Characterization and manipulation of feeding-related neural circuits

Theresia Johanna Maria Goes-Roelofs

Colophon

Cover design: Michel Sinke
Layout: Victor Weigand & Tessa Goes
Printing: Gildeprint

About the cover: The bridge situated in a rough landscape symbolizes a central theme of this thesis; building bridges. Picture taken by the author at Låtefossen, Norway.

ISBN: 978-90-393-7199-2

The research described in this thesis was performed at the Department of Translational Neuroscience, Brain Center Rudolf Magnus, University Medical Center Utrecht and Utrecht University, Utrecht, the Netherlands, and at the Biomedical MR Imaging and Spectroscopy Group, Center for Image Sciences, University Medical Center Utrecht and Utrecht University, Utrecht, the Netherlands.

The work was financially supported by funding from the European Union Seventh Framework Program (FP/2007-2013 under grant agreement number 607310 [Nudge-it]). R.M. Dijkhuizen was supported by a grant from the Netherlands Organization for Scientific Research [NWO-VICI 016.130.662].

Characterization and manipulation of feeding-related neural circuits

Karakterisatie en manipulatie van neurale circuits die betrokken zijn bij voedingsgedrag

(met een samenvatting in het Nederlands)

Proefschrift

ter verkrijging van de graad van doctor aan de Universiteit Utrecht op gezag van de rector magnificus, prof. dr. H.R.B.M. Kummeling, ingevolge het besluit van het college voor promoties in het openbaar te verdedigen op

donderdag 7 november 2019 des ochtends te 10.30 uur

door

Theresia Johanna Maria Goes-Roelofs

geboren op 15 januari 1990 te Zutphen

Promotoren:
Prof. dr. R.A.H. Adan
Prof. dr. R.M. Dijkhuizen

Voor Robert

Ik heb je liever dan geluk

Table of Contents

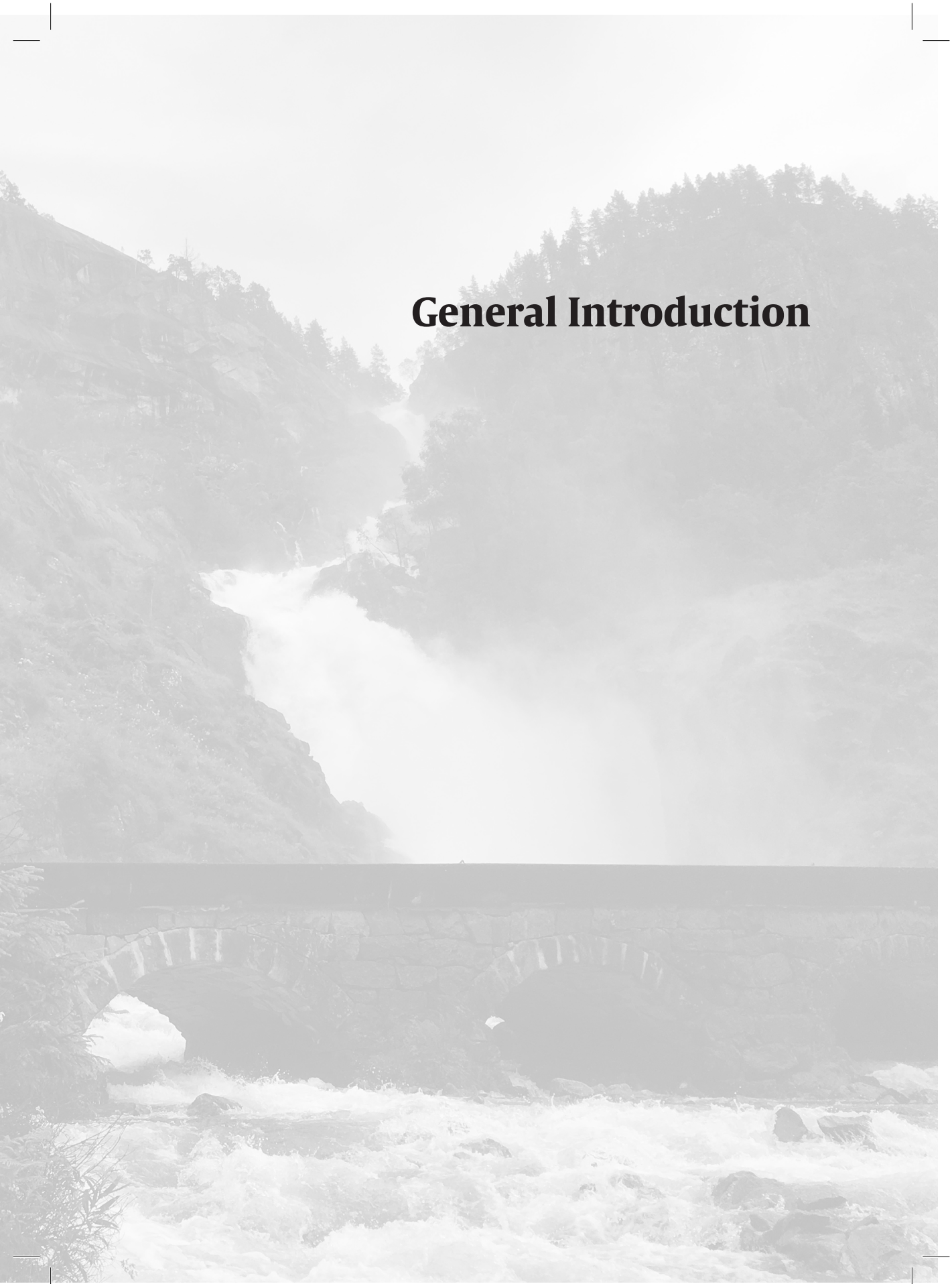

General Introduction

In the past decades neuroscience on understanding mechanisms underlying behavior has moved from lesion studies and pharmacological interventions towards high-tech molecular, cellular and circuit level experiments. Developments in neuroimaging, electrophysiology and genetics provided another dimension and explained many of the earlier lesion and pharmacology studies at a deeper level. Still, there are gaps in knowledge related to how events that are initiated at cellular level impact on ensemble activity in neural circuits, which eventually leads to changes in behavior. How to bridge these different levels of understanding is topic of this thesis.

Tools, techniques, and the main limitations of translational neuroscience

In nowadays neuroscience research many different tools and techniques have been developed that allow investigation of the brain on either a microscopic or a macroscopic level. Different techniques aim to elucidate the cellular working mechanisms of the brain, mostly done in rodent experiments, or aim to resolve on a global level how different brain regions interact to regulate specific behaviors, mostly done in human experiments. Some examples of current state of the art neuroscience technologies in animal models include electrophysiology to perform neural recordings at the cellular level, fiber photometry to perform neural recordings at the population level, chemogenetics to manipulate brain activity at the population level, and optogenetics to manipulate brain activity at the population level with a high temporal resolution. Likewise, neuroimaging modalities in humans like magnetic resonance imaging (MRI), enabling non-invasive whole-brain mapping of neural activity and functional networks, have revolutionized the field of cognitive neuroscience.

Even though the use of these innovative techniques enables us to dive into the functioning of the brain, a critical gap still remains to exist: coupling knowledge about the functioning of the brain from different levels remains difficult. It still is a significant challenge to directly link neurophysiological knowledge of micro-scale cellular activation and connectivity to large-scale neural network activity and connectivity. Besides, there is a huge need for comparable experiments being performed in both rodent models and humans, to investigate how preclinical data translates to humans; another bridge between different levels of understanding that still has to be built.

To start building these bridges, both between microscopic and macroscopic level, as well as between rodent and human neuroscience, we applied, combined, and improved some of the abovementioned techniques to study the regulation of ingestive behavior. The regulation of energy balance and ingestive behavior is not only a good target to start illustrating novel neuroscience approaches because

it is highly conserved and therefore comparable between rodents and humans, it also is a very relevant system; dysregulation of the neural networks involved in the regulation of ingestive behavior and energy balance often leads to serious problems, such as overweight and obesity.

Ingestive behavior and obesity

Obesity is a growing major health challenge[1]; since 1975 the prevalence of obesity has nearly tripled[2] and we have reached the point that most of the world's population live in countries where overweight kills more people than underweight[2]. Overweight and obesity come along with increased risks of developing diabetes, cardiovascular diseases, musculoskeletal disorders, and different types of cancer[2–4], and are thereby responsible for 3.4 million deaths in 2010 worldwide, 4% of years of life lost and 4% of disability-adjusted life-years[3]. This indicates the large socioeconomic burden the growing prevalence of overweight and obesity has on society, and the need for effective interventions.

Obesity is preventable and many people seem aware of the risk factors for developing overweight or obesity, namely increased intake of energy-dense food and decreased physical activity. However, to prevent putting on weight, to lose weight, or to stay lean after dieting appears to be more difficult and complex than simply making the decision to limit calorie intake and increase exercising. A major difficulty in the treatment of obesity is that most people who successfully lost weight during dieting, fail to incorporate the new way of eating into their lifestyle and habits and relapse into their previous unhealthy eating behavior, as a result of which they regain most, if not all or more, of their initial body weight[5]. Rather than a mere nutritional need, we sometimes experience that certain cues can trigger so called hedonic feeding. Hedonic feeding is defined as the consumption of food by a sated individual, simply because he or she experiences the food as a tasty reward and not because he or she needs the food from a homeostatic viewpoint[6]. Cues that can trigger hedonic feeding are environmental cues, such as advertisements, the smell or wrapping of food, or stressors and other emotions[6,7]. It has been known since long that obese individuals are more reactive to food cues and emotions as triggers that initiate feeding[8,9], however, the neural pathways underlying excessive calorie consumption are still not completely understood.

Studying the neural circuits involved in ingestive behavior

The ultimate goal is to understand the regulation of ingestive behavior so that we are able to help people make healthy food choices and to adequately prevent obesity. That is, to steer peoples (feeding) behavior in such a way that energy intake equals energy expenditure in a healthy weight condition and that energy intake

is lower than energy expenditure when body weight is too high. Therefore, we must first know why and how unhealthy food choices that lead to overeating are made. Many different factors and processes influence feeding behavior and their complex interactions complicate a clear elucidation of the working mechanisms underlying feeding behavior. These interacting factors and processes include the body's homeostasis with all the hormones and signaling molecules that are part of it, the process of satiation, the motivation for food, food choice behavior, environmental factors that influence food intake, stress or other emotions, and the genetic and epigenetic predispositions that influence all of these factors. To start resolving how these factors interact and synergistically regulate energy balance and ingestive behavior, we need neuroscientific approaches that bridge different levels of understanding. Thus far, neuroscientists have used a variety of different tools and approaches to unravel the neural circuits involved in the regulation of ingestive behavior, however, these techniques often only focus on a specific level of understanding. Critical gaps in our understanding of the neural mechanisms regulating feeding behavior remain present. For example, there is a gap in our understanding of molecular and cellular mechanisms that guide feeding behavior in freely moving rodents on the one hand, and of neural activity measures in humans exposed to feeding-related stimuli on the other. How changes at the cellular level translate into neural network changes that eventually underly a change in behavior, remains unknown. Still, research has led to valuable knowledge about the neural circuits underlying the regulation of ingestive behavior. Of the multitude of neural circuits involved, two more general systems are relevant for this thesis: the homeostatic system including highly conserved neuroendocrine circuitry and the hedonic system comprising reward- and motivation-related circuitry. Although these two systems comprise largely overlapping elements, they will be described as separate systems for the sake of clarity. It is, however, strongly recommended to keep in mind that the interplay between both systems is of essential importance for the regulation of feeding behavior.

The homeostatic circuitry involved in feeding behavior

The homeostatic system comprises highly conserved neuroendocrine circuitry, in which feeding hormones, such as leptin and ghrelin, play pivotal roles. Leptin is an anorexigenic peptide hormone derived from adipose tissue. The level of circulating leptin is roughly proportional to the amount of fat mass in the body[10–13], and leptin acts via its receptor to signal the amount of energy reserves in the periphery to the brain[10–13]. Leptin inhibits feeding and promotes energy expenditure[12,14] by, amongst others, inhibiting neurons in the arcuate

nucleus of the hypothalamus that make a potent orexigen, neuropeptide Y (NPY), and by activating other neurons in the arcuate nucleus of the hypothalamus that express the anorexigenic factor pro-opiomelanocortin (POMC).

Ghrelin is an orexigenic peptide hormone with opposite functions to leptin, as it stimulates hunger sensation, food intake, adiposity and feeding-associated behaviors[12,15–21]. It is mainly produced by the stomach[15] and to a smaller extend by a subset of hypothalamic neurons[22], and is released into the blood during periods of energy depletion; pre-prandial or during a fast. In the hypothalamus, ghrelin activates NPY neurons, which subsequently inhibit POMC neurons. The dominance of one of the two neuronal populations in the arcuate nucleus, NPY or POMC, is an important determinant for how much we will eat.

The hypothalamus continues to be recognized for its central role in integrating and relaying homeostatic information to regulate feeding behavior[23–25]. The arcuate nucleus of the hypothalamus contains, amongst others, leptin- and ghrelin sensitive NPY and POMC neurons and thereby senses and integrates a wide array of homeostatic signals. These NPY and POMC subpopulations of arcuate nucleus neurons are linked and output to the lateral hypothalamus (LH), the nucleus of the solitary tract (NTS), and the paraventricular nucleus (PVN) of the hypothalamus[24,26], which regulates the hypothalamo-pituitary-adrenal axis (also called the HPA axis or 'stress axis') and the sympathetic nervous system.

When we eat, neural and endocrine signals relay information about food volume and content from the gut to 'satiety' centers in the brainstem and subsequently to leptin- and ghrelin-sensing neurons in the hypothalamus[27]. The nucleus of the solitary tract (NTS) is one of these 'satiety' centers as it is considered a major hub that integrates satiation signals[23]; it receives visceral information via the vagal nerve, as well as information form higher brain centers that project onto and modulate this brain stem nucleus and sometimes overrule visceral information streams[24]. A subpopulation of NTS neurons also expresses leptin receptors[28], suggestive of sensitivity of the NTS itself to neuroendocrine signals. This leptin receptor-expressing subpopulation of NTS neurons projects onto the LH and the ventral tegmental area (VTA) and may affect food intake through actions on dopamine signaling[23] (see *The hedonic circuitry involved in feeding behavior*). The NTS relays meal-related information to the PVN, the dorsal medial hypothalamus (DMH), and the VTA[23]. Via these mechanism and connections, the brain stem nuclei, including the NTS, integrate and respond to acute and long-term changes in energy homeostasis[23].

The hedonic circuitry involved in feeding behavior

Food intake is not just a simple matter of homeostatic balance and

circulating hormones that signal when and how much we should eat to maintain a perfect energy balance. Other factors, such as motivation for food, rewards, environmental cues, stressors, and emotions influence our food choices and feeding behavior as well. The interplay between the homeostatic and hedonic regulation of feeding behavior is of major importance for a well-functioning organism. It is known that leptin and ghrelin not only impact on the homeostatic aspects of feeding behavior, but also influence the hedonic aspects. Both hormones affect the incentive motivation for and the hedonic enjoyments of food; leptin decreases the motivation to work for food, while ghrelin increases it[6,12,16–18,20,29–32,33]. It has been shown that leptin affects motivation for food and reward-related feeding behavior by influencing dopaminergic and GABAergic neurons in the VTA[12,28,34,35] and that ghrelin impacts on neurons in the VTA and nucleus accumbens (NAcc)[12,17,29,36–38].

The hedonic system comprises reward- and motivation-related neural circuitry, including a multitude of brain regions among which the LH, VTA, NAcc, and medial prefrontal cortex (mPFC)[16,17,31,39]. Besides being a major nucleus involved in the homeostatic regulation of feeding behavior, the LH also forms an important component of the hedonic regulation of feeding because it modulates the incentive salience of food[14,37,39–42]. The LH projects onto the VTA[6,14,28] and probably forms one of the crucial inputs that conveys information about energy balance to the VTA[6]. The VTA mediates incentive salience (i.e. 'attractiveness'), motivational properties of positive stimuli and events, the recognition of reward, and reward prediction error[43,44] by integrating peripheral, hypothalamic, cortical, limbic, and mid-/hindbrain information[6,45]. The VTA is the source structure of the brain's reward circuitry and sends projections to the limbic forebrain including the ventral striatum (NAcc) and the prefrontal cortex[31].

The VTA-NAcc projection, known as the mesolimbic projection, is considered to be the core of the mesolimbic dopamine (DA) system involved in reward and motivational behaviors[12,42,46]. The NAcc is thought to be responsible for the hedonic aspects of eating, by generating the hedonic response to metabolically relevant taste stimuli, for example sweet and fatty tastes[20,47]. Some suggest that the NAcc contains an hedonic hotspot and actively generates affective reactions to taste by causing increases in 'liking' as well as 'wanting' for food rewards[48]. Moreover, the NAcc coordinates responses to rewarding and aversive stimuli[44] and the VTA-NAcc projection is considered to be crucial for the recognition of rewards and for initiating their consumption, in the case of food rewards[44,49]. Activity in the VTA-NAcc projection induces the release of dopamine in the NAcc, which binds to excitatory dopamine D1 receptors and inhibitory dopamine D2 receptors on local medium spiny neurons[44,50,51]. Downstream of the striatum, the

GABAergic D1 receptor-expressing striatal neurons project directly to the internal part of the globus pallidus and to the substantia nigra reticulate (SNr) and thereby inhibit these structures[44,50,51]. The SNr sends inhibitory GABAergic projections to the thalamus, resulting in disinhibition, thus activation of the thalamus upon VTA-NAcc activity. Activity in the mesolimbic projection also leads to dopamine binding to inhibitory D2 receptors, which are expressed on GABAergic medium spiny neurons in the NAcc that project via an extra inhibitory loop to the external part of the globus pallidus/ventral pallidum, and subsequently with another inhibitory projection to the internal part of the globus pallidus/SNr[44,50,51]. Activity of this so-called indirect pathway would result in net inhibition of the thalamus. Since the indirect pathway is D2-receptor dominant and dopamine D2 receptors are inhibitory, the release of dopamine upon activation of the mesolimbic pathway results in inhibition of the inhibitory indirect pathway, leading to activation of the thalamus. The direct and indirect pathways converge at the level of the thalamus, which will be activated as a consequence of mesolimbic activation. The thalamus consists of many thalamic nuclei that project to and activate (amongst others) cortical areas like the cingulate, infralimbic, prelimbic and agranular insular cortices, forming a striato-pallido-thalamo-cortical circuit[52–54].

The dorsal anterior cingulate cortex, the prelimbic cortex, and the infralimbic cortex together form the medial prefrontal cortex (mPFC), which is a second major output area of the VTA. The VTA-mPFC projection, known as the mesocortical projection, is more involved in the generic motivational value of certain stimuli[55], cue-reward association learning[6], impulse control, decision making[56], salience attribution, error detection and inhibition[57–59].

As said, the LH, VTA, NAcc, and mPFC together compose a neural circuit involved in the homeostatic and hedonic regulation of feeding behavior[16,17,31,39,59]. However, as outlined above, many more brain areas are involved and form complex networks all affecting (certain parts of) the regulation of feeding behavior. How the homeostatic and hedonic circuitries exactly interact remains largely unknown. Probably, the traditional idea that homeostatic and hedonic systems interact in some way to regulate feeding behavior, should be replaced by an updated vision on the brains neural networks, namely that it all forms a much larger, highly interactive system that unifies reward, cognition, emotion, and homeostasis[25].

Building bridges in neuroscience

In order to help elucidating such a complex system that unifies both homeostatic and hedonic aspects of the regulation of feeding behavior, many different tools have been exploited. However, how microscopic and macroscopic

elements relate and integrate to regulate ingestive behavior and how this system translates between rodents and humans still forms a gap in our current knowledge and understanding. Essential steps from the mechanistic understanding of neuronal signaling at the cellular level, via understanding of neural network activity at the whole-brain level that can be achieved from rodent models, to the global associational data from imaging studies in humans must be taken to bring us closer towards a more complete understanding of the regulation of energy balance and ultimately to prevention of obesity. To take these steps, we need accurate and integrative approaches that exploit the same experimental tools in both rodents and humans, that use newly developed tools, or that combine novel tools. Using, developing, and combining technologies that address how molecular and cellular feeding-related events translate into changes at the neural circuit level, and how these changes translate into feeding-related behavior, will provide us with a more complete understanding of the functioning of the complex networks involved in the regulation of energy balance and feeding behavior. This will be a first step towards therapies and interventions that will help people to make healthier food choices and maintain a healthy body weight. Furthermore, the approaches taken in this thesis with the aim to build bridges between different levels of understanding the brain will also be valuable for other fields of neuroscience, not related to studying the regulation of energy balance and ingestive behavior.

Aims and approaches

The aim of this thesis is to contribute to building bridges between different levels of understanding feeding behavior-related neural circuitry (Figure 1): to date it not only remains difficult to combine molecular knowledge of neuronal working mechanisms with knowledge of complete neural networks or with the entire brain, but also the translational step from rodents to humans is still difficult to make. We aimed to provide molecular insights into the organization of neural networks, as well as to show the translational value of the preclinical studies performed in this thesis for human research. We chose to study the neural circuits involved in ingestive behavior, because this behavior is highly conserved between species and the malfunctioning of these neural systems has major health consequences. Therefore, we also aimed to understand the organization of neural networks involved in ingestive behavior. More specifically, we wanted to characterize these neural networks and understand how specific brain regions within these networks connect and process feeding-related information.

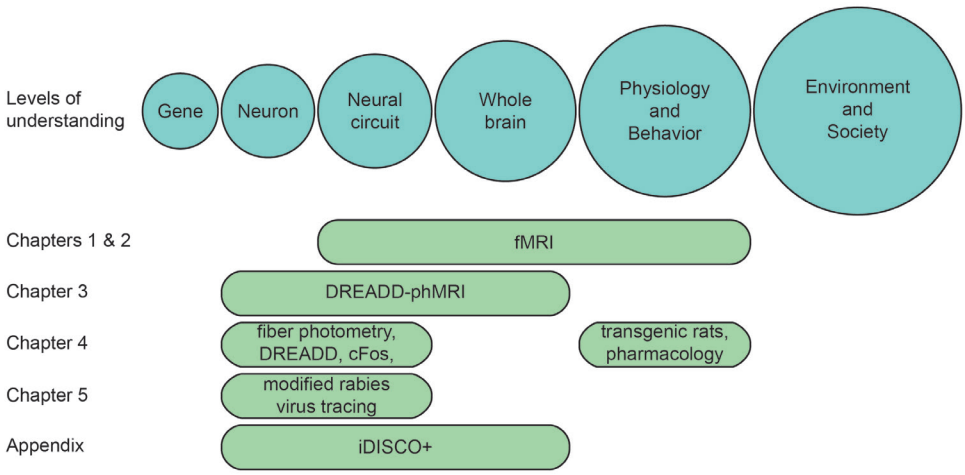

Figure 1. The different levels of understanding in nowadays neuroscience research and the approaches utilized in this thesis to bridge the gaps between these levels. In the different chapters of this thesis, I aimed to contribute to building bridges between different neuroscientific levels of understanding feeding-related behavior. These different levels range from microscopic to the macroscopic. This thesis is focused on building bridges between different levels ranging from neurons to physiology and behavior. cFos, cFos immunohistochemistry; DREADD, Designer Receptors Exclusively Activated by Designer Drug technology; iDISCO+, optimized version of the improved immunolabeling-enabled 3-dimensional imaging of solvent-cleared organs protocol.

Outline of the thesis

In order to get a better understanding of the organization and functioning of feeding-related neural networks, we employed different techniques to visualize and manipulate feeding-related neural pathways ranging from microscopic to macroscopic level (Figure 1).

At the macroscopic level, particularly in the field of studying ingestive behavior, many human neuroimaging experiments have been performed. Unfortunately, it remains difficult to translate this wealth of knowledge to a preclinical setting, which would be beneficial in order to combine it with more information on the underlying cellular mechanisms. On the other hand, many preclinical data on the cellular working mechanism involved in ingestive behavior is already available, but is still difficult to translate to humans. To bring the two fields closer together, we aimed to set up a preclinical neuroimaging experiment with a paradigm translatable to those used in human neuroimaging experiments. In this way, we are able to study whether comparable neural circuits are involved and if data can be translated between rodent and human studies. **Chapter 1** studies the different effects of oro-sensory stimulation, i.e. tasting, and gastric distention on brain activation patterns in rats. Besides, it assesses the influence

of different states of homeostatic energy balance on the responses to tasting and gastric distention. Using functional MRI (fMRI) during the manipulation of the oral or gastric environment, we aimed to determine if findings from rat studies translate to human findings, as described in literature. The approach described in this chapter adds to the aim to establish the translational value of preclinical experiments and offers a new avenue to deepen our understanding of the process of satiation on a macroscopic level. Thereby, it also adds to the aim to understand how specific brain regions process feeding-related information.

As functional MRI studies in humans may also include measurements of functional connectivity, in addition to brain activation responses, we wanted to bring rodent and human neuroimaging closer together by similarly assessing functional network connectivity in a rodent model using resting state fMRI (rs-fMRI). We hypothesized that the organization of neural networks involved in feeding behavior would depend on status of homeostatic energy balance, that is, on being hungry or satiated. Therefore, as a follow-up study to chapter 1, **chapter 2** employs the approach developed in chapter 1 to study the effects of status of homeostatic energy balance and tasting a sweet taste on functional connectivity and signal amplitude in neural networks using rs-fMRI. This chapter thereby adds to the aims to build a bridge between preclinical and human studies, and to characterize feeding-related neural networks to get a better understanding of how brain regions within these networks connect to process feeding-related information.

Although human neuroimaging studies have truly revolutionized the field of cognitive neuroscience, it is still very difficult to bridge findings of this field to preclinical findings. Chapters 1 and 2 aimed to start building this bridge by performing comparable experiments in rodents as done in humans, but an essential link still misses: to understand how neuronal mechanisms at a cellular level underlie the indirect measure of neural activity as retrieved with MRI on a whole-brain level. We aimed to get more insight into this missing link, the coupling of cellular activation and neural circuit activity, by activating specific neurons while at the same time measuring the whole-brain effects using MRI. **Chapter 3** describes the development of a novel approach to locally induce brain activation in specific neural pathways using chemogenetics and to globally map this induced activation and its whole-brain effects using pharmacological Magnetic Resonance Imaging (phMRI). Chemogenetics (Designer Receptors Exclusively Activated by Designer Drugs (DREADD)-technology) enabled us to specifically target the mesolimbic or mesocortical pathways, which are known for their involvement in regulating certain aspects of feeding behavior[30,31,56,60]. Using different MRI techniques, we aimed to elucidate how local induced activation

impacts on global brain activity and on network connectivity. The combination of chemogenetics and MRI provides insights into how neuronal activation at cellular level underlies neural circuit activity at whole-brain level, thereby adding to the aim to understand how microscopic and macroscopic neuronal mechanisms together regulate behavior.

Chapter 4 assesses the influence of homeostatic need on the motivational drive for a specific nutrient. Thereby, it addresses the interaction of different feeding-related neural networks, being a network that senses the homeostatic sodium state of the body and the mesocorticolimbic network that drives motivation. It is already known that homeostatic and motivational neural circuits interact in some way, but via which specific neurons these information streams converge, remains to be elucidated. Also, exactly assessing activity of these neurons as well as manipulating activity and assessing the consequences of changes in activity on a behavioral level, remains a critical step in building a bridge between the microscopic and the macroscopic level. Using a combination of fiber photometry, chemogenetics, pharmacology, and cFos immunohistochemistry we aimed to verify the direct involvement of the mesocorticolimbic system in sodium appetite in rats, by measuring from and manipulating this neural circuit. With this study we aimed to obtain molecular insights into network organization, and to determine how the brain regions involved affect feeding behavior.

At the microscale, we aimed to deepen our understanding of the cellular network organization of feeding-related brain regions with the experiment described in **chapter 5**. Here we assessed the monosynaptic inputs to neurons in the lateral hypothalamus (LH) that express leptin receptors. Although chemical antero- and retrograde tracing technologies have already provided connectivity maps, it is only since the last years that the specific inputs to genetically identifiable neurons can be mapped. For instance, it is known that neurons from the arcuate nucleus project to the LH, but it is poorly understood which subpopulations of LH neurons receive these synaptic inputs. Using modified rabies virus tracing technology and a Cre/LoxP recombination system, we specifically targeted a subpopulation of neurons, thereby mapping anatomical connections in a model system of ingestive behavior. This chapter thus adds to the aim to obtain microscopic level insight into the organization of feeding-related neural networks.

To be able to visualize microscale connections on a macroscale level, we optimized and applied a brain clearing protocol as described in the **Appendix**. Neurons that express leptin receptors, and thus are involved in the regulation of ingestive behavior, were stained. Subsequently brains were made transparent, so that the neurons and connections which expressed leptin receptors became

visible. The Appendix thereby adds to the aims to visualize microscopic neural pathways on a macroscopic level, and to reveal the molecular organization of feeding-behavior related neural networks.

Finally, the **General Discussion** integrates findings from the experimental chapters and puts these findings in a broader perspective, namely, how this knowledge of cellular working mechanisms and knowledge of neural networks can be combined and translated between rodent and human studies, and how this helps us to better understand the regulation of feeding behavior.

References

1. Ng, M. et al. Global, regional, and national prevalence of overweight and obesity in children and adults during 1980-2013: A systematic analysis for the Global Burden of Disease Study 2013. Lancet 384, 766–781 (2014).
2. World Health Organisation, W. Factsheet Obesity and Overweight. http://www.who.int/mediacentre/factsheets/fs311/en/ factsheet 311 (2017).
3. Lim, S. S. et al. A comparative risk assessment of burden of disease and injury attributable to 67 risk factors and risk factor clusters in 21 regions, 1990-2010: A systematic analysis for the Global Burden of Disease Study 2010. Lancet 380, 2224–2260 (2012).
4. Haslam, D. W. & James, W. P. T. Obesity. Lancet 366, 1197–1209 (2005).
5. Tsai, A. G. & Wadden, T. A. Review Systematic Review : An Evaluation of Major Commercial Weight Loss Programs in the United States. Ann Intern Med. 142, (2005).
6. Meye, F. J. & Adan, R. A. H. Feelings about food: the ventral tegmental area in food reward and emotional eating. Trends Pharmacol. Sci. 35, 31–40 (2014).
7. Johnson, A. W. Eating beyond metabolic need: How environmental cues influence feeding behavior. Trends Neurosci. 36, 101–109 (2013).
8. Lowe, M. R. & Fisher, E. B. Emotional reactivity, emotional eating, and obesity: A naturalistic study. J. Behav. Med. 6, 135–149 (1983).
9. Grosshans, M. et al. Association of leptin with food cue-induced activation in human reward pathways. Arch. Gen. Psychiatry 69, 529–537 (2012).
10. Davis, J. F., Choi, D. L. & Benoit, S. C. Insulin, Leptin and Reward. Trends Endocrinol. Metab. 21, 1–12 (2011).
11. Friedman, J. M. & Halaas, J. L. Leptin and the regulation of body weight in mammals. Nature 395, 763–70 (1998).
12. Palmiter, R. D. Is dopamine a physiologically relevant mediator of feeding behavior? Trends Neurosci. 30, 375–81 (2007).

13. Robertson, S. A., Leinninger, G. M. & Myers, M. G. Molecular and neural mediators of leptin action. Physiol. Behav. 94, 637–42 (2008).
14. Leinninger, G. M. et al. Leptin acts via leptin receptor-expressing lateral hypothalamic neurons to modulate the mesolimbic dopamine system and suppress feeding. Cell Metab. 10, 89–98 (2009).
15. Kojima, M. et al. Ghrelin is a growth-hormone-releasing acylated peptide from stomach. Nature 402, 656–60 (1999).
16. Menzies, J. R. W., Skibicka, K. P., Leng, G. & Dickson, S. L. Ghrelin, reward and motivation. Endocr. Dev. 25, 101–11 (2013).
17. Menzies, J. R. W., Skibicka, K. P., Egecioglu, E., Leng, G. & Dickson, S. L. Peripheral Signals Modifying Food Reward. Appet. Control. Handb. Exp. Pharmacol. 209, 131–158 (2012).
18. Naleid, A. M., Grace, M. K., Cummings, D. E. & Levine, A. S. Ghrelin induces feeding in the mesolimbic reward pathway between the ventral tegmental area and the nucleus accumbens. Peptides 26, 2274–9 (2005).
19. Wellman, P. J. et al. Brain reinforcement system function is ghrelin dependent: studies in the rat using pharmacological fMRI and intracranial self-stimulation. Addict. Biol. 17, 908–19 (2011).
20. Lockie, S. H. & Andrews, Z. B. The hormonal signature of energy deficit: Increasing the value of food reward. Mol. Metab. 2, 329–336 (2013).
21. van der Lely, A. J., Tschöp, M., Heiman, M. L. & Ghigo, E. Biological, physiological, pathophysiological, and pharmacological aspects of ghrelin. Endocr. Rev. 25, 426–57 (2004).
22. Cowley, M. a et al. The distribution and mechanism of action of ghrelin in the CNS demonstrates a novel hypothalamic circuit regulating energy homeostasis. Neuron 37, 649–61 (2003).
23. Chambers, A. P., Sandoval, D. A. & Seeley, R. J. Integration of satiety signals by the central nervous system. Curr. Biol. 23, R379–R388 (2013).
24. Grill, H. J. Leptin and the systems neuroscience of meal size control. Front. Neuroendocrinol. 31, 61–78 (2010).
25. Berthoud, H. R., Münzberg, H. & Morrison, C. D. Blaming the Brain for Obesity: Integration of Hedonic and Homeostatic Mechanisms. Gastroenterology 152, 1728–1738 (2017).
26. Cone, R. D. et al. The arcuate nucleus as a conduit for diverse signals relevant to energy homeostasis. Int. J. Obes. 25, S63-7 (2001).
27. Murphy, K. G. & Bloom, S. R. Gut hormones and the regulation of energy homeostasis. Nature 444, 854–859 (2006).

28. Leinninger, G. M. et al. Leptin action via neurotensin neurons controls orexin, the mesolimbic dopamine system and energy balance. Cell Metab. 14, 313–23 (2011).
29. Abizaid, A. et al. Ghrelin modulates the activity and synaptic input organization of midbrain dopamine neurons while promoting appetite. J. Clin. Invest. 116, 3229–3239 (2006).
30. Malik, S., McGlone, F., Bedrossian, D. & Dagher, A. Ghrelin modulates brain activity in areas that control appetitive behavior. Cell Metab. 7, 400–409 (2008).
31. van Zessen, R., van der Plasse, G. & Adan, R. A. H. Contribution of the mesolimbic dopamine system in mediating the effects of leptin and ghrelin on feeding. Proc. Nutr. Soc. 71, 435–445 (2012).
32. Fulton, S., Woodside, B. & Shizgal, P. Modulation of Brain Reward Circuitry by Leptin. Science (80-.). 287, 125–128 (2000).
33. Figlewicz, D. P., MacDonald Naleid, A. & Sipols, A. J. Modulation of food reward by adiposity signals. Physiol. Behav. 91, 473–8 (2007).
34. Figlewicz, D. P., Evans, S. B., Murphy, J., Hoen, M. & Baskin, D. G. Expression of receptors for insulin and leptin in the ventral tegmental area/substantia nigra (VTA/SN) of the rat. Brain Res. 964, 107–15 (2003).
35. Hommel, J. D. et al. Leptin receptor signaling in midbrain dopamine neurons regulates feeding. Neuron 51, 801–10 (2006).
36. Skibicka, K. P., Hansson, C., Alvarez-Crespo, M., Friberg, P. & Dickson, S. L. Ghrelin directly targets the ventral tegmental area to increase food motivation. Neuroscience 180, 129–37 (2011).
37. Skibicka, K. P. & Dickson, S. L. Ghrelin and food reward: the story of potential underlying substrates. Peptides 32, 2265–73 (2011).
38. Zigman, J. M., Jones, J. E., Lee, C. E., Saper, C. B. & Elmquist, J. K. Expression of ghrelin receptor mRNA in the rat and the mouse brain. J. Comp. Neurol. 494, 528–48 (2006).
39. Kelley, A. E., Baldo, B. A. & Pratt, W. E. A proposed hypothalamic-thalamic-striatal axis for the integration of energy balance, arousal, and food reward. J. Comp. Neurol. 493, 72–85 (2005).
40. Harris, G. C., Wimmer, M. & Aston-Jones, G. A role for lateral hypothalamic orexin neurons in reward seeking. Nature 437, 556–9 (2005).
41. Narayanan, N. S., Guarnieri, D. J. & DiLeone, R. J. Metabolic hormones, dopamine circuits, and feeding. Front. Neuroendocrinol. 31, 104–12 (2010).
42. Nestler, E. J. Is there a common molecular pathway for addiction? Nat. Neurosci. 8, 1445–9 (2005).

43. Berridge, K. C. The debate over dopamine's role in reward: the case for incentive salience. Psychopharmacology (Berl). 191, 391–431 (2007).
44. Russo, S. J. & Nestler, E. J. The brain reward circuitry in mood disorders. Nat. Rev. Neurosci. 14, 609–625 (2013).
45. Watabe-Uchida, M., Zhu, L., Ogawa, S. K., Vamanrao, A. & Uchida, N. Whole-Brain Mapping of Direct Inputs to Midbrain Dopamine Neurons. Neuron 74, 858–873 (2012).
46. Kelley, A. E. & Berridge, K. C. The neuroscience of natural rewards: relevance to addictive drugs. J. Neurosci. 22, 3306–11 (2002).
47. Peciña, S. & Berridge, K. C. Hedonic hot spot in nucleus accumbens shell: where do mu-opioids cause increased hedonic impact of sweetness? J. Neurosci. 25, 11777–86 (2005).
48. Berridge, K. C., Ho, C.-Y., Richard, J. M. & DiFeliceantonio, A. G. The tempted brain eats: pleasure and desire circuits in obesity and eating disorders. Brain Res. 1350, 43–64 (2010).
49. Koob, G. F. & Le Moal, M. Addiction and the Brain Antireward System. Annu. Rev. Psychol. 59, 29–53 (2008).
50. Humphries, M. D. & Prescott, T. J. The ventral basal ganglia, a selection mechanism at the crossroads of space, strategy, and reward. Prog. Neurobiol. 90, 385–417 (2010).
51. Kenny, P. J., Voren, G. & Johnson, P. M. Dopamine D2 receptors and striatopallidal transmission in addiction and obesity. Curr. Opin. Neurobiol. 23, 1–4 (2013).
52. Groenewegen, H. J. Organization of the Afferent Connections of the Mediodorsal Thalamic Nucleus in the Rat, Related To the Mediodorsal Prefrontal Topography. Neuroscience 24, 379–431 (1988).
53. Ikemoto, S. Dopamine reward circuitry: two projection systems from the ventral midbrain to the nucleus accumbens-olfactory tubercle complex. Brain Res Rev. 56, 27–78 (2007).
54. Groenewegen, H. J., Berendse, H. W. & Haber, S. N. Organization of the output of the ventral striatopallidal system in the rat: Ventral pallidal efferents. Neuroscience 57, 113–142 (1993).
55. Bassareo, V., De Luca, M. A. & Di Chiara, G. Differential Expression of Motivational Stimulus Properties by Dopamine in Nucleus Accumbens Shell versus Core and Prefrontal Cortex. J. Neurosci. 22, 4709–19. (2002).
56. Kelley, A. E., Baldo, B. a, Pratt, W. E. & Will, M. J. Corticostriatal-hypothalamic circuitry and food motivation: integration of energy, action and reward. Physiol. Behav. 86, 773–95 (2005).

57. Volkow, N. D. et al. Low Level of Brain Dopamine D_2 Receptors in Methamphetamine Abusers: Association With Metabolism in the Orbitofrontal Cortex. Am. J. Psychiatry 158, 2015–2021 (2001).
58. Volkow, N. D. et al. Profound Decreases in Dopamine Release in Striatum in Detoxified Alcoholics: Possible Orbitofrontal Involvement. J. Neurosci. 27, 12700–12706 (2007).
59. Volkow, N. D., Wang, G.-J., Tomasi, D. & Baler, R. D. The addictive dimensionality of obesity. Biol. Psychiatry 73, 811–8 (2013).
60. Salamone, J. D. & Correa, M. The mysterious motivational functions of mesolimbic dopamine. Neuron 76, 470–485 (2012).

Chapter 1

Good taste or gut feeling: what fulfills? Oro-sensory stimulation and gastric distention generate distinct brain activation patterns in rats

Theresia J.M. Roelofs[a,b], Mieneke C.M. Luijendijk[a], Annette van der Toorn[b], Guido Camps[d], Paul A.M. Smeets[d,e], Rick M. Dijkhuizen[b], Roger A.H. Adan[a,c]

[a]Department of Translational Neuroscience, Brain Center Rudolf Magnus, University Medical Center Utrecht and Utrecht University, Universiteitsweg 100, 3584 CG Utrecht, the Netherlands
[b]Biomedical MR Imaging and Spectroscopy Group, Center for Image Sciences, University Medical Center Utrecht and Utrecht University, Bolognalaan 50, 3584 CJ Utrecht, the Netherlands
[c]Institute of Neuroscience and Physiology, The Sahlgrenska Academy at the University of Gothenburg, Sweden
[d]Division of Human Nutrition and Health, Wageningen University & Research, Stippeneng 4, 6708 WE, Wageningen, The Netherlands
[e]Image Sciences Institute, Brain Center Rudolf Magnus, University Medical Center Utrecht, Heidelberglaan 100, 3584 CX Utrecht, The Netherlands

Satiation is influenced by a variety of signals including gastric distention and oro-sensory stimulation, but the neural processes involved remain largely unclear. We here developed a high-field functional MRI (fMRI) protocol to test how oro-sensory stimulation and gastric distention affect brain activation under different states of energy balance in rats. Repeated tasting of sucrose induced positive and negative fMRI responses in the VTA and septum, respectively, and gradual neural activation in the anterior insula. Gastric distention induced more extensive brain activation, involving the insular cortex and the brain stem nucleus of the solitary tract (NTS). These neural responses were not significantly influenced by status of energy balance. Our findings are largely in line with human studies that have shown that the NTS is involved in processing visceral information and that the anterior insula plays a key role in processing sweet taste oro-sensory signals. Furthermore, gastric distention and sucrose tasting induced responses in mesolimbic areas, which may reflect the rewarding effects of a full stomach and sweet taste. The similarity of these rodent data to human neuroimaging data demonstrates the translational value of the approach and offers a new avenue to deepen our understanding of the process of satiation.

INTRODUCTION

Imbalance between intake and burning of calories, as in overconsumption, can result in obesity, which is a major health risk in Western society. Feeding behavior, which is tightly regulated, is influenced by a variety of internal and external factors, which are processed in the brain[1]. Satiation, leading to ending an initiated meal, is one of the key processes determining feeding behavior. Satiation is influenced by, among other factors, gastric distention and oro-sensory stimulation[2–4]. Identification of neural correlates of satiation could aid in understanding and eventually handling of disturbances in satiation that lead to overconsumption and obesity.

Several brain regions, such as the brain stem nucleus of the solitary tract (NTS) and parabrachial nucleus, and the orbitofrontal cortical regions, insula, and anterior cingulate cortex, process visceral information that leads to satiation[5–13]. Processing of oro-sensory stimulation, including taste, involves partly the same brain regions, and activates the insula, the postcentral gyrus, and the hypothalamus[14]. Besides being involved in processing interoceptive signals from the gut, the anterior insula contains the primary taste cortex and is thus involved in processing gustatory stimulation such as sweet and bitter taste[14–17]. Studies in rodents have demonstrated that the NTS is a major hub that integrates satiation signals[18]. Levels of the anorectic hormone cholecystokinin (CCK), released from

the intestines, are strongly associated with satiation, and CCK activates the vagal nerve that projects onto NTS neurons. Higher brain centers project onto and modulate NTS neurons, such that CCK becomes less effective. By this means meal sizes become larger in negative energy balance[19].

During eating, gastric stretch and taste are processed simultaneously. It is not completely understood where these signals converge, whether repeated stimulation gradually builds up a neural signal, and how this contributes to satiation and meal termination[20]. Gastric distention by itself is sufficient to increase brain activity in reward- and eating behavior-related areas such as the midbrain, hypothalamus, amygdala, and hippocampus[3,21–23]. Simultaneous oro-sensory stimulation and gastric distention activates more areas involved in gustation and reward than gastric distention alone, namely the thalamus, amygdala, putamen and left precuneus[3]. However, the separate effects of oro-sensory stimulation and gastric distention and their specific contribution to the process of satiation remain to large extent unknown.

A complicating factor is that the neural response to gustatory stimuli does not only depend on the type of stimulus, but also on hunger and feeding status[24–29]. Hungry subjects have been shown to display a relatively strong neural response to tasting in the insula, thalamus and substantia nigra, while sated subjects exhibited lower responses in the parahippocampus, hippocampus, amygdala, and anterior cingulate cortex[24]. Another study found that the left putamen and left amygdala were more responsive to taste stimuli in a hungry compared to a fed state[30]. Furthermore, it has been shown that the median cingulate, ventrolateral prefrontal cortex, anterior insula and thalamus play a key role in tasting calories, and that this process is dependent on hunger status, since these regions integrate hunger status with stimulus relevance[25]. On the other hand, studies in macaque monkeys did not find an effect of hunger on the neural response to tasting[31,32], thus indicating the complicated nature of studying neural responses to taste and gastric signals under different states of energy balance in conscious animals.

The aim of our study was to develop and apply a novel standardized functional imaging approach in rats which allows separating the effects of oro-sensory stimulation and gastric distention on brain activation of satiation-related brain areas. Since the behavioral response to and stress induced by gastric distention and taste would compromise the processing of gastric and oro-sensory stimulation, the experiments were performed in mildly anesthetized animals. By separately assessing the effects of taste stimulation and gastric distention, we aimed to find the neural correlates of the two stimuli, to identify common activated areas, and to determine the influence of status of homeostatic energy balance on the detected neural responses.

METHODS

Animals

Experiments were approved by the Animal Ethics Committee of the University Medical Center Utrecht, the Netherlands, and were conducted in agreement with Dutch laws ('Wet op de Dierproeven', 1996) and European regulations (Guideline 86/609/EEC).

We used adult male Wistar rats (Crl:WU, Charles River, Sulzfeld, Germany), which were housed individually under controlled temperature and humidity conditions, and under a 12h light/dark cycle (lights on at 7:00 a.m.). Animals had *ad libitum* access to water, and a perspex tube was provided as cage enrichment. Half of the animals had *ad libitum* access to chow, while the other half were food-restricted starting one week prior to scanning. Food restriction involved providing 10 grams of chow per day till the animal reached 90% of its initial body weight. Body weight was maintained at 90% of the initial weight until MRI was performed. Mean (± standard deviation) bodyweight upon arrival of all animals was 240 (±6) g; the food-restricted group had a mean body weight upon arrival of 242 (±7) g, the *ad libitum*-fed group of 239 (±6) g. Mean body weight at time of scanning for the food-restricted group was 296(±17) g, and for the *ad libitum*-fed group 354(±34) g.

Animal preparations and MRI

We conducted *in vivo* MRI measurements on a 9.4 T horizontal bore MR system equipped with a 400 mT/m gradient coil (Agilent). In this setup, we used a home-built 90 mm diameter Helmholtz volume coil for signal excitation, and an inductively coupled 25 mm diameter surface coil for signal reception.

Anesthesia was induced with 3-5% isoflurane in O_2/air (1:4) and animals were endotracheally intubated for mechanical ventilation. A home-built intragastric (IG) balloon device, constructed from a Portex vinyl rubber tubing (inner diameter 1 mm, outer diameter 2 mm; Smiths Industries, Hythe, Kent, England) and a thin-walled silicone 'extruding balloon' tubing (Dentsleeve BE 2.5) fixed together with silicon paste, was inserted via the esophagus. The balloon was filled with water (at ca. 37°C). For sucrose tasting, two Portex polyethylene tubes (PE90, inner diameter 0.86 mm, outer diameter 1.27 mm; Smiths Industries, Hythe, Kent, England) were placed above the tongue; one was used to flush the oral cavity with a 30% sucrose solution, which is palatable to rats[33–35], the second tube was used to rinse the oral cavity with water, in order to remove sucrose from the mouth quickly.

After animals were positioned inside the scanner, anesthesia was reduced to 1.5% isoflurane in O_2/air (1:4). We maintained anesthesia at 1.5% during the

entire MRI protocol. End-tidal CO_2 was monitored with a capnograph (Microcap, Oridion Medical 1987 Ltd., Jerusalem, Israel). Body temperature was maintained at 37.0 ± 1.0°C.

First, we acquired anatomical images using a balanced steady-state free precession (bSSFP) sequence, with 4 phase cycling angles (0°, 90°, 180°, 270°), repetition time (TR)/echo time (TE)=5/2.5 ms, flip angle=20°, field-of-view (FOV)=40x32x24 mm^3, and matrix size=160x128x96 voxels (scan time: 10 min). The resulting spatial resolution was 250 µm in all directions.

Subsequently, we executed a block-design functional MRI protocol during which rats underwent gastric distention or oral sucrose flushing sequentially. fMRI data were acquired with a 3D gradient echo EPI sequence. The read-out and first phase-encode dimensions were covered in a single-shot EPI, the second phase-encode dimension used linear phase encoding. We acquired 680 images with an acquisition time of 974.4 ms per volume (total scan time: 11 minutes and 3 seconds), and TR/TE=34.8/20 ms, flip angle=13°, FOV=36x36x16.8 mm^3 and matrix size=60x60x28 (isotropic spatial resolution=600 µm). During fMRI acquisition the IG balloon was temporarily inflated with 5 mL of water five consecutive times during 50 seconds to induce gastric distention (IG balloon inflation was done in the first 5 seconds, deflation in the last 5 seconds of this period). The volume of balloon inflation was based on a post-mortem assessment of gastric volume and on another study in which gastric distention was performed in rats[36]. Each inflation period was followed by a rest period of 60 seconds during which the IG balloon was in a deflated state. Functional MRI during oral sucrose flushing was executed with a comparable block-design paradigm. 1.8 mL sucrose was flushed through the mouth over a period of 40 seconds, followed by a rinse with water (1 mL in 10 seconds) and a rest period of 60 seconds. This was repeated five times. The two fMRI paradigms were executed ten minutes after each other as outlined in Figure 1a.

After MRI acquisition, we checked whether the tubes, through which sucrose and water were flushed, were still correctly positioned in the rat′s mouth. In all rats, the mouth tubes were correctly placed. The rats were euthanized by an overdose of isoflurane, followed by intracardial perfusion-fixation with cold 0.1M phosphate-buffered saline (PBS) first and 4% paraformaldehyde (PFA) dissolved in PBS thereafter. Post-mortem inspection of IG balloon placement demonstrated that all balloons were correctly positioned inside the stomach.

MRI data processing and analysis

Anatomical MRI

Non-uniformity correction was performed on anatomical images using

n3, and brain masks were obtained by applying the *Brain Extraction Tool* to the anatomical images, both as provided by *FSL* (FMRIB's Software Library, http://fmrib.ox.ac.uk/fsl, version 5.0.9). The individual anatomical images were masked and registered to an anatomical MRI template that was matched to a 3D model of a rat brain atlas[37] using the affine intermodal image registration tool *FLIRT* (FMRIBs Linear Image Registration Tool, v6.0). Co-registered anatomical images were averaged to acquire an anatomical template in atlas space. The original individual anatomical images were registered to this anatomical template using *FLIRT* followed by *FNIRT* (FMRIBs Nonlinear Image Registration Tool, build 508). Inverse coefficients were calculated to register regions of interest (ROIs) from atlas space to individual anatomical space.

Functional MRI

All block-design functional MR images were corrected for subject motion using *MCFLIRT* and image intensity non-uniformity correction was performed using *n3* (solely for registration purposes), both as provided by *FSL*. Using *FLIRT*, fMRI images were registered to the same fMRI image of a single representative rat. Co-registered images were averaged to create a template specific for each fMRI paradigm (i.e. gastric distention and sucrose tasting). These templates were made to obtain proper brain masks, to exclude any tissue outside the brain from analyses. Therefore, we applied the *Brain Extraction Tool* from *FSL* to the templates, registered the individual data to the templates using *FLIRT* and calculated the inverse coefficients, to be able to register the brain masks from template space to individual fMRI space.

Functional MRI data were normalized to the baseline (corresponding to the first 90 MR volumes) using *FSLMATHS* from *FSL*. In order to create a general fMRI template, i.e. a template for all block-design fMRI data of this experiment, on which a two-level generalized linear model (GLM)-based analysis could be performed, individual fMRI data were registered to a representative fMRI dataset (from a single animal's sucrose flushing experiment) using *FLIRT* followed by *FNIRT*. All co-registered fMRI images were averaged to create this general fMRI template. Individual normalized fMRI data were again registered to this template using *FLIRT*, to ensure the same amount of registration deformations per dataset. On first level of the GLM-based analysis we analyzed the individual normalized fMRI data comparable to the approach as described in [38]. For this analysis a block-design function with 40 (for sucrose tasting) or 50 (for gastric distention) seconds on-periods and 70 (for sucrose tasting) or 60 (for gastric distention) seconds off-periods, convolved with a hemodynamic response function (HRF), was used as a regressor. This resulted for each animal in whole-brain activation maps

(Z-maps) for both fMRI paradigms. Subsequently, we assessed the differences in brain responses to sucrose tasting and gastric distention on the group level by comparing the specific Z-maps resulting from the subject level analysis in a GLM-based analysis. We also compared the Z-maps of the hungry and satiated groups to assess possible effects of status of homeostatic energy balance on brain activation responses to the treatments. FDR correction for multiple testing was performed on first (when shown separately) and second level GLM results, and an FDR-corrected Z-value of (-)1.96, corresponding to a p-value of 0.05, was taken as cutoff value for activation maps.

To calculate mean blood oxygenation level-dependent (BOLD) signal intensity over time per ROI, the inverse coefficients for the above described registration from individual anatomical space to anatomical template space were applied to register the ROIs to individual anatomical space. Individual fMRI data were registered to individual anatomical images using *FLIRT*, the inverse coefficients were calculated, and individual anatomical images were then registered to individual fMRI images using *FNIRT*. These coefficients were applied to the ROIs for registration to individual fMRI space. Mean signal intensity was calculated per ROI from normalized fMRI data. ROIs extracted from two rat brain atlases[37,39] included the left and right medial prefrontal cortex (mPFC), orbitofrontal cortex (OFC), cingulate cortex, insula, nucleus accumbens (NAcc), caudate putamen (CPu), septum, sensorimotor cortex, thalamus, lateral hypothalamus (LH), ventral tegmental area (VTA), substantia nigra (SN), and nucleus of the solitary tract (NTS) (Figure 1b).

RESULTS

No effect of status of homeostatic energy balance on brain responses to sucrose tasting or gastric distention

To measure brain responses to tasting (sucrose flushing through the mouth) and gastric distention (water-filled intragastric balloon inflation), we developed and performed a block-design functional MRI protocol in 16 rats that received both treatments sequentially. To rule out possible confounding effects of treatment order, we evenly distributed tasting or gastric distention as first treatment in both groups. In addition, to assess the effect of status of homeostatic energy balance, rats were randomly assigned to two equally sized groups (n=8), in which they were either fed *ad libitum* or food-restricted (Figure 1a). Due to artefacts in the fMRI data (probably Nyquist N/2 ghosts) resulting from technical issues, three animals had to be excluded from all analyses. Final group sizes were: food-restricted group, n=6; *ad libitum*-fed group, n=7. We performed a two-level generalized linear model (GLM)-based analysis. On the first level we calculated

individual whole-brain activation maps (Z-maps) per treatment, and on the second level we assessed the differences in brain responses to the two treatments as well as the differences in responses between food-restricted and *ad libitum*-fed rats. The latter part of the second level GLM-based analyses revealed no significant differences in activation responses between food-restricted and *ad libitum*-fed rats (Supplementary Figure 1) Therefore, we pooled the data from both groups for further analyses.

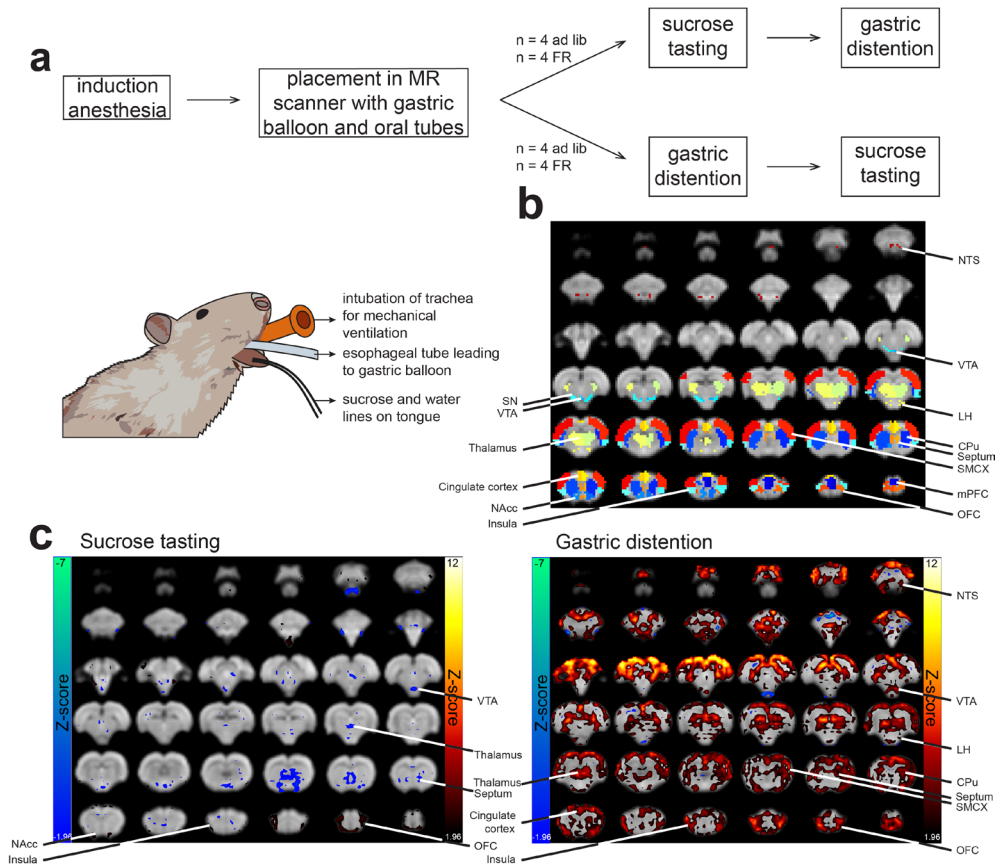

Figure 1. Experimental overview and whole-brain pattern of activation to sucrose tasting and gastric distention. a) Overview of experimental protocol and set-up. b) Regions of interest overlaid on fMRI template. c) Whole-brain group average activation patterns in response to sucrose tasting (left) and gastric distention (right). Z-scores represent FDR-corrected values. Significantly activated regions are shown in hot colors; significantly deactivated regions are shown in cold colors. CPu, caudate putamen; mPFC, medial prefrontal cortex; LH, lateral hypothalamus; NAcc, nucleus accumbens; NTS, nucleus of the solitary tract; OFC, orbitofrontal cortex; SMCX, sensorimotor cortex; SN, substantia nigra; VTA, ventral tegmental area.

Neural responses to oro-sensory stimulation and gastric distention

Group average brain activation patterns in response to sucrose tasting and gastric distention are shown in Figure 1c. Significantly activated or deactivated brain regions are listed in Table 1. Sucrose tasting induced brain activation in the anterior region of the insular cortex, the orbitofrontal cortex (OFC), and in voxels at the border of the nucleus accumbens (NAcc) and ventral pallidum (VP) (Figure 1c, left panel; Table 1). Negative BOLD responses were detected in the septum, the central region of the thalamus, and in voxels right below the ventral tegmental area (VTA). Gastric distention led to brain activation in the insular cortex, orbitofrontal cortex (OFC), cingulate cortex, caudate putamen (CPu), lateral hypothalamus (LH), septum, thalamus, sensorimotor cortex, VTA, caudal cortical areas, e.g. the retrosplenial cortex (RSC), and the brain stem nucleus of the solitary tract (NTS) (Figure 1c, right panel; Table 1). Some voxels in and around the pontine nucleus (caudal to the VTA) showed a negative BOLD response upon gastric distention.

Comparison of the responses to the two treatments with a second level GLM-based analysis showed that the insular cortex, cingulate cortex, CPu, LH, thalamus, some parts of the sensorimotor cortex, VTA, RSC, and some NTS voxels were more significantly activated in response to gastric distention than to sucrose tasting (Supplementary Figure 2). There were no brain areas exhibiting a significantly stronger response to sucrose tasting as compared to gastric distention.

Figure 2 displays the normalized BOLD signal time-course in ROIs in which we detected significant activation or deactivation in response to sucrose tasting or gastric distention. In response to gastric distention, BOLD signal intensity in the left thalamus increased upon inflation of the balloon and (partially) recovered upon deflation. Comparable response patterns to gastric distention were detected in the insula and NTS. On the contrary, in response to sucrose tasting, we detected a decrease in signal intensity in the thalamus, followed by recovery after water flushing. In the septum we found a similar but stronger negative correlation of the BOLD response to sucrose tasting, which was more prominent during water flushing (which was done in the time frame between the downward phases of the two regressors in Figure 2). Although we did not find a significant correlation to the regressor in the GLM-based analysis in the insula in response to sucrose tasting (Figure 1c), we did detect a considerable gradual BOLD signal elevation in this ROI; signal intensity started to increase with the first sucrose tasting challenge, further increased upon the second and third sucrose tasting challenge, and remained elevated during the rest of the scan period. Although the signal in the VTA was more affected by noise than the other ROIs, and the response to the

Table 1. Brain regions exhibiting significant positive or negative BOLD responses during sucrose tasting or gastric distention

Treatment	Activated regions	Z-score	Activated part of ROI (%)	Deactivated regions	Z-score	Deactivated part of ROI (%)
Sucrose tasting	Insula left	2.5	17	Septum left	-2.4	30
	Insula right	2.6	30	Septum right	-2.3	17
	OFC left	2.5	38	Thalamus left	-2.1	4
	OFC right	2.6	30	Thalamus right	-2.2	4
	NAcc left *	2.8	6	Voxels caudal to the VTA		
	NAcc right *	3.1	6			
	VP left *	2.1	9			
	VP right *	-	0			
Gastric distention	Insula left	3.8	86	Voxels in/around pontine nucleus		
	Insula right	4.2	81			
	OFC left	4.2	85			
	OFC right	4.2	85			
	Cingulate cortex left	3.9	74			
	Cingulate cortex right	4.0	88			
	CPu left	3.4	83			
	CPu right	3.2	64			
	LH left	3.4	46			
	LH right	3.3	50			
	Septum left	2.7	50			
	Septum right	2.9	55			
	Thalamus left	4.1	84			
	Thalamus right	4.1	75			
	Sensorimotor cortex left	3.9	78			
	Sensorimotor cortex right	3.7	59			
	VTA left	3.7	60			
	VTA right	2.7	43			
	NTS left	4.0	78			
	NTS right	4.2	69			
	Caudal cortical areas, like the RSC					

Z-scores are calculated as mean FDR-corrected Z-score across significantly (de)activated voxels within regions of interest. A Z-score of (-)1.96 corresponds to a p-value of 0.05. *Activation was detected at the border of the NAcc and VP; when these areas are considered as one ROI the left NAcc-and-VP had a mean Z-score of 2.6 and 7% of the total voxels in this region was significantly activated; the right NAcc-and-VP had a mean Z-score of 3.1 in 4% of the voxels. CPu, caudate putamen; LH, lateral hypothalamus; NAcc, nucleus accumbens; NTS, nucleus of the solitary tract; OFC, orbitofrontal cortex; RSC, retrosplenial cortex; VP, ventral pallidum; VTA, ventral tegmental area.

first sucrose tasting challenge was, if anything, negative, we detected an increase in mean signal intensity in response to the second, third, and fourth sucrose tasting challenge in the VTA. However, the GLM-based analysis in voxels right below the VTA revealed a negative response (Figure 1c). We found no significant VTA response to gastric distention (Supplementary Figure 3). Signal intensity time courses for all left and right ROIs are shown in Supplementary Figure 3.

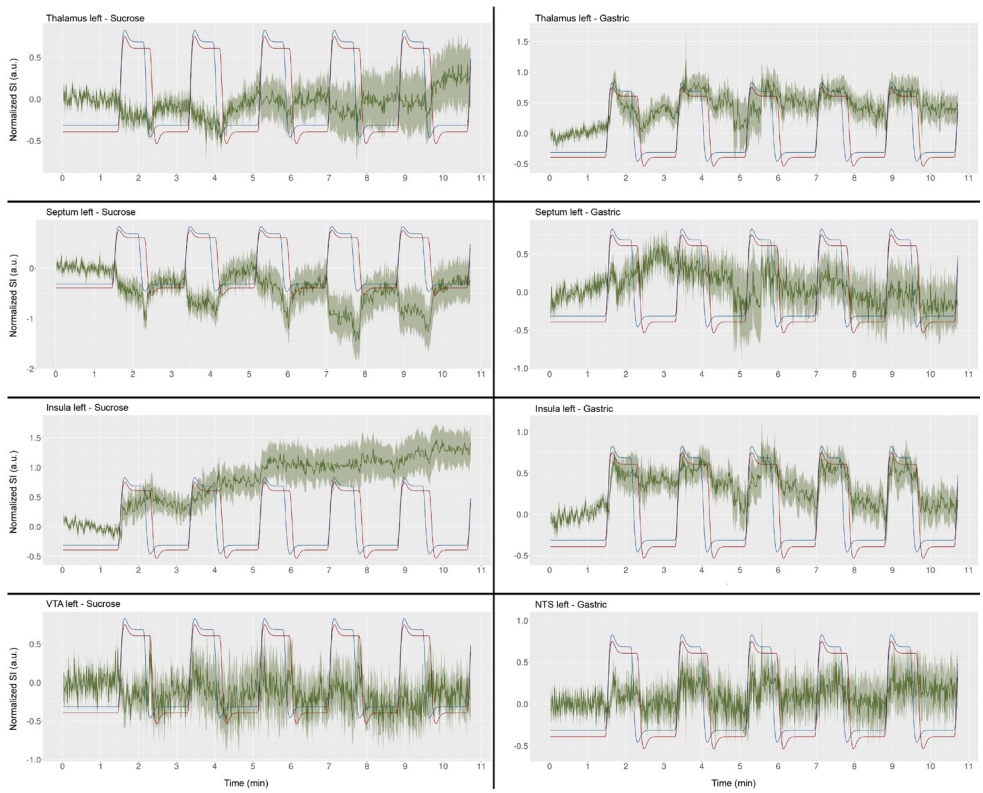

Figure 2. Mean BOLD responses to sucrose tasting (left) and gastric distention (right). Normalized BOLD signal time-courses are shown for different ROIs, displayed over the entire scan period. The blue line represents the HRF for the sucrose tasting paradigm; the red line represents the HRF for the gastric distention paradigm. Difference in the downward phases of both regressors is time needed to flush the mouth with water after a sucrose tasting. a.u., arbitrary units; NTS, nucleus of the solitary tract; SI, signal intensity; VTA, ventral tegmental area.

DISCUSSION

In this study we developed and applied a new method that enables functional neuroimaging during oral and gastric sensory stimulation in rats in a single experimental setting. Functional MRI during manipulation of the gastric

environment in rats has already been proven feasible[36,40], but to the best of our knowledge this had not yet been accomplished together with a taste stimulation paradigm in a single experimental setting in rats. Direct comparison of the brain activation patterns in response to sucrose tasting and gastric distention enabled us to distinguish specific contributions of both factors to satiation-related neural signaling. Our findings are in agreement with results from human studies and provide novel insights in the involvement of brain regions in processing oro-sensory and gastric information. Importantly, we demonstrate activation of several brain regions upon oro-sensory and gastric stimulation in anaesthetized rats which underscores that these areas are activated in the absence of consciousness.

In accordance with literature, we detected activation in the anterior part of the insular cortex upon sucrose tasting[14–17,41–44]. In a human fMRI study with healthy volunteers[15], significant activation upon sucrose tasting was detected in the anterior insular (putative primary taste) cortex. Other studies[14,16,41,45] also detected activation in the middle and anterior parts of the insula upon sweet taste. In our rat study, we found that the insula became activated in response to the first sucrose stimulation, and subsequent mouth rinses with sucrose had an additive effect on insula activation, as seen from the regional rise in BOLD signal intensity. It is unlikely that this was induced by residual sucrose that was not washed out with the 10-second rinses of water, since other brain areas did not show this effect and responded according to the block-designed treatment paradigm. We speculate that the rising response in the anterior insula, which contains the primary taste cortex, reflects lasting neuronal activation that builds up with re-exposure to sucrose. Perhaps, this neural correlate contributes to an increase in satiation by longer oral exposure to food or taste[46–49].

Since sucrose tasting is rewarding for rats, we also expected a response in the VTA, which is an essential part of the reward system. Although the activation maps revealed a negative correlation between stimulus presentation and BOLD signal intensity in some voxels caudal to the VTA, the mean signal time course in the whole VTA demonstrated activation responses to individual tasting challenges. The difference in findings between the whole-brain voxel-based GLM analysis and the ROI analysis may be explained by the difference in spatial dimensions of the two analyses: whereas the ROI analyses encompassed the mean response for the entire VTA region, the voxel-based GLM analysis allowed for detection of sub regional (de)activation at the single voxel level.

The detected activation in some voxels at the border of the NAcc and VP in response to sucrose tasting is in line with an activated VTA. The VTA projects directly to the NAcc, as part of the mesolimbic projection. We speculate that upon

sucrose tasting-induced activation of the mesolimbic projection, dopamine is released in the NAcc, which binds to inhibitory D2 receptors on local GABAergic neurons that project to the VP. Consequent disinhibition would lead to activation of the VP[50–52].

We also observed deactivation of the septum upon sucrose tasting, which aligns with findings from Sweeney and Yang[53], who showed that chemogenetic or optogenetic inhibition of the septum increased food intake. Thus, perhaps food intake and consequent tasting deactivate the septum and its inhibitory action in a feedback loop.

We detected significant activation in the NTS, which is known to be involved in the processing of visceral signals, in response to gastric distention. This effect was stronger as compared to sucrose tasting-induced activation of the NTS.

Min and colleagues previously reported that gastric distention increases BOLD signal in regions such as the NTS and hypothalamus[36]. Furthermore, they detected activation in the hippocampus, amygdala, thalamus, cerebellum, and the cingulate, insular and motor and sensory cortices. We detected a comparable activation pattern, with additional activation in the OFC, cingulate cortex, dorsal and ventral striatal regions, VTA, and caudal cortical areas. Also in human studies, similar areas were found to be activated in response to gastric distention: Wang et al. detected activation in the sensorimotor cortices, right insula, left posterior amygdala, left posterior insula and left precuneus in response to gastric balloon inflation[21]. Spetter et al. found that gastric distention with a liquid increased brain activity in reward- and eating behavior-related areas such as the midbrain, hypothalamus, amygdala, and hippocampus[3]. Other studies reported activation in the dorsal brain stem, the left inferior frontal gyrus, the bilateral insula, and the right subgenual anterior cingulate cortex in response to gastric distention[11]; activation in the right insula in response to balloon-induced distention[54], and activation in the opercular part of the inferior frontal gyrus upon manipulation of gastric content volume[55] or upon gastric stimulation with a liquid meal after 36 h fasting[29].

In addition to activation in orbitofrontal regions and insular regions analogous with findings in humans, our study in rats exhibited gastic distention-induced responses in mesolimbic areas like the VTA, NAcc, and CPu. These areas are known to be involved in motivation- and reward-related behaviors[50,52] and may therefore be associated with the rewarding effects of a full stomach.

Due to the use of anesthesia, gastric distention should be a neutral stimulus to the animals. It can be discussed that inflation of a gastric balloon with

5 mL is aversive to awake rats, however, since they are under anesthesia there a no consious processes of possible aversion. Moreover, balloon inflation of 5 mL is within the phsyiological range, since the volume was based on a post-mortem assesment of gastric volume in a pilot animal and on a study in which gastric balloon inflation was performed previously[36]. In this reference study gastric balloons were inflated with 8 mL of saline, however, a slower increase in volume (2 ml/min during 4 minutes) was used, and animals were heavier.

In contrast to human fMRI studies[24–28,30], but in line with early macaque studies[31,32], we did not detect differences in the response to tasting (or gastric distention) between *ad libitum*-fed and food-deprived animals. Our measurements may have lacked sensitivity to detect possible subtle differences. Moreover, in our study rats were mildly anesthetized, which would obscure potentially augmenting effects of awareness of physiological state.

The need for anesthesia may appear as a limitation, however, the alternative of scanning awake rats with a paradigm as used in the current study comes with many more limitations, such as confounding effects of consciousness on the responses to either stimuli, stress induced by the scanning procedure itself as well as by the stimuli, and motion artefacts. Still, it is possible that isoflurane anesthesia affects the responses to tasting and gastric distention in a different way; full taste sensation could require more conscious awareness than gastric distention does, and thereby the use of anesthesia could have affected the results for the two stimuli in a different way. To our knowledge there are currently no studies investigating the possible different influences of anesthesia on taste and gastric distention responses.

Due to the unfortunate drop out of three animals, our sample size was relatively low. The power of this study could be increased by repeating the experiment with a larger sample size. However, even with this relatively low number of animals per group, the power was still high enough to detect the effects of taste and gastric distention, which were found to be comparable to human data.

Another limitation of this study is that we only assessed brain responses to gastric distention using a gastric balloon. Studies have shown that gastric distention is different from gut nutrient sensing, and as a consequence brain patterns in response to gastric balloon distention are different from those in response to actual feeding, thus nutrients entering the stomach. A difficulty with the latter is that a block design paradigm is impossible when food is entering the stomach, which has to be emptied first. Using a balloon, we were able to scan

animals using the same block design for gastric distention as well as for sucrose tasting. In a follow-up study it should be investigated how brain responses differ between these different paradigms.

To summarize, we developed and applied a translational functional MRI approach that is useful to study feeding-related neural signals in rats under standardized and controlled settings. The detected patterns of brain activation in response to oro-sensory stimulation and gastric distention align well with findings from human neuroimaging studies (e.g.[3,20]), and uncovered additional brain regions involved in processing taste and gastric distention signals. Future studies may use the described neuroimaging approach to assess the effects of manipulation of specific satiation pathways, for example by chemo- or optogenetics, by simultaneous oro-sensory and gastric stimulation, or by manipulating feeding and hunger status, to further unravel the role of these pathways and elucidate mechanisms underlying regulation of satiation. Ultimately, this may aid in the identification of therapeutic targets and establishment of intervention strategies to reduce overconsumption and prevent obesity.

REFERENCES

1. Smeets, P. A. M., Charbonnier, L., van Meer, F., van der Laan, L. N. & Spetter, M. S. Food-induced brain responses and eating behaviour. Proc. Nutr. Soc. 71, 511–520 (2012).
2. Blundell, J. E. & Halford, J. C. Regulation of nutrient supply: the brain and appetite control. Proc. Nutr. Soc. 53, 407–418 (1994).
3. Spetter, M. S., de Graaf, C., Mars, M., Viergever, M. A. & Smeets, P. A. M. The sum of its parts-effects of gastric distention, nutrient content and sensory stimulation on brain activation. PLoS One 9, e90872 (2014).
4. Wijlens, A. G. M. et al. Effects of oral and gastric stimulation on appetite and energy intake. Obesity (Silver Spring). 20, 2226–32 (2012).
5. Beckstead, R. M., Morse, J. R. & Norgren, R. The nucleus of the solitary tract in the monkey: projections to the thalamus and brain stem nuclei. J. Comp. Neurol. 190, 259–282 (1980).
6. Beckstead, R. M. & Norgren, R. An autoradiographic examination of the central distribution of the trigeminal, facial, glossopharyngeal, and vagal nerves in the monkey. J. Comp. Neurol. 184, 455–472 (1979).
7. Flynn, F. G. Anatomy of the insula functional and clinical correlates. Aphasiology 13, 55–78 (1999).

8. Fussey, I. F., Kidd, C. & Whitwam, J. G. Activity evoked in the brain stem by stimulation of C fibres in the cervical vagus nerve of the dog. Brain Res 49, 436–440 (1973).
9. Hurleygius, K. M. & Neafsey, E. J. The Medial Frontal-Cortex and Gastric-Motility - Microstimulation Results and Their Possible Significance for the Overall Pattern of Organization of Rat Frontal and Parietal Cortex. Brain Res. 365, 241–248 (1986).
10. Ongür, D. & Price, J. L. The organization of networks within the orbital and medial prefrontal cortex of rats, monkeys and humans. Cereb. cortex 10, 206–219 (2000).
11. Stephan, E. et al. Functional Neuroimaging of Gastric Distention. J. Gastrointest. Surg. 7, 740–749 (2003).
12. Terreberry, R. R. & Neafsey, E. J. Rat medial frontal cortex: a visceral motor region with a direct projection to the solitary nucleus. Brain Res. 278, 245–249 (1983).
13. Vogt, B. A., Finch, D. M. & Olson, C. R. Functional heterogeneity in cingulate cortex: The anterior executive and posterior evaluative regions. Cereb. Cortex 2, 435–443 (1992).
14. Gagnon, L., Kupers, R. & Ptito, M. Neural correlates of taste perception in congenital blindness. Neuropsychologia 70, 227–234 (2015).
15. de Araujo, I. E. & Rolls, E. T. Representation in the Human Brain of Food Texture and Oral Fat. J. Neurosci. 24, 3086–3093 (2004).
16. Small, D. M. et al. Dissociation of neural representation of intensity and affective valuation in human gustation. Neuron 39, 701–711 (2003).
17. Small, D. M. Taste representation in the human insula. Brain Struct. Funct. 214, 551–561 (2010).
18. Chambers, A. P., Sandoval, D. A. & Seeley, R. J. Integration of satiety signals by the central nervous system. Curr. Biol. 23, R379–R388 (2013).
19. Grill, H. J. Leptin and the systems neuroscience of meal size control. Front. Neuroendocrinol. 31, 61–78 (2010).
20. Small, D. M., Zatorre, R. J., Dagher, A., Evans, A. C. & Jones-Gotman, M. Changes in brain activity related to eating chocolate: from pleasure to aversion. Brain 124, 1720–33 (2001).
21. Wang, G. J. et al. Gastric distention activates satiety circuitry in the human brain. Neuroimage 39, 1824–1831 (2008).
22. Geeraerts, B. et al. Different regional brain activity during physiological gastric distension compared to balloon distension: A H215O-PET study. Neurogastroenterol. Motil. 23, 533–544 (2011).

23. Van Oudenhove, L. et al. Cortical deactivations during gastric fundus distension in health: Visceral pain-specific response or attenuation of 'default mode' brain function? A H215O-PET study. Neurogastroenterol. Motil. 21, 259–271 (2009).
24. Haase, L., Cerf-Ducastel, B. & Murphy, C. Cortical activation in response to pure taste stimuli during the physiological states of hunger and satiety. Neuroimage 44, 1008–1021 (2009).
25. van Rijn, I., de Graaf, C. & Smeets, P. A. M. Tasting calories differentially affects brain activation during hunger and satiety. Behav. Brain Res. 279, 139–147 (2015).
26. Smeets, P. A. M. et al. Effect of satiety on brain activation during chocolate tasting in men and women. Am. J. Clin. Nutr. 83, 1297–1305 (2006).
27. Haase, L., Green, E. & Murphy, C. Males and females show differential brain activation to taste when hungry and sated in gustatory and reward areas. Appetite 57, 421–434 (2011).
28. Thomas, J. M. et al. Satiation attenuates BOLD activity in brain regions involved in reward and increases activity in dorsolateral prefrontal cortex : an fMRI study in healthy volunteers. 697–704 (2015). doi:10.3945/ajcn.114.097543.The
29. Del Parigi, A. et al. Tasting a liquid meal after a prolonged fast is associated with preferential activation of the left hemisphere. Neuroreport 13, 1141–1145 (2002).
30. Ely, A. V. et al. Response in taste circuitry is not modulated by hunger and satiety in women remitted from bulimia nervosa. J. Abnorm. Psychol. 126, 519–530 (2017).
31. Yaxley, S., Rolls, E. T., Sienkiewicz, Z. J. & Scott, T. R. Satiety does not affect gustatory-evoked activity in the nucleus tractus solitarius or opercular cortex of the alert cynomolgus monkey. Chem. Senses 10, 442 (1985).
32. Rolls, E. T., Scott, T. R., Sienkiewicz, Z. J. & Yaxley, S. The responsiveness of neurones in the frontal opercular gustatory cortex of the macaque monkey is independent of hunger. J. Physiol. 397, 1–12 (1988).
33. La Fleur, S. E., Luijendijk, M. C. M., Van Rozen, A. J., Kalsbeek, A. & Adan, R. A. H. A free-choice high-fat high-sugar diet induces glucose intolerance and insulin unresponsiveness to a glucose load not explained by obesity. Int. J. Obes. 35, 595–604 (2011).
34. La Fleur, S. E., Van Rozen, A. J., Luijendijk, M. C. M., Groeneweg, F. & Adan, R. A. H. A free-choice high-fat high-sugar diet induces changes in arcuate neuropeptide expression that support hyperphagia. Int. J. Obes. 34, 537–546 (2010).

35. La Fleur, S. E. et al. A reciprocal interaction between food-motivated behavior and diet-induced obesity. Int. J. Obes. 31, 1286–1294 (2007).
36. Min, D. K., Tuor, U. I. & Chelikani, P. K. Gastric distention induced functional magnetic resonance signal changes in the rodent brain. Neuroscience 179, 151–158 (2011).
37. Paxinos, G. & Watson, C. The rat brain in stereotaxic coordinates. (Academic Press, 2007).
38. Mandeville, J. B., Liu, C. H., Vanduffel, W., Marota, J. J. A. & Jenkins, B. G. Data collection and analysis strategies for phMRI. Neuropharmacology 84, 65–78 (2014).
39. WaxholmSpace. http://software.incf.org/software/waxholm-space. (2014).
40. Min, D. K., Tuor, U. I., Koopmans, H. S. & Chelikani, P. K. Changes in differential functional magnetic resonance signals in the rodent brain elicited by mixed-nutrient or protein-enriched meals. Gastroenterology 141, 1832–1841 (2011).
41. Turner, C. E., Byblow, W. D., Stinear, C. M. & Gant, N. Carbohydrate in the mouth enhances activation of brain circuitry involved in motor performance and sensory perception. Appetite 80, 212–219 (2014).
42. Frank, S., Kullmann, S. & Veit, R. Food related processes in the insular cortex. Front. Hum. Neurosci. 7, 1–6 (2013).
43. Rolls, E. T. Brain mechanisms underlying flavour and appetite. Philos. Trans. R. Soc. B Biol. Sci. 361, 1123–1136 (2006).
44. Small, D. M. & Prescott, J. Odor/taste integration and the perception of flavor. Exp. Brain Res. 166, 345–357 (2005).
45. Spetter, M. S., Smeets, P. A. M., de Graaf, C. & Viergever, M. A. Representation of sweet and salty taste intensity in the brain. Chem. Senses 35, 831–840 (2010).
46. Lasschuijt, M. P. et al. Comparison of oro-sensory exposure duration and intensity manipulations on satiation. Physiol. Behav. 176, 76–83 (2017).
47. Zijlstra, N., Mars, M., De Wijk, R. A., Westerterp-Plantenga, M. S. & De Graaf, C. The effect of viscosity on ad libitum food intake. Int. J. Obes. 32, 676–683 (2008).
48. Zijlstra, N. et al. Effect of viscosity on appetite and gastro-intestinal hormones. Physiol. Behav. 97, 68–75 (2009).
49. Bolhuis, D. P. et al. Slow food: Sustained impact of harder foods on the reduction in energy intake over the course of the day. PLoS One 9, 1–7 (2014).

50. Humphries, M. D. & Prescott, T. J. The ventral basal ganglia, a selection mechanism at the crossroads of space, strategy, and reward. Prog. Neurobiol. 90, 385–417 (2010).
51. Kenny, P. J., Voren, G. & Johnson, P. M. Dopamine D2 receptors and striatopallidal transmission in addiction and obesity. Curr. Opin. Neurobiol. 23, 1–4 (2013).
52. Russo, S. J. & Nestler, E. J. The brain reward circuitry in mood disorders. Nat. Rev. Neurosci. 14, 609–625 (2013).
53. Sweeney, P. & Yang, Y. An Inhibitory Septum to Lateral Hypothalamus Circuit That Suppresses Feeding. J. Neurosci. 36, 11185–11195 (2016).
54. Ly, H. G. et al. Differential brain responses to gradual intragastric nutrient infusion and gastric balloon distension: A role for gut peptides? Neuroimage 144, 101–112 (2017).
55. Camps, G., Veit, R., Mars, M., de Graaf, C. & Smeets, P. A. Just add water: Effects of added gastric distention by water on gastric emptying and satiety related brain activity. Appetite 127, 195–202 (2018).

ACKNOWLEDGEMENTS

This work was supported by the European Union Seventh Framework Program (FP/2007-2013) [grant number 607310 (Nudge-it)]. The funding source had no involvement in the collection, analysis, or interpretation of the data, nor in the writing or submission of this article. We especially thank Gerard van Vliet for technical assistance and hardware development, Wim Otte for assistance and advice on data analyses, Michel Sinke for assistance on R scripting, Milou Straathof, Jeroen Verharen, Julia Boonzaier, and Geralda van Tilborg for fruitful discussions on the experimental procedure and set-up, troubleshooting, and analyses of the data.

AUTHOR CONTRIBUTIONS

T.J.M.R., R.M.D., and R.A.H.A. designed the experiments. T.J.M.R., M.C.M.L, and A.v.d.T. performed the experiments. T.J.M.R. analyzed the data. G.C., P.A.M.S., R.M.D., and R.A.H.A. inputted on data interpretation and the manuscript. T.J.M.R., R.M.D., and R.A.H.A. wrote the manuscript. All authors reviewed the paper.

COMPETING INTERESTS

The authors declare no competing interests.

SUPPEMENTARY FIGURES

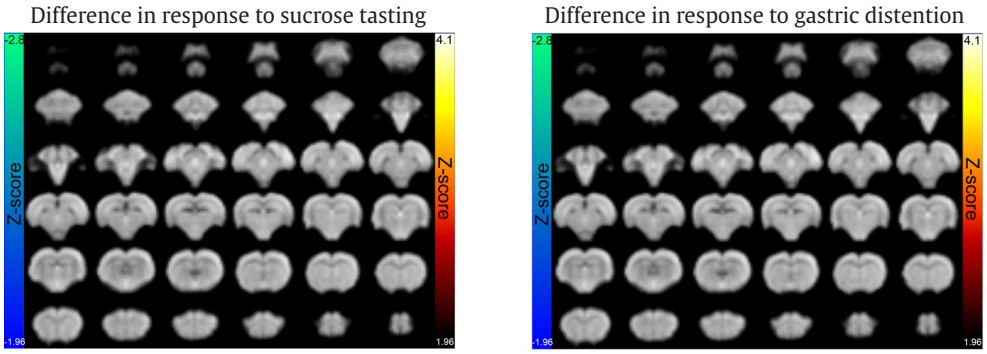

Supplementary Figure 1. Difference in response to sucrose tasting (left) and gastric distention (right) between ad libitum-fed and food-restricted animals. After FDR correction for multiple testing no significant differences in response to either sucrose tasting or gastric distention were detected. Z-scores represent FDR-corrected values.

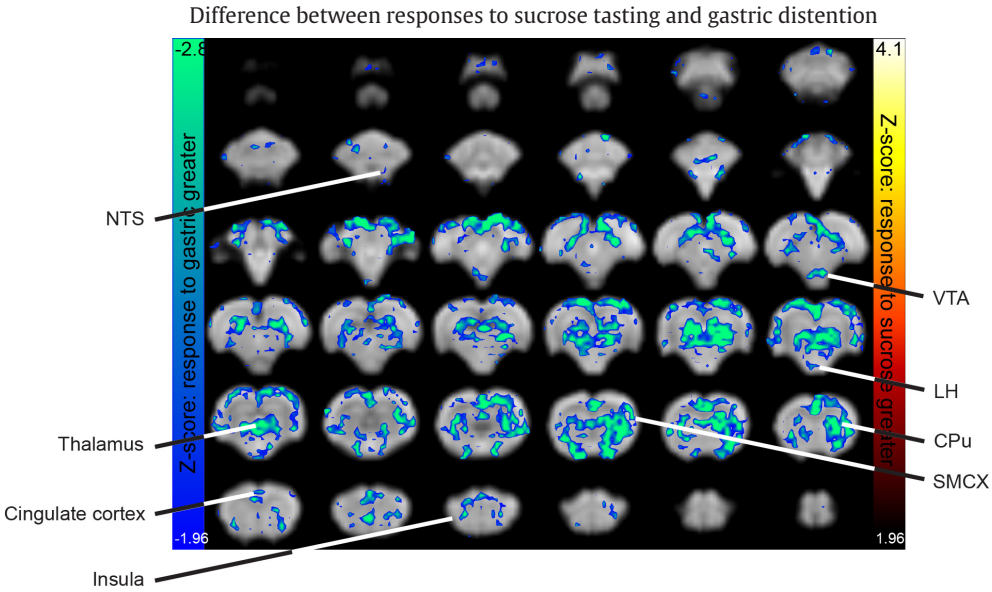

Supplementary Figure 2. Comparison between the response to sucrose tasting and the response to gastric distention. Regions that were more significantly activated in the response to sucrose tasting as compared to gastric distention are shown in hot colors; regions that were more significantly activated in response to gastric distention as compared to sucrose tasting are shown in cold colors. Z-scores represent FDR-corrected values. CPu, caudate putamen; LH, lateral hypothalamus; NTS, nucleus of the solitary tract; SMCX, sensorimotor cortex; VTA, ventral tegmental area.

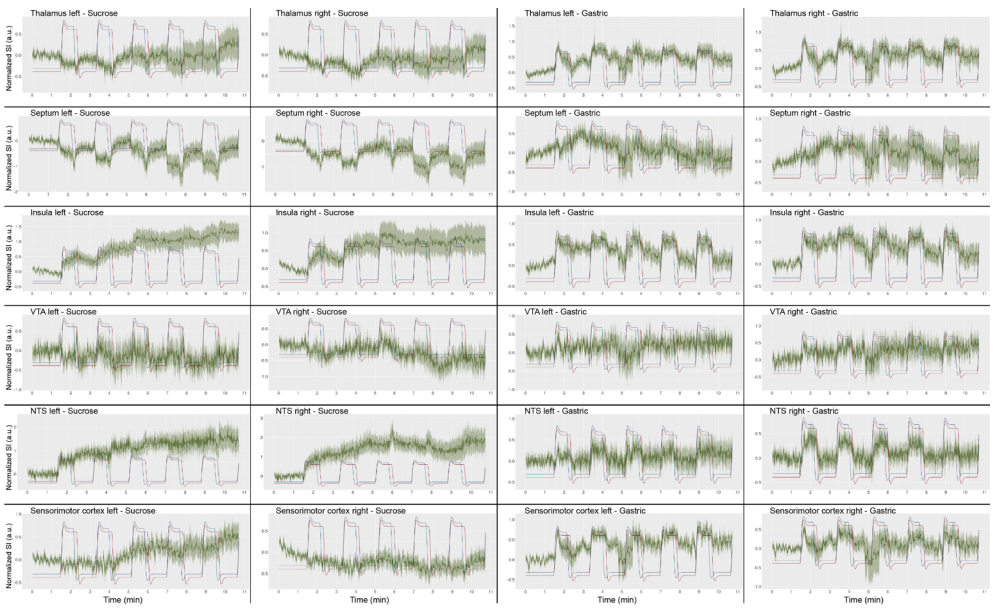

Supplementary Figure 3. Mean BOLD responses to sucrose tasting (two left columns) and gastric distention (two right columns). Normalized BOLD signal time-courses are shown for left and right ROIs. Left ROIs are displayed in the first and third column; right ROIs in the second and fourth column. All signal time-courses are displayed over the entire scan period. The blue line represents the HRF for the sucrose tasting paradigm; the red line represents the HRF for the gastric distention paradigm. Difference in the downward phases of both regressors is time needed to flush the mouth of the rats with water after a sucrose tasting. a.u., arbitrary units; NTS, nucleus of the solitary tract; SI, signal intensity; VTA, ventral tegmental area.

Chapter 2

Diet as connecting factor: functional brain connectivity in relation to food intake and sucrose tasting, assessed with resting-state functional MRI in rats

Theresia J.M. Roelofs[a,b], Milou Straathof[b], Annette van der Toorn[b], Willem M. Otte[b,c], Roger A.H. Adan[a], Rick M. Dijkhuizen[b]

[a]Department of Translational Neuroscience, UMC Utrecht Brain Center, University Medical Center Utrecht and Utrecht University, Universiteitsweg 100, 3584 CG Utrecht, the Netherlands
[b]Biomedical MR Imaging and Spectroscopy Group, Center for Image Sciences, University Medical Center Utrecht and Utrecht University, Bolognalaan 50, 3584 CJ Utrecht, the Netherlands
[c]Department of Child Neurology, UMC Utrecht Brain Center, University Medical Center Utrecht and Utrecht University, Universiteitsweg 100, 3584 CG Utrecht, the Netherlands

Under review at Journal of Neuroscience Research

Eating disorders and obesity form a major health problem in Western Society. To be able to provide adequate treatment and prevention, it is necessary to understand the neural mechanisms underlying the development of eating disorders and obesity. Specific brain networks have been shown to be involved in feeding behavior. We therefore hypothesized that functional connectivity in neural networks involved in feeding behavior is dependent on the status of homeostatic energy balance, thus on being hungry or satiated. To test our hypothesis, we measured functional connectivity and amplitudes of neural signals within neural networks in relation to food intake and sucrose tasting in rats. Therefore, sixteen male Wistar rats, of which eight were food-restricted and eight were satiated, underwent resting-state functional magnetic resonance imaging (rs-fMRI) at 9.4 T. Subsequently, half of these animals underwent a sucrose tasting procedure followed by a second rs-fMRI scan. Functional connectivity and amplitude of low-frequency signal fluctuations were statistically analyzed in a linear mixed model.

Although we did not detect a significant effect of food intake on functional connectivity before sucrose tasting, there was a trend towards interaction between group (satiated vs. hungry) and treatment (sucrose tasting). Functional connectivity between feeding-related regions tended to decrease stronger upon sucrose tasting in satiated rats as compared to food-restricted rats. Furthermore, rs-fMRI signal amplitudes decreased stronger upon sucrose tasting in food-restricted rats, as compared to satiated rats. These findings indicate that food intake and sucrose tasting can affect functional network organization, which may explain specific patterns in feeding behavior.

SIGNIFICANCE STATEMENT

Our study demonstrates the potential of translational functional neuroimaging studies in rodents to elucidate how hunger, satiation and sweet taste affect functional connectivity between different brain regions. Our results show that these factors may affect functional networks in the brain, which may explain specific feeding behaviors.

KEYWORDS

Magnetic Resonance Imaging, rat brain, feeding behavior, neuroimaging

INTRODUCTION

Disturbed regulation of feeding behavior and energy balance can lead to eating disorders and obesity. Obesity is a growing global health problem; most of

the world's population lives in countries where more people die from overweight than from underweight[1]. Even though obesity is preventable, its prevalence rises, which comes along with increasing risks of developing cardiovascular diseases, diabetes, musculoskeletal disorders and different types of cancer[1].

To combat obesity with adequate treatment and by prevention, it is necessary to get more insight into the exact neural processes and mechanisms of action underlying the development of overweight and obesity. Those neural processes involve multiple brain areas, associated with different aspects of the regulation of body weight, of which the role may vary between different states of homeostatic energy balance. These brain areas are functionally connected in neural networks, of which the organization may also differ depending on the status of homeostatic energy balance, thus on being hungry or satiated. An altered functional organization of these neural networks may result in different responses to food and food-related cues, and could explain different feeding behaviors.

The organization of neural networks in relation to status of homeostatic energy balance has recently been investigated in several human neuroimaging studies. Wright and colleagues reported that fasting and satiation led to changes in functional connectivity of the insula and the hypothalamus as measured with resting-state functional MRI (rs-fMRI)[2]. The authors speculated that these regions form a network that regulates energy balance through cognitive control over eating. In another rs-fMRI study, higher functional connectivity of the right supramarginal gyrus (as seed region) to the right midbrain, the bilateral midcingulate area and the left hippocampus was measured when participants were in a hungry state as compared to a satiated state[3]. According to the authors, the observed pattern of connectivity of the right supramarginal gyrus with the mesolimbic system in the hungry state, could be related to the feeling of hunger, which is a very salient need that requires fulfilling and consequent recruitment of the mesolimbic system to drive motivational behavior. In line with these findings, Avery et al. reported a significant relationship between hunger status and functional connectivity of the left orbitofrontal cortex (OFC) to limbic regions[4]. They found that functional connectivity between the left OFC and mid insula decreased when hunger deceased after a meal. However, this relationship was absent in obese participants.

Other studies failed to show differences in functional connectivity between hungry and satiated healthy participants. Simon et al.[5] and Al-Zubaidi et al.[6] found no significant changes in functional connectivity as a result of hunger, although in the latter study the amplitudes of rs-fMRI signals were increased in the posterior cingulate cortex and the anterior precuneus. A study that investigated

the effect of weight loss on resting-state functional connectivity in obese subjects also failed to detect a main effect of satiety on functional connectivity[7].

The discrepancies in human rs-fMRI studies on the relationship between status of homeostatic energy balance and neural network organization may be at least partly explained by a high level of methodological variation. To the best of our knowledge, there have been no studies that investigated organization of neural networks in the resting brain in relation to food intake or tasting in animal models. Min and colleagues have successfully applied fMRI to map brain regions that respond to intragastric infusion of nutrients[8] or to gastric distention with an intragastric balloon[9]. However, resting state functional connectivity in large-scale neural networks was not assessed in these studies. Therefore we set out to use an animal model to measure functional network status in hungry and satiated subjects in a tightly controlled and highly standardized experimental setup. Furthermore, this setup would also allow assessment of the influence of sucrose tasting without interference of the cognitive component associated with differences in the level of satiation. To that aim, we performed rs-fMRI in anesthetized food-restricted or satiated rats, before and after sucrose tasting. We hypothesized that functional connectivity between areas involved in feeding behavior and areas involved in reward and motivation would be higher when animals are hungry, and that this functional connectivity would decline in response to sucrose tasting.

MATERIALS AND METHODS

Animals

Experiments were approved by the Animal Ethics Committee of the University Medical Center Utrecht, the Netherlands, and were conducted in agreement with Dutch laws ('Wet op de Dierproeven', 1996) and European regulations (Guideline 86/609/EEC).

We used 16 adult male Wistar rats (Crl:WU, Charles River, Sulzfeld, Germany) with a mean (± standard deviation) body weight of 240 (±6) gram upon arrival. Rats were housed individually under controlled temperature and humidity conditions, and under a 12h light/dark cycle (lights on at 7:00 a.m.). Animals had *ad libitum* access to water, and a perspex tube was provided as cage enrichment. Rats were randomly assigned to two equally sized groups. One group of rats (n=8) had *ad libitum* access to chow, the other group (n=8) was food-restricted (Figure 1a). Food restriction started one week prior to scanning and involved a diet of 10 grams of chow per day till the animal reached 90% of its initial bodyweight. When this point was reached before the actual day of scanning, animals received the amount of chow needed to maintain this bodyweight (which differed per rat,

but was always between 10-20 grams of chow). The experimenter could not be blinded to group assignment, since animal caretaking and MRI scanning were done by the same person. Rats' mean (± standard deviation) body weight at time of scanning was 324 (±40) gram.

In vivo MRI acquisition

We conducted *in vivo* MRI measurements using a 9.4 T horizontal bore MR system equipped with a 100 mT/m gradient coil (Agilent). We used a home-built 90 mm diameter Helmholtz volume coil for signal excitation, and an inductively coupled 25 mm diameter surface coil for signal reception. Anesthesia was induced with 3-5% isoflurane in O_2/air (1:4), and animals were endotracheally intubated for mechanical ventilation. For fMRI-based detection of activation in response to sucrose tasting, two Protex polyethylene tubes were placed above the tongue. The polyethylene tubes enabled sucrose delivery and water rinsing while the animal was inside the MR scanner.

After animals were positioned inside the scanner, anesthesia was reduced to 1.5% isoflurane in O_2/air (1:4). We maintained anesthesia at 1.5% during the entire MRI protocol. End-tidal CO_2 was monitored with a capnograph (Microcap, Oridion Medical 1987 Ltd., Jerusalem, Israel). Body temperature was maintained at 37.0 ± 1.0°C.

We first acquired anatomical images using a balanced steady-state free precession (bSSFP) sequence, with 4 phase cycling angles (0°, 90°, 180°, 270°), repetition time (TR)/echo time (TE)=5/2.5 ms, flip angle=20°, field-of-view (FOV)=40x32x24 mm, and matrix size=160x128x96 voxels (scan time: 10 min). The resulting spatial resolution of these anatomical images was 250 µm in all directions.

Next, we conducted rs-fMRI, for which we used a 3D gradient echo echo planar imaging (EPI) sequence. The read-out and first phase-encode dimensions were covered in a single-shot EPI, while linear phase encoding was used for the second phase-encode dimension. We acquired 800 images with an acquisition time of 862.4 ms per volume (total scan time: 11 minutes and 30 seconds), and TR/TE=30.8/16 ms, flip angle=13°, FOV=36x36x16.8 mm, matrix size=60x60x28, and thus an isotropic spatial resolution of 600 µm.

After the rs-fMRI scan, half of the animals (n=4 in both the food-restricted and *ad libitum*-fed groups) underwent fMRI during sucrose tasting, which consisted of five repetitions of sucrose application on the tongue. After sucrose tasting a second rs-fMRI scan was performed (Figure 1a).

MRI data processing and analysis

Anatomical MRI data

Non-uniformity correction was performed on anatomical images using *n3*, and brain masks were obtained by applying the *Brain Extraction Tool* to the anatomical images, both as provided by *FSL* (FMRIB's Software Library, www.fmrib.ox.ac.uk/fsl, version 5.0.9). The individual anatomical images were masked and registered to an anatomical MRI template that was matched to a 3D model of a rat brain atlas[10], using the affine intermodal image registration tool *FLIRT* (FMRIBs Linear Image Registration Tool, v6.0). Co-registered anatomical images were averaged to acquire an anatomical template in atlas space. The original individual anatomical images were registered to this anatomical template using *FLIRT* followed by *FNIRT* (FMRIBs Nonlinear Image Registration Tool). Inverse coefficients were calculated to register regions of interest (ROIs) from atlas space to individual anatomical space. ROIs extracted from the rat brain atlas[10] consisted of the left and right ventral tegmental area (VTA), nucleus accumbens (NAcc), insula, medial hypothalamus (MH), lateral hypothalamus (LH), medial prefrontal cortex (mPFC), orbitofrontal cortex (OFC), caudate putamen (CPu), and nucleus of the solitary tract (NTS) (Figure 1b).

Resting-state fMRI data processing

All rs-fMRI images were corrected for subject motion using *MCFLIRT*, and image intensity non-uniformity correction was performed using *n3* (solely for registration purposes). Using *FLIRT*, rs-fMRI images were registered to a mean rs-fMRI image of a single representative rat. Co-registered images were averaged to create an rs-fMRI template specific for this batch of animals. To exclude tissue outside the brain, brain masks were obtained by applying the *Brain Extraction Tool* from *FSL* to the template. Since this tool is difficult to apply to rodent resting-state data, the brain mask for the rs-fMRI template was somewhat increased in size, resulting in inclusion of some non-brain voxels. To obtain a more accurate brain mask, the initial brain mask was registered to individual space using *FLIRT*, and the mean image of each rat's rs-fMRI scan was masked using this initial mask. The individual masked mean rs-fMRI images were subsequently registered into Waxholm atlas space[11] using *FLIRT*, and a mean of these registered images was calculated to create a reference image in atlas space. Using *FNIRT* the masked individual mean rs-fMRI images were nonlinearly registered to this reference image, and inverse coefficients were calculated to register the optimized masks from atlas space to individual fMRI space. These optimized masks were obtained by averaging the co-registered individual images in reference space, and subsequently thresholding this average image to exclude all non-brain voxels. The

resulting masks optimally delineated the brain and were registered into individual space using the previously calculated coefficients. The ROIs were registered into individual space using the same coefficients. The individual rs-fMRI data as well as the ROIs in individual space were masked using the optimized final masks.

Resting-state fMRI data analysis – whole-brain connectivity maps

Rs-fMRI data were band-pass filtered between 0.01 and 0.1 Hz using 3dFourier as provided by *AFNI* (Analysis of Functional NeuroImages, Version Debian-16.2.07, https://afni.nimh.nih.gov/). Temporal signal to noise ratio (tSNR) was calculated per individual animal using *FSLMATHS* as implemented in *FSL*. The resulting tSNR map was used to mask out voxels with tSNR < 10 and this mask was applied to the 4D filtered rs-fMRI data and to the registered ROIs. This resulted in occasional exclusion of individual voxels from ROIs. Functional connectivity maps displaying the Fisher-transformed z' of Pearson correlation coefficient r were calculated using *fcmap* as provided by *FSL*, with the left or right VTA, NAcc, insula, MH, LH, mPFC, OFC, CPu, or NTS as seed ROI. These individual functional connectivity maps were registered to the reference image in atlas space, in order to perform group analysis. Mean seed-to-whole-brain functional connectivity maps were calculated for food-restricted animals and for *ad libitum*-fed animals using *FSLMATHS*.

Mean functional connectivity maps as described above were also calculated after animals tasted sucrose.

Resting-state fMRI data analysis – ROI analyses

Functional connectivity matrices were obtained from the Fisher-transformed z' of Pearson correlation coefficients r between ROIs using *FSL* and MATLAB (The MathWorks Inc., version R2014a). Average functional connectivities between specific ROIs were compared between the different groups. We assessed functional connectivity between homologous ROIs in both hemispheres (interhemispheric functional connectivity) as well as between ROIs within hemispheres (intrahemispheric functional connectivity). To statistically compare functional connectivity values and signal amplitude values on a group level in the pre-sucrose data, we performed a linear mixed model analysis within the *nlme* package[12] with the factor group (*ad libitum* or food-restricted) as between-subject variable and with correction for multiple comparisons. For the pre- and post-sucrose tasting data combined, we performed a linear mixed model analysis with correction for multiple comparisons within the *nlme* package[12] with the factor group (*ad libitum* or food-restricted) as between-subject variable and the factor time (pre- and post-sucrose tasting) as within-subject variable. Comparison of

functional connectivities (intra- and interhemispherically) between groups was done for ROIs that are known to be involved in the regulation of energy balance and feeding behavior. These ROIs included the VTA, NAcc, insula, MH, LH, mPFC, OFC, CPu, and NTS (Figure 1b). This was done for pre-sucrose tasting data to assess the influence of status of homeostatic energy balance and for post-sucrose tasting data to assess the influence of status of homeostatic energy balance after sucrose tasting.

Resting-state fMRI data analysis – fractional amplitude of low frequency fluctuations

As a measure of the magnitude of brain activity, we assessed the fractional amplitude of low frequency fluctuations (fALFF), calculated from the rs-fMRI BOLD signals as the ratio of the power of each frequency in the low-frequency range (0.01-0.1 Hz) to that of the entire frequency range[6,13]. The fractional ALFF has been shown to be more sensitive than ALFF and also corrects for physiological noise[13]. We transformed the time series of the unfiltered motion-corrected resting-state fMRI data to a frequency domain using *fslpspec* as provided by *FSL*. The resting-state fMRI data were temporally band-pass filtered ($0.01 < Hz < 0.1$). Power spectra were calculated in *fslpspec*. The resulting 4D power spectra of filtered and unfiltered data were used to calculate cumulative 3D power spectra per rat using *FSLMATHS*. The cumulative power spectra from the filtered data were divided by the cumulative power spectra of the unfiltered data to achieve fALFF maps for each rat. Individual fALFF maps were registered to the resting-state reference image in atlas space using the coefficients described earlier. We compared mean fALFF maps between the groups (*ad libitum*-fed versus food-restricted groups) by calculating the mean of all fALFF maps per group. Using a second level GLM-based analysis followed by an FDR correction for multiple comparisons, we compared mean fALFF maps between the two groups. This was done for pre- as well as post-sucrose tasting data.

In addition to the whole-brain fALFF analysis, we compared fALFF between *ad libitum*-fed and food-restricted animals in a feeding behavior-related network comprising the following ROIs: VTA, NAcc, insula, MH, LH, mPFC, OFC, CPu, and NTS. This was done for pre-sucrose tasting data to assess the influence of status of homeostatic energy balance on fALFF; on post-sucrose tasting data to assess the influence of status of homeostatic energy balance on fALFF after sucrose tasting; and on the sucrose tasting-induced differences in fALFF.

RESULTS

Three animals (one from the food-restricted group that also underwent sucrose tasting; one from the *ad libitum*-fed group that also underwent sucrose

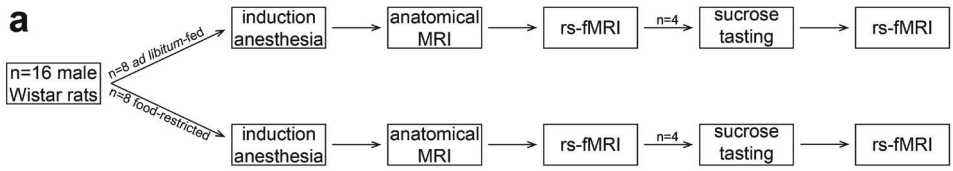
a
n=16 male Wistar rats
n=8 ad libitum-fed
n=8 food-restricted
induction anesthesia
anatomical MRI
rs-fMRI
n=4
sucrose tasting
rs-fMRI
induction anesthesia
anatomical MRI
rs-fMRI
n=4
sucrose tasting
rs-fMRI

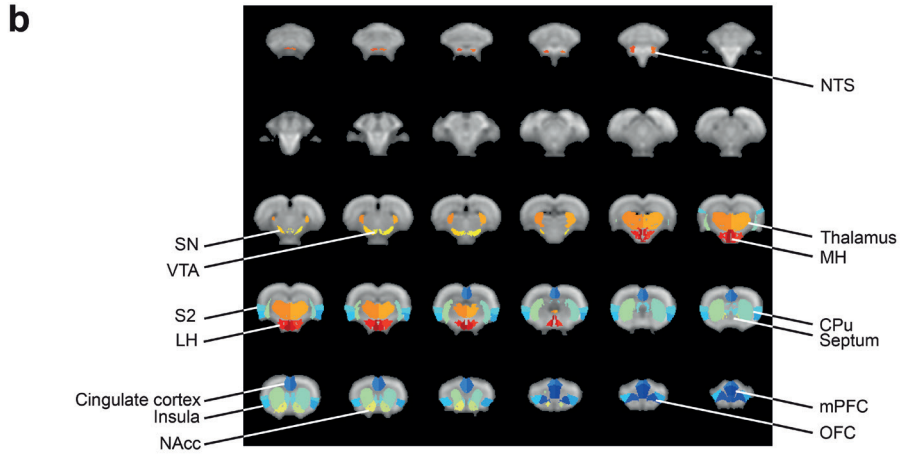
b
NTS
SN
VTA
S2
LH
Cingulate cortex
Insula
NAcc
Thalamus
MH
CPu
Septum
mPFC
OFC

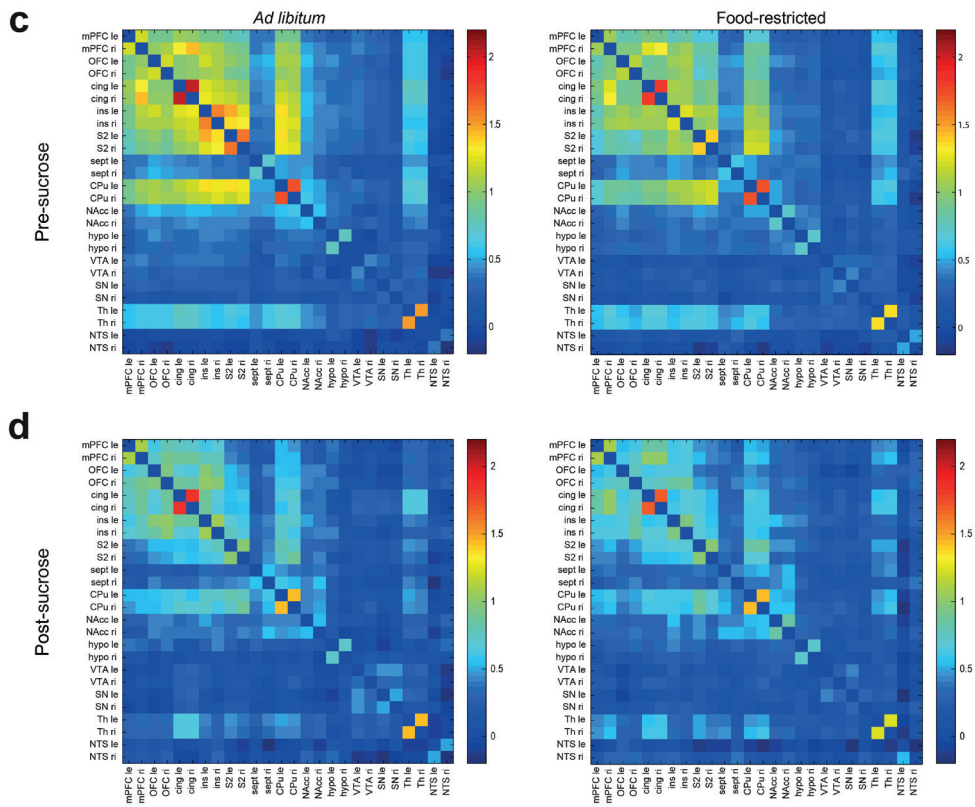
c
Ad libitum
Food-restricted
Pre-sucrose
d
Post-sucrose

Figure 1. Novel experimental resting state fMRI approach allows detection of alterations in functional connectivity as a result of food intake and sucrose tasting. a) Experimental outline. b) Regions of interest (ROIs) as used in the study. c) Inter- and intrahemispheric functional connectivity between different ROI combinations assessed in ad libitum-fed (left) and food-restricted rats (right) prior to sucrose tasting. Functional connectivity is shown as Fisher-transformed z' of Pearson correlation coefficient r. d) Inter- and intrahemispheric functional connectivity between different ROI combinations assessed in ad libitum-fed (left) and food-restricted rats (right) after sucrose tasting. cing, cingulate cortex; CPu, caudate putamen; hypo, hypothalamus; ins, insula; le, left; LH, lateral hypothalamus; MH, medial hypothalamus; mPFC, medial prefrontal cortex; NAcc, nucleus accumbens; NTS, nucleus of the solitary tract; OFC, orbitofrontal cortex; ri, right; S2, secondary somatosensory cortex; sept, septum; SN, substantia nigra; Th, thalamus; VTA, ventral tegmental area.

tasting; and one animal from the food-restricted group that did not underwent sucrose tasting) had to be excluded from the study due to significant MRI artefacts. The final group sizes for pre-sucrose tasting data were n=6 for the food-restricted group, and n=7 for the *ad libitum* group. Final group sizes for post-sucrose tasting data were n=3 for the food-restricted and *ad libitum*-fed groups, respectively.

A general decrease in functional connectivity upon food restriction

Functional connectivities between different ROIs in the food-restricted and *ad libitum*-fed groups prior to sucrose tasting are displayed as connectivity matrices in Figure 1c. Functional connectivity was clearly stronger between anterior cortical regions, such as the mPFC, OFC, cingulate cortex, CPu, insula, and S2, than between more posterior regions, such as the NAcc, hypothalamus, VTA and SN. The functional connectivity matrices displayed a generally lower functional connectivity in the food-restricted group. After sucrose tasting functional connectivities were generally lower (Figure 1d). At group level, we found no significant difference between *ad libitum*-fed and food-restricted animals before sucrose tasting (p = 0.69 for interhemispheric functional connectivity; p = 0.57 for intrahemispheric functional connectivity). However, there was a trend for interaction between group and time (group level statistics: estimate, -0.095; 95% confidence interval, -0.199 – 0.010; t(142) = -1.783; p = 0.0768).

Seed-based functional connectivity maps for different unilateral ROIs before sucrose tasting are shown in Figure 2 (for left ROIs as seed region) and Supplementary Figure 1 (for right ROIs as seed region). In general, these functional connectivity maps revealed strong interhemispheric connectivity between homologous areas, and strong connectivity with cortical areas. A comparable pattern was observed after sucrose tasting (Supplementary Figure 2). Comparison of seed-based functional connectivity patterns between *ad libitum*-fed and food-restricted rats before sucrose tasting, revealed a generally stronger functional connectivity for all ROIs in the *ad libitum*-fed group prior to sucrose tasting.

Figure 2. Food intake-dependent functional connectivity maps with different seed regions. Mean functional connectivity maps were obtained by calculation of the Fisher-transformed z' of Pearson correlation coefficient r and display functional connectivity for ad libitum-fed rats (left) and food-restricted rats (right) prior to sucrose tasting. Different left ROIs were used as seed regions: CPu, caudate putamen; LH, lateral hypothalamus; MH, medial hypothalamus; mPFC, medial prefrontal cortex; NAcc, nucleus accumbens; NTS, nucleus of the solitary tract; OFC, orbitofrontal cortex; VTA, ventral tegmental area.

This is also apparent in Figure 3, which shows the interhemispheric functional connectivity between homologous ROIs (Figure 3a), and the intrahemispheric functional connectivity between the VTA and the other ROIs (Figure 3b). However, group level statistics, including post-sucrose data, did not reveal a statistically significant effect (p = 0.687 for interhemispheric functional connectivity; p = 0.566 for intrahemispheric functional connectivity).

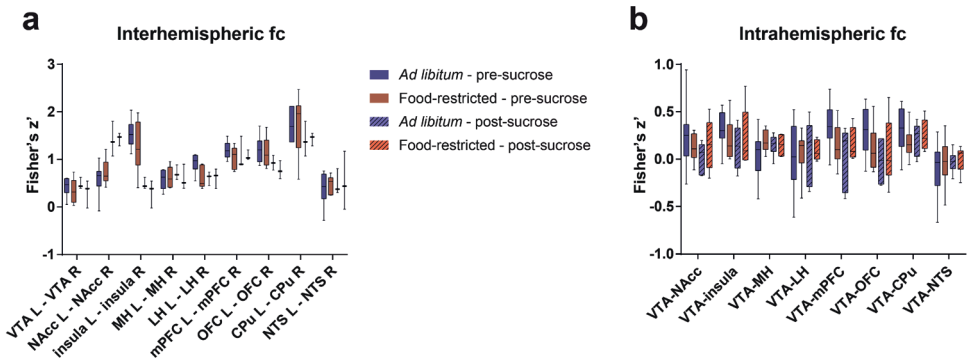

Figure 3. Inter- and intrahemispheric functional connectivity in food-restricted and ad libitum-fed rats before and after sucrose tasting. a) Functional connectivity between homologous ROIs, interhemispheric functional connectivity, and b) functional connectivity between the left VTA and left ROI plus the right VTA and the right ROI, intrahemispheric functional connectivity, compared between ad libitum-fed and food-restricted animals pre- and post-sucrose tasting. Boxplots represent the minimum, first quartile, median, third quartile, and maximum functional connectivity values. No significant differences were detected in pre-sucrose tasting data ($p = 0.69$) for interhemispheric functional connectivity; $p = 0.57$ for intrahemispheric functional connectivity). After sucrose tasting, interhemispheric functional connectivities tended to be lower in the ad libitum-fed group compared to the food-restricted group (trend towards interaction effect with group level statistics: estimate, -0.0946; 95% confidence interval, -0.1994 – 0.0103; $t(142) = -1.7826$; $p = 0.0768$). Fc, functional connectivity; L, left; R, right; CPu, caudate putamen; LH, lateral hypothalamus; MH, medial hypothalamus; mPFC, medial prefrontal cortex; NAcc, nucleus accumbens; NTS, nucleus of the solitary tract; OFC, orbitofrontal cortex; VTA, ventral tegmental area.

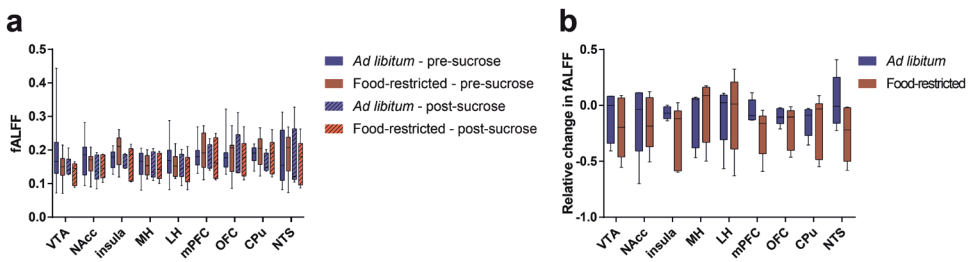

Figure 4. Fractional Amplitude of Low Frequency Fluctuations (fALFF) in satiated and food-restricted rats before and after sucrose tasting. a) fALFF in different ROIs were significantly different between pre- and post-sucrose tasting (group level statistics: estimate, 0.0191; 95% confidence interval, 0.0072 – 0.0311; $t(160) = 3.1592$; $p = 0.0019$), probably explained by a decrease in fALFF upon sucrose tasting. There was also a significant group and time interaction effect at the ROI level (group level statistics: estimate, 0.0209; 95% confidence interval, 0.0040 – 0.0378; $t(160) = 2.4396$; $p = 0.0158$). b) The relative difference in fALFF of post- as compared to pre-sucrose data, compared between ad libitum-fed and food-restricted rats, did not reveal significant differences. Boxplots represent the minimum, first quartile, median, third quartile, and maximum fALFF values. CPu, caudate putamen; LH, lateral hypothalamus; MH, medial hypothalamus; mPFC, medial prefrontal cortex; NAcc, nucleus accumbens; NTS, nucleus of the solitary tract; OFC, orbitofrontal cortex; VTA, ventral tegmental area.

Difference in fALFF between satiated and food-restricted rats

Mean fALFF maps are shown in Supplementary Figure 3. We detected a significant effect of time (sucrose tasting) on fALFF at the ROI level, as well as a significant interaction effect between group and time. The time effect (group level statistics: estimate, 0.0191; 95% confidence interval, 0.0072 – 0.0311; t(160) = 3.1592, p = 0.0019) probably reflects a decrease in fALFF upon sucrose tasting (see Figure 4), whereas the group and time interaction effect at the ROI level (group level statistics: estimate, 0.0209; 95% confidence interval, 0.0040 – 0.0378; t(160) = 2.4396; p = 0.0158) might be related to an overall stronger decrease in fALFF upon sucrose tasting in food-restricted animals as compared to *ad libitum*-fed animals (Figure 4b).

DISCUSSION

In this study we explored whether status of homeostatic energy balance, based on food intake, and sucrose tasting are reflected in resting-state functional connectivity and amplitudes of rs-fMRI signals within neural networks involved in feeding behavior. With a recently developed protocol, we acquired rs-fMRI scans in food-restricted and *ad libitum*-fed rats before and after sucrose tasting, similar to paradigms used in human neuroimaging studies on the regulation of feeding behavior. Our data revealed a trend towards higher functional connectivity in *ad libitum*-fed rats compared to food-restricted rats. Analysis of the fractional amplitude of the low-frequency resting-state signals revealed a decrease in fALFF in response to sucrose tasting.

The observed functional connectivity between the insula, cingulate cortex, and frontal cortices in rats agrees with studies in humans that have revealed a resting-state network linked to limbic brain regions[6,14]. The anterior insula contains the primary taste cortex and is involved in processing gustatory stimulation, but also in processing interoceptive signals from the gut[15–18]. Limbic regions such as the VTA and the SN, are involved in reward and motivational behavior, and are as such also involved in feeding behavior[19]. In the current study, we detected higher functional connectivity of cortical areas, such as the insula, mPFC, and cingulate cortex to these limbic structures in *ad libitum*-fed rats as compared to food-restricted rats. This is in contrast to our hypothesis, since we expected higher functional connectivity between areas involved in feeding behavior, reward and motivation in hungry animals, in line with some human fMRI studies that reported higher functional connectivity in hungry as compared to satiated subjects[3,4]. On the other hand, Wright and colleagues found decreases as well as increases in functional connectivity upon fasting[2], and other studies failed to show an effect of satiety condition on functional connectivity[5–7].

Our linear mixed model analysis revealed a trend towards an interaction between food intake and sucrose tasting. This indicates that hunger status may have an effect on how neural networks respond to a feeding-related stimulus. Others have shown that resting-state neural signals are affected by meal consumption or glucose administration[6,20]. However, our results should be interpreted with caution, since the number of animals per group was low in the sucrose tasting experiment.

The fALFF has previously been suggested as a sensitive marker to assess homeostatic changes in the brain[6]. We detected a significant decrease in fALFF upon sucrose tasting in both groups, as well as an interaction effect. This could potentially be related to a parallel decrease in functional connectivity upon sucrose tasting.

A limitation of the current study is the small sample size. Especially the post-sucrose tasting data should be interpreted with caution, since both the food-restricted and the *ad libitum*-fed groups consisted of only three rats after sucrose tasting. In addition, we were not able to scan animals during actual feeding behavior under awake conditions. Although sucrose tasting mimics an aspect of the natural process of satiation, we cannot exclude potential differences in the effects on neural network signaling.

In conclusion, our fMRI experiments in rats show that food intake and sucrose tasting can lead to specific changes in the connectivity and activity of neural networks involved in feeding behaviors. The applied paradigms are comparable to those used in human neuroimaging studies, reflecting its translational value. Our proof-of-principle study could provide a starting point for future studies to further disentangle the complex interaction between (changes in) status of homeostatic energy balance and brain signaling, which can aid in elucidation of behavioral phenotypes of feeding in health and disease. Such studies could include assessment of possible variations in neural network organisation between lean and obese rats, which have a differently regulated status of energy balance.

ACKNOWLEDGEMENTS

We especially thank Gerard van Vliet for technical assistance and hardware development, and Michel Sinke and Jeroen Verharen for advice and assistance on data analyses and visualization.

AUTHOR CONTRIBUTIONS

Conceptualization, T.J.M.R., R.A.H.A., R.M.D.; Methodology, T.J.M.R., A.v.d.T., R.A.H.A., R.M.D.; Software, A.v.d.T., W.M.O.; Validation, T.J.M.R., M.S.; Investigation, T.J.M.R.; Formal Analysis, T.J.M.R., M.S., W.M.O.; Resources, T.J.M.R., A.v.d.T., W.M.O., R.A.H.A., R.M.D.; Data curation, T.J.M.R.; Writing – Original Draft, T.J.M.R.; Writing – Review & Editing, T.J.M.R., M.S., R.A.H.A., R.M.D.; Visualization, T.J.M.R.; Supervision, R.A.H.A., R.M.D.; Project Administration, T.J.M.R.; Funding acquisition, R.A.H.A., R.M.D..

GRANT INFORMATION

This work was supported by the European Union Seventh Framework Program (FP/2007-2013) [grant number 607310 (Nudge-it)], and by the Netherlands Organization for Scientific Research [NWO-VICI 016.130.662]. The funding sources had no involvement in the collection, analysis, or interpretation of the data, nor in the writing or submission of this article.

CONFLICT OF INTEREST STATEMENT

The authors declare no conflict of interest of any type.

REFERENCES

1. World Health Organisation, W. Factsheet Obesity and Overweight. http://www.who.int/mediacentre/factsheets/fs311/en/ factsheet 311 (2017).
2. Wright, H. et al. Differential effects of hunger and satiety on insular cortex and hypothalamic functional connectivity. Eur. J. Neurosci. 43, 1181–1189 (2016).
3. Yousuf, M., Heldmann, M., Göttlich, M., Münte, T. F. & Doñamayor, N. Neural processing of food and monetary rewards is modulated by metabolic state. Brain Imaging Behav. 0, 0 (2017).
4. Avery, J. A. et al. Obesity is associated with altered mid-insula functional connectivity to limbic regions underlying appetitive responses to foods. J. Psychopharmacol. 31, 1475–1484 (2017).
5. Simon, J. J. et al. Integration of homeostatic signaling and food reward processing in the human brain. JCI Insight 2, 1–17 (2017).
6. Al-Zubaidi, A., Heldmann, M., Mertins, A., Jauch-Chara, K. & Münte, T. F. Influences of Hunger, Satiety and Oral Glucose on Functional Brain Connectivity: A Multimethod Resting-State fMRI Study. Neuroscience 382, 80–92 (2018).
7. Lepping, R. J. et al. Resting-state brain connectivity after surgical and behavioral weight loss. Obesity 23, 1422–1428 (2015).

8. Min, D. K., Tuor, U. I., Koopmans, H. S. & Chelikani, P. K. Changes in differential functional magnetic resonance signals in the rodent brain elicited by mixed-nutrient or protein-enriched meals. Gastroenterology 141, 1832–1841 (2011).
9. Min, D. K., Tuor, U. I. & Chelikani, P. K. Gastric distention induced functional magnetic resonance signal changes in the rodent brain. Neuroscience 179, 151–158 (2011).
10. Paxinos, G. & Watson, C. The rat brain in stereotaxic coordinates. (Academic Press, 2007).
11. Papp, E. A., Leergaard, T. B., Calabrese, E., Johnson, G. A. & Bjaalie, J. G. Waxholm Space atlas of the Sprague Dawley rat brain. Neuroimage 97, 374–386 (2014).
12. Pinheiro, J., Bates, D., DebRoy, S., Sarkar, D. & R core team. nlme: Linear and nonlinear Mixed Effects Models. (2018). Available at: https://cran.r-project.org/package=nlme.
13. Zou, Q. H. et al. An improved approach to detection of amplitude of low-frequency fluctuation (ALFF) for resting-state fMRI: Fractional ALFF. J. Neurosci. Methods 172, 137–141 (2008).
14. Zuo, X. N. et al. The oscillating brain: Complex and reliable. Neuroimage 49, 1432–1445 (2010).
15. de Araujo, I. E. & Rolls, E. T. Representation in the Human Brain of Food Texture and Oral Fat. J. Neurosci. 24, 3086–3093 (2004).
16. Gagnon, L., Kupers, R. & Ptito, M. Neural correlates of taste perception in congenital blindness. Neuropsychologia 70, 227–234 (2015).
17. Small, D. M. Taste representation in the human insula. Brain Struct. Funct. 214, 551–561 (2010).
18. Small, D. M. et al. Dissociation of neural representation of intensity and affective valuation in human gustation. Neuron 39, 701–711 (2003).
19. Kelley, A. E., Baldo, B. A., Pratt, W. E. & Will, M. J. Corticostriatal-hypothalamic circuitry and food motivation: integration of energy, action and reward. Physiol. Behav. 86, 773–95 (2005).
20. De Silva, A., Salem, V., Matthews, P. M. & Dhillo, W. S. The use of functional MRI to study appetite control in the CNS. Exp. Diabetes Res. 2012, (2012).

SUPPLEMENTARY FIGURES

Supplementary Figure 1. Functional connectivity maps with different right ROIs as seed regions from ad libitum-fed and food-restricted rats. Mean functional connectivity maps were obtained by calculation of the Fisher-transformed z' of Pearson correlation coefficient r and display functional connectivity for ad libitum-fed rats (left) and food-restricted rats (right). Different right ROIs were used as seed regions: CPu, caudate putamen; LH, lateral hypothalamus; MH, medial hypothalamus; mPFC, medial prefrontal cortex; NAcc, nucleus accumbens; NTS, nucleus of the solitary tract; OFC, orbitofrontal cortex; VTA, ventral tegmental area.

Supplementary Figure 2. Functional connectivity maps after sucrose tasting with different seed regions from ad libitum-fed and food-restricted rats. Mean functional connectivity maps were obtained by calculation of the Fisher-transformed z' of Pearson correlation coefficient r and show functional connectivity for ad libitum-fed (left) and food-restricted rats (right) post-sucrose tasting. Different left ROIs were used as seed regions: CPu, caudate putamen; LH, lateral hypothalamus; MH, medial hypothalamus; mPFC, medial prefrontal cortex; NAcc, nucleus accumbens; NTS, nucleus of the solitary tract; OFC, orbitofrontal cortex; VTA, ventral tegmental area.

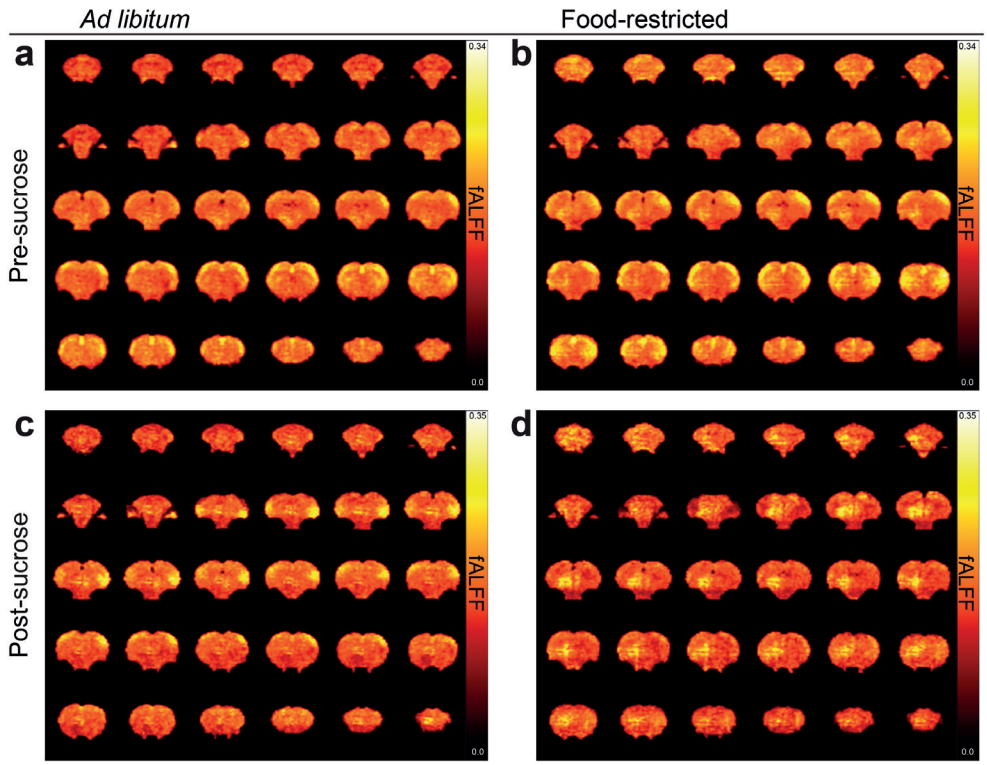

Supplementary Figure 3. Mean fractional Amplitude of Low Frequency Fluctuations (fALFF) maps in different states of energy balance. a) Whole-brain fALFF pre-sucrose tasting in ad libitum-fed rats. b) Whole-brain fALFF pre-sucrose tasting in food-restricted rats. c) Whole-brain fALFF post-sucrose tasting in ad libitum-fed rats. d) Whole-brain fALFF post-sucrose tasting in food-restricted rats.

Chapter 3

A novel approach to map induced activation of neuronal networks using chemogenetics and functional neuroimaging in rats: A proof-of-concept study on the mesocorticolimbic system

Theresia J.M. Roelofs[a,b], Jeroen P.H. Verharen[a], Geralda A.F. van Tilborg[b], Linde Boekhoudt[a], Annette van der Toorn[b], Johannes W. de Jong[a], Mieneke C.M. Luijendijk[a], Willem M. Otte[b,c], Roger A.H. Adan[a,1], Rick M. Dijkhuizen[b,1]

[a]Department of Translational Neuroscience, Brain Center Rudolf Magnus, University Medical Center Utrecht, Universiteitsweg 100, 3584 CG Utrecht, the Netherlands

[b]Biomedical MR Imaging and Spectroscopy Group, Center for Image Sciences, University Medical Center Utrecht, Bolognalaan 50, 3584 CJ Utrecht, the Netherlands

[c]Department of Pediatric Neurology, Brain Center Rudolf Magnus, University Medical Center Utrecht, Heidelberglaan 100, 3584 CX Utrecht, the Netherlands

[1]Shared senior authorship.

Published in NeuroImage 156: 109-118 (2017)

Linking neural circuit activation at whole-brain level to neuronal activity at cellular level remains one of the major challenges in neuroscience research. We set up a novel functional neuroimaging approach to map global effects of locally induced activation of specific midbrain projection neurons using chemogenetics (Designer Receptors Exclusively Activated by Designer Drugs (DREADD)-technology) combined with pharmacological magnetic resonance imaging (phMRI) in the rat mesocorticolimbic system. Chemogenetic activation of DREADD-targeted mesolimbic or mesocortical pathways, i.e. projections from the ventral tegmental area (VTA) to the nucleus accumbens (NAcc) or medial prefrontal cortex (mPFC), respectively, induced significant blood oxygenation level-dependent (BOLD) responses in areas with DREADD expression, but also in remote defined neural circuitry without DREADD expression. The time-course of brain activation corresponded with the behavioral output measure, i.e. locomotor (hyper)activity, in the mesolimbic pathway-targeted group. Chemogenetic activation specifically increased neuronal activity, whereas functional connectivity assessed with resting state functional MRI (rs-fMRI) remained stable. Positive and negative BOLD responses distinctively reflected simultaneous ventral pallidum activation and substantia nigra pars reticulata deactivation, respectively, demonstrating the concept of mesocorticolimbic network activity with concurrent activation of the direct and indirect pathways following stimulation of specific midbrain projection neurons. The presented methodology provides straightforward and widely applicable opportunities to elucidate relationships between local neuronal activity and global network activity in a controllable manner, which will increase our understanding of the functioning and dysfunctioning of large-scale neuronal networks in health and disease.

KEYWORDS
Chemogenetics, DREADD-technology, Functional imaging, Mesocorticolimbic system, Pharmacological fMRI

INTRODUCTION

Neuroimaging studies in humans, enabling non-invasive whole-brain mapping of functional networks, have revolutionized the field of cognitive neuroscience. Likewise, neuronal recordings at the cellular level in animal models have provided insights into precise neuronal activity underlying specific behaviors. However, the ability to directly link large-scale neural network activation to micro-scale neuronal circuit activity remains a significant challenge.

Recent developments in chemogenetics and optogenetics have provided

unique experimental tools to selectively activate or inhibit targeted neuronal populations or projections in animals[1–4]. Chemogenetic stimulation of neurons using Designer Receptors Exclusively Activated by Designer Drugs (DREADD)-technology induces physiologically relevant neuronal activation by increasing neuronal excitability similar to physiological activation via native muscarinic receptors[2]. One of the possible ways to take advantage of DREADD-technology is to manipulate specific projection neurons. This can be achieved by intracerebrally delivering floxed activating designer receptors (hM3Dq DREADDs) through adeno-associated viral vectors (AAVs) in the region of origin of the projection, in combination with Cre-recombinase in the projection region through retrograde traveling canine adenoviral vector (CAV2-CRE). The Cre-recombinase enzyme recombines the floxed receptors, leading to their expression on the targeted projection neurons specifically[5]. The DREADDed projection can subsequently be activated by peripheral injection of the designer ligand clozapine-*N*-oxide (CNO)[3].

One of the neural systems that has been extensively investigated both in humans and animal models, is the mesocorticolimbic system, which is implicated in many physiological (e.g. reward-related behavior, feeding behavior, decision making, and learning) and pathological (e.g. eating disorders, addiction, and depression) behaviors[6–13]. Key pathways of this system include the mesolimbic projection from ventral tegmental area (VTA) to nucleus accumbens (NAcc), and the mesocortical projection from VTA to medial prefrontal cortex (mPFC). Activation of dopamine neurons in the mesolimbic system (involved in reward processing) modulates downstream activity of direct and indirect pathway neurons[14–16]. The strict classical division of the direct and indirect pathways based on medium spiny neurons (MSNs) expressing excitatory dopamine D1- and inhibitory dopamine D2-receptors, respectively, has recently been debated by Kupchik et al. (2015), who showed that mouse ventral pallidum (VP) neurons, originally classified as part of the ventral stream indirect pathway[15,17], receive inputs from the NAcc via D1- as well as D2-receptor expressing MSNs[18]. It is therefore difficult to predict how these combined excitatory and inhibitory inputs will impact on large-scale mesocorticolimbic network activity. This emphasizes the need for accurate and integrative assessment of neuronal signaling from cellular to network level.

The goal of our study was to develop and apply a method that combines chemogenetics and functional imaging to map whole-brain neural network activity upon activation of a specific neuronal projection. To that aim we employed DREADD-technology to target neurons in the rat brain in a projection-specific manner[5]. To measure the effect of chemogenetic activation of neuronal pathways on global network activity, we applied blood oxygenation level-dependent (BOLD) functional magnetic resonance imaging (fMRI) in a similar fashion as

pharmacological fMRI (phMRI), which allows detection of neural activation induced by brain-targeted drugs[19–22]. We applied this on the mesocorticolimbic system to elucidate the effect of its activation on global neural network activity.

METHODS AND MATERIALS

Animals

Experiments were approved by the Animal Ethics Committee of the University Medical Center Utrecht, The Netherlands, and were conducted in agreement with Dutch laws ('Wet op de Dierproeven', 1996) and European regulations (Guideline 86/609/EEC).

Healthy male Wistar rats (Crl:WU, Charles River, Sulzfeld, Germany) were housed in pairs under controlled temperature and humidity conditions, with a 12h-light/dark cycle (lights on at 7:00 a.m.). Animals had *ad libitum* access to water and chow, and a perspex tube as cage enrichment. Mean (± standard deviation) body weight before MRI was 480 (± 40) g.

Intracerebral viral vector injection

Rats were divided into five groups to specifically target individual neuronal projections. In three groups DREADD expression was induced in the VTA-NAcc projection (VTA-NAcc group, n=13), the VTA-mPFC projection (VTA-mPFC group, n=11), or the VTA-basolateral amygdala (BLA) projection (VTA-BLA group, n=10) by injecting AAV5-hSyn-DIO-hM3D(Gq)-mCherry into the VTA and CAV2-CRE into projection sites (Fig. 1a). Two additional groups served as control: a Sham group (total: n=8) in which rats received sham vectors either in the VTA-NAcc, the VTA-mPFC or the VTA-BLA projection (AAV5-hSyn-DIO-ChR2-eYFP into the VTA and CAV2-CRE into projection sites), and a Saline group (total: n=11) which had DREADD expression in either the VTA-NAcc, the VTA-mPFC or the VTA-BLA projection and which were treated with saline during MRI, instead of the selective DREADD ligand clozapine-N-oxide (CNO, kindly provided by Bryan Roth, and NIMH Chemical Synthesis and Drug Supply Program)[3]. Viral vector injections were performed as follows: before surgery, rats were anesthetized by an intramuscular injection of a combination of 0.315 mg/kg fentanyl and 10 mg/kg fluanisone (Hypnorm, Janssen Pharmaceutica, Belgium), supplemented with an additional injection when needed. Xylocaine was sprayed on the skull for local anesthesia (Lidocaine 100 mg/ml, AstraZeneca BV, the Netherlands). Using a stereotaxic apparatus (David Kopf), 1 µl of $1.0\times10^{\wedge9}$ genomic copies/µl of AAV5-hSyn-DIO-hM3D(Gq)-mCherry (UNC Vector Core, USA) was injected bilaterally in the VTA of animals in the experimental groups, as described in Boender et al. (2014) (Fig. 1a). Depending on group assignment, 1 µl of $1.25\times10^{\wedge9}$ genomic copies/

µl of the retrograde vector CAV2-CRE (IGMM, France) was injected bilaterally into the NAcc, the prelimbic part of the mPFC, or the BLA (coordinates relative to Bregma for NAcc: AP+1.20 mm, ML±2.80 mm at an angle of 10°, DV-7.50 mm; for mPFC: AP+2.70 mm, ML±1.40 mm at an angle of 10°, DV-4.90 mm; for BLA: AP-2.20 mm, ML±5.00 mm, DV-9.20 mm). Rats in the Sham group received CAV2-CRE injections similarly as other groups, but received 1 µl AAV5-hSyn-DIO-ChR2-eYFP (1.0×10^9 genomic copies/µl) bilaterally into the VTA.

MRI experiments started at least two months after viral injections, when virus expression is known to be stabilized.

Home cage locomotor activity

Locomotor activity upon CNO or saline injection was assessed in ten VTA-NAcc and nine VTA-mPFC animals. Rats were temporarily housed individually in 43x43x90-cm PhenoTyper® 9000 home cages (Noldus IT, Wageningen, the Netherlands). PhenoTyper cages were equipped with infrared video cameras to monitor locomotor activity. After habituation, CNO or saline was administered and locomotor activity was tracked from the moment of injection. CNO and saline were given in a counter-balanced design, 24 h apart. Total distance moved was analyzed with EthoVision XT11 (Noldus IT, Wageningen, the Netherlands), using locally weighted scatterplot smoothing.

In vivo MRI

In vivo MRI measurements were conducted using a 9.4 T MR system equipped with a 400 mT/m gradient coil (Agilent). A home-built 90 mm diameter Helmholtz volume coil and an inductively coupled 25 mm diameter surface coil were used for signal excitation and reception, respectively. Animals were endotracheally intubated for mechanical ventilation with 1.5% isoflurane in O_2/air (1:4) (ventilation rate: 45-55). A cannula was placed intraperitoneally (i.p.) for injection of CNO or saline. CNO (kindly provided by Bryan Roth, and NIMH Chemical Synthesis and Drug Supply Program) was dissolved in saline (0.9% NaCl) at a concentration of 0.3 mg/ml[5,23]. End-tidal CO_2 was monitored with a capnograph (Microcap, Oridion Medical 1987 Ltd., Jerusalem, Israel). Body temperature was maintained at 37.0 ± 1.0°C.

phMRI data were acquired using a gradient echo multi slice (GEMS) sequence, with TR/TE=500/15 ms, flip angle=50°, FOV=32x32x12.5 mm^3, matrix size=128x128x25 voxels, resolution=250x250x500 μm^3, two averages, and a total scan time of 2 min and 8 s per image series. After 10 baseline image series (21.3 min), 1.0 ml/kg CNO or saline was injected i.p. Representative GEMS images are shown in Supplementary Fig. S1.

Next, resting state-fMRI (rs-fMRI) was conducted one hour after CNO injection. For this purpose a 3D gradient echo Echo Planar Imaging (EPI) sequence was used. The read-out and first phase-encode dimensions were covered in a single-shot EPI, the second phase-encode dimension using linear phase encoding. 800 images were acquired with an acquisition time of 730.8 ms per volume (total scan time: 9 min and 45 s), and TR/TE=26.1/15 ms, flip angle=13°, FOV=32.4x32.4x16.8 mm^3, matrix size=54x54x28, and thus an isotropic spatial resolution of 600 µm. Representative EPI images are shown in Supplementary Fig. S2.

Immunohistochemistry

Rats were euthanized by an overdose of isoflurane, followed by intracardial perfusion-fixation as described in Boender et al. (2014). Time between CNO or saline injection and perfusion-fixation was around 90 min to allow synthesis of the peptide product of the immediate early gene cFos. After extraction, brains were post-fixated in 4% paraformaldehyde at 4°C for at least 24 h and stored in 30% sucrose and 0.1% NaN_3 in PBS. For immunohistochemical assessment of virus expression, 40 µm slices were collected and blocked in 10% normal horse serum (NHS) and 0.25% Triton X-100 in PBS. Subsequently, slices were incubated overnight at 4°C in primary antibodies rabbit anti-dsRed (1:500, Clontech 632496) and mouse anti-tyrosine hydroxylase (TH, 1:1000, Millipore MAB318) in 2% NHS and 0.1% Triton X-100 in PBS. Rabbit anti-dsRed was directed against mCherry, a red fluorescent tag coupled to the designer receptor. hM3D(Gq)-mCherry was visualized with incubation in secondary antibody Alexa-568- or Alexa-594-labeled goat anti-rabbit (1:500, Abcam ab175471 and A11037), and TH with incubation in Alexa-488-labeled goat anti-mouse (1:1000, Abcam, ab150113), all in 2% NHS and 0.1% Triton X-100 in PBS. Sections were coverslipped with FluorSave (Merck Millipore).

For histochemical quantification of activated neurons at the time of sacrifice, brain sections were stained for cFos. Sections were pre-heated in a 10mM sodium citrate solution to 80°C for antigen retrieval, and subsequently incubated in 1% Triton X-100 in PBS, followed by incubation in 0.9% H_2O_2 and 20% methanol in PBS to remove endogenous peroxidase activity. Subsequent blocking in 3% NHS and 0.3% Triton X-100 in PBS, was followed by overnight incubation in primary antibody goat anti-cFos (1:500, Santa Cruz, sc-52-G) in 2% NHS in PBS. Next, slices were incubated in biotinylated secondary antibody horse anti-goat (1:200, Vector, BA-9500) in 1% NHS in PBS, and subsequently in Biotin/Avidin (1:1000, Vectastain) in PBS. This complex was visualized by exposing the slices for exactly 15 min to a solution of liquid DAB (3,3'-Diaminobenzidine, Dako) and 3%

nickel ammonium sulphate. All sections were dehydrated using increasing series of ethanol, cleared in xylene, and coverslipped with Entallan (Merck Millipore).

Immunofluorescent sections were photographed by confocal laser scanning microscopy (Olympus Fluoview FV1000). Expression of mCherry on neuronal somas was quantified on an ordinal scale by one of the authors who was blinded for group assignment of the rats. DAB-treated slices stained for cFos were photographed using a Zeiss Axioskop 2 light microscope. In slices comprising the VTA (on average 2-4 per rat), the VTA was manually delineated in ImageJ (Version 1.48v, National Institutes of Health), and cFos-positive neurons within this area were counted using the cell counter plugin in ImageJ.

Pharmacological fMRI data processing

Pharmacological MR images were corrected for subject motion using *MCFLIRT*; image intensity non-uniformity correction was performed using *n3* (solely for registration purposes); and brain masks were obtained using the *Brain Extraction Tool*, all as implemented in *FSL* (FMRIB's Software Library, http://www.fmrib.ox.ac.uk/fsl, version 5.0.9). Using the affine intermodal image registration tool *FLIRT* (FMRIBs Linear Image Registration Tool) phMRI images were registered to an in-house anatomical MRI template that was matched to a 3D model of a rat brain atlas[24] to create an average phMRI template. PhMRI data were registered to this template, using *FLIRT* followed by *FNIRT* (FMRIBs Nonlinear Image Registration Tool, build 508). PhMRI data were normalized to baseline (average of the ten scans prior to CNO or saline injection). To calculate whole-brain activation maps, phMRI data were smoothed (Gaussian kernel, full width at half maximum = 0.4 mm) and a generalized linear model (GLM)-based analysis was applied to the smoothed phMRI data for each specific group, as described in Mandeville et al. (2014), using the group-specific mean smoothed BOLD signal time-course in the VTA as a regressor. FDR correction for multiple testing was performed and an FDR-corrected Z-value of (-)1.96, corresponding to a p-value of 0.05, was taken as cutoff value for activation maps.

Resting state fMRI data processing

For analyses of rs-fMRI data, images were motion-corrected using *MCFLIRT*, followed by image intensity non-uniformity correction using *n3* (solely for registration purposes). For all animals, rs-fMRI images were registered to images from a single representative rat using *FLIRT* to create an average rs-fMRI data set, which served as a rs-fMRI template. A brain mask of this template was obtained using the *Brain Extraction Tool* in *FSL*. Subsequently the phMRI template, which was matched to an in-house 3D model of a rat brain atlas as described in

the data processing section of pharmacological fMRI data, was registered to the rs-fMRI template using *FLIRT*, which allowed consistent ROI analyses of individual rs-fMRI data. Rs-fMRI data were band-pass filtered between 0.01 and 0.1 Hz. Temporal signal to noise ratio (tSNR) was calculated per individual animal using *FSLMATHS* as implemented in *FSL*. The resulting tSNR map was used to mask out voxels with tSNR < 10 and was applied on the 4D filtered rs-fMRI data. Functional connectivity matrices were obtained by calculation of the Fisher-transformed z′ of Pearson correlation coefficients *r*.

Data analysis

Locomotor activity over time was analyzed using a mixed factorial ANOVA (repeated measures GLM) analysis, with Greenhouse-Geisser correction for sphericity, in SPSS (v. 16.0). Total locomotor activity per condition was analyzed using a paired-samples t-test and independent-samples t-test in SPSS, to compare the effect between treatments and between groups. Four comparisons were made, with Bonferroni correction.

For fMRI analysis, ROIs extracted from the rat brain atlas included the VTA, NAcc, and mPFC. S2, not part of the mesocorticolimbic system, was used as control ROI. BOLD signal time-courses were derived from the phMRI data. Two outlier tests, iterative Grubb′s test (GraphPad Software QuickCalcs, http://graphpad.com/quickcalcs/grubbs1/) and iterative Dixon′s Q-test[25], were performed on post-injection mean BOLD signal values in the ROIs. The total BOLD response was calculated as area under the curve from the BOLD signal time-course, with mean baseline BOLD signal intensity set to 0. BOLD signal intensity below baseline was interpreted as a negative response, allowing for negative total BOLD response values. Differences in total BOLD response were first compared between the two control groups, to specifically test for any effect of CNO itself, using an independent samples t-test in SPSS. Next, for all ROIs, total BOLD response values were compared between the CNO-injected groups using one-way ANOVA analysis in SPSS, with Bonferroni correction. Total BOLD response was compared to the number of cFos-positive neurons using a one-tailed Pearson′s product-moment correlation test in SPSS. The number of cFos-expressing neurons was compared between the groups using a one-way ANOVA test in SPSS, with Bonferroni correction.

Functional connectivity values calculated from the rs-fMRI experiments were compared between the two control groups using an independent samples t-test in SPSS, to check if CNO by itself had any effect on functional connectivity. Subsequently, functional connectivity values were compared between CNO-injected groups using a one-way ANOVA in SPSS, with Bonferroni correction.

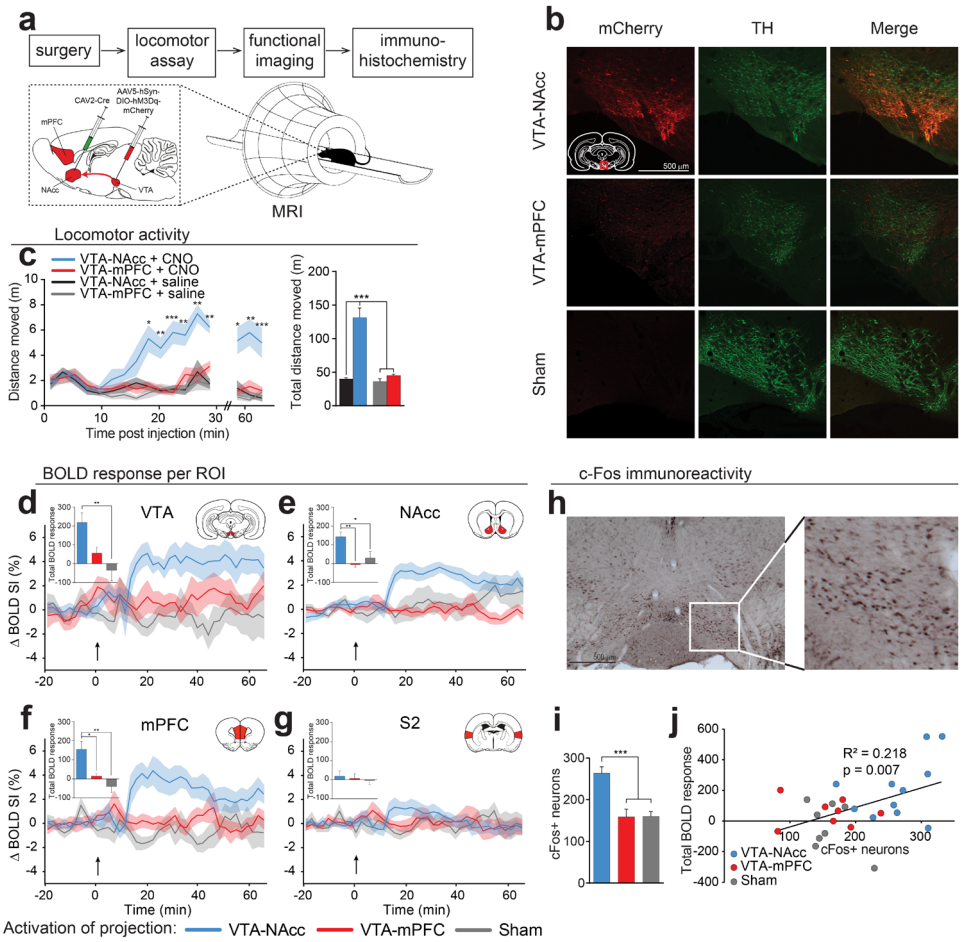

Fig 1. Novel DREADD-phMRI approach reveals changes in neuronal activity with corresponding time-course as behavioral output and validated by cFos immunohistochemistry. (a) Experimental design. Using a two-vector DREADD approach, only VTA neurons projecting to the NAcc (VTA-NAcc group) or to the mPFC (VTA-mPFC group) express the activating DREADDs. Projection specificity was obtained by injection of AAV5-hSyn-DIO-hM3D(Gq)-mCherry (UNC Vector Core, USA) bilaterally in the VTA, as described in Boender et al. (2014), and the retrograde vector CAV2-CRE (IGMM, France) into the target area. Activation of the targeted pathway in the VTA-NAcc group is schematically represented by the red arrow. (b) Representative images of DREADD expression. DREADD expression is shown in red. TH (tyrosine hydroxylase, a marker for dopamine neurons) was stained in green. DREADD expression was correctly targeted to the VTA. The VTA-NAcc group showed higher expression of DREADDs as compared to the VTA-mPFC group. In the Sham group no DREADDs were expressed. (c) Locomotor activity after CNO or saline injection. A significant interaction effect on total locomotor activity was measured between injection type (CNO or saline), group and time point ($F=3.8$, $p=0.002$). Total distance moved (right graph; mean ± SEM) was significantly different between CNO-injected VTA-NAcc animals (n=10) and other groups ($p<0.001$, VTA-mPFC group; n=9). Figure legend continues on next page.

Continuation of figure legend 1. Locomotor activity after CNO injection in the VTA-NAcc group started to increase 10 min after injection and was significantly elevated after approximately 20 min which remained up to at least 1 h (*p<0.05, ** p<0.01, *** p<0.001). (d-g) BOLD signal time-courses in the VTA, NAcc, mPFC, and S2, respectively (mean ± SEM) before and after injection of CNO in the VTA-NAcc group, the VTA-mPFC group, and the Sham control group. CNO was injected after 21 min of baseline scanning (arrows). Changes in BOLD signal intensity are presented as percentage change from baseline. The insets show the total BOLD response over the entire phMRI time-course (a.u., mean ± SEM). BOLD signal in the VTA of VTA-NAcc animals started to increase 10 min after injection of CNO and reached a plateau level of 4% higher than baseline after 15-20 min (d). Total BOLD response in the VTA-NAcc (inset) was significantly higher than in the Sham group (p=0.004). The VTA in animals from the VTA-mPFC group exhibited a smaller BOLD response, which was not significantly different from the Sham group. Positive BOLD responses in the NAcc (e) and mPFC (f) of the VTA-NAcc group, reached plateau levels of about 3% higher than baseline at 15-20 min after CNO injection, and were significantly elevated as compared to the Sham group (p=0.018 for NAcc, and p=0.003 for mPFC). Significant responses in the NAcc or mPFC were absent in the VTA-mPFC group. The BOLD signal time-course in the control area S2, not part of the mesocorticolimbic system, remained stable and no significant differences in BOLD signal were found between groups (g). See also Supplementary Figure S3a for results in the Saline group. (h) Representative image of cFos staining in the VTA of a VTA-NAcc animal, which showed cFos expression after CNO injection. (i) The VTA-NAcc groups expressed significantly more cFos-positive neurons in the VTA as compared to the VTA-mPFC and Sham groups (p<0.0005, mean ± SEM). (j) A positive correlation was found between the number of cFos-positive neurons in the VTA and the total BOLD response in the VTA (r=0.467, p=0.007). Δ BOLD SI (%): delta BOLD signal intensity in percentages; AAV5: adeno-associated virus serotype 5; CAV2-Cre: canine adenovirus-2 expressing Cre-recombinase; DIO: double-floxed inverted open reading frame; hSyn: human synapsin promotor; mPFC: medial prefrontal cortex; NAcc: nucleus accumbens; S2: secondary somatosensory cortex; VTA: ventral tegmental area. Brain slice insets are adapted from Paxinos and Watson (2005).

RESULTS

Immunohistochemical assessment of virus expression demonstrated that injections were correctly targeted and resulted in DREADD expression in VTA-NAcc, VTA-mPFC and VTA-BLA projections, representing three different experimental groups. Fig. 1b shows representative examples of DREADD expression in the VTA, which was most abundant in the VTA-NAcc group, in which viral expression was detected on somas in the VTA and on axons in the NAcc core and shell region. No DREADD expression was detected in the rats that received sham vectors (Sham group).

The VTA-BLA group had to be excluded from further analysis, due to low BOLD signal-to-noise ratio in the BLA, caused by air-tissue susceptibility artifacts from the ear cavities. In addition, outlier tests identified two animals from the Saline group with irregular BOLD signal time-courses as outliers, which were excluded from all analyses. Three animals in the VTA-mPFC group showed considerable DREADD expression in the dorsal medial striatum (DMS) and in the

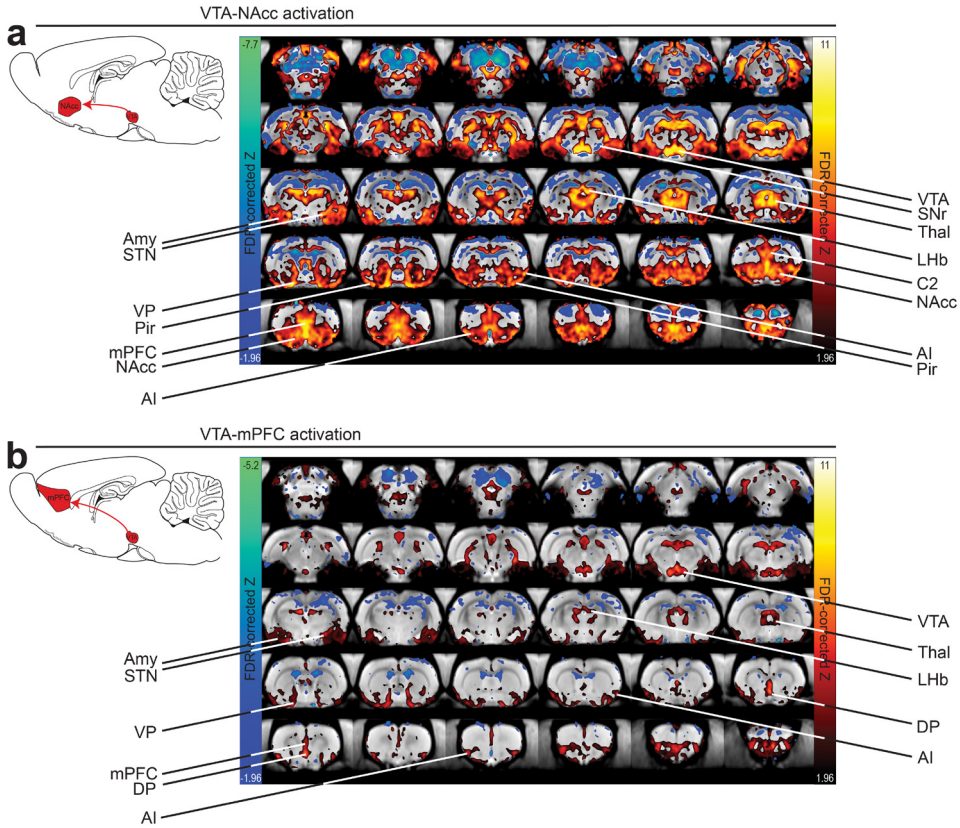

Fig. 2. Detection of network activity in defined neural circuitry in DREADD-targeted animals. The insets on the top left indicate the projection targeted with DREADD-technology. (a) In the VTA-NAcc group, BOLD signal time-course in the NAcc showed strongest correlation to the VTA signal time-course, but correlated responses were also detected in the ventral pallidum (VP), agranular insular cortex (AI), secondary cingulate cortex (C2), amygdaloid nucleus (Amy), piriform cortex (Pir), and thalamic nuclei (Thal). A negative BOLD response was detected in the substantia nigra pars reticulata (SNr). Minor negative signal correlations were detected outside the targeted network. (b) In the VTA-mPFC group, BOLD signal time-course in the mPFC was positively correlated to the VTA signal time-course (mainly infralimbic part and medial prelimbic part). Furthermore, positive signal responses were detected in the VP, AI, Amy, dorsal peduncular cortex (DP), and thalamic nuclei. Also minor negative responses were detected. In both the VTA-NAcc (a) and VTA-mPFC group (b), significant BOLD responses were detected in the subthalamic nucleus (STN) and lateral habenula (LHb). However, caution is needed in interpreting these signals (see Discussion). Insets adapted from Paxinos and Watson (2005).

medial substantia nigra (SN), indicating that CAV2-Cre virus particles targeted to the mPFC spread to the DMS, and AAV virus particles injected in the VTA spread to the SN. These animals were excluded from further analyses. Final group sizes

for phMRI assessment with CNO activation were: VTA-NAcc group: n=13; VTA-mPFC group: n=8; Sham group: n=8. The Saline group in which animals received saline instead of CNO during phMRI consisted of nine animals.

For rs-fMRI analyses, one animal from the VTA-NAcc group, one animal from the VTA-mPFC group, and one animal from the Sham group had to be excluded due to signal distortions.

Locomotor activity

A well-known behavioral output of mesolimbic activation is locomotor (hyper)activity[5,12,26–28]. To assess the time course of functional chemogenetic activation, locomotor activity was measured after CNO or saline injections. Total distance moved in the VTA-NAcc group was significantly increased after i.p. injection of CNO as compared to saline (Fig. 1c). Locomotion increased from ten minutes after CNO injection and remained elevated for at least one hour. This confirmed functional chemogenetic activation and indicated the time frame in which injection of CNO results in a behavioral output. In the VTA-mPFC group locomotor activity was unaffected, as expected.

DREADD-induced activation in mesocorticolimbic regions

We applied pharmacological fMRI in animals with projection-specific DREADD expression in the mesolimbic or mesocortical projection (Fig. 1a). During acquisition, animals were under 1.5% isoflurane anesthesia to allow investigation of the effect of chemogenetic activation of defined neuronal projections on global brain activity without interference of conscious processes, differences in arousal state, or stress. Furthermore, the use of anesthetized rats allowed us to compare results to previous optogenetics-fMRI studies which used the same anesthetic[29–33].

Chemogenetic activation by CNO administration resulted in clear BOLD responses in mesocorticolimbic regions of interest (ROIs) in animals with DREADD expression (Fig. 1d-f). Increased BOLD signal upon injection of CNO remained elevated during the entire phMRI acquisition (i.e., 1 h after CNO injection) (Fig. 1d-f). Significant responses were absent in animals without DREADD expression (Sham group) (Fig. 1d-g), in DREADD-expressing animals that received saline (Saline group) (Supplementary Fig. S3a), and in the control area, the secondary somatosensory cortex (S2), which is not part of the mesocorticolimbic system (Fig. 1g).

Strongest BOLD responses were measured in the VTA-NAcc group. BOLD signal in the VTA started to increase 10 min after injection of CNO and reached a plateau level of 4% higher than baseline after 15-20 min (Fig. 1d). In the NAcc and mPFC, positive BOLD responses reached plateau levels of 3% higher than

baseline (Fig. 1e-f). Total BOLD responses in the VTA, NAcc and mPFC of the VTA-NAcc group (insets Fig. 1d-f) were significantly higher than in the Sham group. The VTA in animals from the VTA-mPFC group exhibited a considerably smaller BOLD response (inset Fig. 1d). Significant responses in the NAcc or mPFC regions were absent in the VTA-mPFC group. cFos staining was performed to estimate the number of activated neurons and to correlate this to the phMRI-based

Table 1. Brain regions exhibiting significant positive (activated) or negative (deactivated) BOLD responses after CNO injection in rats with projection specific DREADD expression.

DREADD-targeted projection	Activated regions	Z-score	Activated part of ROI (%)	Deactivated regions	Z-score	Deactivated part of ROI (%)
VTA-NAcc	VTA	7.0	71	SNr	-3.4	34
	NAcc	6.6	99	IC	-5.0	90
	mPFC	5.9	87	Cerebellar regions	-	-
	VP	4.5	94	Dorsal cortical areas outside targeted network	-	-
	AI	5.2	88			
	C2	4.7	84			
	Amy	5.0	80			
	Pir	5.1	87			
	Thalamic nuclei (mainly: IAM, AM, VA, IMD, MDT, CL, PC)	6.0	83			
	STN[a]	4.7	81			
	LHb[a]	5.2	75			
VTA-mPFC	VTA	4.4	64	IC	-2.8	77
	mPFC (predominantly IL and medial PL)	3.2	33	Dorsal cortical areas outside targeted network	-	-
	VP	3.1	39			
	AI	3.5	50			
	Amy	3.2	60			
	DP	3.1	25			
	Thalamic nuclei (mainly: IAM, AM, IMD, MDT, CL, PC)	3.2	29			
	STN[a]	2.7	42			
	LHb[a]	2.7	25			

Z-scores are calculated as mean FDR-corrected Z-score across significantly (de)activated voxels within regions of interest. A Z-score of (-)1.96 corresponds to a p-value of 0.05. Z-scores in thalamus are calculated within the sub regions mentioned in the left column. a Activity in these regions should be interpreted with caution, because of possible partial volume effects. AI, agranular insular cortex; AM, anteromedial thalamic nucleus; Amy, amygdaloid nucleus; C2, secondary cingulate cortex; CL, centrolateral thalamic nucleus; DP, dorsal peduncular cortex; IAM, interanteromedial thalamic nucleus; IC, inferior colliculae; IL, infralimbic region of medial prefrontal cortex; IMD, intermediodorsal thalamic nucleus; LHb, lateral habenula; MDT, mediodorsal thalamic nucleus; mPFC, medial prefrontal cortex; NAcc, nucleus accumbens; PC, paracentral thalamic nucleus; Pir, piriform cortex; PL, prelimbic region of medial prefrontal cortex; SNr, substantia nigra pars reticulata; STN, subthalamic nucleus; VA, ventral anterior thalamic nucleus; VP, ventral pallidum; VTA, ventral tegmental area.

measure of neuronal activity. Immunohistochemical analysis showed increased cFos expression in the VTA after CNO injection in animals from the VTA-NAcc group (Fig. 1h), which was significantly higher compared to the Sham and VTA-mPFC groups (Fig. 1i). A significant positive correlation was found between the DREADD-induced BOLD activation response and the number of cFos-positive neurons (Fig. 1j).

DREADD-induced activation of whole-brain networks

To study the causal effects of chemogenetic activation of specific neuronal projections on global brain network activity, we assessed the changes

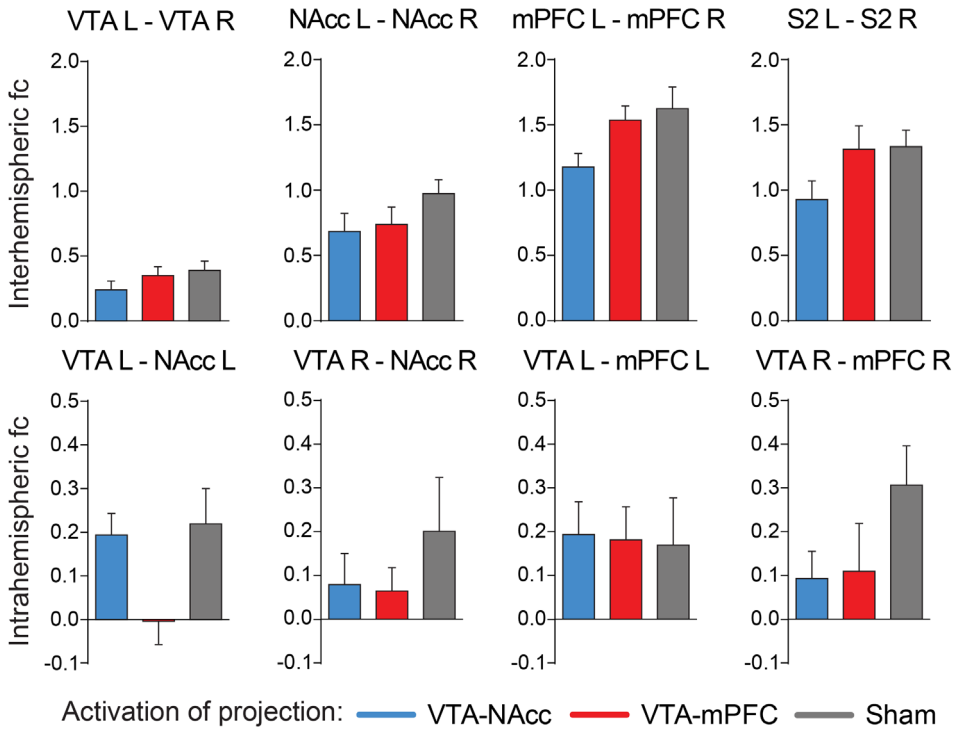

Fig. 3. Unaffected inter- and intrahemispheric functional connectivity. Interhemispheric functional connectivity (fc; mean ± SEM) between bilateral ROIs (upper graphs), and intrahemispheric fc (mean ± SEM) between the left/right VTA and the left/right NAcc or mPFC. Fc is expressed as the Fisher-transformed correlation coefficient (z'). No statistically significant differences in inter- nor in intrahemispheric fc were found between any of the groups. Only intrahemispheric fc between the left and right mPFC showed a trend of reduction in the VTA-NAcc group (p=0.05). See also Supplementary Fig. S3b and S3c for functional connectivity in the Saline group. fc: functional connectivity; mPFC: medial prefrontal cortex; NAcc: nucleus accumbens; S2: secondary somatosensory cortex; VTA: ventral tegmental area.

in BOLD signal upon CNO injection at whole-brain level. Fig. 2 shows whole-brain DREADD-induced activation maps of the VTA-NAcc (Fig. 2a) and VTA-mPFC (Fig. 2b) groups, calculated using a generalized linear model (GLM) with the VTA activation response as input signal. Positive and negative BOLD responses were observed throughout the entire brain. Significantly activated or deactivated brain regions are listed in Table 1. In general, the extent of activation was smaller in the VTA-mPFC group as compared to the VTA-NAcc group (Fig. 2 and Table 1).

To check whether DREADD-induced BOLD responses in not directly targeted brain areas were true network effects and not caused by ectopic DREADD expression, we determined the degree of DREADD expression on neuronal somas in primary targeted as well as non-targeted brain regions that showed BOLD responses. No DREADD expression was found in non-targeted regions; one VTA-NAcc animal had considerable expression in the substantia nigra pars reticulata (SNr); and two VTA-NAcc animals had poor expression in the SNr (Supplementary Fig. S4).

Functional connectivity

The effect of chemogenetic activation of mesolimbic and mesocortical pathways on intra- and interhemispheric functional connectivity (fc) was assessed with resting state-fMRI (rs-fMRI) after injection of CNO or saline. Strongest fc was observed between homologous cortical regions, i.e. left and right mPFC, and left and right S2 (Fig. 3 and Supplementary Fig. S3b and S3c). In contrast to our phMRI findings, rs-fMRI did not reveal significant differences in fc of the ROIs between the experimental groups, only interhemispheric fc of the left and right mPFC showed a trend towards being decreased in the VTA-NAcc group as compared to the Sham group (p=0.05).

DISCUSSION

We successfully combined DREADD-technology and pharmacological fMRI to map whole-brain network activity caused by activation of specific midbrain neurons in rats. We detected robust positive BOLD signal responses in DREADD-targeted brain regions, as well as positive and negative BOLD responses in remotely connected direct and indirect pathways of the mesocorticolimbic network. The measured time-course of activation of the VTA-NAcc projection matched with the time-course of increased locomotor activity, a behavioral output of mesolimbic dopamine stimulation. Neuronal activation of the VTA was histologically confirmed by increased cFos expression, although there was quite some variation associated with background expression of cFos. Chemogenetic activation specifically affected neuronal activity, as functional connectivity

between mesocorticolimbic regions, as assessed by resting state-fMRI, was not significantly altered by DREADD activation.

Activation of directly targeted projection areas

DREADD-induced activation of VTA neurons projecting to the NAcc caused a significant positive BOLD signal response in the VTA and NAcc, starting 10 min after injection of CNO, in correspondence with the timing of locomotor hyperactivity. In contrast, animals in the VTA-mPFC group exhibited only a weak BOLD signal response in the VTA and mPFC. Likewise, the extent of activation on the whole-brain map of this group was smaller. These findings are likely explained by the lower number of neurons in the VTA-mPFC projection as compared to the VTA-NAcc projection. This was confirmed with immunohistochemistry, showing less DREADD expression in the VTA of VTA-mPFC animals as compared to VTA-NAcc animals. It is unlikely that issues with the CAV or AAV vectors caused low DREADD expression, since the same vectors were used in the VTA-NAcc and Saline groups, which showed high DREADD expression. Although the activation response in the mPFC of VTA-mPFC animals failed to reach statistical significance in the ROI analysis, encompassing the entire mPFC, significant subregional activation was detectable on the statistical activation maps at single voxel level.

Activation and deactivation of connected network regions

phMRI data from the VTA-NAcc group demonstrated that downstream connected brain regions were also activated. Surprisingly, VTA-mPFC activation resulted in an activation pattern that largely overlapped with the activation pattern upon VTA-NAcc stimulation. However, the NAcc was not activated in the VTA-mPFC group, which suggests that projections originating from mPFC neurons (that receive input from the VTA) activate the mesocorticolimbic system independent of accumbens activity. Future studies that allow detailed assessment of the connections of neurons within this network, for example using confocal microscopy of brain slices or light sheet microscopy of cleared whole-brain tissue, may provide improved insights in the structural organization of these networks.

We have found that on average 80% of DREADD-expressing NAcc-projecting VTA neurons and 72% of mPFC-projecting VTA neurons are TH-positive, thus dopaminergic (unpublished data). Activity in the VTA-NAcc projection induces release of dopamine in the NAcc, which binds to excitatory dopamine D1 receptors and inhibitory dopamine D2 receptors on local MSNs[14–16]. Consequent excitation or inhibition via the direct or indirect pathways explains the observed positive or negative BOLD responses in connected network regions, as outlined below.

The observed negative BOLD responses in the SNr concur with activation of D1-dominant direct pathway MSNs, which project directly to the SNr with GABAergic control[14–16]. Three out of thirteen animals in the VTA-NAcc group expressed some DREADDs in the medial part of the SNr, probably due to minor leakage from the VTA injection site. Circuit-wise, the SNr, which is inhibited by GABAergic control from D1-dominant MSNs and which is also GABAergic itself, subsequently disinhibits the thalamus. The thalamus indeed displayed strong activation in the VTA-NAcc and VTA-mPFC groups. Activation of the indirect pathway would result in net inhibition of the thalamus via an extra inhibitory loop from D2-expressing GABAergic MSNs projecting to VP/globus pallidus externus, which also inhibits the SNr[14–16]. The release of dopamine upon mesocorticolimbic activation binds inhibitory D2 receptors on indirect pathway MSNs, leading to inhibition of the indirect pathway. The observed activation of the VP after stimulation of the VTA-NAcc projection presumably results from disinhibition via the D2-dominant GABAergic projection from NAcc MSNs to the VP[14–16]. Although it was recently described that the VP does not only receive input from the NAcc via D2-, but also via D1-expressing MSNs[18], our study shows that the net effect of VTA-NAcc activation is an activation of the VP, likely resulting from disinhibition via D2 GABAergic MSNs. At the level of the thalamus, the direct and indirect pathways converge. Direct pathway activation combined with indirect pathway inhibition synergistically activates the thalamus and cortical output areas of the mesocorticolimbic system, as was observed in our data.

The mediodorsal nucleus of the thalamus (MDT), which showed a positive activation response in the VTA-NAcc and VTA-mPFC groups but no DREADD expression, activates the cingulate, infralimbic, prelimbic and agranular insular cortices, forming a striato-pallido-thalamo-cortical circuit[34–36]. These forebrain circuits involving basal ganglia, thalamus and (pre)frontal cortical areas, run via the direct as well as the indirect pathway. This entire neural circuit, commonly known as the direct and indirect striatal output pathways, exhibited significant BOLD responses. The subthalamic nucleus (STN) and lateral habenula (LHb), forming an integrated part of this circuit, were both significantly activated upon VTA-NAcc as well as VTA-mPFC stimulation. However, phMRI signals in the STN and LHb should be interpreted with caution, because of their small size and close proximity to larger areas with strong responses.

The detection of simultaneous direct and indirect pathway activity demonstrates the ability of DREADD-phMRI to gauge network activity upon activation of specific neuronal pathways. Previously, fMRI has been successfully employed to map and measure optogenetically-induced changes in BOLD fMRI signals[29,31–33,37–40]. In contrast to our study, some optogenetics-fMRI papers in

which the VTA was targeted in TH::Cre animals reported clear activation of the dorsal striatum[29,39,40]. Since the medial SN is located adjacent to the lateral VTA and projects to the DMS[41], we believe that unintended targeting of the medial SN together with the VTA may have resulted in activation of the dorsal part of the striatum. By using a Cav2-Cre approach, we exclusively targeted VTA neurons projecting to the NAcc (in the VTA-NAcc group) and prevented coactivation of VTA-DMS neurons.

Our study revealed BOLD responses which were considerably stronger compared to earlier studies employing optogenetics-fMRI in the same neural networks[29,31,33,39]. Chemogenetics offers a valuable alternative, since it bypasses potential optogenetics-related artifacts in BOLD signal caused by optic probe implantation, laser-induced tissue heating and unspecific light-induced activation of visual pathways[42,43]. Chemogenetics is easily applied, allows for selective activation of specific neuronal cell-types and projections, and can be straightforwardly combined with fMRI[44]; [45]. A disadvantage of chemogenetically induced activation, however, is the lack of control of the activation duration, for example due to incomplete understanding of CNO′s pharmacokinetic properties.

Recently, Lee et al. showed that activation of direct and indirect pathway MSNs results in opposing brain-wide responses[31]. They specifically targeted D1 or D2 receptor-expressing neurons using optogenetics and, with fMRI, confirmed the long-standing hypothesis that the direct and indirect pathways exert antagonistic control over neural networks. Our results nicely match the results described by Lee and colleagues, and corroborate the potential of phMRI to detect these defined pathways. The robust BOLD signal responses detected in our study illustrate the suitability and potential of DREADD-technology when combined with functional neuroimaging.

Stable functional connectivity

Despite the clear detection of chemogenetically induced BOLD responses with phMRI, rs-fMRI revealed no significant changes in inter- and intrahemispheric functional connectivity between mesocorticolimbic ROIs. This result suggests that chemogenetic activation of specific pathways only affects activity of the targeted areas and leaves functional connectivity unaffected. Although this may appear as a discrepancy, the underpinnings of brain activation and functional connectivity are conceptually different. Brain activation reflects an external stimulus-induced increase in neuronal activity (measured by model-fitting for phMRI), whereas functional connectivity reflects intrinsic spontaneous neuronal signal synchronization (measured from interregional temporal correlation for rs-fMRI). Although functional connectivity is a determining factor for network

activation, it does not consequentially change when networks are activated.

Our findings of an absent apparent effect of neuronal activation on functional connectivity seem in contrast with results from Ferenczi et al (2016) who reported that an optogenetically induced increase in excitability of mPFC neurons led to significant modulation of resting state networks. Differences in stimulation paradigm, neuronal signaling and awake vs. anesthetized may explain the dissimilar effects on functional connectivity. Ferenczi et al. stimulated predominantly excitatory glutamatergic pyramidal neurons in the mPFC using optogenetics in awake rats and used a different rs-fMRI protocol. They induced neuronal activation directly before the rs-fMRI acquisition, whereas our rs-fMRI data were acquired 1 h after CNO injection. This may have weakened a possible effect on functional connectivity in our study. However, our phMRI data and previous behavioral data[23] indicate that DREADD-induced neuronal activation persists for more than an hour. Although fMRI in awake rats may allow for better translation to human fMRI data, the use of anesthetized animals enabled us to specifically study the causal effects of chemogenetically induced activation, without interference of conscious processing, arousal state, stress or pain.

Conclusions

Our proof-of-principle study demonstrates that DREADD-phMRI offers a potent new tool to assess large-scale network activity – at whole-brain level – in response to activation of specific neuronal pathways – at cellular level. We showed that activation of mesocorticolimbic projection neurons triggered network activity patterns that provided new insights in the involvement of the direct and indirect pathways. Because of the relative ease of use and physiological nature of the induced neuronal activation, we envision a broad range of applications for DREADD-phMRI. The potential to modulate and monitor activity of neuronal circuits with DREADD-phMRI provides a novel tool to bridge the gap between fundamental neuroscience and (human) neuroimaging studies, giving better insights in the functioning and dysfunctioning of neural networks.

ACKNOWLEDGMENTS

This work was supported by the European Union Seventh Framework Program (FP/2007-2013) [grand number 607310 (Nudge-it)], and by the Netherlands Organization for Scientific Research [NWO-VICI 016.130.662]. The funding sources had no involvement in the collection, analysis, or interpretation of the data, nor in the writing or submission of this article. We thank Caroline van Heijningen for assistance on immunohistochemistry and Gerard van Vliet for technical assistance.

REFERENCES

1. Deisseroth, K. Optogenetics : 10 years of microbial opsins in neuroscience. Nat. Neurosci. Hist. Comment. 18, 1213–1225 (2015).
2. Urban, D. J. & Roth, B. L. DREADDs (Designer Receptors Exclusively Activated by Designer Drugs): Chemogenetic Tools with Therapeutic Utility. Annu. Rev. Pharmacol. Toxicol. 55, 399–417 (2015).
3. Armbruster, B. N., Li, X., Pausch, M. H., Herlitze, S. & Roth, B. L. Evolving the lock to fit the key to create a family of G protein-coupled receptors potently activated by an inert ligand. Proc. Natl. Acad. Sci. U. S. A. 104, 5163–5168 (2007).
4. Boyden, E. S., Zhang, F., Bamberg, E., Nagel, G. & Deisseroth, K. Millisecond-timescale, genetically targeted optical control of neural activity. Nat. Neurosci. 8, 1263–1268 (2005).
5. Boender, A. J. et al. Combined use of the canine adenovirus-2 and DREADD-technology to activate specific neural pathways in vivo. PLoS One 9, e95392 (2014).
6. Wang, G. J. et al. Decreased dopamine activity predicts relapse in methamphetamine abusers. Mol. Psychiatry 17, 918–925 (2012).
7. Malik, S., McGlone, F., Bedrossian, D. & Dagher, A. Ghrelin modulates brain activity in areas that control appetitive behavior. Cell Metab. 7, 400–409 (2008).
8. Breiter, H. C. et al. Acute effects of cocaine on human brain activity and emotion. Neuron 19, 591–611 (1997).
9. Schultz, W. Updating dopamine reward signals. Curr. Opin. Neurobiol. 23, 229–238 (2013).
10. van Zessen, R., van der Plasse, G. & Adan, R. A. H. Contribution of the mesolimbic dopamine system in mediating the effects of leptin and ghrelin on feeding. Proc. Nutr. Soc. 71, 435–445 (2012).
11. Wise, R. A. Dopamine, learning and motivation. Nat. Rev. Neurosci. 5, 483–494 (2004).
12. Salamone, J. D. & Correa, M. The mysterious motivational functions of mesolimbic dopamine. Neuron 76, 470–485 (2012).
13. Rogers, R. D. The roles of dopamine and serotonin in decision making: evidence from pharmacological experiments in humans. Neuropsychopharmacology 36, 114–132 (2011).
14. Humphries, M. D. & Prescott, T. J. The ventral basal ganglia, a selection mechanism at the crossroads of space, strategy, and reward. Prog. Neurobiol. 90, 385–417 (2010).

15. Russo, S. J. & Nestler, E. J. The brain reward circuitry in mood disorders. Nat. Rev. Neurosci. 14, 609–625 (2013).
16. Kenny, P. J., Voren, G. & Johnson, P. M. Dopamine D2 receptors and striatopallidal transmission in addiction and obesity. Curr. Opin. Neurobiol. 23, 1–4 (2013).
17. Richard, J. M. & Berridge, K. C. Nucleus accumbens dopamine/glutamate interaction switches mode to generate desire versus dread: D1 alone for appetitive eating but D1 and D2 together for fear. Jounal Neurosci. 31, 12866–12879 (2012).
18. Kupchik, Y. M. et al. Coding the direct/indirect pathways by D1 and D2 receptors is not valid for accumbens projections. Nat. Neurosci. 18, 1230–1232 (2015).
19. Dijkhuizen, R. M. & Nicolay, K. Magnetic resonance imaging in experimental models of brain disorders. J. Cereb. Blood Flow Metab. 23, 1383–1402 (2003).
20. Honey, G. & Bullmore, E. Human pharmacological MRI. Trends Pharmacol. Sci. 25, 366–374 (2004).
21. Leslie, R. A. & James, M. F. Pharmacological magnetic resonance imaging: a new application for functional MRI. Trends Pharmacol. Sci. 21, 314–318 (2000).
22. Jenkins, B. G. Pharmacologic magnetic resonance imaging (phMRI): Imaging drug action in the brain. Neuroimage 62, 1072–1085 (2012).
23. Boekhoudt, L. et al. Does activation of midbrain dopamine neurons promote or reduce feeding? Int. J. Obes. 1–34 (2017). doi:10.1038/ijo.2017.74
24. Paxinos, G. & Watson, C. The rat brain in stereotaxic coordinates. (Academic Press, 2005).
25. Verma, S. P. & Quiroz-Ruiz, A. Critical values for 22 discordancy test variants for outliers in normal samples up to sizes 100, and applications in science and engineering. Rev. Mex. Ciencias Geol. 23, 302–319 (2006).
26. Meredith, G. E., Baldo, B. A., Andrezjewski, M. E. & Kelley, A. E. The structural basis for mapping behavior onto the ventral striatum and its subdivisions. Brain Struct. Funct. 213, 17–27 (2008).
27. Cousins, M. S., Sokolowski, J. D. & Salamone, J. D. Different effects of nucleus accumbens and ventrolateral striatal dopamine depletions on instrumental response selection in the rat. Pharmacol. Biochem. Behav. 46, 943–951 (1993).
28. Ikemoto, S. Ventral Striatal Anatomy of Locomotor Activity Induced By Cocaine , D -Amphetamine , Dopamine and D 1 / D 2 Agonists 1. 113, 939–955 (2002).

29. Lohani, S., Poplawsky, A. J., Kim, S.-G. & Moghaddam, B. Unexpected global impact of VTA dopamine neuron activation as measured by opto-fMRI. Mol. Psychiatry 00, 1–10 (2016).
30. Lee, J. H. et al. Global and local fMRI signals driven by neurons defined optogenetically by type and wiring. Nature 465, 788–792 (2010).
31. Lee, H. J. et al. Activation of Direct and Indirect Pathway Medium Spiny Neurons Drives Distinct Brain-wide Responses. Neuron 91, 1–13 (2016).
32. Domingos, A. I. et al. Leptin regulates the reward value of nutrient. Nat. Neurosci. 14, 1562–1568 (2011).
33. Voss, H. U., Ballon, D. J. & Domingos, A. I. Neuronal and hemodynamic source modeling of optogenetic BOLD signals. 2011 IEEE Signal Process. Med. Biol. Symp. 1–6 (2011). doi:10.1109/SPMB.2011.6120104
34. Groenewegen, H. J. Organization of the Afferent Connections of the Mediodorsal Thalamic Nucleus in the Rat, Related To the Mediodorsal Prefrontal Topography. Neuroscience 24, 379–431 (1988).
35. Ikemoto, S. Dopamine reward circuitry: two projection systems from the ventral midbrain to the nucleus accumbens-olfactory tubercle complex. Brain Res Rev. 56, 27–78 (2007).
36. Groenewegen, H. J., Berendse, H. W. & Haber, S. N. Organization of the output of the ventral striatopallidal system in the rat: Ventral pallidal efferents. Neuroscience 57, 113–142 (1993).
37. Lee, J. H. et al. Global and local fMRI signals driven by neurons defined optogenetically by type and wiring. Nature 465, 788–792 (2010).
38. Desai, M. et al. Mapping brain networks in awake mice using combined optical neural control and fMRI. J. Neurophysiol. 105, 1393–1405 (2011).
39. Ferenczi, E. A. et al. Prefrontal cortical regulation of brainwide circuit dynamics and reward-related behavior. Science 351, aac9698-1-aac9698-12 (2016).
40. Decot, H. K. et al. Coordination of Brain Wide Activity Dynamics by Dopaminergic Neurons. Neuropsychopharmacology 42, 1–32 (2016).
41. Boekhoudt, L. et al. Chemogenetic activation of dopamine neurons in the ventral tegmental area, but not substantia nigra, induces hyperactivity in rats. Eur. Neuropsychopharmacol. 26, 1784–1793 (2016).
42. Christie, I. N. et al. fMRI response to blue light delivery in the naïve brain: Implications for combined optogenetic fMRI studies. Neuroimage 66, 634–641 (2013).
43. Schmid, F. et al. True and apparent optogenetic BOLD fMRI signals. Magn. Reson. Med. 00, 1–11 (2016).

44. Gozzi, A. et al. A neural switch for active and passive fear. Neuron 67, 656–666 (2010).
45. Baslow, M. H. et al. Stimulation-induced transient changes in neuronal activity, blood flow and N-acetylaspartate content in rat prefrontal cortex: a chemogenetic fMRS-BOLD study. NMR Biomed. 29, 1678–1687 (2016).

SUPPLEMENTARY FIGURES

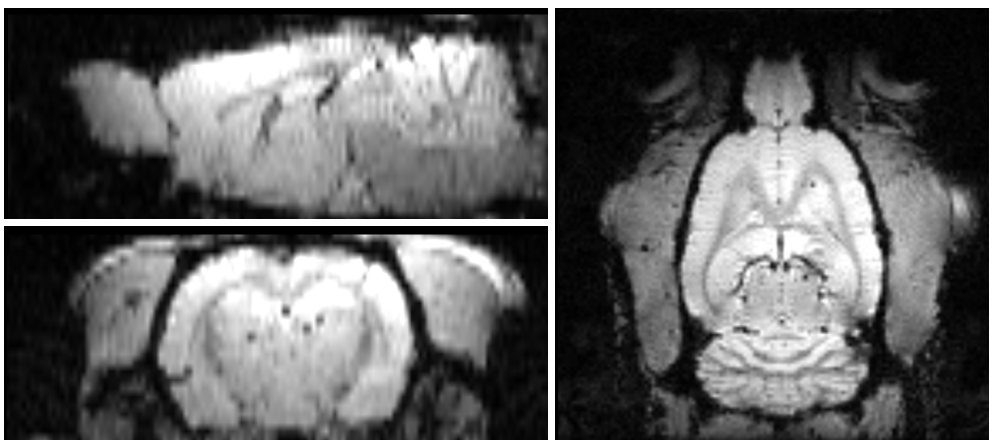

Supplementary Figure S1. Examples of GEMS (phMRI) images of a rat brain. Images show sections in sagittal, coronal, and axial orientation.

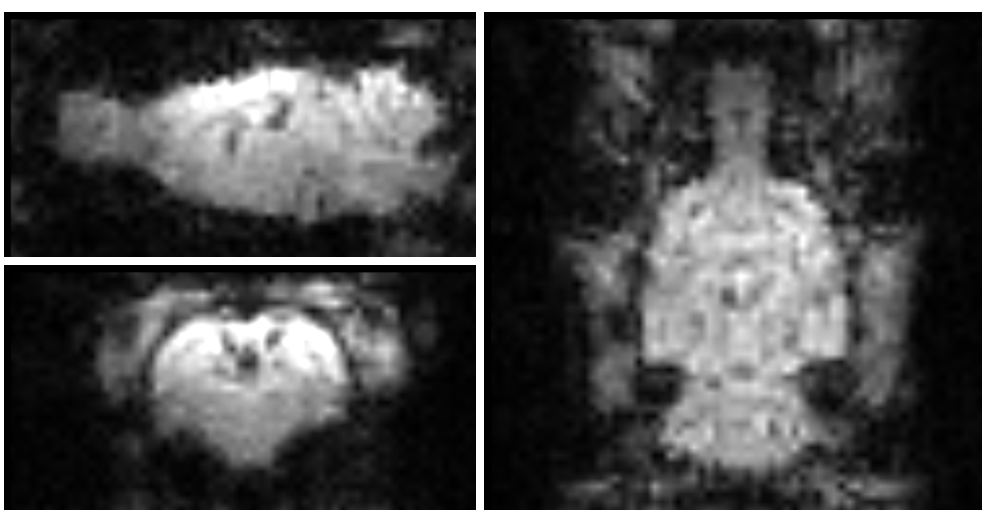

Supplementary Figure S2. Examples of gradient echo EPI (rs-fMRI) images of a rat brain. Images show sections in sagittal, coronal, and axial orientation.

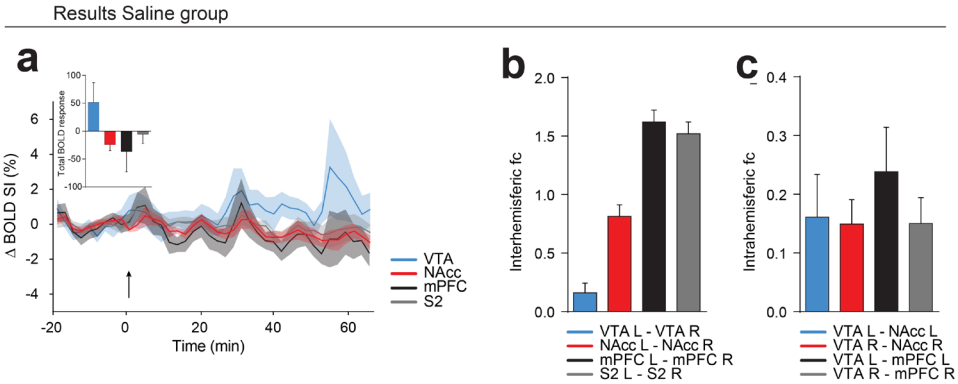

Supplementary Figure S3. Stable BOLD signal time-courses and functional connectivity in the Saline group. (a) No changes in the BOLD signal time-course were detected in the VTA, NAcc, mPFC, and S2 (mean ± SEM) in the Saline group. CNO was injected after 21 minutes of baseline scanning (arrow). Changes in BOLD signal intensity are presented as percentage change from baseline. The inset shows the total BOLD response over the entire phMRI time-course. (b) Interhemispheric functional connectivity (mean ± SEM) between bilateral ROIs. No statistically significant differences in interhemispheric fc were found between the Saline group and the Sham control group (see also Figure 3). (c) Intrahemispheric functional connectivity (mean ± SEM) between the left/right VTA and the left/right NAcc or mPFC. No statistically significant differences in intrahemispheric fc were found between the Saline group and the Sham control group (see also Figure 3). Functional connectivity is expressed as the Fisher-transformed correlation coefficient (z'). Δ BOLD SI (%): delta BOLD signal intensity in percentages; fc: functional connectivity; mPFC: medial prefrontal cortex; NAcc: nucleus accumbens; S2: secondary somatosensory cortex; VTA: ventral tegmental area.

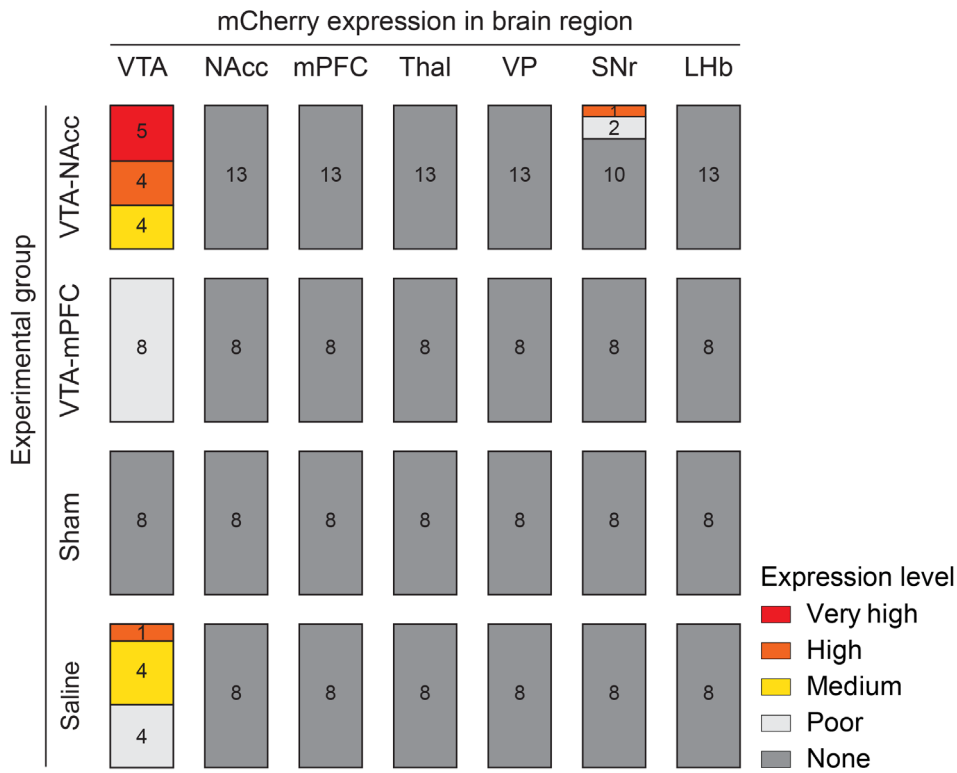

Supplementary Figure S4. DREADD-expression on neuronal somas. The degree of DREADD-expression was scored on an ordinal scale by a blinded co-author. The VTA in all experimental groups, except for the Sham group, was the only brain region with DREADD expression on cell bodies. Except for some expression in the SNr in three animals in the VTA-NAcc group, no expression of DREADDs was found in non-targeted regions. LHb: lateral habenula; mPFC: medial prefrontal cortex; NAcc: nucleus accumbens; SNr: substantia nigra pars reticulate; Thal: thalamus; VP: ventral pallidum; VTA: ventral tegmental area.

Chapter 4

Limbic control over the homeostatic need for sodium

Jeroen P.H. Verharen[1,2,4], Theresia J.M. Roelofs[1,4], Shanice Menting-Henry[1], Mieneke C.M. Luijendijk[1], Louk J.M.J. Vanderschuren[2], Roger A.H. Adan[1,3]

[1] Brain Center Rudolf Magnus, Department of Translational Neuroscience, University Medical Center Utrecht, Utrecht, The Netherlands.
[2] Department of Animals in Science and Society, Division of Behavioural Neuroscience, Faculty of Veterinary Medicine, Utrecht University, Utrecht, The Netherlands.
[3] Institute of Physiology and Neuroscience, Sahlgrenska Academy at the University of Gothenburg, Gothenburg, Sweden.
[4] These authors contributed equally.

Published in Scientific Reports 9:1050 (2019)

The homeostatic need for sodium is one of the strongest motivational drives known in animals. Although the brain regions involved in the sensory detection of sodium levels have been relatively well mapped, data about the neural basis of the motivational properties of salt appetite, including a role for midbrain dopamine cells, have been inconclusive. Here, we employed a combination of fiber photometry, behavioral pharmacology and c-Fos immunohistochemistry to study the involvement of the mesocorticolimbic dopamine system in salt appetite in rats. We observed that sodium deficiency affected the responses of dopaminergic midbrain neurons to salt tasting, suggesting that these neurons encode appetitive properties of sodium. We further observed a significant reduction in the consumption of salt after pharmacological inactivation of the nucleus accumbens (but not the medial prefrontal cortex), and microstructure analysis of licking behavior suggested that this was due to decreased motivation for, but not appreciation of salt. However, this was not dependent on dopaminergic neurotransmission in that area, as infusion of a dopamine receptor antagonist into the nucleus accumbens did not alter salt appetite. We conclude that the nucleus accumbens, but not medial prefrontal cortex, is important for the behavioral expression of salt appetite by mediating its motivational component, but that the switch in salt appreciation after sodium depletion, although detected by midbrain dopamine neurons, must arise from other areas.

INTRODUCTION

In order to obtain all nutrients necessary for survival, organisms need to make adaptive food choices based on their homeostatic needs[1,2]. For example, when an organism's body senses a shortage of a certain nutrient, it may, consciously or not, choose foods that will replenish this need[2,3]. Of all the nutrients, a deficiency in sodium is one of the strongest homeostatic drives known in animals, evoking intense cravings for salty foods after salt deprivation, which has been consistently reported in a wide range of species[4,5]. Although sodium is abundant in modern Western diets, it is relatively scarce in natural resources, which has likely contributed to the development of this homeostatic drive[6,7].

A remarkable observation that illustrates this innate drive for sodium is that rats normally experience a hypertonic sodium solution as aversive, but that this solution is experienced as positive and consumed in high amounts when rats are low on sodium, a phenomenon known as salt appetite[4,5,8,9]. Such a switch in the experience of a flavor from aversive to appetitive, driven by a homeostatic need, is a prime example of how adaptive the interaction between sensory and reward systems can be in order to maintain homeostasis and ensure survival.

Elucidating the mechanisms that underlie this switch may therefore provide interesting insights into the flexibility of brain circuits that mediate reward.

A variety of brain areas has been shown to be involved in salt appetite. Not surprisingly, this includes brain structures involved in the sensory processing of taste, such as the parabrachial nucleus[10] and the nucleus of the solitary tract[11,12]. Other brain areas implicated in salt appetite are the lateral and paraventricular nucleus of the hypothalamus, the preoptic area, the subfornical organ, the central amygdala and the bed nucleus of the stria terminalis (for a review see ref. [13]). Given its role in processing rewarding and aversive stimuli[14,15], a logical candidate for the mediation of salt appetite is the mesocorticolimbic dopamine (DA) system, consisting of DA neurons in the ventral tegmental area (VTA) projecting to the nucleus accumbens (NAc) and medial prefrontal cortex (mPFC). However, data about the involvement of this circuit in salt appetite has been inconclusive. On the one hand, a total ablation of the VTA[16] or DA terminals in the entire brain[17], as well as the infusion of DA receptor agonists or antagonists in the nucleus accumbens[18] does not affect salt appetite, suggesting that motivation for salt bypasses the mesoaccumbens DA pathway. On the other hand, it has been observed that infusion of a delta-opioid receptor antagonist into the VTA decreases salt appetite[18], and that a sodium-depleted state is associated with decreased DA transporter activity[19] and altered spine morphology[20] in the nucleus accumbens. A recent study demonstrated, using fast-scan cyclic voltammetry, that tasting a sodium solution evoked phasic dopamine release in the rat nucleus accumbens shell after sodium deprivation, but not under normal conditions[21]. Furthermore, this study showed that hindbrain neurons projecting to the VTA displayed increased c-Fos expression after salt deprivation. Another recent study showed that optogenetic or chemogenetic activation of VTA DA neurons in mice reduced intake of a high-concentration (but not low-concentration) salt jelly, while chemogenetic inhibition of these same neurons had no effect on salt intake[22].

In this study, we attempted to contribute to the understanding of the involvement of the mesocorticolimbic DA system in salt appetite. Towards this aim, we combined fiber photometry, behavioral pharmacology and c-Fos immunohistochemistry to study *in vivo* VTA DA neuron dynamics during sodium deficiency, and the importance of the NAc and mPFC, the two major output regions of these neurons, for salt appetite. By employing a microstructural analysis of licking behavior, we tried to discern effects of manipulations of the mesocorticolimbic system on the motivation for versus the appreciation of salt. We hypothesized that VTA DA neurons may respond differently to salty solutions during a normal versus sodium-depleted state, and that these changes in DA cell

responsiveness are important for the expression of behaviors associated with salt appetite.

METHODS

Animals

All experiments were approved by the Animal Ethics Committee of the Utrecht University, and were conducted in agreement with Dutch (Wet op de Dierproeven, revised 2014) and European regulations (Guideline 86/609/EEC; Directive 2010/63/EU).

A total of 46 male rats were used in the experiments. Male Long-Evans rats (Rj:Orl; Janvier Labs, France) were used for the micro-infusion experiments (n = 14), male Wistar rats (Crl:WU; Charles River, Germany) were used for c-Fos analysis (n = 22), and TH::Cre transgenic rats (bred in-house by crossing heterozygous TH::Cre+/- male rats with wild type Rj:Orl mates) were used for fiber photometry (n = 6 TH::Cre+ injected with DIO-GCaMP6s and, n = 4 TH::Cre- injected with eYFP). All rats weighted ~250 g at the start of the experiments, were individually housed under controlled temperature (20°C) conditions, with a 12h light/dark cycle (lights off at 7:00 a.m.), and received a wood block as cage enrichment. When not being tested, animals had *ad libitum* access to demineralized water and a 0.45 M sodium chloride solution (or a 5% sucrose solution, prior to the sucrose intake experiment) and standard chow (Special Diet Service, United Kingdom) in the home cage. Preceding sodium intake test days, animals were salt deprived, during which they only had access to demineralized water and a sodium-deficient chow (Teklad Custom Diet, Envigo, United States). Preceding the sucrose intake test days, animals were food restricted, during which they had no access to chow or the sucrose solution for 24 h.

Surgeries

Anesthesia was induced using a mixture of 0.315 mg/kg fentanyl and 10 mg/kg fluanisone (Hypnorm, Janssen Pharmaceutica, Belgium) that was injected intramuscularly. Animals were placed in a stereotaxic apparatus (David Kopf Instruments, USA) and an incision was made along the skull midline.

For fiber photometry experiments, the same surgical procedure was applied as described previously[15]. In brief, TH::Cre rats were injected with 1 µl of AAV5-FLEX-hSyn-GCaMP6s (University of Pennsylvania Vector Core) at a titer of 1×10^{12} particles/ml unilaterally into the right VTA (–5.40 mm AP, ±2.20 mm ML from Bregma, at an angle of 10°, and –8.90 mm DV from the skull). A 400 µm implantable fiber was lowered to 0.1 mm above the injection site and attached with dental cement.

For micro-infusion experiments, 26-gauge stainless steel guide cannulas (Plastics One, USA) were implanted above the NAc (two single cannulas; +1.20 mm anteroposterior (AP), ±2.80 mm mediolateral (ML) from Bregma, at an angle of 10°, and the guide was lowered to -6.80 mm dorsoventral (DV) from the skull) or the mPFC (one double cannula with a width of 1.2 mm; +3.20 mm AP, ±0.60 mm ML from Bregma, and the guide was lowered to -2.60 mm DV from the skull). Cannulas were secured to the skull with screws and dental cement, and dummy injectors were placed inside the cannulas to prevent blockage. Single injectors for the NAc protruded 0.5 mm beyond the guides (targeting -7.30 mm DV from the skull) and double injectors for the mPFC protruded 1 mm beyond the guides (targeting -3.50 mm DV from the skull).

To prevent dehydration of the rats, they were given 10 mL of saline subcutaneous (s.c.) after surgery. Starting on the day of surgery, rats were given carprofen as analgesia (s.c. injection of 5 mg/kg per day for 3 days). All rats were allowed to recover from surgery for at least 7 days before behavioral testing began.

Sodium deprivation

The sodium deprivation protocol has been adapted from ref. [21]. Before the sodium deprivation procedure, all cages were cleaned to prevent the rats from repleting their sodium levels by eating their own feces. Sodium depletion was induced by an s.c. injection of the diuretic drug furosemide (20 mg/kg dissolved in sterile H_2O, given in 2 injections of 10 mg/kg 1 hour apart). Control animals received s.c. saline injections. In the 24h that followed, sodium-depleted animals received sodium-free chow (Teklad Custom Diet, Envigo, United States), and control animals received regular chow (Special Diet Service, United Kingdom). In the first three hours after the first furosemide injection, animals had no access to water, to confirm success of the procedure by observing a body weight loss. After these 3 hours, all animals received demineralized water, which was especially heavily consumed by the animals that were previously injected with furosemide. 24 hours after the first furosemide injection, animals were given a bottle containing a 0.45M NaCl solution, and intake of this solution (as well as intake of the demineralized water, which was already present in the cage) was monitored for 1h using mechanical lickometers that were present in the home cage. Animals were always tested in a counterbalanced fashion, so that half of the animals were first tested in a control state, i.e., 24 h after s.c. saline injection, and the other half in a sodium-depleted state, i.e., 24 h after s.c. furosemide injection. Drinking behavior was assessed as cumulative intake (number of licks), number of licking bouts, and licks per licking bout for both the intake of demineralized water and the 0.45M NaCl solution. A minimum of 5 licks was considered a bout,

which ended when the animals did not lick for at least 1min. Bout analysis was performed in Matlab R2014a (MathWorks Inc., United States).

In vivo fiber photometry

Technical details about our fiber photometry setup have been published elsewhere[15]. In brief, animals were injected with a Cre-dependent GCaMP6s in the right VTA, and a 400 µm fiber was secured 0.1mm dorsal of the injection site. Animals were connected to a 400 µm core fiber optic patch cable through which lock-in amplified blue LED light was delivered. Emission light was captured with a photoreceiver, digitized, and dF/F_0 values were computed with F_0 being defined as the mean of the middle 50% of values in the 30 seconds before each time point F.

Each rat was tested on the behavioral task twice, once in a salt-depleted state and once in a control state, and the task was conducted in operant conditioning chambers (Med Associates, USA). The chambers were equipped with one optical lickometer (delivering both solutions through the same spout), and on the other side of the chamber a house light and auditory tone generator. All animals were food restricted for 24h before the measurement, to increase the motivation for sucrose (making sure the animals lick during every trial).

In the task, a 5-second tone initiated the trial, and the first lick after tone offset triggered the fluid pump, which delivered a droplet of the solution over a period of 5s. If the animal did not make a lick within 5s after tone offset, no reward was obtained and the inter-trial interval of 30s commenced. If the animal did make a lick within 5s after tone offset, the pump delivered a 0.88M sucrose solution in 75% of the trials and a 0.30M NaCl solution in 25% of the trials (in random order). After the 5-second liquid delivery, a 30-second inter-trial interval separated the current trial from the onset of the next trial**.** No cue lights were used and the house light was turned on continuously to prevent the signal to be contaminated by lights from the environment. Individual trial responses were time-locked to the 5-second tone that started the trial and mean dF/F of trial responses to sucrose and of trial responses to sodium was calculated. The number of licks during the trials was assessed using the lickometers that were monitored by MedPC software. The task continued until the animal had made at least 80 trials.

Microinfusions

For the infusion experiments, n = 7 (NAc; all experiments performed in the same animals. see Fig. S3c) and n = 8 (mPFC) rats were used. Animals were habituated to the infusion procedure by infusing saline (0.5 µl/side) the day

before the first experiment. Rats were brought into a salt depleted state or in a control state, as described in the paragraph above, and 24 h later they received infusions with saline (1 µl/side for the NAc, 0.5 µl/side for the mPFC) or a mixture of baclofen (1nmol; Sigma-Aldrich, The Netherlands) and muscimol (0.1 nmol; Sigma-Aldrich, The Netherlands) dissolved in saline (1 µl/side for the NAc, 0.5 µl/side for the mPFC; based on the spread observed in ref. [23]). Furosemide vs saline injections and baclofen-muscimol vs saline infusions were performed in a Latin Square repeated measures design (each animal was tested 4 times). Testing of a single experiment was performed across ~2 weeks, as we allowed the animals to recover after every of the four measurements for at least 48 hours.

Drugs were infused at a rate of 0.5 µl/min, and the injectors were left in place for an additional 30 s after the infusion was complete to allow for diffusion of saline/baclofen-muscimol into the brain. After the infusion procedure, animals were placed back into their home cage, and a bottle with a 0.45 NaCl solution was given 5 minutes later. In the dopamine receptor antagonist infusion experiment, we used the same experimental procedure as in the pharmacological inactivation experiments, except that 25 µg of cis-(Z)-α-flupenthixol dihydrochloride (Sigma-Aldrich, The Netherlands) was infused, dissolved in 1 µl saline.

c-Fos analysis

For c-Fos analysis, 11 animals were brought into a salt-deprived state as described in the procedure above, and 11 animals were used as control animals. 48 hours after the first furosemide injection, all 22 rats received an i.p. injection of sodium pentobarbital and perfused with phosphate-buffered saline (PBS) followed by 4% paraformaldehyde (PFA) in PBS. After extraction, brains were post-fixated in 4% PFA in PBS at 4 °C for 24 h, and stored in a 30% sucrose in PBS solution at 4 °C. For immunohistochemical quantification of the number of activated neurons, brains were stained for the immediate early gene c-Fos. Brain slices (50 µm) were blocked in 3% normal goat serum (NGS) and 0.5% Triton-X-100 in PBS. Slices were incubated overnight in primary antibody rabbit anti-c-Fos (1:1000, Cell Signaling) in 3% NGS in PBS at room temperature. Subsequently, slices were incubated for 2 h in biotinilated antibody goat anti-rabbit (1:200, Vector labs) in 3% NGS in PBS, and afterwards in Biotin/Avidin (1:1000, Vectastain) in PBS for 1 h. This complex was visualized by exposing the slices for 5 min to a solution of liquid DAB (3,3'-Diaminobenzidine, Dako) and 10% nickel ammonium sulphate. All sections were dehydrated using increasing series of ethanol, cleared in xylene and coverslipped with Entallan (Merck Millipore). Sections were photographed by a brightfield microscope with a 10X lense (AxioImager M2). Slices comprising the VTA were manually aligned in illustrator, and ImageJ (Version 1.48 v) was used

to extract the coordinates of c-Fos positive neurons by applying a bandpass filter over the Fourier-transformed image, followed by a search for maximum intensity points. Heatmaps of c-Fos expression were generated based on the coordinates of the c-Fos positive cells using MATLAB (The MathWorks Inc., version R2014a).

Exclusion criteria

One animal was excluded from c-Fos analysis because brain slices were not of sufficient quality. One additional animal was excluded from c-Fos analysis because the brain slices did not show any expression. One animal was excluded from the sucrose intake (after food restriction) experiment, water intake (after water deprivation) experiment and dopamine receptor antagonist infusion experiment, because it was suspected to develop diabetes (it drank excessive amounts of water and sucrose water, and the bedding was continuously wet).

Data analysis and statistics

Data analysis was performed with MATLAB, statistical analysis using GraphPad Prism (GraphPad Software Inc., version 6.0). Statistical comparisons were made using a two-tailed t-test for a single comparison (c-Fos experiment) and a (repeated measures) ANOVA was used for multiple comparisons (all other experiments), followed by a t-test with Šidák's multiple comparisons correction when a significant interaction effect ($P < .05$) was found between the two factors of the ANOVA. Bar graphs represent the mean ± standard error of the mean. In all figures: ns not significant, $^{*}P < 0.05$, $^{**}P < 0.01$, $^{***}P < 0.001$, $^{****}P < 0.0001$.

RESULTS

No changes in c-Fos expression in DA nuclei after sodium deprivation

In an attempt to substantiate the findings of ref.[22], that showed that sodium deprivation did not change baseline activity of VTA DA neurons, we analyzed c-Fos immunoreactivity in a coronal slice of the midbrain that included the VTA and substantia nigra (Fig. 1a; $n = 21$). Based on a typical brain slice, we created a template on which we overlayed all the other slices in order to perform whole-slice automated cell counting. A visual sliding-window analysis revealed fairly similar levels of c-Fos expression between animals in a sodium-depleted state (induced by treatment with the diuretic furosemide; see Methods) versus a control state around these nuclei (Fig. 1b). Indeed, region-of-interest analysis showed no significant differences in the number of c-Fos positive cells in the VTA (Fig. 1c), the substantia nigra pars compacta (SNc; Fig. 1d), or the substantia nigra pars reticulata (SNr; Fig. 1e). Together, these data support the finding that baseline activity of neurons in midbrain DA nuclei was not altered by sodium

deprivation.

Dopamine neurons encode a switch in sodium appreciation

To study how VTA DA neurons respond to the taste of salt during normal and low levels of sodium in the body, we injected a viral vector carrying Cre-dependent GCaMP6s into the VTA of TH::Cre rats (Supplementary Fig. 1) and measured VTA DA neuron dynamics using fiber photometry during a Pavlovian conditioning task. In this task (Fig. 2a), rats (n = 6) learned that a 5-second auditory tone preceded the delivery of a nutritional solution, which was usually a tasty sucrose solution (3 out of 4 trials), but sometimes a NaCl solution (1 out of 4 trials). We tested the responses of the animals to these solutions on two

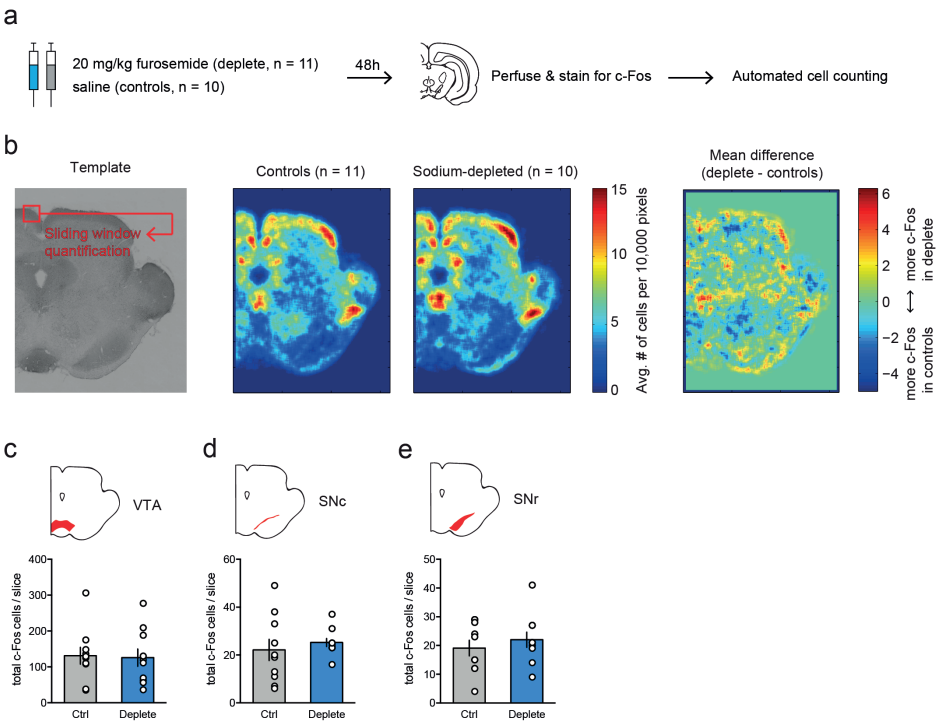

Figure 1. c-Fos analysis of midbrain slices after sodium deprivation. a) Experimental design. b) From left to right: a coronal slice of the midbrain that included the VTA and substantia nigra was used to create a template on which the other midbrain slices were overlayed in order to perform whole-slice automated cell counting – average c-Fos density in control animals (n=11) – average c-Fos density in sodium-depleted animals (n=10) – mean difference in c-Fos expression between controls and depleted animals indicating similar levels of c-Fos expression. c-e) Region-of-interest analysis showed no significant differences in the number of c-Fos positive cells in the VTA (c; t18 = 0.15, p = 0.88), the substantia nigra pars compacta (SNc; d; t18 = 0.64, P = 0.53), or the substantia nigra pars reticulata (SNr; e; t18 = 0.75, P = 0.46).

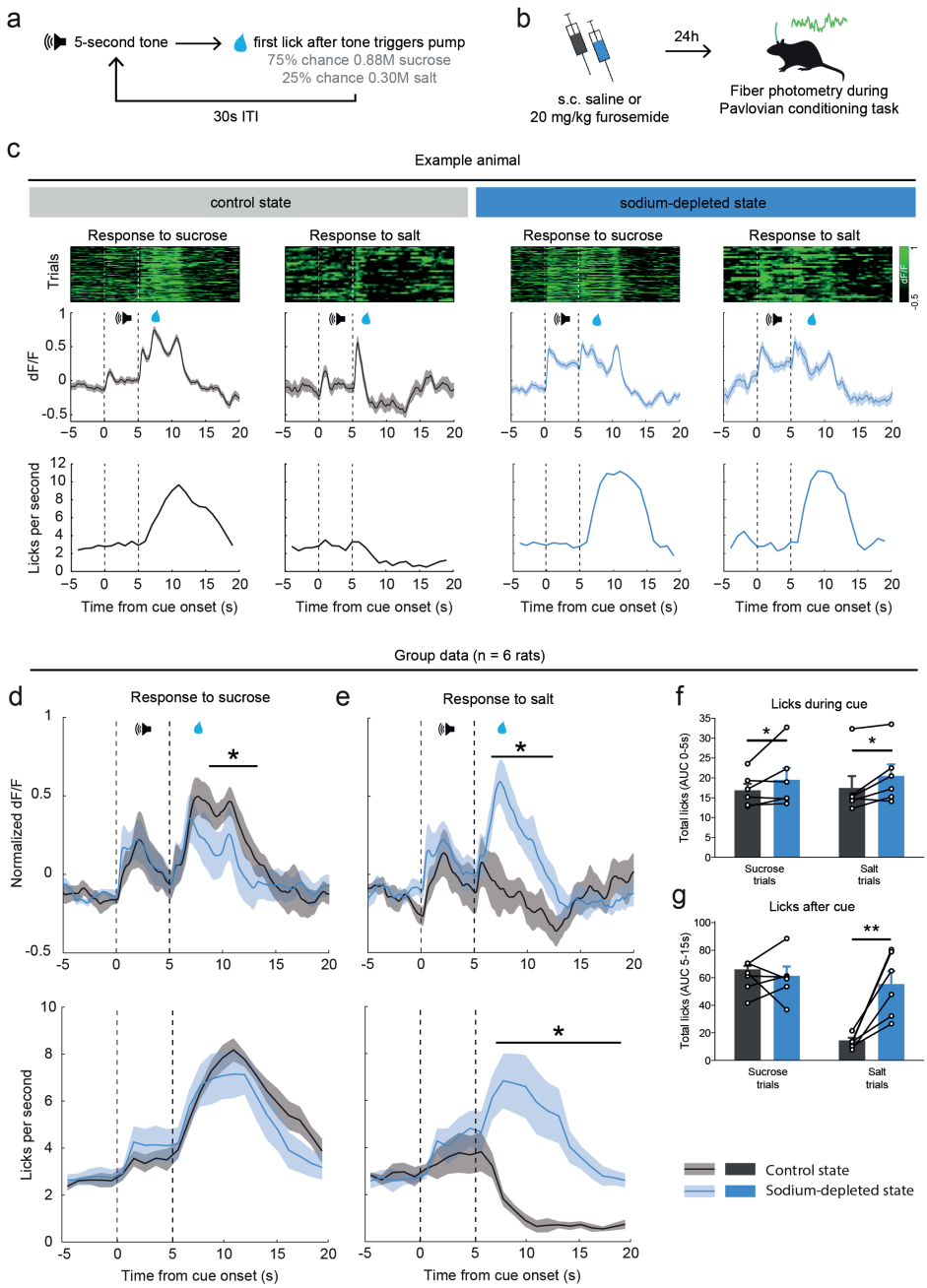

Figure 2. In vivo fiber photometry of VTA DA neurons during sodium depletion. a) The Pavlovian conditioning task that was used for in vivo fiber photometry consisted of a five-second auditory tone followed by delivery of a nutritional solution, being either a sucrose solution (in 75% of trials) or a NaCl solution (in 25% of trials). Figure legend continues on next page.

Continuation of figure legend 2. A 30-second inter trial interval (ITI) separated the trial from the next auditory tone. b) Animals were tested twice; once after a subcutaneous (s.c.) saline injection, i.e. a control state, and once after a furosemide injection, i.e. a sodium-depleted state. Rats were tested after being in a specific state for 24 hours. c) Population responses of VTA DA neurons of an example animal (sampling rate 100 Hz). Shown are the control state (left) and sodium-depleted state (right). Reward was delivered for 5s after the first lick after cue offset (5s). d) (top panel) Sodium depletion decreased VTA DA neuron responses to sucrose (2-way repeated measures ANOVA, main effect of treatment, $F_{1,5} = 2.494$, $p = 0.1751$; treatment × time interaction effect, $F_{2499,12495} = 1.335$, $P < 0.0001$; * post-hoc test significant between 7.9 - 13.1 s post-stimulus). (bottom panel) ANOVA revealed no differences in the number of licks for sucrose between the two treatments (main effect of treatment, $F_{1,5} = 1.307$, $p = 0.3046$; treatment × time interaction effect, $F_{23,115} = 0.9798$, $P = 0.4963$). e) (top panel) Mean responses of all animals to salt indicated that sodium depletion increased VTA DA neuron response to salt (ANOVA, main effect of treatment, $F_{1,5} = 9.463$, $P = 0.0276$; treatment × time interaction effect, $F_{2499,12495} = 2.188$, $P < 0.0001$; * post-hoc test significant between 6.8 - 12.9 s post-stimulus). (bottom panel) Sodium depletion increased the number of licks for salt (ANOVA, main effect of treatment, $F_{1,5} = 10.13$, $P < 0.0001$; treatment × time interaction effect, $F_{23,115} = 10.13$, $P = 0.0016$; * post-hoc Sidak's test, significant 7-18s post-stimulus). f) Salt depletion increased the number of licks during the 5-second cue across both trial types (ANOVA, main effect of treatment, $F_{1,5} = 10.10$, * $P = 0.0246$; but no treatment × tastant interaction effect, $F_{1,5} = 0.03624$, $P = 0.8565$; and no main effect of tastant, $F_{1,5} = 0.6428$, $P = 0.4591$). g) Salt depletion increased the number of licks for salt, but not for sucrose (ANOVA, treatment × tastant interaction effect, $F_{1,5} = 19.93$, $P = 0.0066$; post-hoc Sidak's test, control vs depleted state: sucrose $t5 = 0.017$, $P = 0.9998$; salt $t5 = 6.297$, ** $P = 0.0030$).

occasions: once in a sodium-deficient state, 24h after injection with furosemide, and once under baseline conditions (Fig. 2b).

In the control state, animals vigorously licked for sucrose, but refrained from licking when a sodium solution was delivered, in line with our expectations that high-sodium concentrations are aversive to rats. Accordingly, VTA DA neuron population activity increased during the consumption of sucrose, while the delivery of salt resulted in sub-baseline levels of DA neuron activity. This is illustrated in both an example animal (Fig. 2c, left panel) as well as on a group level (Fig. 2d,e).

In the sodium-depleted state, animals showed increased licking during the reward-preceding cue, although this effect was numerically modest (Fig. 2f). In contrast, sodium depletion strongly increased the number of licks during the delivery of the salty solution, while the number of licks for sucrose was not dependent on the sodium state of the animals (Fig. 2g). The difference in licking for salt after sodium deprivation extends beyond the peaks in DA neuron activity, and this is especially driven by a long attenuation of licking behavior after salt exposure in the control state (Fig. 2e, bottom panels). In line with this appreciation of salt, we observed increased levels of VTA DA neuron activity in response to salt delivery (Fig. 2e), with responses that were even higher than those after sucrose delivery (compare Fig. 2d and e, blue curves). Although numerically more modest

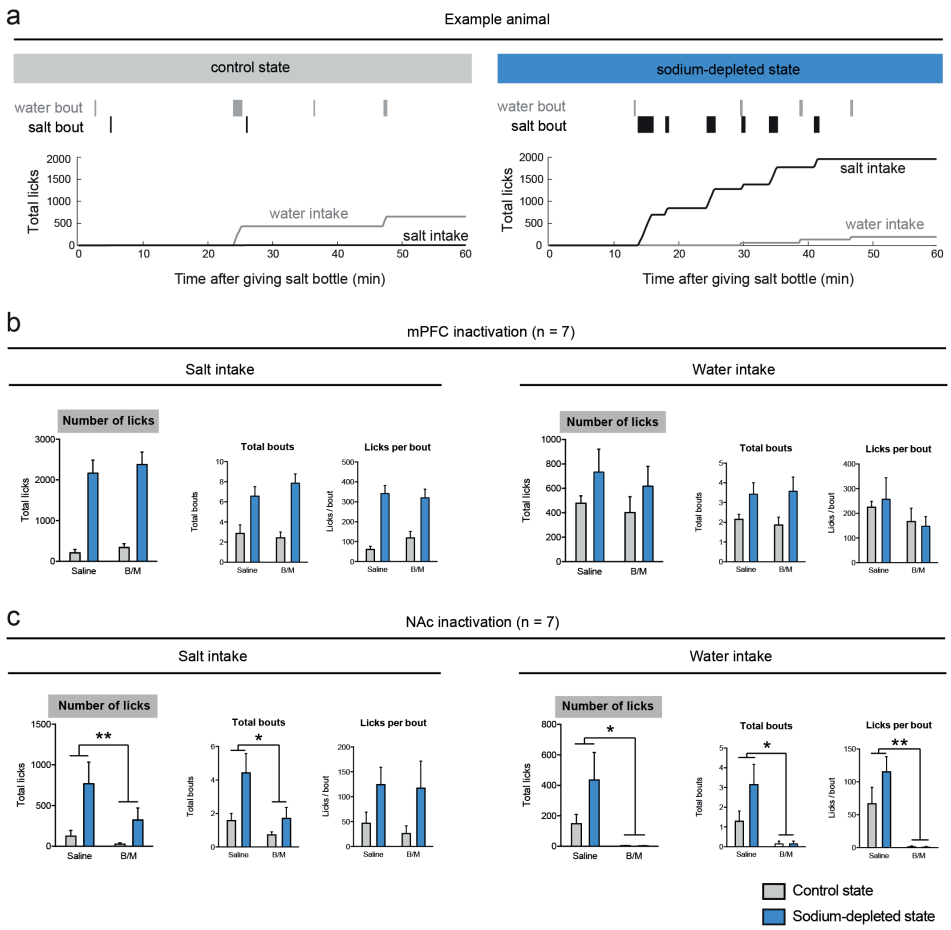

Figure 3. Effects of pharmacological inactivation of VTA target regions on salt appetite. a) Microstructure analysis of licking behavior in an example animal once in a control state (left) and once in a sodium-depleted state (right). At time = 0 min the salt bottle was given back to the animal and its drinking behavior was analyzed as number of licks (grey line for water intake, black line for salt intake). On the upper part of the graph, bout analyses for salt and water intake shows frequency and size of the bouts. b) Effect of mPFC inactivation on salt intake (left) and water intake (right). No main effect of mPFC inactivation by baclofen and muscimol (B/M) of interaction effect was detected. c) Effect of NAc inactivation on salt intake (left) and water intake (right). Inactivation of the NAc decreased sodium intake, which was driven by a decrease in the number of licking bouts. A significant main effect of state was detected for the number of sodium licking bouts, and a trend towards an effect of sodium depletion on the number of licks and bout size. No B/M × state interaction effects were observed. Inactivation of the NAc also abolished water consumption, as a main effect of B/M was found on the number of water licks, driven by effects on the number of bouts and licks per bout. A single asterisk annotation per graph indicates a main effect of B/M; see also the Supplementary statistics table. ** P < 0.01, * P < 0.05

than the changed DA neuron responsiveness to salt, we observed a lower DA neuron activation to sucrose during a salt-depleted state compared to the control state (Fig. 2d). Importantly, we observed no changes in fluorescent activity in animals that were injected with an activity-independent control fluorophore (n = 4; Supplementary Fig. 2), indicating that the observed fluorescent signals were driven by neuronal activity.

In sum, we show that a salty solution under normal conditions is considered aversive by rats, as shown by the termination of licking behavior and sub-baseline levels of VTA DA neuron activity, but that this same solution is considered appetitive in a sodium-depleted state, accompanied by vigorous licking for salt and large peaks in DA neuron activity.

Inactivation of NAc, but not mPFC, diminished drinking behavior without affecting salt appetite

To investigate the behavioral structure of salt appetite, we assessed intake of a 0.45M NaCl solution, as well as intake of demineralized water, by using mechanical lickometers present in the animals' home cages, which measured the numbers of licks per 12s bins (in a within-subjects, counterbalanced design; each animal was tested four times). To gain insight into the appetitive components of sodium appetite, we performed a microstructure analysis of licking behavior, calculating the number of licking bouts that animals made, as well as the size of each of these bouts (Fig. 3a). As expected, animals that were brought into a sodium-depleted state consistently consumed more of the sodium solution, which was driven by an increase in the frequency of licking bouts as well as the size of a licking bout (see Fig. 3 and 5). Note that these animals had ad libitum access to demineralized water, but had no access to salt in the 24h prior to the measurements.

To study the role of the two main VTA DA neuron output regions, the mPFC and NAc, in the regulation of salt appetite, we pharmacologically inactivated the mPFC and the NAc using micro-infusions of a mixture of the GABA receptor agonists baclofen and muscimol (B/M). Rats were brought in a sodium-depleted or a control state for 24h, after which they received infusions with either B/M or saline. Subsequently, animals received a 0.45M NaCl solution, in addition to a bottle of demineralized water that was already present in the cage.

We first assessed salt appetite upon mPFC inactivation (n = 7; Supplementary Fig. 3a). A two-way repeated measures ANOVA revealed increased consumption of the sodium solution in sodium-depleted animals (main effect of state), which was driven by an increase in the frequency of licking bouts as well as by the size of these bouts (Fig. 3b, left panels). Inactivation of the mPFC, however,

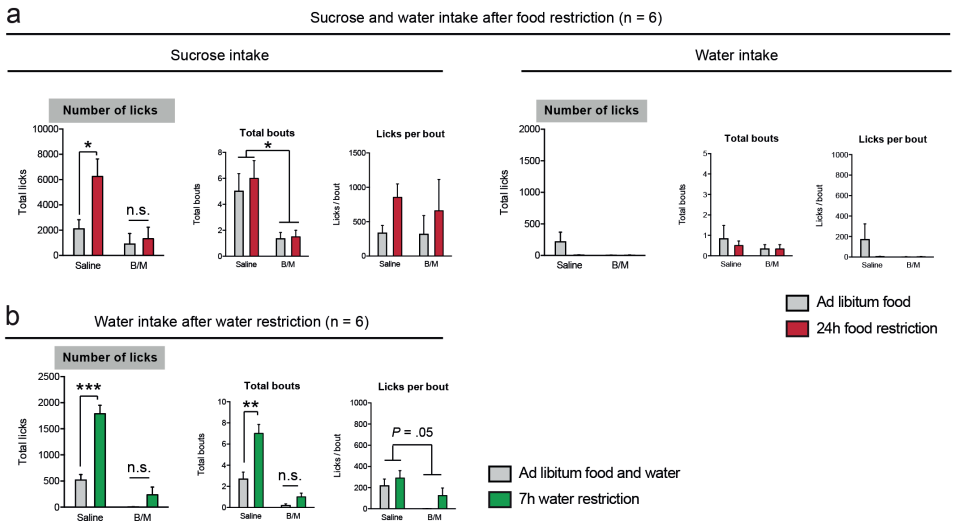

Figure 4. NAc inactivation reduced sucrose and water intake. a) Sucrose (left) and water (right) intake was analyzed when animals were in a food restricted state (red) or in an ad libitum-fed state (grey). A significant B/M × food restriction interaction effect on the number of licks for sucrose was found. Post-hoc tests Sidak's test revealed a significant increase in the number of licks due to food restriction after saline infusion (t5 = 4.77, P = 0.010), but not after B/M infusion (t5 = 0.48, P = 0.877). A decrease in the number of licking bouts was found, which indicates that the interaction effect was mainly driven by a decrease in motivation for sucrose. Food restriction increased the number of licks for sucrose, driven by an increase in licks per bout. Water intake was extremely low and no significant effects could be detected on water licking behavior. b) Water licking behavior was analyzed after water restriction. Water restriction increased the number of water licks, driven by an increase in number of licking bouts. NAc inactivation decreased overall water intake, as a significant main effect of B/M on the number of licks and the number of bouts were detected, as well as a trend towards a main effect of licks per bout. A significant B/M × water restriction interaction effect was observed of the number of licks for water which was driven by an increase in licking after saline infusion (t5 = 10.29, P = 0.0003) but not after B/M infusion (t5 = 1.87, P = 0.23) as revealed by post-hoc Sidak's tests. There was also a significant B/M × water restriction interaction effect on the number of bouts, driven by an increase in bouts after saline (t5 = 7.24, P = 0.0016), but not B/M (t5 = 1.39, P = 0.40) infusion.
A single asterisk annotation per graph indicates a main effect of B/M; a dual asterisk annotation in a graph denotes significance after post-hoc Sidak's test (performed because a significant B/M × restriction interaction was found); see also the Supplementary statistics table.*** P < 0.001, ** P < 0.01, * P < 0.05

did not impact consumption of the sodium solution (Fig. 3b, left panels), nor of demineralized water (Fig. 3b, right panels), as the ANOVA revealed no main effect of B/M or B/M × state interaction effect.

Inactivation of the NAc (n = 7; Supplementary Fig. 3b,c) significantly decreased sodium intake, as the two-way repeated measures ANOVA revealed a main effect of B/M on the licks of salt, which was driven by a decrease in the

number of licking bouts but not by the size of these bouts (Fig. 3c, left panels). However, in a sodium-depleted state, animals still drank a substantial amount of salt, even after B/M infusion (on average 323 ± 148 s.e.m. licks in the 1h recording session). Indeed, there was a significant main effect of sodium depletion (state) on the number of sodium licking bouts, and a trend towards an effect of sodium depletion on the number of licks and bout size. Importantly, no B/M × state interaction effects were observed, indicating that the effects of sodium deprivation on salt intake were still present after NAc inactivation, although numerically more modest.

Licking for water in sodium-deprived and control rats also decreased upon infusion of B/M into the NAc, as a significant main effect of B/M was observed (Fig. 3c, right panels). In contrast to licking for salt, water consumption was almost fully abolished in both groups of rats (on average 4 ± 1-2 s.e.m. licks in the 1h recording session), without a main effect of state or B/M × state interaction effect. Collectively, these data show that inactivation of the NAc decreases intake of salt, but not as strongly as for water.

NAc inactivation abolished sucrose and water intake, even during hunger and thirst

Since we observed that NAc inactivation almost fully abolished water, but not salt intake, we next examined the effects of NAc inactivation on food intake during hunger, and later also assessed the effects of NAc inactivation on water intake during thirst. We used the same experimental design as we had used to assess salt appetite, but instead monitored the intake of a 5% sucrose solution in the home cage after food restriction (n = 6). As such, animals had the choice between a bottle of sucrose (which was delivered to the animal right after the infusion) and a bottle of tap water (which was already present in the home cage of the animals). Animals in the control state, who were *ad libitum*-fed, had access to regular chow before and during the experiment.

We observed a significant B/M × food restriction interaction effect on the number of licks the animals made for sucrose (Fig. 4a, left panels). Post-hoc tests indicated that this was driven by a significant increase in the number of licks for sucrose upon food restriction after saline infusion, but not after B/M infusion. This effect seemed mainly driven by a decrease in the number of licking bouts, as we observed a main effect of B/M on this parameter, but not on the number of licks per bout. In contrast to baseline sucrose consumption, the total intake of water was extremely low (Fig. 4a, right panels), perhaps because the animals' water homeostasis was relatively normal (compared to after sodium deprivation) and the animals had continuous access to water. Together, these data

demonstrate that NAc inactivation reduced consumption of sucrose, and that this is independent of the energy balance of the animal.

Similar effects of NAc inactivation were observed on the intake of water during thirst (Fig. 4b). Water restriction increased the consumption of water (main effect of restriction on licks and the number of licking bouts), and B/M infusion into the NAc decreased overall water intake (significant main effect of B/M on number of licks and number of bouts; trend towards a main effect on the licks per bout). Furthermore, a significant B/M × water restriction interaction effect was observed on the number of licks for water and the number of licking bouts, which was driven by an increase in licking after saline infusion but not after B/M infusion. This indicates that pharmacological inactivation of the NAc abolished water intake, even when animals were thirsty.

DA receptor antagonism in the nucleus accumbens does not alter salt appetite

We next repeated the salt intake experiment in these animals (n = 6), but now infused the DA receptor antagonist α-flupenthixol into the NAc (25 µg/side), to study the importance of DAergic neurotransmission in the NAc for salt appetite. We observed that α-flupenthixol infusion did not affect salt intake, nor did it affect the number of licking bouts or licks per bout (Fig. 5, left panels). However, we did observe a significant effect of α-flupenthixol infusion on water intake (driven by both a decrease in the number of licking bouts and the size of these licking bouts; Fig. 5, right panels). These data suggest that the suppressing

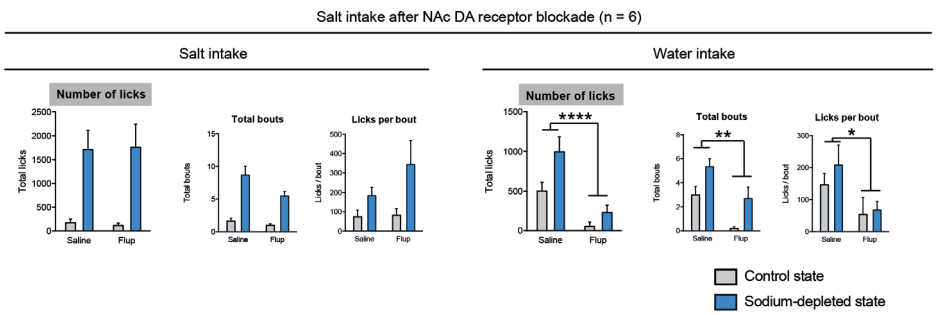

Figure 5. Effects of DA receptor blockade in the NAc on salt appetite. The effects of infusion of the DA receptor antagonist α-flupenthixol (Flup) on salt (left) and demineralized water (right) intake in rats in a sodium-depleted (blue) and control (grey) state. Infusion of α-flupenthixol did not affect salt intake, nor the number of bouts or the number of licks per bout. Water intake was significantly decreased by infusion of the DA receptor antagonist, driven by decreases in both the number of bouts and licks per bout.

A single asterisk annotation per graph indicates a main effect of B/M; see also the Supplementary statistics table. **** P < 0.0001, ** P < 0.01, * P < 0.05

effects of pharmacological inactivation of the NAc on salt intake under sodium-depleted conditions is not driven by DAergic neurotransmission.

DISCUSSION

It is generally assumed that deprivation of a reward increases the motivation to obtain it, ranging from food[24] to social behavior[25] and drugs[26]. However, that a certain food can act either as punisher or as a reinforcer dependent on the homeostatic state of an organism is, to our knowledge, unique to salt. In our study, we demonstrated that VTA DA neurons in rats encoded the appreciation of a salty solution, dependent on the animal's internal sodium levels. As such, tasting salt under normal circumstances resulted in a suppression of licking and sub-baseline levels of DA neuron activity, indicating that this solution was considered aversive. Conversely, salt tasting after sodium depletion evoked vigorous licking for the solution, along with peaks in DA neuron activity that were even larger than the peaks previously observed during sucrose tasting. This finding is consistent with a recent study that demonstrated altered DA release in the nucleus accumbens shell in response to a NaCl solution after sodium deprivation[21]. Another study[22] recently showed that sodium deprivation did not affect baseline activity of VTA DA neurons, *ex vivo* nor *in vivo,* in accordance with our finding that c-Fos expression was not altered in midbrain DA nuclei after furosemide treatment. A methodological consideration here is that we may have missed any acute effects of salt deprivation on c-Fos expression, since the peak in c-Fos expression lies between 60 and 120 minutes after a certain manipulation[27] and our measurement was conducted after 48 hours of deprivation. However, a recent paper found that the same furosemide treatment as used in the current work resulted in strong c-Fos expression after 24 hours of salt deprivation[21]. Earlier work by Geerling et al. shows that even after 8 days of salt deprivation, responsive neurons still show increased c-Fos immunoreactivity[28], perhaps signaling a need state for sodium. This indicates that its chronic effects can be detected if present, and that the lack of altered c-Fos expression upon salt deprivation is most probably due to unaffected baseline activity of midbrain DA neurons. Taken together, the findings from the photometry and c-Fos experiment suggest that sodium deprivation does not simply disinhibit the whole DA system, but that the changes in DA neuron activity are dependent on presentation of the salient salt solution. Thus, the DA system gets engaged upon presentation of the salient (salt) stimulus.

To subsequently investigate which output areas are involved in the regulation of salt appetite, we assessed the effects of inhibiting the two main output regions of the VTA, the NAc and the mPFC, on salt appetite. Several studies have suggested that during free-intake paradigms, the frequency of licking bouts

(i.e., how often the animal initiates drinking) is a measure of incentive salience, or the motivation to obtain reward, whereas the bout size (i.e., the length of a drinking period) informs about the hedonic impact, or appreciation of reward[29–32]. We therefore performed a microstructure analysis of salt licking behavior after pharmacological inactivation of the NAc and demonstrated that the decrease in salt intake was driven by a reduction in the number of licking bouts, but not the size of these bouts, suggesting that the motivation for salt under a situation of salt deprivation was decreased upon NAc inactivation. To assess if this decrease in motivation for salt upon NAc inactivation was also true for other appetites, we investigated sucrose or water intake during food deprivation or water deprivation, respectively. The finding of decreased motivation was replicated in the sucrose intake experiment, where we observed that NAc inactivation reduced the number of sucrose licking bouts, but not the number of licks within these bouts. Together, this suggests that the motivational aspect of salt appetite is reduced by inactivation of the NAc, just as is the motivation for sugar when food restricted. In contrast to these findings, NAc inactivation did have a significant effect on the size of the licking bouts for water, a liquid that has a neutral taste, suggesting that the absence of an effect of NAc activation on the sucrose and salt licking bout size is related to its taste, and that taste acts as the conditioned stimulus for the homeostatic need. In fact, NAc inactivation almost fully suppressed water intake in all of the experiments, even when the animals were thirsty. The observation that this was not the case for salt and sucrose consumption suggests that the attenuated water intake was not the result of a general behavioural impairment, for example because of motor deficits. Interestingly, it has previously been shown that pharmacological inactivation of the medial shell subregion of the NAc leads to an increase in palatable food intake[33]. These findings are difficult to reconcile with the findings from the current study, but may be related to the larger infusion volume that we have used (1µl), that was used in order to inactive the entire NAc, rather than just the medial shell[23]. Indeed, it is well known that the core and shell subregions of the NAc play distinct, complementary roles in the pursuit, consumption and appreciation of palatable food, which likely explains the different effects of inactivating the medial shell versus entire NAc[33–35]. In contrast to inactivation of the NAc, we found no effects of inactivation of the mPFC on salt appetite.

Since we found that VTA DA neurons encode the appreciation of salt dependent on homeostatic state of the animal and that inactivation of the NAc decreased the motivational aspects of salt appetite, we finally inhibited DA receptors locally within the NAc to study the role of NAc DAergic neurotransmission in salt appetite. After pharmacological blockade of NAc DA receptors using

α-flupenthixol, we observed no effects on salt appetite. Interestingly, we did again observe an effect of the DA receptor antagonist on water intake during this experiment, just as after inactivation of the NAc with B/M. This suggests that the motivation for salt does not require NAc DA, but that this is not necessarily the case for other types of motivation.

The lack of effect of NAc DA receptor blockade on salt appetite is somewhat surprising, given that mesoaccumbens DA is considered a driving force behind motivation for rewards[36,37]. Furthermore, previous studies have reported alterations in the mesolimbic dopamine system and its inputs after sodium deprivation, both morphologically[20] and functionally[21]. Our findings are not necessarily conflicting with these data, as we also showed that VTA DA neuron dynamics during salt and sucrose tasting are dependent on the sodium balance of the animal. This suggests altered reward processing after sodium deprivation, which may logically also affect downstream DA release and hence morphological and structural changes to downstream areas. However, we do show that mesolimbic DA neurotransmission is not *necessary* for the behavioral expression of salt appetite.

That said, the finding that a switch in salt appreciation upon a change in body sodium levels is encoded by VTA DA neurons, but that blockade of DA receptors in one of its most important downstream regions does not hamper salt appetite may seem counterintuitive. A possible explanation is that behavioral adaptation to a shortage in sodium is so crucial, since it can be a prerequisite for survival, that it is redundantly coded in the brain, and thus relies on a variety of brain regions. For example, the VTA also projects to the subthalamic nucleus, which projects to the substantia nigra and the ventral pallidum, which again sends efferents to the substantia nigra, lateral hypothalamus, lateral pre-optic area, pedunculopontine nucleus, and brainstem[38]. All these regions form a complex network of the ventral basal ganglia, which could function as backup for dysfunction of the NAc. Furthermore, the VTA is known to directly project to the lateral hypothalamus, also a key region of the reward system, which forms a neural circuit with the parabrachial nucleus and the nucleus of the solitary tract, which has shown to be involved in the sensory and motor aspects of feeding[39,40].

Whether the apparent independence of sodium appetite of NAc DA extends towards other types of motivated behaviors, such as food intake and social behaviors remains an important question. Acute pharmacological NAc DA receptor blockade has been shown to decrease social play behavior in rats, but only when animals are highly motivated to do so (i.e., after social isolation)[25]. Likewise, it reduces sucrose self-administration when the response requirement increases within a session (i.e., a progressive ratio schedule of reinforcement), but

not free chow intake[41]. It is therefore thought that NAc DA is important for certain types of motivated behaviors, most prominently those involving explicit effort or reward-based learning[35,37,42]. Importantly, in our task, the salt solution can be consumed freely and does not involve any learning processes, since the animals had already been exposed to the salty solution before. It is therefore important to note that our conclusions only apply to the general increase in effort-free salt intake that is observed under sodium-depleted conditions.

In sum, we have used a multidisciplinary approach, including c-Fos immunohistochemistry, fiber photometry and behavioral pharmacology, to assess the role of the mesocorticolimbic DA system in salt appetite. We have substantiated findings from earlier studies regarding the role of VTA neurons in salt appetite, and provide novel insights into the role of its target regions in this behavior. We show that the NAc, but not mPFC, is essential for the behavioral expression of salt appetite by mediating its motivational, but not hedonic, component. This role of the NAc in salt appetite is independent of DA, although we show that DA neurons themselves do encode the appreciation of salt.

REFERENCES

1. Yeomans, M. R., Blundell, J. E. & Leshem, M. Palatability: response to nutritional need or need-free stimulation of appetite? Br. J. Nutr. 92, S3-14 (2004).
2. Rangel, A. Regulation of dietary choice by the decision-making circuitry. Nat. Neurosci. 16, 1717–1724 (2013).
3. Hall, K. D., Hammond, R. A. & Rahmandad, H. Dynamic interplay among homeostatic, hedonic, and cognitive feedback circuits regulating body weight. Am. J. Public Health 104, 1169–1175 (2014).
4. Richter, C. Salt appetite of mammals: its dependence on instinct and metabolism. L'Instinct dans le Comport. des animaux l'homme 577, (1956).
5. Roitman, M. F., Schafe, G. E., Thiele, T. E. & Bernstein, I. L. Dopamine and Sodium Appetite: Antagonists Suppress Sham Drinking of NaCl Solutions in the Rat. Behav. Neurosci. 111, 606–611 (1997).
6. Epstein, A. N. Neurohormonal control of salt intake in the rat. Brain Res. Bull. 27, 315–320 (1991).
7. Morris, M. J., Na, E. S. & Johnson, A. K. Salt craving: The psychobiology of pathogenic sodium intake. Physiol. Behav. 94, 709–721 (2008).
8. Berridge, K. C., Flynn, F. W., Schulkin, J. & Grill, H. J. Sodium depletion enhances salt palatability in rats. Behav. Neurosci. 98, 652–660 (1984).
9. Berridge, K. C. & Schulkin, J. Palatability shift of salt-associated incentive during sodium depletion. Q. J. Exp. Psychol. 41B, 121–131 (1989).

10. Menani, J. V, De Luca, L. A. & Johnson, A. K. Lateral parabrachial nucleus serotonergic mechanisms and salt appetite induced by sodium depletion. Am. J. Physiol. 274, R555-60 (1998).
11. Geerling, J. C. & Loewy, A. D. Aldosterone-sensitive neurons in the nucleus of the solitary tract: Efferent projections. J. Comp. Neurol. 497, 223–250 (2006).
12. Jarvie, B. C. & Palmiter, R. D. HSD2 neurons in the hindbrain drive sodium appetite. Nat. Neurosci. (2016). doi:10.1038/nn.4451
13. Geerling, J. C. & Loewy, A. D. Central regulation of sodium appetite. Exp. Physiol. 93, 177–209 (2008).
14. Schultz, W., Dayan, P. & Montague, P. R. A neural substrate of prediction and reward. Science (80-.). 275, 1593–1599 (1997).
15. Verharen, J. P. H. et al. A neuronal mechanism underlying decision-making deficits during hyperdopaminergic states. Nat. Commun. 9, 1–15 (2018).
16. Wolf, G. Hypothalamic regulation of sodium intake: relations to preoptic and tegmental function. Am. J. Physiol. 213, 1433–1438 (1967).
17. Stricker, E. M. & Zigmond, M. J. Effects on homeostasis of intraventricular injections of 6-hydroxydopamine in rats. J. Comp. Physiol. Psychol. 86, 973–994 (1974).
18. Lucas, L. R., Grillo, C. A. & McEwen, B. S. Salt appetite in sodium-depleted or sodium-replete conditions: Possible role of opioid receptors. Neuroendocrinology 85, 139–147 (2007).
19. Roitman, M. F., Patterson, T. A., Sakai, R. R., Bernstein, I. L. & Figlewicz, D. P. Sodium depletion and aldosterone decrease dopamine transporter activity in nucleus accumbens but not striatum. Am. J. Physiol. 276, 1339–1345 (1999).
20. Roitman, M. F., Na, E., Anderson, G., Jones, T. A. & Bernstein, I. L. Induction of a salt appetite alters dendritic morphology in nucleus accumbens and sensitizes rats to amphetamine. J. Neurosci. 22, 1–5 (2002).
21. Fortin, S. M. & Roitman, M. F. Challenges to Body Fluid Homeostasis Differentially Recruit Phasic Dopamine Signaling in a Taste-Selective Manner. J. Neurosci. 38, 6841–6853 (2018).
22. Sandhu, E. C. et al. Phasic Stimulation of Midbrain Dopamine Neuron Activity Reduces Salt Consumption. Eneuro 5, ENEURO.0064-18.2018 (2018).
23. Allen, T. A. et al. Imaging the spread of reversible brain inactivations using fluorescent muscimol. J. Neurosci. Methods 171, 30–38 (2008).

24. Hillebrand, J. J. G., de Wied, D. & Adan, R. A. H. Neuropeptides, food intake and body weight regulation: a hypothalamic focus. Peptides 23, 2283–2306 (2002).
25. Manduca, A. et al. Dopaminergic neurotransmission in the nucleus accumbens modulates social play behavior in rats. Neuropsychopharmacology 41, 2215–2223 (2016).
26. Lu, L., Grimm, J. W., Hope, B. T. & Shaham, Y. Incubation of cocaine craving after withdrawal: A review of preclinical data. Neuropharmacology 47, 214–226 (2004).
27. Curran, T. & Morgan, J. I. Fos: An immediate-early transcription factor in neurons. J. Neurobiol. 26, 403–412 (1995).
28. Geerling, J. C. et al. FoxP2 expression defines dorsolateral pontine neurons activated by sodium deprivation. Brain Res. 1375, 19–27 (2011).
29. Davis, John, D. The Microstructure of Ingestive Behavior. Ann. N. Y. Acad. Sci. 575, 106–121 (1989).
30. Higgs, S. & Cooper, S. J. Evidence for early opioid modulation of licking responses to sucrose and Intralipid: A microstructural analysis in the rat. Psychopharmacology (Berl). 139, 342–355 (1998).
31. D'Aquila, P. S. Dopamine on D2-like receptors 'reboosts' dopamine D1-like receptor-mediated behavioural activation in rats licking for sucrose. Neuropharmacology 58, 1085–1096 (2010).
32. Ostlund, S. B., Kosheleff, A., Maidment, N. T. & Murphy, N. P. Decreased consumption of sweet fluids in mu opioid receptor knockout mice: A microstructural analysis of licking behavior. Psychopharmacology (Berl). 229, 105–113 (2013).
33. Kelley, A. E. Ventral striatal control of appetitive motivation: role in ingestive behavior and reward-related learning. Neurosci. Biobehav. Rev. 27, 765–76 (2004).
34. Cardinal, R. N., Parkinson, J. A., Hall, J. & Everitt, B. J. Emotion and motivation: the role of the amygdala, ventral striatum, and prefrontal cortex. Neurosci. Biobehav. Rev. 26, 321–52 (2002).
35. Floresco, S. B. The Nucleus Accumbens: An Interface between Cognition, Emotion, and Action. Annu. Rev. Psychol. 66, 25–52 (2015).
36. Cools, R. Role of dopamine in the motivational and cognitive control of behavior. Neuroscientist 14, 381–395 (2008).
37. Salamone, J. D. & Correa, M. The mysterious motivational functions of mesolimbic dopamine. Neuron 76, 470–485 (2012).

38. Humphries, M. D. & Prescott, T. J. The ventral basal ganglia, a selection mechanism at the crossroads of space, strategy, and reward. Prog. Neurobiol. 90, 385–417 (2010).
39. Grill, H. J. Leptin and the systems neuroscience of meal size control. Front. Neuroendocrinol. 31, 61–78 (2010).
40. Stice, E., Figlewicz, D. P., Gosnell, B. A., Levine, A. S. & Pratt, W. E. The contribution of brain reward circuits to the obesity epidemic. Neurosci. Biobehav. Rev. 37, 2047–2058 (2013).
41. Randall, P. A. et al. Dopaminergic Modulation of Effort-Related Choice Behavior as Assessed by a Progressive Ratio Chow Feeding Choice Task: Pharmacological Studies and the Role of Individual Differences. PLoS One 7, 1–10 (2012).
42. Salamone, J. D., Correa, M., Mingote, S. M. & Weber, S. M. Beyond the reward hypothesis: Alternative functions of nucleus accumbens dopamine. Curr. Opin. Pharmacol. 5, 34–41 (2005).

ACKNOWLEDGEMENTS

This work was supported by the European Union Seventh Framework Programme under grant agreement number 607310 (*Nudge-IT*), and the Netherlands Organisation for Scientific Research (NWO) under project numbers 912.14.093 (*Shining light on loss of control*).

AUTHOR CONTRIBUTIONS

J.P.H.V., T.J.M.R, L.J.M.J.V. and R.A.H.A designed the experiments. J.P.H.V., T.J.M.R, S.M. and M.C.M.L. performed the experiments. J.P.H.V. and T.J.M.R analyzed the data. J.P.H.V., T.J.M.R, L.J.M.J.V. and R.A.H.A wrote the paper with input from the other authors.

COMPETING INTEREST

The authors declare no competing interests.

SUPPLEMENTARY FIGURES

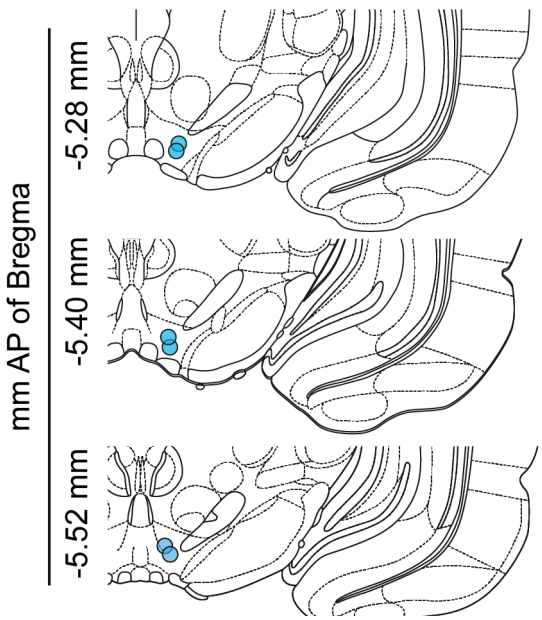

Supplementary Figure 1. Fiber placements of photometry experiments

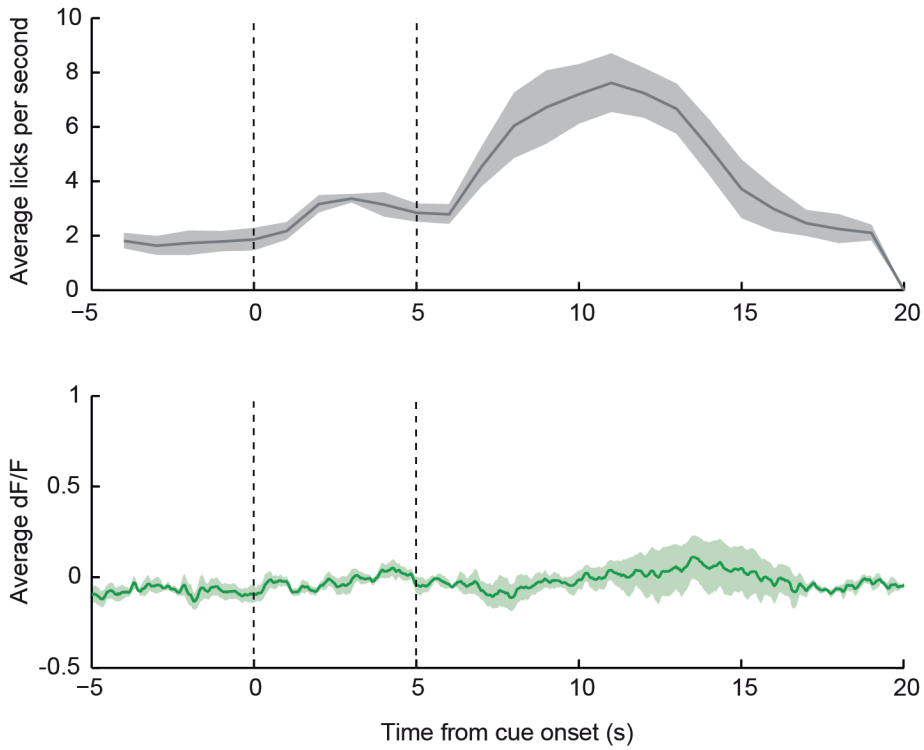

Supplementary Figure 2. In vivo fiber photometry of VTA neurons from animals injected with a YFP control fluorophore. An activity-independent control fluorophore was injected into the VTA of control animals (n=4) and in vivo fiber photometry indicated no changes in fluorescent activity in these controls (lower panel). Upper panel shows the average licking rate of the animals for sucrose reward. Line and shading represent mean and standard error of the mean, respectively.

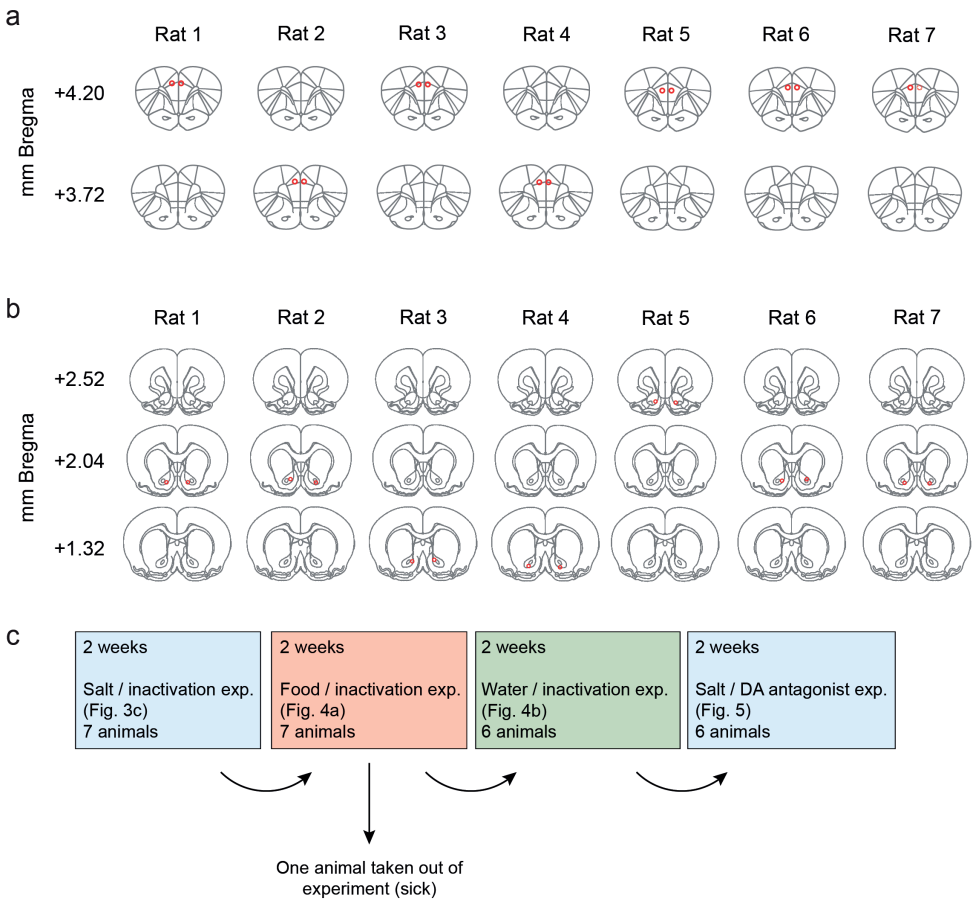

Supplementary Figure 3. Histological verification of guide cannula placement. Correct placement of the guide cannulas used for local infusions was verified for all animals in which the mPFC (a) or the NAc (b) was targeted. Rat 1 from (b) was excluded from figures 4 and 5 because it developed diabetes. (c) Timeline of experiments for animals with cannulas in the NAc. In each block of 2 weeks, animals were tested four times in the free-intake paradigm (in a counterbalanced, semi-random design).

Supplementary statistics table

P values of 2-way repeated measures ANOVA on the outcome parameters of the free-intake assay

	ANOVA factor	Salt intake			Water intake			Sucrose intake		
		# of licks	# of bouts	Licks per bout	# of licks	# of bouts	Licks per bout	# of licks	# of bouts	Licks per bout
Fig. 3b	B/M	*P* = .30	*P* = .42	*P* = .38	*P* = .58	*P* = .91	*P* = .12			
	State	***P* < .001**	***P* < .001**	***P* < .01**	*P* = .06	***P* = .04**	*P* = .90			
	B/M × State	*P* = .80	*P* = .10	*P* = .31	*P* = .89	*P* = .51	*P* = .69			
		# of licks	# of bouts	Licks per bout	# of licks	# of bouts	Licks per bout	# of licks	# of bouts	Licks per bout
Fig. 3c	B/M	***P* < .01**	***P* = .04**	*P* = .59	***P* = .04**	***P* = .01**	***P* < .01**			
	State	*P* = .06	***P* = .02**	*P* = .08	*P* = .14	*P* = .17	*P* = .24			
	B/M × State	*P* = .15	*P* = .20	*P* = .74	*P* = .13	*P* = .16	*P* = .23			
		# of licks	# of bouts	Licks per bout	# of licks	# of bouts	Licks per bout	# of licks	# of bouts	Licks per bout
Fig. 4a	B/M				*P* = .22	*P* = .24	*P* = .32	*P* = .05	***P* = .018**	*P* = .80
	Restriction				*P* = .24	*P* = .75	*P* = .33	***P* = .013**	*P* = .48	***P* = .031**
	B/M × Restriction				*P* = .24	*P* = .68	*P* = .34	***P* = .029**	*P* = .71	*P* = .48
								*post-hoc tests performed **		
		# of licks	# of bouts	Licks per bout	# of licks	# of bouts	Licks per bout	# of licks	# of bouts	Licks per bout
Fig. 4b	B/M				***P* = .0016**	***P* = .0025**	***P* = .05**			
	Restriction				***P* = .0015**	***P* = .0038**	*P* = .18			
	B/M × Restriction				***P* = .0019**	***P* = .0090**	*P* = .66			
					*post-hoc tests performed **	*post-hoc tests performed **				
		# of licks	# of bouts	Licks per bout	# of licks	# of bouts	Licks per bout	# of licks	# of bouts	Licks per bout
Fig. 5	Flup	*P* = .97	*P* = .09	*P* = .16	***P* < 0.0001**	***P* = .0026**	***P* = .03**			
	State	***P* = .011**	***P* = .0002**	*P* = .07	*P* = .09	***P* = .0081**	*P* = .51			
	Flup × State	*P* = .76	*P* = .15	*P* = .25	*P* = .31	*P* = .90	*P* = .69			

** a post-hoc Sidak's test was performed when the ANOVA yielded a significant (P < 0.05) interaction effect*

Chapter 5

Modified rabies virus tracing technology goes viral! Optimization of whole-brain input mapping to leptin receptor-expressing neurons in the lateral hypothalamus by assessing the effect of different TVA titers on tracing efficiency and specificity

Theresia J.M. Roelofs[a,b], Shanice Menting-Henry[a], Lieke M. Gol[a], Annelijn M. Speel[a], Keith M. Garner[a], Mieneke C.M. Luijendijk[a], Vera H. Wielenga[b], Karl-Klaus Conzelmann[d], Roger A.H. Adan[a,c]

[a]Department of Translational Neuroscience, Brain Center Rudolf Magnus, University Medical Center Utrecht, Universiteitsweg 100, 3584 CG Utrecht, the Netherlands

[b]Biomedical MR Imaging and Spectroscopy Group, Center for Image Sciences, University Medical Center Utrecht and Utrecht University, Bolognalaan 50, 3584 CJ Utrecht, the Netherlands

[c]Institute of Neuroscience and Physiology, The Sahlgrenska Academy at the University of Gothenburg, Sweden

[d]Max von Pettenkofer Institute Virology and Gene Center, Medical Faculty, Ludwig-Maximilians-University Munich, Munich 81377, Germany

Leptin is an important hormone in the regulation of homeostatic energy balance and it is known to increase energy expenditure and to decrease appetite and energy intake by action via its receptor, LepRb, which is expressed in a multitude of brain areas. A brain area critically involved in the regulation of food intake which also expresses LepRb is the lateral hypothalamus (LH). Downstream of the LH, signaling pathways are relatively well understood, however, the neuroanatomical inputs to LepRb-expressing LH neurons are unknown. We used rabies virus tracing technology to map these inputs. To optimize this technology for a minor cell population (LepRb is not ubiquitously expressed in LH), we used LepRb-Cre mice and assessed how different titers of the helper virus TVA affected rabies tracing efficiency and specificity. We found that rabies expression is dependent on TVA receptor expression, and also that leakiness of TVA receptors is dependent on the titer of TVA virus used. We concluded that a titer of 1.0-3.0 ×10^7 genomic copies per μl of the TVA virus is optimal for modified rabies tracing. Following these methodological considerations on the use of modified rabies virus tracing technology, we successfully applied the technique to map inputs projecting to LepRb-expressing LH neurons. We discovered that other neurons in the LH itself, the periventricular hypothalamic nucleus (Pe), the posterior hypothalamic nucleus (PH), the bed nucleus of the stria terminalis (BNST), and the paraventricular hypothalamic nucleus (PVN) are the most prominent input areas to LepRb-expressing LH neurons. We conclude that low titers of AAV-TVA are required to reliably map inputs when limited numbers of neurons are present in a given brain region as the LH.

KEYWORDS
Neuroanatomical tract-tracing technique, modified rabies virus tracing technology, leptin, lateral hypothalamus, mice

INTRODUCTION

In order to maintain energy homeostasis and body weight, specific amounts of calories must be consumed to replenish the energy used for physical activity, thermogenesis, and other processes resulting in energy expenditure. A dysregulation of this balance leads to overweight and ultimately obesity, in case of caloric overconsumption. Leptin is an adipocyte-derived cytokine and has a significant role in the regulation of body weight in humans as well as rodents[1–4]. Elevated leptin levels in the blood are associated with increased adiposity, which is a hallmark of obesity[5,6]. Leptin is known to increase energy expenditure, for example by increasing body temperature, and to decrease appetite and energy

intake by action via its receptor, LepRb, which is expressed in a multitude of brain areas[1,2,7–9]. A brain area critically involved in the regulation of food intake which also expresses LepRb, is the lateral hypothalamus (LH)[10–12]. The LH relays information from neural circuits regulating energy balance to the mesolimbic system, such that a perceived negative energy balance results in motivation to initiate behaviors that result in energy intake. However, the upstream neuronal circuitries, thus the neuroanatomical inputs to LepRb-expressing LH neurons, are not known.

Since long viral vectors have been used as methods of neuroanatomical tract tracing[13,14]. Modified rabies virus tracing is a relatively new tracing technique that can be used for qualitative and quantitative analysis of functional neuronal networks in the brain[13–25]. In modified G-deleted rabies virus (RV*d*G) rabies glycoprotein (G), an envelope protein essential for transneuronal transfer of rabies virus[20,26], is deleted from the genome and replaced by green fluorescent protein (GFP). Therefore, RV*d*G needs host-cells to express G for *trans*-complementation in order to spread to presynaptic nerve terminals[20,26,27]. RV*d*G is pseudotyped with the avian ASLV type A (EnvA, Figure 1), that makes use of the avian-specific TVA receptor for entry in recipient cells[20,26]. This restricts entry of RV*d*G to those cells that are genetically designed to express TVA. In the modified rabies virus tracing approach used in the current study, two helper adeno-associated viral vectors (AAV vectors) are injected simultaneously; one that carries TVA-mCherry which, once expressed in target neurons, allows EnvA+RV*d*G to enter, and one that carries rabies G which, once expressed in target neurons, leads to normal infectious properties of the intact RV. To restrict input mapping to LepRb-expressing neurons, TVA and G are Cre-dependent[26,28] and injected in LepRb-Cre mice, allowing TVA and G expression only in LepRb-expressing neurons. When TVA and G are adequately expressed in LepRb-expressing neurons, EnvA+RV*d*G will be injected. RV*d*G will infect target neurons expressing TVA, being LepRb-expressing neurons, and subsequently spread monosynaptically to presynaptic nerve terminals, since only target neurons express G[26–28]. RV expresses GFP, which allows input mapping to LepRb-expressing neurons (Figure 1).

Even though rabies tracing is a highly specific and effective tracing technique, to our knowledge little work has been done on the optimization of titers of the different vectors used. This is crucial, in particular when only few Cre-positive neurons are present in a brain region, such as in the case of LepRb-expressing neurons in the LH. We noticed that during preparation of AAV viruses, a low amount of Cre-dependent TVA is recombined in bacteria (in the absence of Cre-recombinase). Often only control animals are used to check if RV is solely expressed in the presence of TVA[21,27,28], but to our knowledge no

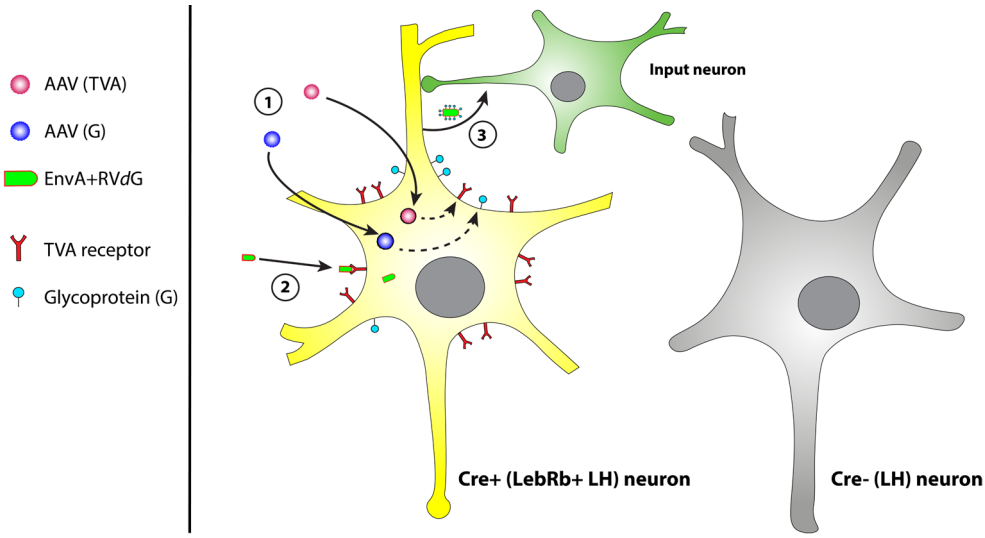

Figure 1. Working mechanism of modified rabies virus tracing technology. a) Modified rabies virus lacks the envelope protein G, which normally allows budding of new host cell-derived membrane-enveloped viral particles that have G on their membrane. Modified rabies is pseudotyped, so that it expresses EvnA+GFP as envelope protein. EnvA makes use of the avian-specific TVA receptor for entry in recipient cells. First (1), an injection with two helper AAV vectors delivers Cre-dependent TVA-mCherry and G in a mouse Cre-line. Only neurons that express Cre will start to express the TVA receptor and G. Second (2), when TVA and G are adequately expressed mice are injected with modified G-deleted rabies virus (RVdG). EnvA+RVdG can only infect host-cells that express the TVA receptor and it needs host-cells to express G for trans-complementation in order to spread to presynaptic nerve terminals. Once EnvA+RVdG entered neurons via the TVA receptor, it replicates and uses G to obtain normal infectious properties. Thereby, it is able to spread monosynaptically to presynaptic nerve terminals. Since these input neurons do not express G, RVdG cannot infect subsequent nerve terminals from upstream input neurons. RVdG expresses GFP, allowing input mapping to Cre-positive neurons.

experiments have been performed to assess the optimal TVA titer for selective and efficient expression of RV and thus for specific and efficient input mapping. Unspecific TVA receptor expression, a possible scenario when a high titer is used, undermines the specificity of RV tracing: little TVA receptor expression is already sufficient for EnvA+RV*d*G infection and subsequent retrograde spread of RV[25]. Leaky TVA receptor expression (expression in the absence of Cre-recombinase) and consequent unspecific RV spread cannot be distinguished from specific RV spread, thus compromising the specificity of tracing[25]. On the contrary, too little TVA expression will result in inefficient infection of EnvA+RV*d*G, thereby probably resulting in missed inputs. An optimal balance between specificity and efficiency of RV tracing is therefore a prerequisite. With the aim to optimize specificity and efficiency of RV tracing, we determined the most optimal TVA titer and finally

used this titer to map inputs to LepRb-expressing LH neurons. Mapping of these inputs will provide more insight into the organization of feeding behavior-related neural-networks.

EXPERIMENTAL PROCEDURES

Animals

Experiments were approved by the Animal Ethics Committee of the University Medical Center Utrecht, The Netherlands, and were conducted in agreement with Dutch ('Wet op de Dierproeven', 2014) and European regulations (Guideline 86/609/EEC; Directive 2010/63/EU).

Healthy female and male wildtype C57BL6/J mice (n=8) and transgenic C57BL6/J mice expressing Cre in leptin receptor-expressing neurons (LepRb-Cre mice; n=12) were housed under controlled temperature and humidity conditions, with a 12h-light/dark cycle (lights on at 7:00 a.m.). Based on their post-surgical condition, mice were housed in pairs or solitary. Animals had *ad libitum* access to water and standard chow, and tissues were provided as cage enrichment. Extra mashed chow was given in the home cage when animals showed signs of weakness after surgery. Mean (± standard deviation) body weight at time of first surgery was 27.0 (± 2.3) g.

Quantitative real-time polymerase chain reaction

Quantitative real-time polymerase chain reaction (qPCR) was performed to determine the level of LoxP recombination of the rAAV-Flex-TCB (CAG-Flex-TCB, plasmid #48332) plasmid using a Quantstudio 6 qPCR instrument and the FastStart Universal SYBR Green mix (Roche). Reactions were performed on sequential log dilutions of the plasmid ranging from 1.0×10^9 to 1.0×10^4 genomic copies per µl, followed by a negative control. Reactions were performed with primer pairs specifically amplifying either the unrecombined, or the recombined version of the plasmid. A primer pair amplifying a segment of the wPRE element of the plasmid was used as a positive/internal control for each reaction. All reactions were performed in an end volume of 10 µl, containing 10 pmol forward and reverse primers, 2 µL genomic DNA template, and 5 µL FastStart SYBR Green mix. Annealing temperature was 60.0 °C. Primer sequences were as follows, all given 5′ to 3′: wPRE forward = CCCGTATGGCTTTCATTTTCTCC; wPRE reverse = CGGGCCACAACTCCTCATAA; non-recombined plasmid forward = AGCCGCGCCATGGTGGCGC; recombined plasmid forward = CGGCATGGACGAGCTGTACAAGTAA; (un)recombined common reverse = CTTTCACAAATTTTGTAATCCAGAGGTTGA. Cycle threshold (CT) values were obtained using the second derivative maximum method in the Quantstudio software. At the titer that resulted in detectable levels of recombined plasmid DNA,

delta CT (dCT) was calculated by subtracting the CT value from the unrecombined version from the recombined version of the plasmid. From this dCT value the amount of recombined plasmids per number of genomic copies was estimated.

Intracerebral viral vector injection

Mice were divided into eight groups; four groups (all n=2) for the wildtype control mice and four groups (n=2, n=2, n=4, n=4) for the LepRb-Cre mice to assess the effect of different titers of TVA vector injection and to map inputs to LepRb-expressing LH neurons. For wildtype control mice, the first group received no TVA or glycoprotein (G) viral vector injection, thus only unilateral rabies injection in the LH to assess necessity of the helper vectors for rabies expression. The other three control groups all received different titers of the Cre-dependent improved TVA viral vector rAAV5-Flex-TCB, being 1.0×10^9, 1.0×10^8, and 1.0×10^7 genomic copies (g.c.)/µl, and always the same titer of 0.9×10^9 g.c./µl of the Cre-dependent G glycoprotein vector AAV8-CA-Flex-RG. The first three LepRb-Cre groups received different titers of rAAV5-Flex-TCB, being 1.0×10^9 (n=4), 1.0×10^8 (n=2), and 1.0×10^7 g.c./µl (n=2), and always the same titer of 0.9×10^9 g.c./µl of AAV8-CA-Flex-RG. In both the wildtype control and the LepRb-Cre groups unilateral injections were made when rAAV5-Flex-TCB was injected with a titer of 1.0×10^9 g.c./µl, when rAAV5-Flex-TCB was injected with a titer of 1.0×10^8 or 1.0×10^7 g.c./µl bilateral injections were made. In the final LepRb-Cre group (n=4) mice were unilaterally injected with 3.0×10^7 g.c./µl of rAAV5-Flex-TCB and 0.9×10^9 g.c./µl of AAV8-CA-Flex-RG.

Viral vector injections were performed as follows: before surgery mice received a subcutaneous injection with carprofen as analgesia (5 mg/kg, s.c., Carporal, AST Farma BV, the Netherlands) and were subsequently anesthetized by an intraperitoneal injection of a combination of 75 mg/kg ketamine (Narketan, Vetoquinol BV, the Netherlands) and 1 mg/kg medetomidine (SedaStart, AST Farma BV, The Netherlands). Xylocaine was sprayed on the skull for local anesthesia (Lidocaine 100 mg/ml, AstraZeneca BV, the Netherlands). Using a stereotaxic apparatus (David Kopf Instruments, USA), 0.2 µl of a mixture of rAAV5-Flex-TCB (coupled to the red fluorophore mCherry; homemade from [25]) and AAV8-CA-Flex-RG (UNC Vector Core, USA) was injected into the lateral hypothalamus (LH; coordinates relative to Bregma: anteroposterior -1.40 mm, mediolateral ±1.80 mm at an angle of 10°, dorsoventral -5.48 mm) at a speed of 0.1 µl/minute. Depending on group assignment 0.2 µl of the mixture was injected unilateral or bilateral (0.2 µl per side). The injection needle was only retracted from the injection position after 10 minutes, to allow for diffusion of the vector mix into the tissue. Injections with G-deleted rabies virus pseudotyped with an avian virus envelope protein,

called EnvA, (SAD-ΔG-eGFP(EnvA)[26,29]) were performed at least 21 days after the first surgery. 1.0 µl of 4.0×10^8 focus forming units (ffu)/ml SAD-ΔG-eGFP(EnvA) was injected into the LH (using the same coordinates as before) at a rate of 0.2 µl/minute. Again, the injection needle was kept in position for 10 minutes after injection, to allow for diffusion of the virus into the tissue. Atipamezole (2.5 mg/kg, SedaStop, AST Farma BV, the Netherlands) was given after surgery to reverse sedative effects. After surgery mice were carefully monitored and the two days following surgery carprofen (5 mg/kg, s.c., Carporal, AST Farma BV, The Netherlands) was administered to relieve post-operative pain.

Tissue preparation

Exactly 8 days after rabies injection mice were euthanized by intraperitoneal injection with an overdose of sodium pentobarbital (Euthanimal, Alfasan BV, The Netherlands) followed by intracardial perfusion-fixation with cold 0.1M phosphate buffered saline (PBS), followed by 4% paraformaldehyde (PFA). Brains were excised and kept at 4°C in PBS containing 4% PFA for at least 24 hours for post-fixation. After post-fixation, brains were transferred to 30% sucrose with 0.1% NaN_3 in PBS and kept at 4°C, after at least another 48 hours brains were frozen and sliced into 40 µm sections using a cryostat (Leica CM3050 S, Germany). Sections were collected as 1 in 6 series and stored in 30% sucrose with 0.1% NaN_3 in PBS at 4°C.

Immunohistochemistry

Sections were washed in PBS and blocked and permeabilized in PBS containing 5% normal goat serum, 5% normal donkey serum, and 0.25% Triton-X-100 for 1 hour at room temperature. Sections were incubated overnight with the primary antibodies rabbit anti-dsRed (1:1000, Clontech Laboratories, USA) to detect mCherry-fused TVA and chicken anti-GFP (1:1000, Abcam, UK) to detect rabies in 2% normal goat serum and 0.1% Triton-X-100 in PBS at 4°C. After washing in PBS, TVA-mCherry was visualized with Alexa-568-labeled goat anti-rabbit IgG (1:500, Abcam, UK) and rabies was visualized with Alexa-488-labeled goat anti-chicken (1:500, Abcam, UK) in 2% normal goat serum and 0.1% Triton-X-100 in PBS. After incubation with secondary antibodies, sections were washed in PBS, incubated with DAPI (4',6-diamidino-2-phenylindole) to visualize cell nuclei, washed in PBS again, mounted and embedded in Fluorsave (Merck Millipore, the Netherlands).

Image analysis

Immunofluorescent sections were photographed using a Zeiss Axio Scope

A1 epifluorescent microscope (Carl Zeiss BV, Germany). Starter cells expressing both TVA and rabies (expressing both fluorophores, thus yellow), TVA-positive neurons (red), and rabies-positive neurons (green) were manually quantified in the entire brain using Fiji (version 1.0, ImageJ, National Institute of Health). Paxinos and Franklin mouse brain atlas was used as reference to identify brain areas expressing TVA and/or rabies[30]. For input mapping, whole-brain inputs were only analyzed if starter cells were discovered in the LH. For the last group of LepRb-Cre mice (n=3), the Paxinos and Franklin mouse brain atlas[30] was used as a reference for initial orientation. Slices were then matched to the corresponding image from the Allen Mouse Brain Atlas[31] using Fiji, and input neurons were counted using the 'multi-point' function in Fiji. All input neurons were counted and ordered to create a list of brain regions that contained at least 1% of the total number of input neurons per mouse.

Data analysis

Statistical analysis was performed using GraphPad Prism (version 7.0e). Independent samples t-tests were used when appropriate. Numbers of starter cells, TVA-positive neurons, and rabies-positive neurons were compared between different groups using a one-way analysis of variance (ANOVA). When a significant effect was discovered, a post-hoc comparison was performed using a Tukey HSD test ($p < 0.05$).

RESULTS

Exclusion criteria

Five mice were excluded (one wildtype control and four LepRb-Cre mice) since no starter cells – the initial TVA- and rabies-infected cells – could be discovered in the LH.

Spontaneous TVA recombination

A quantitative real-time polymerase chain reaction (qPCR) was performed on the rAAV-Flex-TCB plasmid to estimate the amount of recombined TVA receptor DNA during the growth phase of the plasmid, thus prior to, but utilized for AAV production and subsequent injection of the virus, and in the absence of Cre recombinase. CT values of the qPCR on wPRE and unrecombined plasmid were used as guides to determine which concentration could be reliably detected. A CT value higher than 29 was regarded as junk (see Table 1), since WPRE, the internal control, had a CT of ~29. DNA of the unrecombined version of the plasmid was used as reference DNA to calculate delta CT values. The presence of spontaneously recombined plasmid only becomes detectable by qPCR in the

Table 1. CT values from qPCR with different primer pairs directed against the wPRE as a positive control, the unrecombined version of the plasmid, or the recombined version of the plasmid.

TVA titer (genomic copies per µl)	**wPRE**	**Unrecombined plasmid**	**Recombined plasmid**	**Delta CT**
1.0×10^{9}	5.82	5.10	12.50	7.40
1.0×10^{8}	7.73	7.18	16.50	9.32
1.0×10^{7}	10.79	10.39	26.01	15.62
1.0×10^{6}	14.29	14.18	31.71	17.53
1.0×10^{5}	17.33	17.49	32.13	14.64
1.0×10^{4}	20.74	20.70	31.71	11.01
Negative	29.54 ➔ junk	34.15	31.35	

Cycle threshold (CT) values were obtained using the second derivative maximum method in the Quantstudio software. Delta CT values are calculated by subtracting the CT from the unrecombined version of the plasmid from the recombined version of the plasmid.

range of between 1.0×10^{7} genomic copies per µl (g.c./µl) and 1.0×10^{8} g.c./µl starting copies of plasmid. (CT<29, see Table 1). CT values at titers of 1.0×10^{7} g.c./µl and 1.0×10^{8} g.c./µl were 26.01 and 31.71, respectively. This indicates that the highest titer with nearly undetectable recombined versions of TVA DNA lies closer to 1.0×10^{7} g.c./µl than to 1.0×10^{8} g.c./µl. We estimated that a titer between 1.0×10^{7} g.c./µl and 3.0×10^{7} g.c./µl would be optimally specific and efficient. Delta CT at a titer of 1.0×10^{7} g.c./µl was 15.62. Making a rough estimation by taking a difference of 3 CT values to be a log(10) difference in amount of starting DNA (CT values of wPRE increase with steps of ~3 between different sequential log dilutions), this resulted in 1 recombination in every ~160000 genomic copies [log(10) of 15.62/3 = 158489]. This indicated that with an injection of 1 µl of the virus with a titer of 1.0×10^{7} g.c./µl, probably around 62.5 TVA particles will already be recombined and thus possibly be expressed in the absence of Cre recombinase. When a titer of 1.0×10^{8} g.c./µl is used probably around 625 TVA receptor particles will possibly be expressed in the absence of Cre, and with a titer of 1.0×10^{9} g.c./µl probably around 6250 TVA receptor particles will possibly be expressed. However, not every viral particle results in infection. The TVA receptor DNA used is packaged into AAV-particles which need a multiplicity of infection (MOI) of around 100.000 viral genomes per cell[32], indicating that around 100.000 viral particles are needed to efficiently infect one neuron. Lower titers decrease the chance that all neurons will be infected. As there are approximately 100.000 neurons per mm^3 and viral spread following an injection with a volume of 1 µl of 1.0×10^{9} g.c./µl is less than 1 mm^3, injection of 1.0×10^{9} g.c. is sufficient to infect at least 10% of the neurons in such an volume[33,34], assuming that indeed 10.000 neurons get infected with an injection of 1.0×10^{9} g.c. and an MOI of around 100.000 viral genomes per cell. Depending on the amount of targeted neurons, this would indicate that

the amount of AAV-particles carrying a spontaneous recombined TVA receptor leading to infection is neglectable. However, MOIs refer to high efficiency of infection. For rAAV vectors[35], the efficiency of an infectious particle to infect a cell is $0.2–1.0\times10^{-3}$. When we use these assumptions and numbers based on literature and when there are 6250 infectious particles injected, one may expect 1-6 neurons to be injected, which is somewhat lower, but close to what we found.

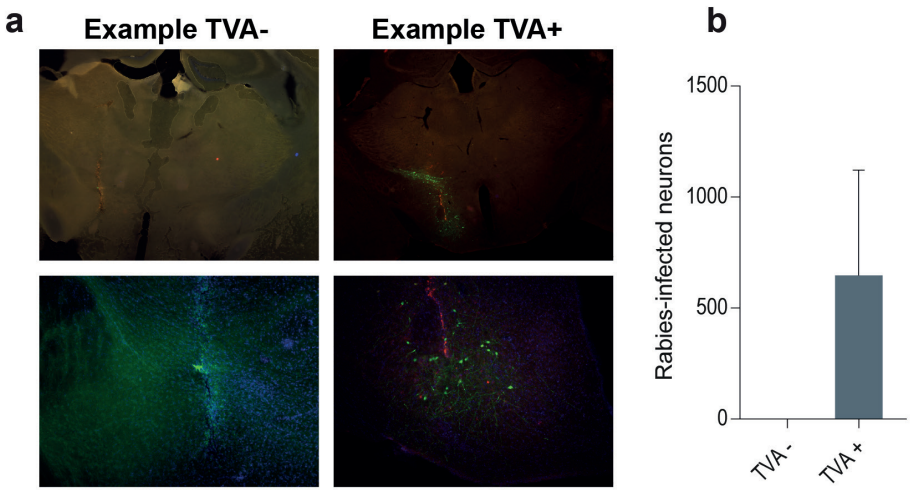

Figure 2. Rabies expression in C57BL6/J control mice with (TVA+) or without (TVA-) a prior injection of 1.0×109 g.c./µl rAAV5-Flex-TCB. a) Representative images of TVA- and TVA+ animals. Zooms are displayed under the original images. b) TVA- mice expressed almost no rabies, while TVA+ mice expressed a remarkable higher level of rabies. No significant difference could be detected using an independent samples t-test; for TVA+ M = 647, SD = 475.2; for TVA- M=1, SD=0; $t(2) = 1.923$, $p = 0.194$.

TVA expression is necessary for rabies expression

Prior to assessing the effects of different TVA titers on efficiency and specificity of rabies tracing, we performed a control experiment to check if TVA expression is indeed necessary for rabies expression to occur. Wildtype C57BL6/J mice were injected in the LH with 1.0×10^9 g.c./µl G-deleted rabies virus, SAD-ΔG-eGFP(EnvA), with (TVA+; n=2) or without (TVA-; n=2) a prior injection of 1.0×10^9 g.c./µl Cre-dependent TVA (rAAV5-Flex-TCB). In the absence of TVA, there was undetectable infection of rabies. TVA-injected mice showed a remarkable higher level of rabies expression than TVA-negative mice (Figure 2), indicating that rabies expression is dependent on TVA expression, but also that TVA receptor expression is leaky.

Leakiness of TVA receptor depends on titer

Since much rabies expression was detected in wildtype control mice that do not express Cre and that were injected with Cre-dependent TVA, rAAV5-Flex-TCB, this demonstrated that rabies was able to infect neurons, and thus that TVA

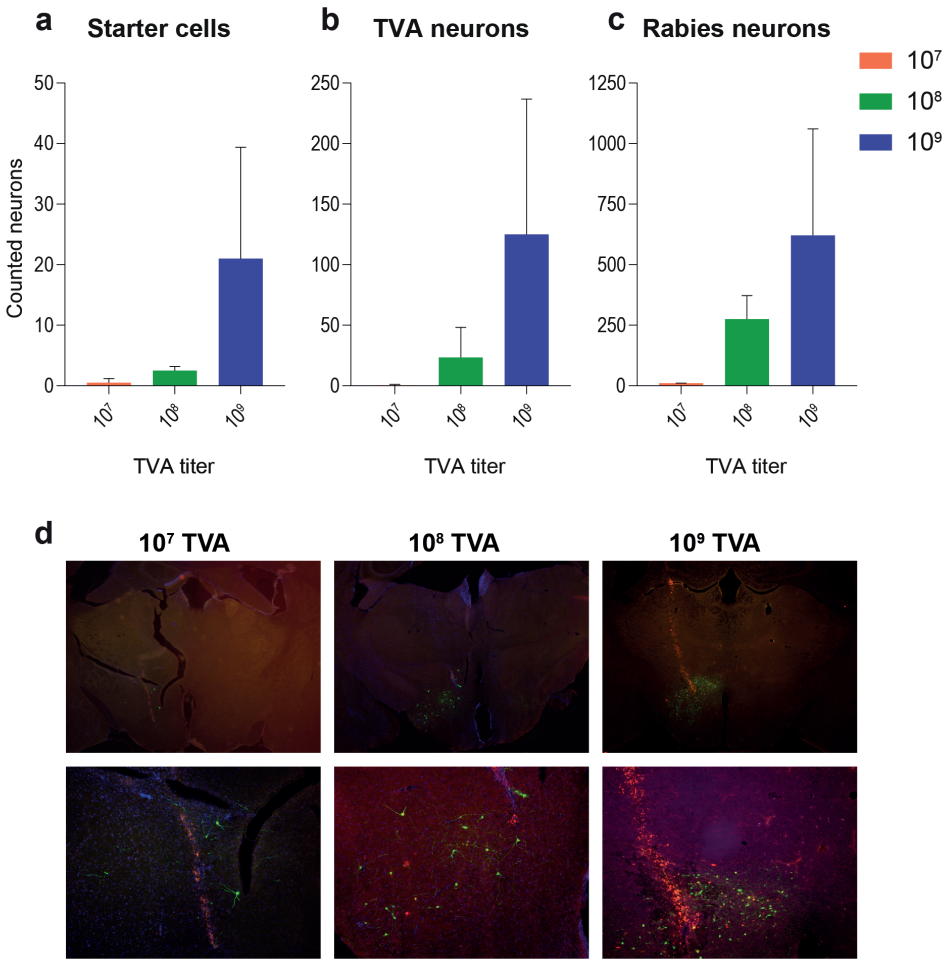

Figure 3. Rabies expression due to TVA leakiness depends on TVA titer. Number of starter cells (a), TVA-expressing neurons (b), and rabies-expressing neurons (c) were quantified in C57BL6/J Cre-negative controle mice that were injected with Cre-dependent TVA and G, followed by SAD-ΔG-eGFP(EnvA) in the LH. Number of starter cells [$F(2,3) = 2.261$, $p = 0.252$], TVA-expressing neurons[$F(2,3) = 2.011$, $p = 0.279$], and rabies-expressing neurons [$F(2,3) = 2.784$, $p = 0.207$] showed a trend towards an increase with TVA titer, also visible in the representative images with zooms per titer underneath in d. Note that injections of 1.0×107 g.c./µl and 1.0×108 g.c./µl rAAV5-Flex-TCB were done bilaterally, whereas 1.0×109 g.c./µl rAAV5-Flex-TCB was done unilaterally. Further, note that the y-axes are different for a, b, and c.

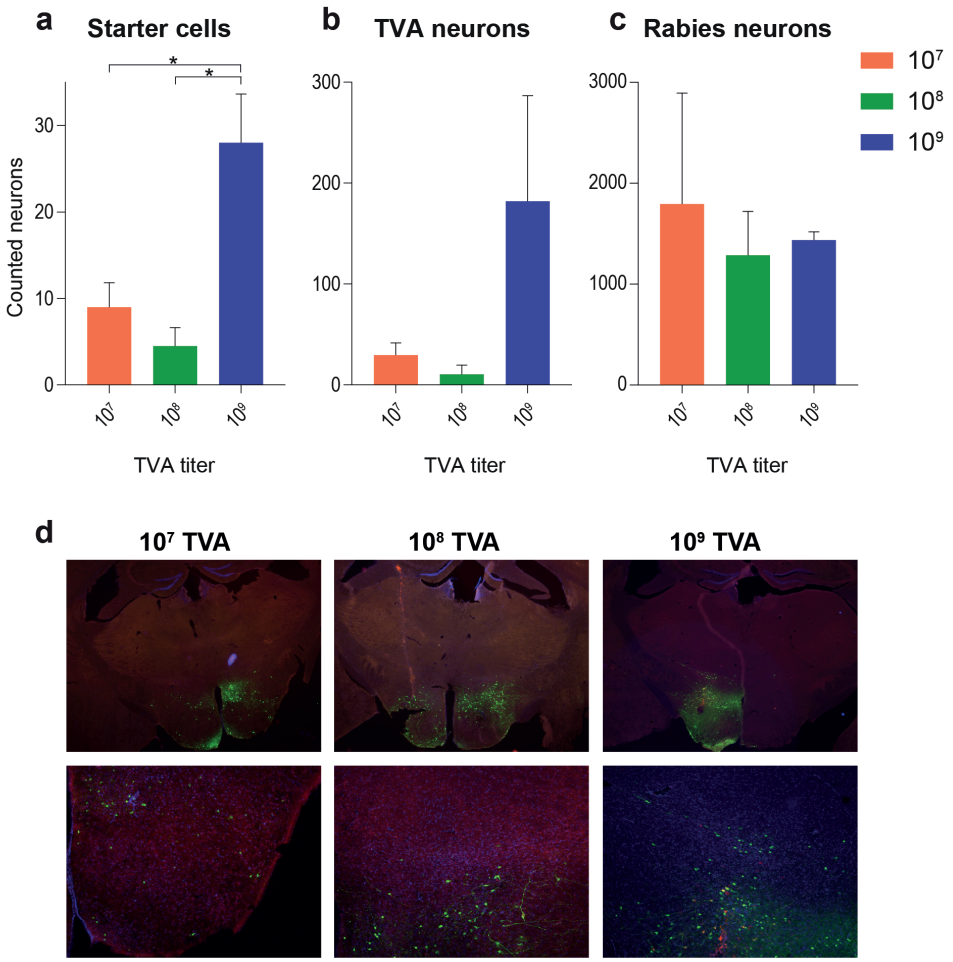

Figure 4. Rabies expression in LepRb-Cre mice. Number of starter cells (a), TVA-expressing neurons (b), and rabies-expressing neurons (c) were quantified in LepRb-Cre mice that were injected with Cre-dependent TVA and G, followed by SAD-ΔG-eGFP(EnvA) in the LH. a) Number of starter cells increased significantly with TVA titer [$F(2,3) = 20.98$, $p = 0.017$]. Post hoc comparison using Tukey HSD test showed that a TVA titer of 1×109 g.c./µl [M = 28, SD = 5.66] resulted in significantly more starter cells than TVA titers of 1×107 g.c./µl [M = 9, SD = 2.83] or 1×108 g.c./µl [M = 4.5, SD = 2.12]. b) TVA-expressing neurons showed a trend towards an increase with TVA titer [$F(2,3) = 4.743$, $p = 0.118$]. c) No difference was found in the number of rabies-expressing neurons [$F(2,3) = 0.293$, $p = 0.765$]. d) These results are also visible in the representative images with zooms per titer underneath. Note that injections of 1×107 g.c./µl and 1×108 g.c./µl rAAV5-Flex-TCB were done bilaterally, whereas 1×109 g.c./µl rAAV5-Flex-TCB was done unilaterally. Further, note that the y-axes are ten-folds different for a, b, and c.

was expressed in the absence of Cre. This suggests that at this high titer, there is leaky expression of TVA resulting in rabies infection. Therefore we reduced the titer of rAAV5-Flex-TCB to determine what the lowest titer of TVA was which still resulted in rabies infection of LepRb-Cre mice, with neglectable infection in wildtype control mice. To this aim, wildtype C57BL6/J mice were injected with either 1.0×10^7, 1.0×10^8, or 1.0×10^9 g.c./µl rAAV5-Flex-TCB in the LH. At least 21 days later these mice were injected with SAD-ΔG-eGFP(EnvA). Expression of starter cells, TVA positive cells, and rabies-infected cells was quantified. Although relatively low numbers of starter cells (infected by both TVA and rabies, Figure 3a) and TVA-positive cells (Figure 3b) were detected, a considerable trend towards an increase in number of both starter and TVA-infected neurons was found upon increasing TVA titer. Increasing TVA titer also increased the number of rabies-infected cells (Figure 3c). The numbers of rabies-infected neurons were higher for all different titers as compared to starter and TVA-positive cells, indicating that rabies needs few starter cells to be able to infect and spread monosynaptically to input neurons. Figure 3d shows representative examples of immunohistochemical stainings of the LH of mice injected with the three different concentrations of rAAV5-Flex-TCB.

Effect of different TVA titers on rabies expression in LepRb-Cre mice

To assess the effect of different TVA titers on number of starter cells, TVA-expressing neurons, and rabies-expressing neurons in the presence of Cre, LepRb-Cre mice were injected with either 1.0×10^7, 1.0×10^8, or 1.0×10^9 g.c./µl rAAV5-Flex-TCB in the LH, followed by SAD-ΔG-eGFP(EnvA) at least 21 days later. Expression of starter cells, TVA-positive neurons, and rabies-infected neurons was quantified. The amount of starter cells in the LH was significantly higher when 1.0×10^9 g.c./µl rAAV5-Flex-TCB was injected as compared to the two lower titers (Figure 4a), even though the injections with 1.0×10^9 rAAV5-Flex-TCB were performed unilaterally and the injections with 1.0×10^7 g.c./µl and 1.0×10^8 g.c./µl rAAV5-Flex-TCB bilaterally. A trend in the same direction was found for TVA-positive cells (Figure 4b). We found no significant differences between 1.0×10^7 g.c./µl and 1.0×10^8 g.c./µl rAAV5-Flex-TCB (Figures 4a and b). No differences in rabies expression were found between the different titers (Figure 4c). Example images of the immunohistochemical sections display the same trends and are shown in Figure 4d.

Inputs to LepRb-expressing LH neurons

In five correctly targeted LepRb-Cre mice, injected with either 1.0×10^7, 1.0×10^8, or 1.0×10^9 g.c./µl rAAV5-Flex-TCB in the LH whole-brain rabies expression

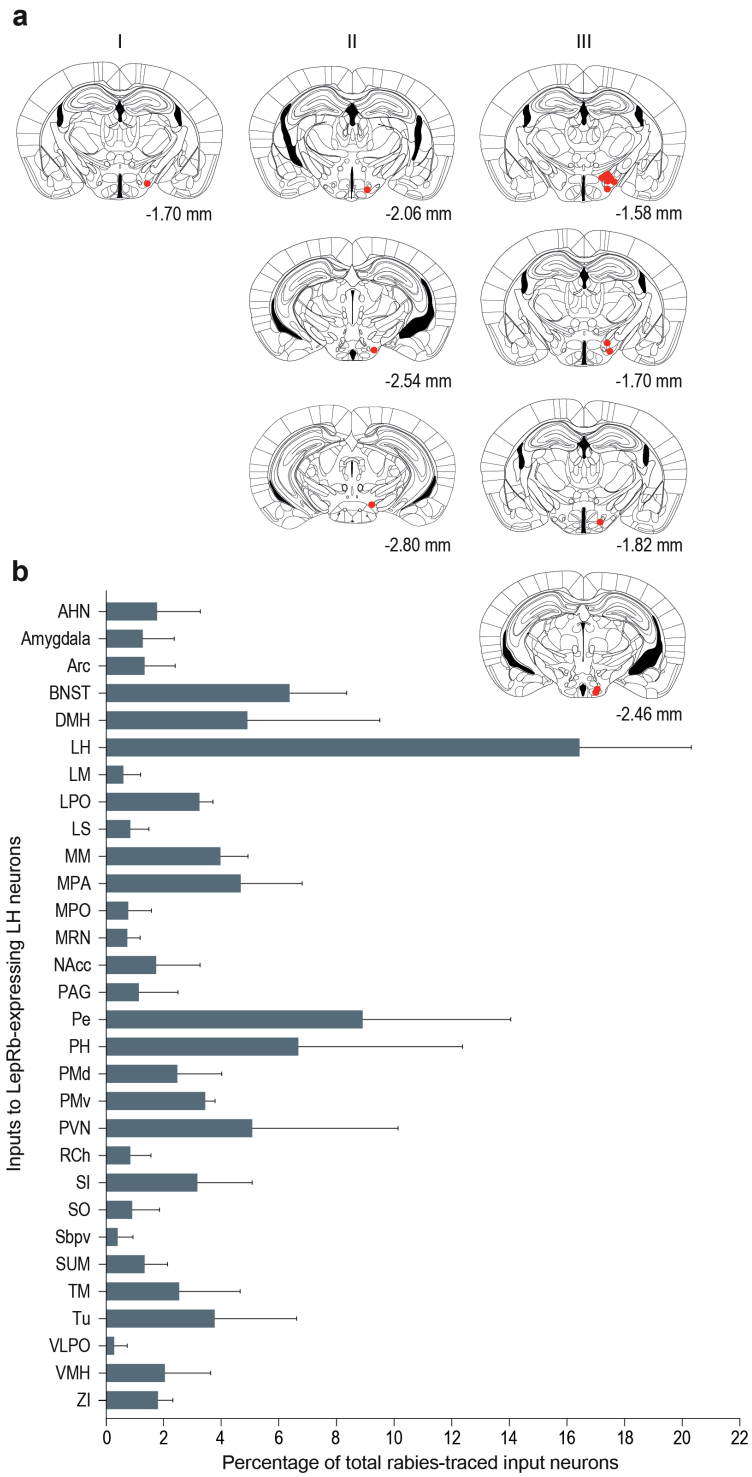
a
I
II
III
-1.70 mm
-2.06 mm
-1.58 mm
-2.54 mm
-1.70 mm
-2.80 mm
-1.82 mm
-2.46 mm
b
AHN
Amygdala
Arc
BNST
DMH
LH
LM
LPO
LS
MM
MPA
MPO
MRN
NAcc
PAG
Pe
PH
PMd
PMv
PVN
RCh
SI
SO
Sbpv
SUM
TM
Tu
VLPO
VMH
ZI
Inputs to LepRb-expressing LH neurons
0
2
4
6
8
10
12
14
16
18
20
22
Percentage of total rabies-traced input neurons

Figure 5. Rabies-traced inputs to LepRb-expressing LH neurons. a) Starter cells found in the different mice that were used for input tracing to LepRb-expressing LH neurons. All three mice were injected with 3.0×107 g.c./µl rAAV5-Flex-TCB unilaterally. Mice in which the starter cells were not correctly targeted to the LH were excluded from the input analysis. b) Different rabies-traced areas that input onto LepRb-expressing LH neurons. Areas were considered as input area, and displayed here, when they consisted of more than 1% of all rabies-traced inputs within one mouse. AHN, anterior hypothalamic nucleus; Arc, arcuate hypothalamic nucleus; BNST, bed nucleus of the stria terminalis; DMH, dorsomedial hypothalamic nucleus; LH, lateral hypothalamus; LM, lateral mammillary nucleus; LPO, lateral preoptic area; LS, lateral septal nucleus; MM, medial mammillary nucleus; MPA, medial preoptic area; MPO , medial preoptic nucleus; MRN, midbrain reticular nucleus; NAcc, nucleus accumbens; PAG, periaqueductal grey; Pe, periventricular hypothalamic nucleus; PH, posterior hypothalamic nucleus; PMd, premammillary nucleus dorsal part; PMv, premammillary nucleus ventral part; PVN, paraventricular hypothalamic nucleus; RCh, retrochiasmatic area; SI, substantia innominata; SO, supraoptic nucleus; Sbpv, subparaventricular zone; SUM, supramammillary nucleus; TM, tuberomammillary nucleus; Tu, tuberal nucleus; VLPO, ventrolateral preoptic nucleus; VMH, ventromedial hypothalamic nucleus; ZI, zona incerta.

was quantified to elucidate the different areas that input onto LepRb-expressing LH neurons (Supplementary Figure 1a). All areas that contained more than 1% of the total amount of input neurons per single mouse were considered input areas (Supplementary Figure 1b). The most prominent input areas to LepRb-expressing LH neurons were the LH itself, the dorsomedial hypothalamic nucleus (DMH), the tuber cinereum area (TC), and the posterior part of the anterior hypothalamic area (AHP). However, these mice were injected with different titers of rAAV5-Flex-TCB. When we, subsequently, assessed the influence of different titers of rAAV5-Flex-TCB on the results of input tracing to LepRb-expressing LH neurons, we found that percentages of input neurons in two brain regions, namely the DMH and the intermediate part of the lateral septal nucleus (LSI), were significantly affected by TVA titer used (Supplementary Figure 2). The percentage of rabies-labeled input neurons detected in the DMH was significantly higher when a TVA titer of 1.0×10^8 g.c./µl was used, as compared to titers of 1.0×10^7 g.c./µl or 1.0×10^9 g.c./µl (Supplementary Figure 2a). In the LSI, using a TVA titer of 1.0×10^8 g.c./µl resulted in a significant lower percentage of rabies-traced input neurons as compared to titers of 1.0×10^7 g.c./µl or 1.0×10^9 g.c./µl (Supplementary Figure 2b). When a titer of 1.0×10^9 g.c./µl was used, significant more neurons were traced in the LSI compared to titers of 1.0×10^7 g.c./µl and 1.0×10^8 g.c./µl (Supplementary Figure 2b).

Although percentages of labeled inputs in other brain regions were not significantly affected by TVA titer, there were clear differences found in many input regions. Therefore, we repeated the experiment in four mice that were injected with the titer found to be optimally specific and efficient in the qPCR experiment and other previously mentioned experiments, being 3.0×10^7 g.c./µl rAAV5-Flex-TCB. Again, only correctly targeted mice were included in the analysis

(n=3, Figure 5a), and areas that contained more than 1% of the total amount of input neurons per single mouse were considered input areas (Figure 5b). We found that the LH itself, the periventricular hypothalamic nucleus (Pe), the posterior hypothalamic nucleus (PH), the bed nucleus of the stria terminalis (BNST), and the paraventricular hypothalamic nucleus (PVN) are the most prominent input areas to LepRb-expressing LH neurons.

DISCUSSION

We found that careful consideration of the titer of Cre-dependent TVA is of utmost importance to avoid non-specific results when using modified rabies virus tracing technology for mapping neuronal circuitries.

Previous studies have shown that modified rabies virus tracing technology is a highly effective and specific method to elucidate neuronal circuits in the brain[13,15,16,21,23,24]. Others mostly used control experiments to assess that rabies virus is dependent on expression of the helper viruses, and thus not leaky[21,27,28]. To the best of our knowledge, however, no studies have investigated the effect of different titers of Cre-dependent TVA on rabies efficiency and specificity. We performed different experiments to assess what the most optimal titer of Cre-dependent TVA was for mapping inputs to LepRb-expressing LH neurons, which still resulted in efficient rabies tracing of inputs in LepRb-Cre mice, but had neglectable infection in wildtype control mice.

Using qPCR we found that probably around 1 in every ~160000 genomic copies of the TVA vector is already recombined during the growth phase of the plasmid, long before injection. This means that with an injection of 1 µl of the virus with a titer of 1.0×10^7 genomic copies per µl around 62.5 TVA particles will already be recombined and may result in expression in the absence of Cre recombinase. To achieve optimal specificity, it is therefore important to inject as little Cre-dependent, unrecombined, TVA particles as possible, so that as little as possible prematurely recombined TVA particles are injected. Of course this has its limitations, because efficiency must be optimal. AAV vectors are known to have a MOI of ~100.000 genomic copies per host cell to be infected, indicating that, in order to obtain optimal efficiency, ~100.000 virus particles per neuron are needed. A decrease in specificity due to leaky expression upon increasing TVA titer was also shown *in vivo*, where wildtype control mice that were injected with high titers of Cre-dependent TVA showed a remarkable high level of rabies expression. This indicates that the TVA receptor is expressed leaky, thus in the absence of Cre recombinase. Using qPCR we found that with a TVA titer of 1.0×10^9 genomic copies per µl around 6250 TVA particles will be spontaneously recombined and may result in infection. Based on an MOI of 100.000 viral particles per cell[32],

6250 would be neglectable. However, our *in vivo* results show that a TVA titer of 1.0×10^9 genomic copies per µl indeed results in unspecific TVA infection. This is problematic for rabies tracing, especially when few Cre+ neurons are present in the target area. Based on our qPCR and *in vivo* results we concluded that a titer of 3.0×10^7 g.c./µl is probably the highest titer with lowest unspecific recombinations. Falsely rabies-labeled input neurons due to leaky TVA receptor expression cannot be distinguished from 'normal' rabies-labeled input neurons, and thereby leaky TVA expression hinders specific tracing[25]. Rabies expression itself was dependent on TVA, since wildtype control mice that were not injected with TVA did not express detectable levels of rabies, consistent with previous studies[21,27,28].

Based on our *in vivo* result that a titer of 1.0×10^7 g.c./µl shows least expression in wildtype control mice, and on our qPCR result that a titer of 3.0×10^7 g.c./µl is probably the highest titer with lowest unspecific recombinations, we considered a rAAV5-Flex-TCB titer between 1.0 and 3.0×10^7 g.c./µl the most optimal titer for modified rabies traced input mapping of LepRb-expressing LH neurons. When Cre+ neurons are present, a low titer of TVA receptors is already sufficient to infect Cre+ neurons. A higher titer of TVA receptors seemingly leads to more starter cells in Cre+ animals, but in fact it only hinders specificity, since it increases the chance of unspecific infection of Cre– neurons. By this means, a too high TVA titer results in many TVA-infected but Cre– neurons, especially in the case of few Cre+ neurons. These unspecifically TVA-infected neurons subsequently become rabies-labeled neurons and are then wrongly considered as input neurons. When many Cre+ neurons are to be infected, this difference in specificity between low and high titers becomes neglectable. However, especially when there are fewer Cre+ neurons it is important to be cautious with a too high TVA titer. Since LepRb-expressing neurons are not ubiquitously expressed in the LH, careful consideration is essential to avoid non-specific results.

Even though the highest titer of rAAV5-Flex-TCB tested, 1.0×10^9 g.c./µl, resulted in more TVA-infected neurons (albeit unspecific), no differences in amount of rabies-labeled neurons were found between the different TVA titers in Cre+ animals. This is because rabies is highly sensitive for TVA receptor expression[25]; rabies only needs few starter cells to be able to infect and spread monosynaptically to input neurons. Thus, the seemingly high efficiency of the highest TVA titer was probably due to leakiness of the vector at this high concentration and does not affect efficiency of rabies labeling.

Furthermore, we showed that, when the lower TVA titer is used for input mapping, many brain regions were found to provide input to LepRb-expressing

LH neurons. The most prominent input areas to LepRb-expressing LH neurons are other neurons in the LH itself, the periventricular hypothalamic nucleus (Pe), the posterior hypothalamic nucleus (PH), the bed nucleus of the stria terminalis (BNST), and the paraventricular hypothalamic nucleus (PVN).

The LH is a central player in the regulation of energy balance, partly because it is a key area where leptin exerts its action upon[10,11,22,36–38]. The LH projects to the periventricular hypothalamic nucleus (Pe)[39]. The Pe also receives projections originating in the anterior hypothalamic area[40,41], paraventricular nucleus of the hypothalamus[42] and is densely innervated by ghrelin-containing projections[43]. A functional MRI study found a ghrelin induced response in the Pe[44], underlining ghrelin sensitivity of the Pe and thereby its involvement in the regulation of feeding behavior. The Pe is known to express the long-form leptin receptors[9] and is now found to project to leptin sensitive LH neurons, thereby linking the working mechanisms of leptin and ghrelin.

The posterior hypothalamic nucleus (PH) plays an important role in autonomic and behavioral control mechanisms, and as such receives inputs from various brain regions, ranging from cortical and subcortical to brainstem and cerebellar regions[45]. The bed nucleus of the stria terminalis, the ventral pallidum, as well as the lateral and medial septal nuclei are some of the many input regions to the PH. Çavdar and colleagues suggested that these inputs areas, together with the PH, are all involved in autonomic regulation and make up different pathways that regulate autonomic and somatomotor activity[45]. Projections of the PH to the LH may therefore relay this autonomic information to the LH, where this autonomic information may be integrated with information about homeostatic energy balance, thus exerting an influence over feeding behavior.

The bed nucleus of the stria terminalis (BNST) is innervated by ghrelin projections, just as the paraventricular hypothalamic nucleus (PVN), the Pe, the arcuate nucleus, the DMH and the LH[43]. It is already known to project to the anterior hypothalamic area[40,46], and to relay cortico-limbic input to the PVN, where this information is integrated with visceral and interoceptive inputs[47]. The ventral part of the BNST sends glutamatergic and GABAergic efferents to the ventral tegmental area, stimulations of which results in aversive and anxiogenic behavioral phenotypes (for stimulation of glutamatergic projections) or rewarding and anxiolytic phenotypes (for stimulation of GABAergic projections)[48]. By this means, BNST circuit elements orchestrate divergent aspects of motivational and emotional processing[48]. Since we found that the BNST is a major input to LepRb-expressing LH neurons, this might indicate that the BNST provides motivational and emotional inputs to the regulation of feeding behavior

The paraventricular hypothalamic nucleus (PVN) is part of a circuit

that is involved in metabolic regulation; it receives GABAergic projections from the LH that promote feeding[49]. The PVN is known to regulate pituitary gland function and feeding, it innervates autonomic preganglionic neurons, and is activated by intravenous leptin[46,50]. It is innervated by leptin-activated neurons in the caudal DMH, which may underlie the neuroendocrine and autonomic effects of leptin mediated by the PVN[46]. The PVN is also innervated by ghrelin-containing axon terminals[43] and receives input from the arcuate nucleus of the hypothalamus, which are NPY and POMC neurons. Local ghrelin boutons in the PVN are in direct apposition to NPY axon terminals[43]. The fact that ghrelin produced in hypothalamic regions signals to the PVN, which is important for metabolic regulation, and that ghrelin synapses are anatomically close to NPY synapses, suggests that hypothalamic ghrelin is part of a central regulatory loop modulating the orexigenic drive. In the PVN, ghrelin increases the activity of NPY axon terminals, thereby probably increases the release of NPY and GABA, that modulate the activity of postsynaptic POMC neurons[43]. The PVN subsequently inputs to leptin sensitive neurons in the LH, thereby combining orexigenic information to neurons sensitive to anorexigenic signals. This underlines the idea that the LH is a central regulator of homeostatic regulation of energy balance.

The current study has some shortcomings. First of all, sample sizes were relatively small. Also, TVA injections with a titer of 1.0×10^9 g.c./µl were done unilaterally, whereas injections with a titer of 1.0×10^7 g.c./µl and 1.0×10^8 g.c./µl were done bilaterally. This complicates comparison of the different titers, however, results were still elucidative since trends in clear directions were detected. Future studies should therefore perform experiments with a larger sample size in which all titers are injected unilaterally, so that intra- and interhemispheric inputs can be assessed within a single mouse, and that titers can be compared more easily.

Modified rabies virus tracing technology also has some limitations. Under most conditions, only a fraction of all inputs to the starter cells are labeled. This can be caused by insufficient expression of G in the starter cells, too few RV*d*G particles entering the starter cells, or a too short time available for trans-synaptic spread before starter cells die[26]. Secondly, since rabies does not label all inputs, the probability of labeling might be different for different input cells. This might be caused by different numbers of synaptic contacts, the subcellular locations of synaptic contacts, or by different expression of receptors for G on axon terminals. This should always be considered when interpreting rabies tracing results[26]. Finally, rabies-infected neurons have a surviving window of around 14 days, which is relatively long in comparison to other neurotropic virus-based tracing techniques, but which is still a short time to perform, for example, other studies

to test rabies-labeled neurons specifically. It is likely that cell health deteriorates before actual cell death; it has been suggested that cell viability is affected by 12 days after rabies infection[51,52]. On the other hand, a timeframe of around 3-10 days is necessary to allow trans-synaptic spread of RV[26], restricting the time window even further. We chose to euthanize animals 8 days after rabies infection, since no differences in structural integrity of neurons or trans-synaptic efficiency could be detected at 8 days compared to 4 days post-infection[25].

In summary, modified rabies virus tracing technology is a highly effective and specific method to elucidate neuronal circuits. However, we place on cautionary note on its use, because we found that specificity of rabies tracing decreases due to leaky TVA receptor expression when TVA titer increases. Since a titer between 1.0-3.0×10^7 g.c./µl shows least expression in wildtype control mice and is efficient for mapping input neurons in LepRb-Cre mice, we recommend this titer as the most optimal rAAV5-Flex-TCB titer for mapping inputs to LepRb-expressing neurons in the LH. We furthermore showed that when a titer of 3.0×10^7 g.c./µl is used for input mapping, LepRb-expressing LH neurons receive inputs from a broad variety of brain areas, but that neurons in the LH, the Pe, the PH, the BNST, and the PVN are the most prominent inputs. Thus, as a final note, before you go viral with modified rabies tracing technology, carefully consider the titer of TVA receptor you use.

REFERENCES

1. Friedman, J. M. & Halaas, J. L. Leptin and the regulation of body weight in mammals. Nature 395, 763–70 (1998).
2. Halaas, J. L. et al. Weight-Reducing Effects of the Plasma Protein Encoded by the Obese Gene. Science (80-.). 269, 543–546 (1995).
3. Rosenbaum, M., Sy, M., Pavlovich, K., Leibel, R. L. & Hirsch, J. Leptin reverses weight loss–induced changes in regional neural activity responses to visual food stimuli. J. Clin. Invest. 118, 2583–2591 (2008).
4. Hinkle, W., Cordell, M., Leibel, R., Rosenbaum, M. & Hirsch, J. Effects of reduced weight maintenance and leptin repletion on functional connectivity of the hypothalamus in obese humans. PLoS One 8, e59114 (2013).
5. Slomp, M. et al. Stressing the importance of choice – validity of a preclinical free-choice high-caloric diet paradigm to model behavioral, physiological, and molecular adaptations during human diet-induced obesity and metabolic dysfunction. J. Neuroendocrinol. e12718 (2019). doi:10.1111/jne.12718

6. Frederich, R. C. et al. Leptin levels reflect body lipid content in mice: evidence for diet-induced resistance to leptin action. Nat. Med. 1, 1311–1314 (1995).
7. Davis, J. F. et al. Leptin Regulates Energy Balance and Motivation through Action at Distinct Neural Circuits. Biol. Psychiatry 69, 668–674 (2012).
8. Enriori, P. J., Sinnayah, P., Simonds, S. E., Garcia Rudaz, C. & Cowley, M. A. Leptin Action in the Dorsomedial Hypothalamus Increases Sympathetic Tone to Brown Adipose Tissue in Spite of Systemic Leptin Resistance. J. Neurosci. 31, 12189–12197 (2011).
9. Elmquist, J. K. Hypothalamic pathways underlying the endocrine, autonomic, and behavioral effects of leptin. Physiol. Behav. 74, 703–708 (2001).
10. Elias, C. F. et al. Leptin Differentially Regulates NPY and POMC Neurons Projecting to the Lateral Hypothalamic Area. Neuron 23, 775–786 (1999).
11. Leinninger, G. M. et al. Leptin acts via leptin receptor-expressing lateral hypothalamic neurons to modulate the mesolimbic dopamine system and suppress feeding. Cell Metab. 10, 89–98 (2009).
12. de Vrind, V. A. J., Rozeboom, A., Wolterink-Donselaar, I. G., Luijendijk-Berg, M. C. M. & Adan, R. A. H. Effects of GABA and Leptin Receptor-Expressing Neurons in the Lateral Hypothalamus on Feeding, Locomotion, and Thermogenesis. Obesity 27, 1123–1132 (2019).
13. Kuypers, H. G. J. M. & Ugolini, G. Viruses as transneuronal tracers. Trends Neurosci. 13, 71–75 (1990).
14. Vercelli, A., Repici, M., Garbossa, D. & Grimaldi, A. Recent techniques for tracing pathways in the central nervous system of developing and adult mammals. Brain Res. Bull. 51, 11–28 (2000).
15. Beier, K. T. et al. Circuit Architecture of VTA Dopamine Neurons Revealed by Systematic Input-Output Mapping. Cell 162, 622–634 (2015).
16. Watabe-Uchida, M., Zhu, L., Ogawa, S. K., Vamanrao, A. & Uchida, N. Whole-Brain Mapping of Direct Inputs to Midbrain Dopamine Neurons. Neuron 74, 858–873 (2012).
17. Grealish, S. et al. Monosynaptic Tracing using Modified Rabies Virus Reveals Early and Extensive Circuit Integration of Human Embryonic Stem Cell-Derived Neurons. Stem Cell Reports 4, 975–983 (2015).
18. Ohara, S. et al. Dual transneuronal tracing in the rat entorhinal-hippocampal circuit by intracerebral injection of recombinant rabies virus vectors. Front. Neuroanat. 3, 1–11 (2009).

19. Ogawa, S. K. & Watabe-Uchida, M. Organization of dopamine and serotonin system: Anatomical and functional mapping of monosynaptic inputs using rabies virus. Pharmacol. Biochem. Behav. 0–1 (2017). doi:10.1016/j.pbb.2017.05.001
20. Osakada, F. & Callaway, E. M. Design and generation of recombinant rabies virus vectors. Nat. Protoc. 8, 1583–1601 (2013).
21. Sun, Y. et al. Cell-type-specific circuit connectivity of hippocampal CA1 revealed through cre-dependent rabies tracing. Cell Rep. 7, 269–280 (2014).
22. Jennings, J. H., Rizzi, G., Stamatakis, A. M., Ung, R. L. & Stuber, G. D. The Inhibitory Circuit Architecture of the Lateral Hypothalamus Orchestrates Feeding. Science 341, 1517–1522 (2013).
23. Ruigrok, T. J. H., Pijpers, A., Goedknegt-Sabel, E. & Coulon, P. Multiple cerebellar zones are involved in the control of individual muscles: A retrograde transneuronal tracing study with rabies virus in the rat. Eur. J. Neurosci. 28, 181–200 (2008).
24. Miyamichi, K. et al. Cortical representations of olfactory input by trans-synaptic tracing. Nature 472, 191–199 (2011).
25. Miyamichi, K. et al. Dissecting Local Circuits : Parvalbumin Interneurons Underlie Broad Feedback Control of Olfactory Bulb Output. Neuron 80, 1232–1245 (2013).
26. Callaway, E. M. & Luo, L. Monosynaptic Circuit Tracing with Glycoprotein-Deleted Rabies Viruses. J. Neurosci. 35, 8979–8985 (2015).
27. Wickersham, I. R. et al. Monosynaptic Restriction of Transsynaptic Tracing from Single, Genetically Targeted Neurons. Neuron 53, 639–647 (2007).
28. Wall, N. R., Wickersham, I. R., Cetin, A., De La Parra, M. & Callaway, E. M. Monosynaptic circuit tracing in vivo through Cre-dependent targeting and complementation of modified rabies virus. Proc. Natl. Acad. Sci. 107, 21848–21853 (2010).
29. Callaway, E. M. Transneuronal circuit tracing with neurotropic viruses. Curr. Opin. Neurobiol. 18, 617–623 (2008).
30. Paxinos, G. & Franklin, K. B. J. The Mouse Brain in Stereotaxic Coordinates. (Academic Press, 2001).
31. Allen Institute for Brain Science. Allen Mouse Brain Atlas. (2004). Available at: http://mouse.brain-map.org/.
32. Ellis, B. L. et al. A survey of ex vivo/in vitro transduction efficiency of mammalian primary cells and cell lines with Nine natural adeno-associated virus (AAV1-9) and one engineered adeno-associated virus serotype. Virol. J. 10, 1–10 (2013).

33. Charvet, C. J., Cahalane, D. J. & Finlay, B. L. Systematic, cross-cortex variation in neuron numbers in rodents and primates. Cereb. Cortex 25, 147–160 (2015).
34. Herculano-Houzel, S. The human brain in numbers: a linearly scaled-up primate brain. Front. Hum. Neurosci. 3, 1–11 (2009).
35. McCarty, D. M., Young, S. M. & Samulski, R. J. Integration of Adeno-Associated Virus (AAV) and Recombinant AAV Vectors. Annu. Rev. Genet. 38, 819–845 (2004).
36. Grossman, S. P., Dacey, D., Halaris, A. E., Collier, T. & Routtenberg, A. Aphagia and Adipsia After Preferential Destruction of Nerve Cell Bodies in Hypothalamus. Science (80-.). 202, 537–539 (1978).
37. Sweeney, P. & Yang, Y. An Inhibitory Septum to Lateral Hypothalamus Circuit That Suppresses Feeding. J. Neurosci. 36, 11185–11195 (2016).
38. Stricker, E. M., Swerdloff, A. F. & Zigmond, M. J. Intrahypothalamic injections of kainic acid produce feeding and drinking deficits in rats. Brain Res. 158, 470–473 (1978).
39. Bjorklund, A., Hokfelt, T. & Swanson, L. W. The hypothalamus. in Handbook of chemical neuroanatomy 1–124 (Elsevier, 1987).
40. Mitra, A., Guèvremont, G. & Timofeeva, E. Stress and sucrose intake modulate neuronal activity in the anterior hypothalamic area in rats. PLoS One 11, 1–21 (2016).
41. Saper, C. B., Swanson, L. W. & Cowan, W. M. The efferent connections of the anterior hypothalamic area of the rat, cat and monkey. J. Comp. Neurol. 182, 575–599 (1978).
42. Groenewegen, H. J. Organization of the Afferent Connections of the Mediodorsal Thalamic Nucleus in the Rat, Related To the Mediodorsal Prefrontal Topography. Neuroscience 24, 379–431 (1988).
43. Cowley, M. A. et al. The distribution and mechanism of action of ghrelin in the CNS demonstrates a novel hypothalamic circuit regulating energy homeostasis. Neuron 37, 649–61 (2003).
44. Wellman, P. J. et al. Brain reinforcement system function is ghrelin dependent: studies in the rat using pharmacological fMRI and intracranial self-stimulation. Addict. Biol. 17, 908–19 (2011).
45. Çavdar, S. et al. The afferent connections of the posterior hypothalamic nucleus in the rat using horseradish peroxidase. J. Anat. 198, 463–472 (2001).
46. Elmquist, J. K., Ahima, R. S., Elias, C. F., Flier, J. S. & Saper, C. B. Leptin activates distinct projections from the dorsomedial and ventromedial hypothalamic nuclei. Proc. Natl. Acad. Sci. U. S. A. 95, 741–6 (1998).

47. van Swieten, M. M. H., Pandit, R., Adan, R. a H. & van der Plasse, G. The neuroanatomical function of leptin in the hypothalamus. J. Chem. Neuroanat. (2014). doi:10.1016/j.jchemneu.2014.05.004
48. Jennings, J. H. et al. Distinct extended amygdala circuits for divergent motivational states. Nature 496, 224–228 (2013).
49. Wu, Z. et al. GABAergic Projections from Lateral Hypothalamus to Paraventricular Hypothalamic Nucleus Promote Feeding. J. Neurosci. 35, 3312–3318 (2015).
50. Garza, J. C., Kim, C. S., Liu, J., Zhang, W. & Lu, X.-Y. Adeno-associated virus-mediated knockdown of melanocortin-4 receptor in the paraventricular nucleus of the hypothalamus promotes high-fat diet-induced hyperphagia and obesity. J. Endocrinol. 197, 471–482 (2008).
51. Osakada, F. et al. New rabies virus variants for monitoring and manipulating activity and gene expression in defined neural circuits. Neuron 71, 617–631 (2011).
52. Wickersham, I. R., Finke, S., Conzelmann, K. K. & Callaway, E. M. Retrograde neuronal tracing with a deletion-mutant rabies virus. Nat. Methods 4, 47–49 (2007).

ACKNOWLEDGEMENTS

This work was supported by the European Union Seventh Framework Program (FP/2007-2013) [grant number 607310 (Nudge-it)]. The funding source had no involvement in the collection, analysis, or interpretation of the data, or in the writing of this article. We thank Inge Wolterink for assistance with vector injections.

SUPPLEMENTARY FIGURES

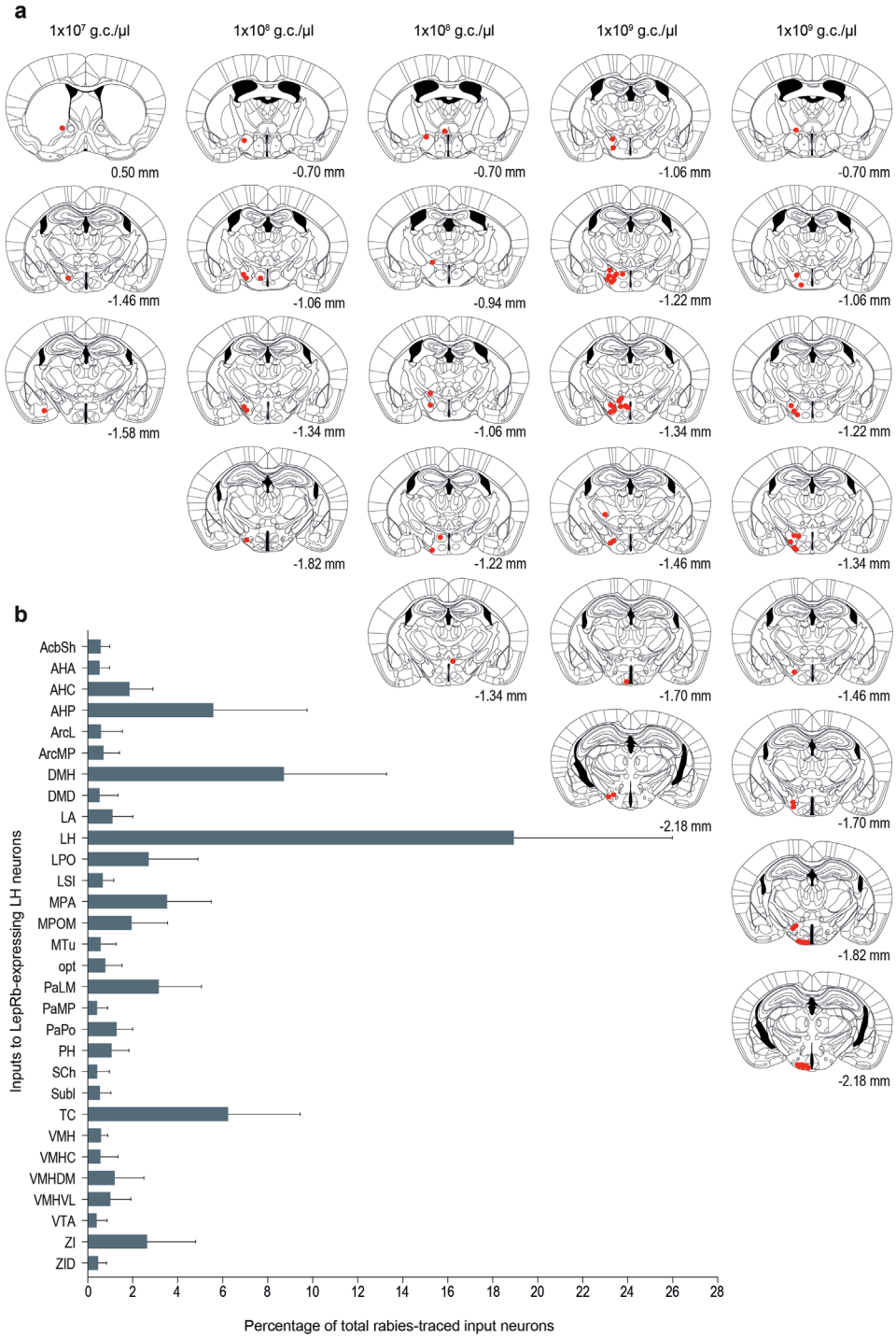

Supplementary Figure 1. Rabies-traced inputs to LepRb-expressing LH neurons using different titers of TVA receptor helper vector. a) Starter cells found in the different mice that were used for input tracing to LepRb-expressing LH neurons. Mice in which the starter cells were not correctly targeted to the LH were excluded from the input analysis. Second mouse with 1.0×108 g.c./µl rAAV5-Flex-TCB (in the middle) was correctly targeted to the LH and therefore included in the analysis, even though some starter cells were detected outside the LH. b) Different rabies-traced areas that input onto LepRb-expressing LH neurons. Areas were considered as input area, and displayed here, when they consisted of more than 1% of all rabies-traced inputs within one mouse. AcbSh, nucleus accumbens shell; AHA, anterior hypothalamic area anterior part; AHC, anterior hypothalamic area central part; AHP, anterior hypothalamic area posterior part; ArcL, arcuate hypothalamic nucleus lateral part; ArcMP, arcuate hypothalamic nucleus medial posterior part; DMH, dorsomedial hypothalamic nucleus; DMD, dorsomedial hypothalamic nucleus dorsal part; LA, lateroanterior hypothalamic nucleus; LH, lateral hypothalamic nucleus; LPO, lateral preoptic area; LSI, lateral septal nucleus intermediate part; MPA, medial preoptic area; MPOM , medial preoptic nucleus medial part; MTu, medial tuberal nucleus; opt, optical tract; PaLM, paraventricular hypothalamic nucleus lateral magnocellular part; PaMP, paraventricular hypothalamic nucleus medial parvicellular part; PaPo, paraventricular hypothalamic nucleus posterior part; PH, posterior hypothalamic area; SCh, suprachiasmatic nucleus; Subl, subincertal nucleus; TC, tuber cinereum area; VMH, ventromedial hypothalamic nucleus; VMHC, ventromedial hypothalamic nucleus central part; VMHDM, ventromedial hypothalamic nucleus dorsomedial part; VMHVL, ventromedial hypothalamic nucleus ventrolateral part; VTA, ventral tegmental area; ZI, zona incerta; ZID, zona incerta dorsal part.

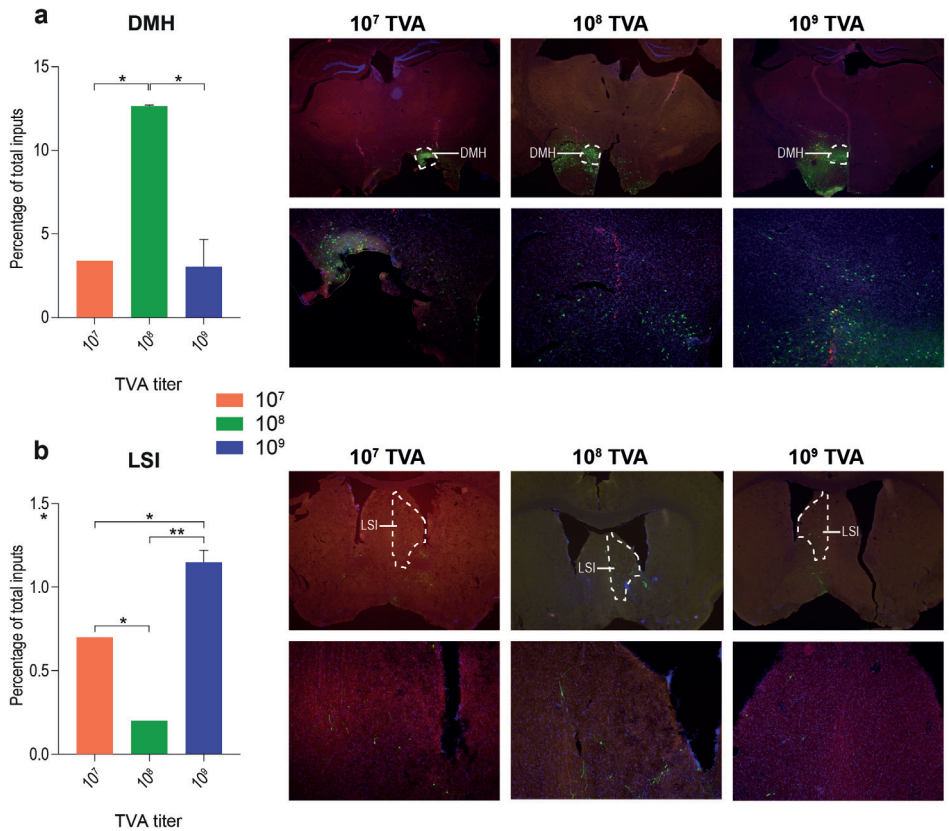

Supplementary Figure 2. TVA titer affects rabies tracing in the DM and LSI. a) The effect of different TVA titers on the percentages of traced input neurons in the dorsomedial hypothalamic nucleus (DMH). An ANOVA test revealed that a titer of 1×108 g.c./µl resulted in significantly more rabies-traced input neurons in the DMH than with the other two titers [$F(2,2) = 40.76$, $p = 0.024$]. Post hoc comparison (Tukey HSD): 1×107 g.c./µl [M = 3.4, SD = 0] and 1×109 g.c./µl [M = 3.05, SD = 1.63] both significantly less rabies-traced neurons than 1×108 g.c./µl [M = 12.65, SD = 0.07]. Representative immunohistochemical images with zooms underneath are shown on the right. b) The effect of different TVA titers on the percentages of traced input neurons in the intermediate part of the lateral septal nucleus (LSI). An ANOVA revealed that a titer of 1×109 g.c./µl resulted in significantly more traced input neurons [$F(2,2) = 180.6$, $p = 0.006$] Post hoc comparison (Tukey HSD) furthermore indicated that 1×107 g.c./µl [M = 0.7, SD = 0] and 1×109 g.c./µl [M = 1.15, SD = 0.07] both resulted in significantly less rabies-traced neurons than 1×108 g.c./µl [M = 0.2, SD = 0], and that a titer of 1×108 g.c./µl resulted in significantly less rabies-traced input neurons than 1×107 g.c./µl. On the right representative images (top) with zooms (bottom) are shown.

Appendix

Visualizing the invisible: brain clearing reveals leptin receptor-expressing neurons and their projections

Theresia J.M. Roelofs[a,b], Nefeli Kakava-Georgiadou[a], Roger A.H. Adan[a,c]

[a]Department of Translational Neuroscience, Brain Center Rudolf Magnus, University Medical Center Utrecht and Utrecht University, Universiteitsweg 100, 3584 CG Utrecht, the Netherlands
[b]Biomedical MR Imaging and Spectroscopy Group, Center for Image Sciences, University Medical Center Utrecht and Utrecht University, Bolognalaan 50, 3584 CJ Utrecht, the Netherlands
[c]Institute of Neuroscience and Physiology, The Sahlgrenska Academy at the University of Gothenburg, Sweden

We used the optimized version of the improved immunolabeling-enabled 3-dimensional imaging of solvent-cleared organs (iDISCO+) protocol to visualize leptin receptor-expressing neurons in 3D. For this aim we used transgenic C57BL6/J mice that expressed Cre-recombinase in leptin receptor-expressing neurons (LepRb-Cre) and that were crossed with tdTomato reporter mice. These LepRb-Cre × L-tdTomato mice (n = 7) permanently expressed tdTomato in leptin receptor-expressing cells. We optimized antibody concentration used in the iDISCO+ protocol and visualized leptin receptor-expressing neurons in the intact mouse brain using light sheet fluorescent microscopy.

INTRODUCTION

Immunohistochemistry has served neuroscience research since ages with specific and detailed information about expression of a broad variety of different proteins in the brain. A disadvantage of this method, however, is that post-mortem brain samples need to be sliced in thin sections, which complicates correct anatomical localization of the staining in three dimensions (3D), quantification of complete structures, and alignment of protein expression data with a brain atlas or imaging data of other modalities, for example with Magnetic Resonance Imaging (MRI) data. To overcome these hurdles and make alignment of post-mortem protein expression data with atlases or other 3D *in vivo* imaging data easier, brain clearing is a very convenient solution. Already in 1914 Spalteholz described that it is possible to make biological samples optically transparent by methods that reduce the internal differences in refractive index within tissue, thereby reducing scatter and enabling visualization of deeper structures[1]. More recently, newer techniques have been described that allow for immunofluorescent staining and clearing of the entire mouse brain. A 3-dimensional imaging of solvent cleared organs (3DISCO) protocol was first described in 2012[2] and improved into an immunolabeling-enabled 3-dimensional imaging of solvent-cleared organs (iDISCO) protocol in 2014[3]. This protocol was further optimized into the iDISCO+ protocol[4], which induces less sample shrinkage and better preserves brain morphology than its predecessor versions of the protocol.

We applied the iDISCO+ protocol to brains of mice that permanently express the reporter protein tdTomato in leptin receptor-expressing neurons, with the aim to visualize all leptin receptor-expressing neurons and their axonal projections in the mouse brain in 3D.

EXPERIMENTAL PROCEDURES

Animals

Experiments were approved by the Animal Ethics Committee of the University Medical Center Utrecht, The Netherlands, and were conducted in agreement with Dutch ('Wet op de Dierproeven', 2014) and European regulations (Guideline 86/609/EEC; Directive 2010/63/EU).

Healthy transgenic C57BL6/J mice that expressed Cre-recombinase in leptin receptor-expressing neurons (LepRb-Cre) were crossed with tdTomato reporter mice. These LepRb-Cre × L-tdTomato mice ($n = 7$) permanently expressed tdTomato in leptin receptor-expressing cells. Mice were housed under controlled temperature and humidity conditions, with a 12h-light/dark cycle (lights on at 7:00 a.m.). Animals had *ad libitum* access to water and standard chow, and tissues were provided as cage enrichment.

Brain preparation and staining

For brain preparation and staining the protocol described by Renier et al.[4] was used. This entailed the following procedures. Adult LepRb-Cre × L-tdTomato mice were euthanized by an intraperitoneal injection with an overdose of sodium pentobarbital (Euthanimal, Alfasan BV, The Netherlands) followed by intracardial perfusion-fixation with cold 0.1M phosphate buffered saline (PBS) and 4% paraformaldehyde (PFA). Brains were excised and post-fixed overnight in PBS containing 4% PFA at 4°C. After post-fixation, samples were washed twice in PBS for 1h. Subsequently, brains were washed in 20% methanol in MilliQ water for 1h, next in 40% methanol for 1h, 60% methanol for 1h, 80% methanol for 1h, and finally twice in 100% methanol for 1h. Brains were then bleached with ice cold 5% H_20_2 (consisting of 1 volume of 30% H_20_2 and 5 volumes of methanol) at 4°C overnight. Next, brains were slowly re-equilibrated at room temperature and re-hydrated in 80% methanol in MilliQ water for 1h, followed by re-hydration steps in 60% methanol for 1h, 40% methanol for 1h, 20% methanol for 1h, and finally twice in PBS with 0.2% TritonX-100 for 1h. These brains were then incubated in PBS with 0.2% TritonX-100, 20% DMSO, and 0.3M glycine at 37°C for 36h, blocked in PBS with 0.2% TritonX-100, 10% DMSO, and 6% Normal Donkey Serum (NDS) at 37°C for 2 days, and incubated in primary antibody solutions in 0.2% PBS-Tween with 10 µg/mL heparin (PTwH), 5% DMSO, and 3% NDS at 37°C for 7 days. Although tdTomato is a red fluorescent reporter protein, we immunostained the brains to obtain higher signal. Concentrations of the primary antibodies tested, rabbit anti-dsRed (Rb-anti-dsRed) or rabbit anti-red fluorescent protein (Rb-anti-RFP), and of the secondary antibody, donkey anti-rabbit-Alexa647 (D-anti-Rb 647), are summarized in Table 1. After incubation with the primary antibody

solution, brains were washed in PTwH for 24 h (during this day the PTwH solution was renewed 5 times), and subsequently incubated with the secondary antibody solution (D-anti-Rb 647 in PTwH with 3% NDS) at 37°C for another 7 days. Finally, the brains were washed in PTwH for 1 day before clearing and imaging.

Table 1. Different combinations of antibodies and their concentrations tested

Brain number	1° Rb-anti-dsRed	1° Rb-anti-RFP	2° D-anti-Rb 647
1	1:750		1:500
2	1:750		1:750
3	1:1000		1:500
4	1:1000		1:750
5		1:1500	1:2000
6		1:3000	1:2000
7		1:6000	1:2000

Concentrations of antibodies are all given as ratio antibody:solution.

Brain clearing using iDISCO+

Brain clearing was performed as described by Renier et al.[4]. This further optimized version of the improved 3-dimensional imaging of solvent cleared organs (i3DISCO) protocol[3] is based on the original 3DISCO protocol developed by Ertürk et al.[2,5] and is termed iDISCO+.

Brains were dehydrated in increasing steps of methanol in MilliQ water, starting with 20% methanol for 1 h, followed by 40% methanol for 1h, 60% methanol for 1 h, 80% methanol for 1h, and finally twice 100% methanol for 1h. Next, the brains were incubated overnight in methanol/Dichloromethan (1/2) (DCM, Sigma 270997-12X100ML) until the brains sank to the bottom of the Eppendorf tubes. Hereafter, the brains were washed twice in 100% DCM for 20 minutes to remove the methanol. The brains were then incubated (without being shaken) in DiBenzyl Ether (DBE, Sigma 108014-1KG) until they were cleared. They were stored in DBE at room temperature till they were imaged.

Light sheet fluorescent microscopy

Cleared brains were imaged in coronal orientation on an Ultramicroscope II (LaVision BioTec) light sheet microscope equipped with Inspector software (LaVision BioTec, version 5.0285.0). The light sheet microscope comprises an Olympus MVX-10 Zoom body (0.63-6.3×) equipped with an Olympus MVPLAPO 2× objective lens that includes dipping cap correction optics (LV OM DCC20) with a working distance of 5.7 mm. Images were taken with a sCMOS camera (Andor Neo) with a field of view of 2560 × 2160 pixels and a pixel size of 6.5 × 6.5 μm^2. The following laser filter combinations were used: Coherent OBIS 488-50

LX Laster with 525/50 nm emission filter, Coherent OBIS 561-100 LS Laser with 615/40 emission filter, Coherent OBIS 647-120 LX with 676/29 emission filter.

Brains were scanned with double-sided illumination, a sheet numerical aperture of 0.148348 (which results in a sheet thickness of 5 µm), and a step-size of (probably) 3 µm using the horizontal focusing light sheet scanning method with the optimal amount of steps and the included contrast blending algorithm. The effective magnification for all images was (around) 1.36× (zoom body * objective and dipping lens = ~0.63× * 2.152×).

Image processing

Imaris (Bitplane, http://www.bitplane.com/imaris/imaris) 3D imaging software was used for image processing. Data were first loaded into Imaris, converted from 16-bit to 8-bit images, and saved as a 3D Imaris file. These files were visually analysed, using the 3D rendering, rotation, zoom, and ortho and oblique slicer options 3D movies were created. All images presented here are snapshots of the actual 3D data.

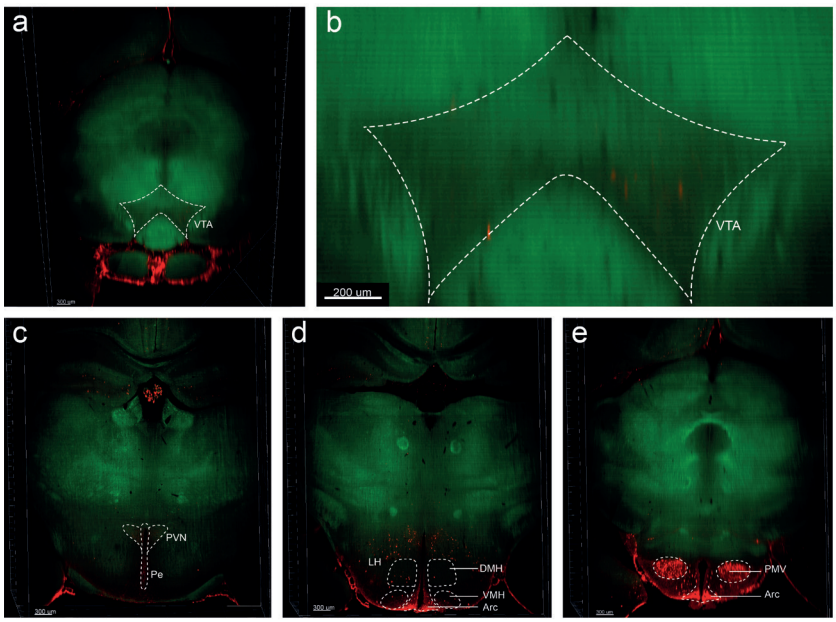

Figure 1. Coronal cross-sectional images throughout the 3-dimensional stained and cleared mouse brain. a) Cross-section showing leptin receptor-expressing neurons in the ventral tegmental area (VTA). b) Zoom of a cross-section through the VTA. Cross-sectional images showing leptin receptor-expressing neurons in the paraventricular hypothalamic nucleus (PVN, c), the periventricular hypothalamic nucleus (Pe, c), in the lateral hypothalamus (LH, d), arcuate nucleus of the hypothalamus (Arc, d and e), the dorsomedial hypothalamus (DMH, d), and the ventromedial hypothalamus (VMH, d), and the ventral part of the premammilary nucleus (PMV, e).

RESULTS

All seven LepRb-Cre × L-tdTomato mice brains were successfully cleared and red fluorescence showing LepRb expression was visible (data not shown). In brains 1 till 4, in which the primary antibody Rb-anti-dsRed was used, staining was suboptimal; only somata of LepRb-expressing neurons were visible, but no axonal fibers. Furthermore, intense red fluorescent signal was visible on the surface of the brain, probably caused by accumulation of the primary antibody (data not shown).

With the aim to overcome these issues, a different primary antibody was tested in brains 5 till 7. Also, the concentrations of both primary and secondary antibodies were lowered. In brains 5 till 7 the 'ring' of high signal intensity on the edges of the brain was still visible, but was less intense compared to brains 1 till 4. Especially in brains 6 and 7 signal of the staining was good; somata and axonal fibers of LepRb-expressing neurons were visible. However, in brain 7, in which the lowest concentration of primary antibody was used, signal intensity was much lower as compared to brain 6. Therefore, antibodies and concentrations thereof of brain 6 were most optimal.

Using Imaris 3D imaging software, brains were visually analysed and 3D movies as well as snapshots were made (only snapshots are printed here). Snapshots of brain 6, which was treated with the optimal antibody concentrations, are shown Figures 1 and 2. The remainder of the 'ring' of high signal intensity is visible in both figures.

Somata as well as axonal tracts of LepRb-expressing neurons were visible in the stained and cleared brain of mouse 6, treated with 1:3000 Rb-anti-RFP and 1:2000 D-anti-Rb 647. Axons could be followed in 3-dimensional rendering movies, but are more difficult to see in snapshots shown in Figures 1 and 2. Some hotspots of LepRb-expressing neurons were the ventral tegmental area (VTA, Figures 1a and 1b), the paraventricular hypothalamic nucleus (PVN, Figure 1c) the periventricular hypothalamic nucleus (Pe, Figure 1c), the lateral hypothalamus (LH), arcuate nucleus of the hypothalamus (Arc), the dorsomedial hypothalamus (DMH), and the ventromedial hypothalamus (VMH, Figure 1d), and the ventral part of the premammilary nucleus (PMV, Figure 1e).

To give some idea of the possibilities iDISCO+ offers, Figure 2 shows coronal as well as sagittal cross-sections through the LH, Arc, DHM and VMH on the same location (as indicated by the dotted line in the sagittal cross-section, Figures 2a and b). The same was done for the PMV and the Arc; in Figure 2c the coronal cross-section taken from location indicated by the dotted line in the sagittal cross-section through the PMV and Arc in Figure 2d is shown. In Figure 2d, the sagittal section through the PMV and Arc, shows some expression in the

dorsomedial hypothalamus (DMH) and ventromedial hypothalamus (VMH) as well.

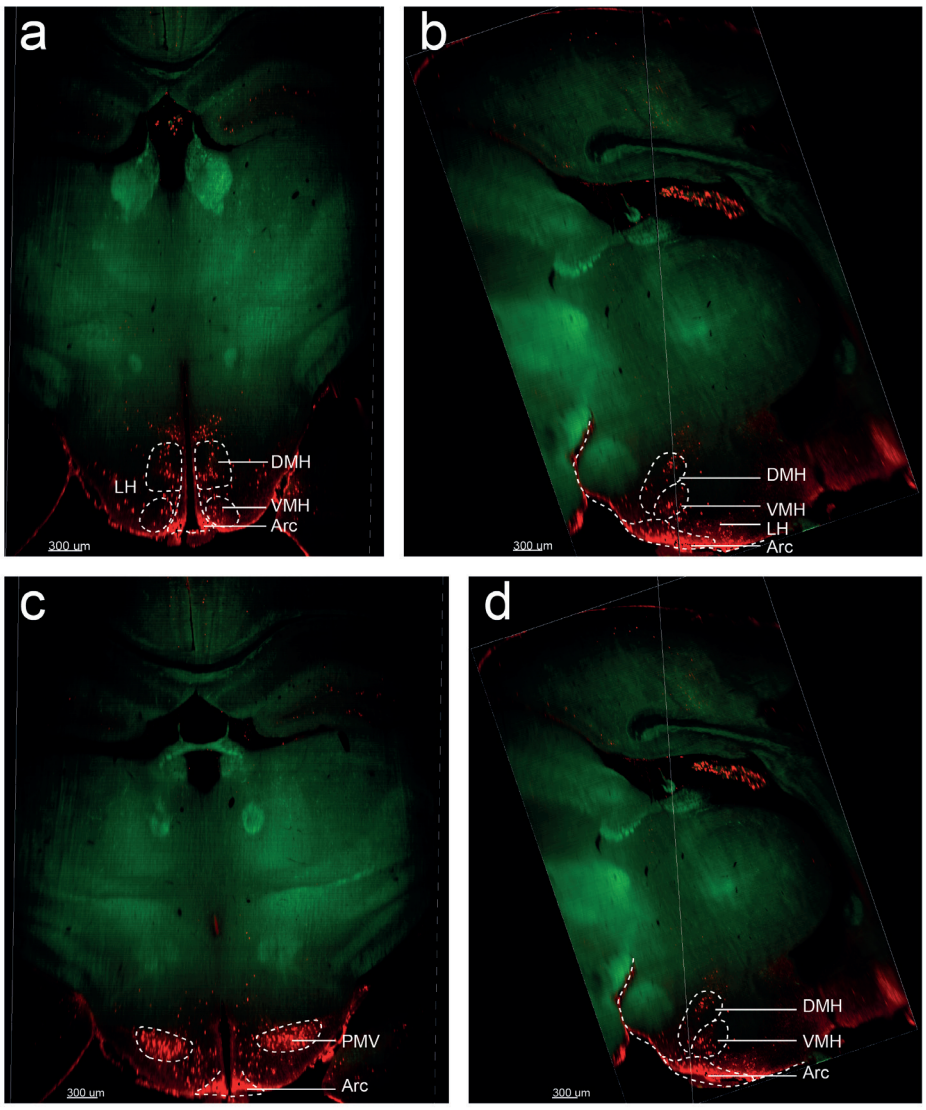

Figure 2. Cross-sections visualizing the same planes in both coronal and sagittal orientation. a) Coronal cross-section through the LH, DMH, VMH, and Arc. b) Sagittal cross-section through the LH, DMH, VMH, and Arc. The dotted line represents the place where the coronal cross-section is taken, as visualized in a. c) Coronal cross-section through the PMV and Arc. d) Sagittal cross-section through the PMV and Arc. The dotted line again represents the place where the coronal cross-section is taken, as visualized in c. Arc, arcuate nucleus of the hypothalamus; DMH, dorsomedial hypothalamus; LH, lateral hypothalamus; PMV, ventral part of the premammilary nucleus; VMH, ventromedial hypothalamus.

DISCUSSION

With the optimized iDISCO+ protocol for brain staining and clearing we used, sample shrinkage is less than with previous versions of this brain clearing protocol and therefore brain morphology is better preserved. In the green channel inner brain structures are visualized by autofluorescence. Autofluorescence of large cleared samples is most prominent in the blue-green spectrum, therefore we used a fluorophore in the far-red spectrum to achieve best signal-to-noise ratio[3]. Since inner structures are well visible and brain morphology is nicely preserved, automated registration of the images rains onto a reference brain atlas is relatively easy. This was not done in the current study, but would definitely be valuable to be able to systematically assess whole-brain protein expression. It would also be valuable for automated comparison between different brains or for comparison of these post-mortem protein expression imaging data to imaging data from other modalities, for example when a brain is first imaged *in vivo* using Magnetic Resonance Imaging (MRI) and subsequently cleared and imaged with light sheet fluorescence microscopy.

In the current study, LepRb expression was detected in a multitude of brain areas, among which the LH, DMH, VMH, Arc, PVN, Pe, PMV, and VTA. These areas are all involved in feeding behavior (see introduction of this thesis), which explains their expression of leptin receptors. However, the complete pattern of leptin receptor expression throughout the entire mouse brain should be analysed more systematically. In future studies, more mouse brains should be stained, cleared, and analysed thoroughly. In the current study, we immunohistochemically stained leptin receptors, to obtain better signal-to-noise ratio than the originally present tdTomato reporter tag. Future studies should perform double staining, for example against leptin receptors and tyrosine hydroxylase (TH), allowing assessment of the genetic identity of LepRb-expressing neurons,. When for example a TH and LepRb double staining is performed, this would allow to assess if LepRb-expressing neurons are dopaminergic. Furthermore, whole-brain quantification of LepRb expression should be done. When 3-dimensional Imaris images are registered to a reference atlas of the mouse brain, whole-brain quantification of protein expression can be achieved relatively easy. This could for example be done using the Mouse Brain Atlas from Paxinos and Franklin[6] or using the digital Allen Mouse Brain Atlas[7]. The latter atlas even contains data from LepRb-Cre mice, that could be used to align new data to, or to verify if LepRb-expressing areas found are in line with results from the Allen Brain Atlas. Since axons can be followed 3-dimensionally, iDISCO+ is also a great tool to assess structural connectivity between different LepRb-expressing brain regions. This measure of structural connectivity could then also be compared with for

example functional connectivity as measured by functional MRI or with structural connectivity data from the Allen Brain Atlas[8].

The 'ring' of high signal intensity along the edges of the brain hardly hinders analysis of protein expression, since it can be removed digitally from the Imaris images. However, it does hinder LepRb expression analysis in brain areas that are close to the edge of the brain, such as the Arc. Therefore, the staining protocol and/or the light sheet microscopy imaging procedure should be further improved to reduce this high signal intensity along the edges.

Summarizing, iDISCO+ is a powerful tool to visualize all leptin receptor-expressing neurons and their axonal projections in the mouse brain in a 3-dimensional way. Although axonal tracts are difficult to see in 2-dimensional snapshots of the original data, 3-dimensional images allow for identification and tracking of these axon bundles. Future studies should focus on further optimization of the staining and imaging protocol to be able to quantify whole-brain leptin receptor expression, also in brain regions near the edge of the brain, and on alignment of these data to a reference brain atlas, to other cleared mouse brains, and to imaging data from other modalities.

REFERENCES

1. Spalteholz, W. Über das Durchsichtigmachen von menschlichen und tierischen Präparaten und seine theoretischen Bedingungen, nebst Anhang: Über Knochenfärbung. Leipzig, S. Hirzel (1914).
2. Ertürk, A. et al. Three-dimensional imaging of solvent-cleared organs using 3DISCO. Nat. Protoc. 7, 1983–1995 (2012).
3. Renier, N. et al. iDISCO: a simple, rapid method to immunolabel large tissue samples for volume imaging. Cell 159, 896–910 (2014).
4. Renier, N. et al. Mapping of Brain Activity by Automated Volume Analysis of Immediate Early Genes. Cell 165, 1789–1802 (2016).
5. Ertürk, A. & Bradke, F. High-resolution imaging of entire organs by 3-dimensional imaging of solvent cleared organs (3DISCO). Exp. Neurol. 242, 57–64 (2013).
6. Paxinos, G. & Franklin, K. B. J. The Mouse Brain in Stereotaxic Coordinates. (Academic Press, 2001).
7. Allen Institute for Brain Science. Allen Mouse Brain Atlas. (2004). Available at: http://mouse.brain-map.org/.
8. Allen Institute for Brain Science. Allen Mouse Brain Connectivity Atlas. (2011). Available at: http://connectivity.brain-map.org/.

General Discussion

In this thesis I aimed to contribute to building bridges between different levels of understanding in current neuroscience research, by developing, applying, improving, and combining microscopic and macroscopic techniques aimed to unravel how ingestive behavior is regulated. We noted that, despite all kinds of advanced and innovative tools, it was still difficult to combine knowledge about the functioning of the brain and, more specifically, about regulation of ingestive behavior from a micro-scale cellular level with knowledge from a macro-scale neural network level. Also, true translation between preclinical and human data remains rare.

To start building these bridges, both between microscopic and macroscopic level, as well as between rodent and human neuroscience, we aimed to obtain molecular insights into the organization of neural networks involved in the regulation of ingestive behavior, and developed and applied preclinical experiments that have the potential to better translate to the clinic. Thereby, our work covers the entire range from macroscopic to microscopic level (see Figure 1 for an overview of the chapters along the macro- to microscopic scale). The work described in this thesis was focused on neural networks involved in the regulation of ingestive behavior, and by characterizing and manipulating these networks, we gained new insights into how brain regions within these networks connect and process feeding-related information.

Ingestive behavior assessed on a macroscopic level

In **chapter 1** of this thesis, we developed a preclinical protocol that was used to assess activation in response to manipulation of the oral or gastric environment. (For 'Highlights of this thesis' see Box 1.) Rats received a gastric balloon, which was inflated five times during a functional Magnetic Resonance Imaging (fMRI) scan, and mouth tubes, through which sucrose was flushed for five times during fMRI followed by water to rinse the mouth. We found that sucrose tasting induced positive fMRI responses in the ventral tegmental area (VTA) and negative responses in the septum. Moreover, we found a gradual neural activation in the anterior insula. Manipulation of the gastric environment, comparable to the feeling of a full stomach, induced a more widespread activation pattern, involving the orbitofrontal cortex, insular cortex, lateral hypothalamus, and the brain stem nucleus of the solitary tract.

Since a relatively comparable protocol was used in rats as is used in humans[1–3], we consider the translational value of this work to be high. This is underlined by our findings, which were largely in line with human studies that have shown that the anterior insula may play a key role in processing sweet taste oro-sensory signals[4–12] and that the nucleus of the solitary tract is involved in

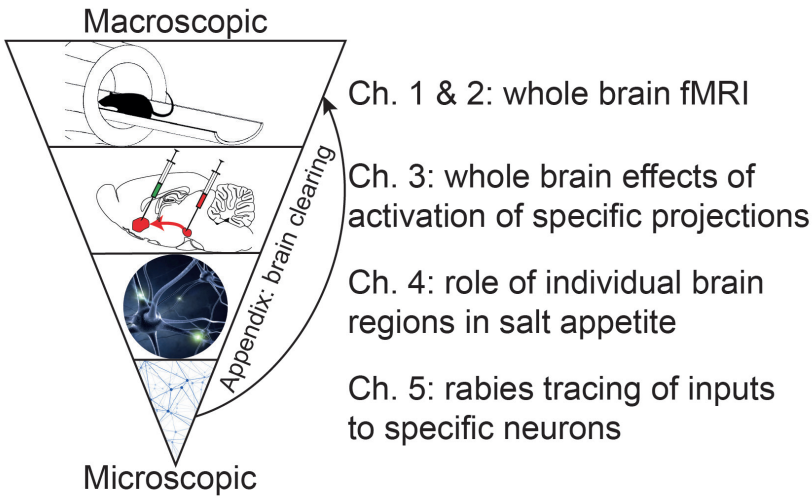

Figure 1. The different chapters of this thesis along a macroscopic to microscopic scale.

processing visceral information[1] (for reviews see refs. [13–15]). Furthermore, we found an additive signal in the insula over time in response to sweet tasting, which might be indicative of satiation that builds up upon repeated taste exposure[16–19]. The responses in mesolimbic areas induced by sucrose tasting or gastric distention may be associated with the rewarding effects of sweet taste and eating, which normally result in a filled stomach. These findings, that align with and corroborate findings described in human literature, show the translational value of preclinical (fMRI) experiments and give insight into how specific brain regions process feeding-related information and contribute to the process of satiation. Although it might be a point of discussion whether our rats experienced satiation (see 'Methodological considerations'), we think that the insular cortex is a key player in the regulation of satiation.

After assessing the neural activation responses to taste and gastric distention, we wondered what the differences in neural network connectivity in the resting brain were between hungry and satiated animals, both before and after they tasted sucrose. In **chapter 2** we measured functional connectivity and amplitudes of neural signals within neural networks in the resting brain using resting state fMRI. We hypothesized that functional connectivity between areas involved in feeding behavior and areas involved in reward and motivation would be stronger in food-restricted, and thus hungry animals, to make them alert to detect feeding-related stimuli in their environment and to prime them to initiate feeding behavior. For this same reason, we expected that functional connectivity would decline after sucrose tasting. The results were, however, not in line with our expectation. The data namely showed that functional connectivity between

brain regions involved in feeding behavior and motivation was not significantly different between *ad libitum*-fed rats and food-restricted rats, but that it tended to be higher in *ad libitum*-fed rats. We found a trend towards interaction between status of homeostatic energy balance (thus being hungry or satiated) and sucrose tasting; intrahemispheric functional connectivity tended to decrease stronger upon sucrose tasting in *ad libitum*-fed rats as compared to food-restricted rats. Furthermore, rs-fMRI signal amplitudes decreased stronger upon sucrose tasting in food-restricted rats as compared to *ad libitum*-fed rats. These findings suggest that status of homeostatic energy balance, thus being either hungry or satiated, and tasting sucrose interact in complex ways and can affect functional network organization, which may explain specific patterns in feeding behavior. Cortical as well as limbic areas were involved, showing that ingestive behavior is associated with different neural systems, that are all integratively regulated[20,21].

Our findings in chapter 2 underline the idea raised in the General Introduction of this thesis, that the homeostatic and hedonic systems that regulate ingestive behavior are not two separate systems that interact on some points, but that they probably form a much larger, highly interconnected system that unifies reward, cognition, emotion, and homeostatis[22]. This work, thereby, helped to characterize feeding-related neural networks, and shed light on how brain regions within these networks may connect and interact to process feeding-related information and to regulate ingestive behavior.

From macroscopic towards microscopic level

In chapters 1 and 2 I set out to form a bridge from preclinical to human neuroscience research by developing fMRI protocols that are exchangeable between the lab and the clinic, and by translating our preclinical findings to what is known from human literature. In chapters 3 to 5 and Appendix I focused on bridging the macroscopic and the microscopic level. We provided insight into the cellular underpinnings of behavior and neural network activity and connectivity, by combining more macroscopic, whole-brain techniques, such as fMRI, resting state fMRI, whole-brain (cFos) immunohistochemistry, behavioral pharmacology, and whole-brain clearing, with more microscopic, cellular techniques, such as chemogenetics, fiber photometry, and modified rabies tracing technique.

In **chapter 3** we developed a novel method that combines Designer Receptors Exclusively Activated by Designer Drug (DREADD)-technology and functional neuroimaging, and applied it to map whole-brain neural network activity in response to activation of specific neuronal projections. We targeted the mesocorticolimbic system, since it is of major importance for, amongst others, the regulation of feeding behavior. Two of its key pathways are the

Box 1. Highlights of this thesis

Chapter 1

We developed a new method that enables functional neuroimaging during oral and gastric sensory stimulation in rats in a single experimental setting.

This method showed that activity in the anterior insular cortex gradually increases upon repeated exposure, a possible neural correlate of an increase in satiation upon longer oral exposure to food, that many brain regions, known from human literature to be involved in processing oro-sensory and gastric signals, are also activated in rats, and that mesolimbic areas are activated in response to a sweet taste and gastric distention, which may be associated with rewarding effects.

Chapter 2

Translational functional neuroimaging studies in rodents have to potential to elucidate how homeostatic energy balance and tasting sucrose affect functional network organization.

Functional connectivity between feeding-related regions tended to be higher in satiated than in hungry rats, but tended to decrease stronger upon sucrose tasting in satiated rats. This is indicative of a complex interaction of energy balance and changes hereof by sweet tasting, that may affect functional networks and hence ingestive behavior.

Chapter 3

We introduced a novel method – DREADD-phMRI – that combines chemogenetics with functional imaging to map whole-brain network activity in response to projection-specific activation, and thereby bridges functional brain studies from cell to systems level.

DREADD-phMRI of the mesocorticolimbic system revealed distinctive direct and indirect dopamine pathway activation.

Chapter 4

Using a multidisciplinary approach we found that the nucleus accumbens, but not the medial prefrontal cortex, is essential for the behavioral expression of salt appetite by mediating its motivational, but not the hedonic, component.

Although we found that dopamine neurons do encode the appreciation of salt, the role of the nucleus accumbens in salt appetite is independent of dopamine.

Chapter 5

For correct mapping of neuronal circuitries using modified rabies virus tracing technology it is of utmost importance to careful chose an optimally specific and efficient titer of the vector delivering the Cre-dependent TVA receptors.

The most prominent inputs to leptin receptor-expressing neurons in the lateral hypothalamus originate from other neurons in the lateral hypothalamus, from the periventricular hypothalamic nucleus, the posterior hypothalamic nucleus, the bed nucleus of the stria terminalis, and the paraventricular hypothalamic nucleus.

Appendix

Brain clearing using the optimized immunolabeling-enabled 3-dimensional imaging of solvent-cleared organs (iDISCO+) protocol visualizes leptin-receptor expressing neurons and their axonal projection trajectories in the mouse brain.

D

mesolimbic pathway projecting from the VTA to the nucleus accumbens (NAcc) and the mesocortical pathway projecting from the VTA to the medial prefrontal cortex (mPFC). The VTA-NAcc projection is involved in, amongst others, reward processing, learning and motivation, also related to ingestive behavior[23–30]. The VTA-mPFC projection is involved in many behaviors, including association learning, decision making, and inhibition[31–36]. (For more detailed descriptions of both projections, see General Introduction of this thesis.)

To get more insight into how activation of those two projections on a cellular level affects neural activity on a whole-brain level, we activated the projections in rats while scanning the animals using pharmacological fMRI (phMRI). In response to chemogenetic activation, we detected robust positive blood oxygenation level-dependent (BOLD) signal responses in DREADD-targeted as well as in remotely connected areas. We detected changes in activity in brain regions belonging to the direct and indirect pathways of the mesocorticolimbic system[26,37–39]. For example, ventral pallidum activation and the substantia nigra pars reticulata deactivation were detected, demonstrating the concept of mesocorticolimbic network activity with concurrent activation of the direct and indirect pathways upon stimulation of specific midbrain projection neurons. The detection of simultaneous direct and indirect pathway activity demonstrated the ability of DREADD-phMRI to gauge network activity upon activation of specific neuronal pathways. Moreover, these findings might also underline the concept of one system that integratively regulates feeding behavior, framed in the General Introduction of this thesis, because the direct and indirect pathways appear to be activated synergistically.

Besides, we found that VTA-mPFC and VTA-NAcc stimulation resulted in largely overlapping activation patterns. However, the NAcc was not activated upon VTA-mPFC stimulation, which suggested that projections originating from mPFC neurons (that receive input from the VTA) activate the mesocorticolimbic system independent of accumbens activity. Chemogenetic activation specifically increased neuronal activity in primarily targeted and remotely connected brain regions, whereas functional connectivity between different brain regions remained stable. Further, we confirmed behavioral relevance of activation of these pathways by testing locomotor activity in response to VTA-NAcc activation; the time-course of the increase in locomotor activity exactly corresponded with the time-course of the increase in BOLD responses. Using cFos immunohistochemistry we validated that neuronal activity on a cellular level underlies neural activity as detected by phMRI.

This work showed that neuronal activation of single projections results in extended neural activity that can be detected with phMRI. Thereby, it provided

insight into the cellular underpinnings of the indirect measure of neural activity as retrieved with fMRI data. This knowledge about cellular mechanisms that underlie the fMRI signal applies to clinical fMRI findings as well, and forms a step on the way to bridge the macroscopic view of the MRI field with the more microscopic view of preclinical neuroscience. Furthermore, this DREADD-phMRI technology provides widely applicable opportunities to elucidate relationships between local neuronal activity and global network activity in a controllable manner. This technique provided more understanding of the functioning of the direct and indirect pathways, and can increase our understanding of the functioning and dysfunctioning of large-scale neuronal networks in health and disease.

In **chapter 4** we went further down the scale towards the microscopic level, while still combining the microscale, cellular techniques with more macroscale, behavioral output measures. We set out to study the contribution of the mesocorticolimbic system to sodium appetite, which refers to the process of salt becoming appetitive when an animal is deprived from salt. Of all the nutrients, a deficiency in sodium is one of the strongest homeostatic drives, evoking intense cravings for salty foods after salt deprivation[40–43]. Salt has the unique property that it can be aversive when the body's sodium levels are normal, and rewarding, when the body experiences a sodium deficiency. How neural circuits exactly regulate this 'switch' in salt appreciation depending on the body's needs remains unelucidated, and studies about a direct involvement of the dopamine system in salt appetite have been inconclusive[44–47]. Therefore, we studied the involvement of the dopamine system in salt appetite by applying fiber photometry, chemogenetics, behavioral pharmacology, and cFos immunohistochemistry in animals in which we manipulated their homeostatic sodium balance. We salt-deprived rats by injecting them with a diuretic and replacing their water and food by demineralized water and sodium-deficient food. By measuring neuronal activity from the mesocorticolimbic system, pharmacologically inactivating the NAcc or the mPFC, blocking dopamine neurotransmission, and assessing the consequences of these manipulations for behavior, we started bridging microscale with macroscale data. We applied a microstructural analysis of licking behavior[48–50] to data of rats licking for salt, sucrose, or water during free-intake paradigms after different manipulations. By doing so, we were able to tear the different aspects of sodium appetite apart; we found that the nucleus accumbens mediates the motivational aspect of sodium appetite, but not the hedonic aspect of salt, and that this does not depend on dopaminergic neurotransmission in the NAcc. This work thereby provided neuronal insight in mechanism underlying network organization, and indicated possible mechanisms via which the brain

regulates feeding behavior.

At the end of the macro- to microscopic scale, we wanted to assess the neuronal inputs to individual neurons in the lateral hypothalamus, a major hotspot in the regulation of energy homeostasis[51,52]. Leptin is an adipocyte-derived cytokine and has a significant role in the regulation of body weight in humans as well as rodents[53–56]. It increases energy expenditure, for example by increasing body temperature, and decreases appetite and energy intake by action via its receptor, LepRb, which is expressed in a multitude of brain areas, among which the LH[53,54,57–59]. LepRb-expressing LH neurons innervate the VTA, thereby relaying homeostatic information to the mesolimbic dopamine system, providing integration of homeostatic and hedonic regulation of energy balance. However, the neuronal inputs to LepRb-expressing neurons in the LH are still unknown. Therefore, in **chapter 5** we wanted to deepen our understanding of the cellular organization of this feeding-related neural network by mapping the inputs to this specific population of neurons.

To do so, we made use of modified rabies virus tracing technology, which allows mapping of monosynaptic inputs to genetically identifiable neurons. First, we optimized the technology, because we found that using a high titer of the TVA helper vector resulted in a high degree of non-specific input labelling. We discovered that carefully choosing the TVA virus titer, thus finding the optimal balance between specificity and efficiency of expression, is crucial for correct input mapping. Hereafter, we applied modified rabies tracing technology to map the inputs to LepRb-expressing LH neurons and found that other neurons in the LH itself, the periventricular hypothalamic nucleus, the posterior hypothalamic nucleus, the bed nucleus of the stria terminalis, and the paraventricular hypothalamic nucleus are the most prominent input areas. Thereby, this work provided microscopic level insights into the cellular organization of neuronal networks involved in feeding behavior.

Finally, in the **Appendix** we visualized microscopic neuronal pathways on a macroscopic level. We applied the optimized version of the improved immunolabeling-enabled 3-dimensional imaging of solvent-cleared organs (iDISCO+) protocol to brains of mice that permanently express the reporter protein tdTomato in LepRb-expressing neurons. We visualized individual leptin receptor-expressing neurons and their axonal projections in the entire mouse brain in a 3-dimensional way, which improves understanding of the molecular organization of feeding behavior-related neural networks.

Methodological considerations

All experiments described in this thesis have been performed in rats or mice. Especially in the first two chapters, where we aimed to develop a neuroimaging protocol that translates well to humans, it remains difficult to judge if we succeeded in bringing preclinical and human neuroscience research closer together. We did develop a protocol with which we were able to assess the effects of food restriction, *ad libitum* access to food, tasting sucrose, or gastric distention on neural activity and connectivity, and we did find brain areas that responded to these different stimuli and that aligned with what we know from human literature. Yet, we still cannot be sure if this protocol with the stimuli used does assess the same process as is assessed in comparable human experiments, being satiation. Even though we tested the volume of the gastric balloon *ex vivo* before using it *in vivo* so that it matched a filled stomach in inflated state, we cannot conclude that repeated in- and deflation of a gastric balloon resembles the feeling of a full stomach, and thus the natural process of eating. The option of pumping nutrients into the stomach would be more translational, but also complicates parsing the different effects of gastric stretch and nutrients inside the stomach. Furthermore, applying nutrients into the animal's stomach would have complicated the use of a block design paradigm, which would have resulted in reduced statistical power.

More or less the same question applies to whether or not our rats were truly satiated or hungry at the start of the experiments. Because we used a relatively stringent protocol to food-restrict the animals, we know that they were in a negative energy balance. However, whether they felt hungry or not at the very moment of scanning, remains questionable. The animals that had free access to food, were in positive energy balance. But we do not know if they ate the moment before being scanned and therefore felt satiated or not. These issues will probably remain complicating when performing animal research. An advantage of using rodents instead of human subjects is that other experimental conditions can be fully controlled and therefore the level of standardization is high. For example, the frequency and duration of a taste stimulus or gastric stretch, the rats' general preference for a tastant, as well as its genetic background, are all known variables and therefore don't confound the results. Using rodents and the high level of standardization also facilitates parsing different aspects of behavior. For example, in the protocols described in chapters 1 and 2, the effects of tasting, gastric distention, and status of homeostatic energy balance could be assessed separately.

Another consideration is the use of anesthesia for all fMRI experiments performed in this thesis. We decided to use a low level of isoflurane anesthesia,

first of all, to avoid movement and stress, and second, in the case of chapters 1 and 2, to avoid possible behavioral responses to satiation which would result in extra activation of brain regions involved in the behavioral response to satiation instead of the sensory process of satiation alone. Of course, the translational value of our studies would increase if animals could be scanned awake, just as most human studies. Especially in chapter 1, where we wanted to assess the process of getting satiated, one may wonder how the use of anesthesia affects the responses to the normally 'conscious' process of getting satiated. Unfortunately, time did not allow for the extensive training required to scan rats awake without high levels of fear and stress. In chapter 3, however, I would consider the use of mildly anesthetized animals an advantage; no stress, fear, or pain is caused to the animals, which also may confound fMRI findings. Moreover, the use of anesthetized rats enabled us to specifically study the causal effects of chemogenetically induced activation, without interference of conscious processing or arousal state.

When we dove deeper into the mechanistic underpinnings of ingestive behavior, for example by studying the 'switch' in salt appreciation in rats that were salt-deprived, a fundamental question that arose was what the actual translational value of preclinical experiments is where homeostatic state, in this case salt homeostasis, is manipulated to almost 'unnatural' levels. Although we as humans are not often seriously salt-deprived, at least not in the current society, the underlying mechanisms by which the brain encodes and regulates a switch in appreciation of a certain nutrient based on its homeostatic state, remain highly translational. The same applies to studying the inputs to leptin receptor-expressing neurons in the lateral hypothalamus; even though this research is fundamental in nature, it is relevant to study these inputs; it is commonly accepted that although the brains of rodents and humans are different, the same basic principles apply. Because the brains of humans and rodents show structural and functional similarities, the translational value of these fundamental experiments is relevant.

Future directions

The work described in this thesis made a genuine effort to bridge microscopic and macroscopic, as well as preclinical and human studies. By doing so, we tried to increase our understanding of the regulation of ingestive behavior. Even though we relatively well managed to build the first parts of the bridges between the different fields in nowadays neuroscience research, more work has to be done to bring the different fields of view closer together. Even more work needs to be done to completely understand the organization and functioning of neural networks regulating ingestive behavior. Some bridges that, once built,

would pave the way to a better understanding of the relationship between the regulation of energy balance from a microscopic and a macroscopic perspective, as well as from a preclinical and a human research perspective, would be the following.

- Future experiments along the line of those described in chapters 1 and 2 should be performed in exactly the same manner in humans and rodents. For example trained, awake rats should be scanned while tasting different substances, while experiencing gastric distention, while nutrients are being pumped into the stomach, or while eating, so that the complete picture of the process of satiation, including conscious processing, can be drawn and compared to humans.
- Ideally, experiments that are performed to study the process of satiation should include simultaneous oro-sensory stimulation and gastric distention, to study whether the effects of tasting and gastric distention are summative or maybe more than the sum of their parts.
- Effort should be put into generating new brain atlases for humans and rodents with exactly the same names for brain regions that are functionally the same. This could be done based on genetic identity of brain areas in humans and rodents, on structural connections between areas, or on function, but ideally those three characteristics should all be taken into account. Nowadays, it remains difficult to combine, for example, neuroimaging results from humans and rodents, since many brain regions that have the same function are named differently in humans compared to rodents. However, this assumes that brains from different species can be compared one on one, which is difficult. Generating atlases with exactly the same names might therefore not be possible, but at least deserves thorough investigation.
- DREADD-phMRI experiments should be performed that are specifically targeted on certain cell types within a neuronal projection, e.g. activating dopamine neurons within the VTA-NAcc projection. When these results are subsequently compared to results from activating the entire VTA-NAcc projection, specific consequences of activation of, and possibly roles for, these neurons can be deduced.
- The full potential of iDISCO+, described in the Appendix, should be exploited. Not only should automated registration be performed, in order to be able to automatically compare brains of different mice, to quantify amounts of stained neurons, and to analyze complete patterns of specific neurons, this brain clearing technique should also be combined with other techniques, such as modified rabies virus tracing technology to visualize inputs to specific cell types in a specific area on whole brain level; with diffusion tensor imaging (DTI) to compare structural connectivity assessed by the two different imaging

modalities; and with resting state fMRI to compare structural connectivity as assessed by iDISCO+ with functional connectivity as assessed by rs-fMRI.

- And finally, future experiments along the line described in this thesis should decipher how the processes and mechanism they aim to unravel lead to or contribute to healthy or unhealthy feeding behavior.

Eventually, the ultimate goal is to completely understand the organization and functioning of feeding-related neural networks, and thereby understand how ingestive behavior and energy balance are regulated. This would allow for manipulations to the system that regulates ingestive behavior, so that this behavior can be steered in order to prevent overweight and obesity. In order to unravel the mechanisms underlying these pathological states, that can only be assessed macroscopically in humans, translational research and the use of animal models remain essential. To increase our understanding of the regulation of ingestive behavior, to be able to bridge different levels of understanding, and to relate molecular and cellular mechanisms to disease states novel tools need to be developed and implemented, as I tried in this thesis.

REFERENCES

1. Wang, G. J. et al. Gastric distention activates satiety circuitry in the human brain. Neuroimage 39, 1824–1831 (2008).
2. Ely, A. V. et al. Response in taste circuitry is not modulated by hunger and satiety in women remitted from bulimia nervosa. J. Abnorm. Psychol. 126, 519–530 (2017).
3. Frank, G. et al. The evaluation of brain activity in response to taste stimuli–a pilot study and method for central taste activation as assessed by event related fMRI. J. Neurosci. Methods 131, 99–105 (2003).
4. Small, D. M. & Prescott, J. Odor/taste integration and the perception of flavor. Exp. Brain Res. 166, 345–357 (2005).
5. de Araujo, I. E. & Rolls, E. T. Representation in the Human Brain of Food Texture and Oral Fat. J. Neurosci. 24, 3086–3093 (2004).
6. Small, D. M. Taste representation in the human insula. Brain Struct. Funct. 214, 551–561 (2010).
7. Small, D. M. et al. Dissociation of neural representation of intensity and affective valuation in human gustation. Neuron 39, 701–711 (2003).
8. Gagnon, L., Kupers, R. & Ptito, M. Neural correlates of taste perception in congenital blindness. Neuropsychologia 70, 227–234 (2015).
9. Turner, C. E., Byblow, W. D., Stinear, C. M. & Gant, N. Carbohydrate in the mouth enhances activation of brain circuitry involved in motor performance and sensory perception. Appetite 80, 212–219 (2014).

10. Frank, S., Kullmann, S. & Veit, R. Food related processes in the insular cortex. Front. Hum. Neurosci. 7, 1–6 (2013).
11. Rolls, E. T. Brain mechanisms underlying flavour and appetite. Philos. Trans. R. Soc. B Biol. Sci. 361, 1123–1136 (2006).
12. Spetter, M. S., Smeets, P. A. M., de Graaf, C. & Viergever, M. A. Representation of sweet and salty taste intensity in the brain. Chem. Senses 35, 831–840 (2010).
13. Travagli, R. A., Hermann, G. E., Browning, K. N. & Rogers, R. C. Brainstem Circuits Regulating Gastric Function. Annu. Rev. Physiol. 68, 279–305 (2006).
14. Browning, K. N. & Travagli, R. A. Plasticity of vagal brainstem circuits in the control of gastrointestinal function. Auton. Neurosci. Basic Clin. 161, 6–13 (2011).
15. Smeets, P. A. M., Charbonnier, L., van Meer, F., van der Laan, L. N. & Spetter, M. S. Food-induced brain responses and eating behaviour. Proc. Nutr. Soc. 71, 511–520 (2012).
16. Lasschuijt, M. P. et al. Comparison of oro-sensory exposure duration and intensity manipulations on satiation. Physiol. Behav. 176, 76–83 (2017).
17. Zijlstra, N. et al. Effect of viscosity on appetite and gastro-intestinal hormones. Physiol. Behav. 97, 68–75 (2009).
18. Zijlstra, N., Mars, M., De Wijk, R. A., Westerterp-Plantenga, M. S. & De Graaf, C. The effect of viscosity on ad libitum food intake. Int. J. Obes. 32, 676–683 (2008).
19. Bolhuis, D. P. et al. Slow food: Sustained impact of harder foods on the reduction in energy intake over the course of the day. PLoS One 9, 1–7 (2014).
20. Simon, J. J. et al. Integration of homeostatic signaling and food reward processing in the human brain. JCI Insight 2, 1–17 (2017).
21. Al-Zubaidi, A., Heldmann, M., Mertins, A., Jauch-Chara, K. & Münte, T. F. Influences of Hunger, Satiety and Oral Glucose on Functional Brain Connectivity: A Multimethod Resting-State fMRI Study. Neuroscience 382, 80–92 (2018).
22. Berthoud, H. R., Münzberg, H. & Morrison, C. D. Blaming the Brain for Obesity: Integration of Hedonic and Homeostatic Mechanisms. Gastroenterology 152, 1728–1738 (2017).
23. Palmiter, R. D. Is dopamine a physiologically relevant mediator of feeding behavior? Trends Neurosci. 30, 375–81 (2007).
24. Lockie, S. H. & Andrews, Z. B. The hormonal signature of energy deficit: Increasing the value of food reward. Mol. Metab. 2, 329–336 (2013).

25. Nestler, E. J. Is there a common molecular pathway for addiction? Nat. Neurosci. 8, 1445–9 (2005).
26. Russo, S. J. & Nestler, E. J. The brain reward circuitry in mood disorders. Nat. Rev. Neurosci. 14, 609–625 (2013).
27. Kelley, A. E. & Berridge, K. C. The neuroscience of natural rewards: relevance to addictive drugs. J. Neurosci. 22, 3306–11 (2002).
28. Peciña, S. & Berridge, K. C. Hedonic hot spot in nucleus accumbens shell: where do mu-opioids cause increased hedonic impact of sweetness? J. Neurosci. 25, 11777–86 (2005).
29. Berridge, K. C., Ho, C.-Y., Richard, J. M. & DiFeliceantonio, A. G. The tempted brain eats: pleasure and desire circuits in obesity and eating disorders. Brain Res. 1350, 43–64 (2010).
30. Koob, G. F. & Le Moal, M. Addiction and the Brain Antireward System. Annu. Rev. Psychol. 59, 29–53 (2008).
31. Meye, F. J. & Adan, R. A. H. Feelings about food: the ventral tegmental area in food reward and emotional eating. Trends Pharmacol. Sci. 35, 31–40 (2014).
32. Bassareo, V., De Luca, M. A. & Di Chiara, G. Differential Expression of Motivational Stimulus Properties by Dopamine in Nucleus Accumbens Shell versus Core and Prefrontal Cortex. J. Neurosci. 22, 4709–19. (2002).
33. Kelley, A. E., Baldo, B. A., Pratt, W. E. & Will, M. J. Corticostriatal-hypothalamic circuitry and food motivation: integration of energy, action and reward. Physiol. Behav. 86, 773–95 (2005).
34. Volkow, N. D. et al. Low Level of Brain Dopamine D2 Receptors in Methamphetamine Abusers: Association With Metabolism in the Orbitofrontal Cortex. Am. J. Psychiatry 158, 2015–2021 (2001).
35. Volkow, N. D. et al. Profound Decreases in Dopamine Release in Striatum in Detoxified Alcoholics: Possible Orbitofrontal Involvement. J. Neurosci. 27, 12700–12706 (2007).
36. Volkow, N. D., Wang, G.-J., Tomasi, D. & Baler, R. D. The addictive dimensionality of obesity. Biol. Psychiatry 73, 811–8 (2013).
37. Humphries, M. D. & Prescott, T. J. The ventral basal ganglia, a selection mechanism at the crossroads of space, strategy, and reward. Prog. Neurobiol. 90, 385–417 (2010).
38. Kenny, P. J., Voren, G. & Johnson, P. M. Dopamine D2 receptors and striatopallidal transmission in addiction and obesity. Curr. Opin. Neurobiol. 23, 1–4 (2013).

39. Kupchik, Y. M. et al. Coding the direct/indirect pathways by D1 and D2 receptors is not valid for accumbens projections. Nat. Neurosci. 18, 1230–1232 (2015).
40. Richter, C. Salt appetite of mammals: its dependence on instinct and metabolism. L'Instinct dans le Comport. des animaux l'homme 577, (1956).
41. Berridge, K. C., Flynn, F. W., Schulkin, J. & Grill, H. J. Sodium depletion enhances salt palatability in rats. Behav. Neurosci. 98, 652–660 (1984).
42. Berridge, K. C. & Schulkin, J. Palatability shift of salt-associated incentive during sodium depletion. Q. J. Exp. Psychol. 41B, 121–131 (1989).
43. Roitman, M. F., Schafe, G. E., Thiele, T. E. & Bernstein, I. L. Dopamine and Sodium Appetite: Antagonists Suppress Sham Drinking of NaCl Solutions in the Rat. Behav. Neurosci. 111, 606–611 (1997).
44. Wolf, G. Hypothalamic regulation of sodium intake: relations to preoptic and tegmental function. Am. J. Physiol. 213, 1433–1438 (1967).
45. Stricker, E. M. & Zigmond, M. J. Effects on homeostasis of intraventricular injections of 6-hydroxydopamine in rats. J. Comp. Physiol. Psychol. 86, 973–994 (1974).
46. Fortin, S. M. & Roitman, M. F. Challenges to Body Fluid Homeostasis Differentially Recruit Phasic Dopamine Signaling in a Taste-Selective Manner. J. Neurosci. 38, 6841–6853 (2018).
47. Sandhu, E. C. et al. Phasic Stimulation of Midbrain Dopamine Neuron Activity Reduces Salt Consumption. Eneuro 5, ENEURO.0064-18.2018 (2018).
48. Davis, John, D. The Microstructure of Ingestive Behavior. Ann. N. Y. Acad. Sci. 575, 106–121 (1989).
49. Higgs, S. & Cooper, S. J. Evidence for early opioid modulation of licking responses to sucrose and Intralipid: A microstructural analysis in the rat. Psychopharmacology (Berl). 139, 342–355 (1998).
50. D'Aquila, P. S. Dopamine on D2-like receptors 'reboosts' dopamine D1-like receptor-mediated behavioural activation in rats licking for sucrose. Neuropharmacology 58, 1085–1096 (2010).
51. Leinninger, G. M. et al. Leptin acts via leptin receptor-expressing lateral hypothalamic neurons to modulate the mesolimbic dopamine system and suppress feeding. Cell Metab. 10, 89–98 (2009).
52. Elias, C. F. et al. Leptin Differentially Regulates NPY and POMC Neurons Projecting to the Lateral Hypothalamic Area. Neuron 23, 775–786 (1999).
53. Friedman, J. M. & Halaas, J. L. Leptin and the regulation of body weight in mammals. Nature 395, 763–70 (1998).

54. Halaas, J. L. et al. Weight-Reducing Effects of the Plasma Protein Encoded by the Obese Gene. Science (80-.). 269, 543–546 (1995).
55. Rosenbaum, M., Sy, M., Pavlovich, K., Leibel, R. L. & Hirsch, J. Leptin reverses weight loss–induced changes in regional neural activity responses to visual food stimuli. J. Clin. Invest. 118, 2583–2591 (2008).
56. Hinkle, W., Cordell, M., Leibel, R., Rosenbaum, M. & Hirsch, J. Effects of reduced weight maintenance and leptin repletion on functional connectivity of the hypothalamus in obese humans. PLoS One 8, e59114 (2013).
57. Davis, J. F. et al. Leptin Regulates Energy Balance and Motivation through Action at Distinct Neural Circuits. Biol. Psychiatry 69, 668–674 (2012).
58. Enriori, P. J., Sinnayah, P., Simonds, S. E., Garcia Rudaz, C. & Cowley, M. A. Leptin Action in the Dorsomedial Hypothalamus Increases Sympathetic Tone to Brown Adipose Tissue in Spite of Systemic Leptin Resistance. J. Neurosci. 31, 12189–12197 (2011).
59. Elmquist, J. K. Hypothalamic pathways underlying the endocrine, autonomic, and behavioral effects of leptin. Physiol. Behav. 74, 703–708 (2001).

D

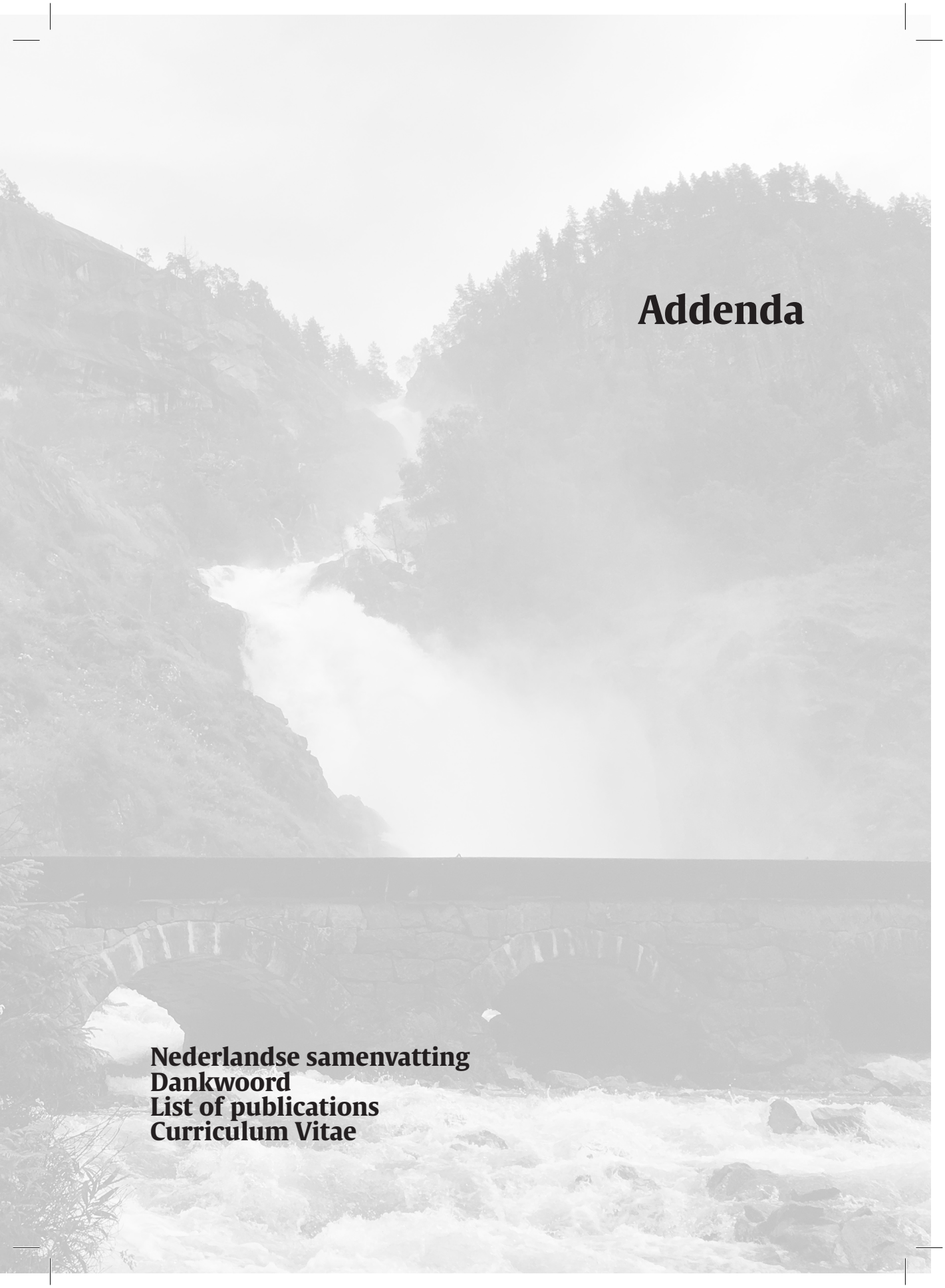

Addenda

Nederlandse samenvatting
Dankwoord
List of publications
Curriculum Vitae

Nederlandse Samenvatting

In de afgelopen decennia zijn er revolutionaire technieken ontwikkeld die totaal nieuwe mogelijkheden op het gebied van hersenwetenschappelijk onderzoek geboden hebben. Werd er vroeger vooral veel gebruik gemaakt van bijvoorbeeld laesie-studies en farmacologische interventies voor hersenwetenschappelijk onderzoek naar de mechanismen die ten grondslag liggen aan gedrag, tegenwoordig worden er daarnaast ook zeer geavanceerde technieken ingezet die de werkingsmechanismen van het brein op microscopisch of macroscopisch niveau proberen te ontrafelen. Voorbeelden hiervan zijn verschillende beeldvormende technieken in mens en proefdier, zoals 'Magnetic Resonance Imaging' (MRI), technieken om hersencellen te activeren of juist te inhiberen, zoals chemogenetica, en technieken om activiteit van hersencellen te meten, zoals 'fiber photometry'. Ondanks al deze innovatieve technieken ontbreekt echter nog steeds de kennis over hoe cellulaire activiteit op microscopisch niveau zich precies verhoudt tot neurale activiteit op macroscopisch niveau in het hele brein. Tevens blijft het lastig om kennis die vergaard is door hersenwetenschappelijk onderzoek in proefdieren te relateren aan kennis die vergaard is in humaan onderzoek. In dit proefschrift heb ik getracht bruggen te bouwen tussen zowel enerzijds neurofysiologische kennis over de microscopische, moleculaire en cellulaire werkingsmechanismen van de hersenen en anderzijds de macroscopische, netwerk-gerelateerde kennis over het functioneren van de hersenen, als tussen kennis verkregen uit proefdieronderzoek en humaan onderzoek. Om dit te doen, hebben we nieuwe technieken ontwikkeld en bestaande en nieuwe technieken gebruikt, gecombineerd en geoptimaliseerd.

Alle experimenten die in dit proefschrift beschreven staan, waren gefocust op het karakteriseren en manipuleren van de neurale circuits die betrokken zijn bij de regulatie van energie balans en in ons geval specifiek bij de regulatie van voedselinname. Regulatie van energie balans en voedselinname is niet alleen een goed onderwerp van studie om nieuwe benaderingen in hersenwetenschappelijk onderzoek te illustreren en de bovengenoemde bruggen te slaan vanwege het feit dat het zo sterk geconserveerd is tussen mens en (proef)dier, het is daarnaast ook een uiterst relevant systeem om te onderzoeken. Ontregeling van neurale netwerken die betrokken zijn bij de regulatie van energie balans en voedselinname leidt namelijk vaak tot serieuze problemen, zoals overgewicht en obesitas.

Obesitas is een nog altijd groeiend probleem; sinds 1975 is de prevalentie van obesitas bijna verdrievoudigd en we hebben inmiddels het punt bereikt waarbij het merendeel van de wereldbevolking in landen leeft waar er meer mensen sterven door overgewicht dan door ondergewicht. Overgewicht en

obesitas leiden tot een verhoogde kans op het ontwikkelen van diabetes, cardiovasculaire aandoeningen, spieraandoeningen en verschillende soorten kanker. De consequenties op sociaal, maatschappelijk en economisch niveau zijn daardoor enorm. Dit illustreert de noodzaak om effectieve interventies te ontwikkelen en de relevantie om meer kennis over het systeem dat voedselinname reguleert te vergaren.

Het doel van dit proefschrift was om de eerder genoemde bruggen te slaan en daardoor de kennis vanuit verschillende invalshoeken in hersenwetenschappelijk onderzoek te kunnen combineren, om zo tot een beter inzicht in de regulatie van voedingsgerelateerd gedrag te komen. Ik heb getracht inzicht te krijgen in de moleculaire mechanismen die ten grondslag liggen aan de macroscopische kennis over de regulatie van voedingsgerelateerd gedrag. Tevens heb ik getracht meer microscopische en macroscopische kennis te vergaren, om daarmee uiteindelijk meer inzicht te krijgen in hoe de neurale netwerken die betrokken zijn bij de regulatie van voedingsgerelateerd gedrag georganiseerd zijn en hoe ze functioneren. Hierbij ben ik op macroscopisch niveau begonnen in hoofdstukken 1 en 2; deze hoofdstukken beschrijven experimenten waarin ik gekeken heb naar het gehele brein van ratten, om hiermee een brug te kunnen slaan naar humaan onderzoek. In hoofdstukken 3 en 4 worden macroscopische en microscopische technieken gecombineerd. Hoofdstuk 5 staat aan het eind van de macroscopische naar microscopische schaal, waarbij ik gekeken heb naar individuele neuronen. De Appendix combineert dit uiterste van de microscopische schaal weer met het macroscopische perspectief, waardoor individuele neuronen in een compleet en intact brein bekeken kunnen worden. Kortom, ik wilde de neurale circuits die betrokken zijn bij de regulatie van voedingsgerelateerd gedrag karakteriseren en manipuleren, om zo beter te gaan begrijpen hoe specifieke hersengebieden binnen deze circuits in verbinding staan en voedingsgerelateerde informatie verwerken. Daarnaast heb ik ook geprobeerd de vertaalslag van proefdieronderzoek naar humaan onderzoek te verbeteren. Omdat een echte vertaalslag tussen mens en dier een uitdaging blijft, heb ik allereerst geprobeerd om de waarde van proefdieronderzoek voor humaan onderzoek aan te tonen.

Om te beginnen heb ik in hoofdstukken 1 en 2 een preklinisch protocol ontwikkeld waarmee zowel de hersenactiviteit in reactie op smaak en maagrek, als de functionele connectiviteit bij hongerige of verzadigde ratten gemeten kan worden met behulp van MRI. Dit protocol is redelijk vergelijkbaar met protocollen die in humaan onderzoek gebruikt worden, waardoor de waarde van dit werk voor humaan onderzoek relevant is. We hebben gevonden dat verschillende hersengebieden, die bij mensen betrokken zijn bij de regulatie van energie

balans en voedingsgerelateerd gedrag, ook bij ratten een rol spelen. Daarnaast hebben we ontdekt dat in een gebied dat belangrijk is voor verzadiging, de insula, de activiteit langzaam stijgt naarmate een rat vaker een suikeroplossing proeft. Dit zou kunnen betekenen dat de insula een belangrijk gebied is voor de regulatie van verzadiging en dat verzadiging langzaam ontstaat naarmate iets vaker geproefd wordt. Verder vonden we activiteit in gebieden die horen bij het mesocorticolimbische systeem dat betrokken is bij motivationeel gedrag en beloning. Dit lijkt erop te duiden dat iets zoets proeven en het ervaren van maagrek geassocieerd zijn met de belonende effecten van zoetigheid en een gevulde maag.

De functionele connectiviteit tussen verschillende gebieden in de hersenen van hongerige en verzadigde ratten, voor- en nadat ze iets zoets geproefd hadden of maagrek ervaren hadden, liet zien dat er een complexe interactie bestaat tussen de status van energie balans, dus de mate van verzadiging, en een verandering van deze balans door een voedingsgerelateerde stimulus, dus smaak of maagrek. We vonden dat er veel gebieden betrokken zijn en functioneel verbonden zijn en dat deze dus op een complexe manier interacteren om voedingsgerelateerd gedrag te reguleren.

De eerste twee hoofdstukken hebben bijgedragen aan het bouwen van een brug tussen proefdieronderzoek en humaan onderzoek, aangezien we protocollen hebben ontwikkeld en toegepast die vergelijkbaar zijn met humane protocollen, en resultaten hebben gevonden die overeenkwamen met die van humane experimenten. Verder hebben we door de experimenten die beschreven staan in de eerste twee hoofdstukken kennis opgedaan over de organisatie van voedingsgerelateerde neurale netwerken, over hoe bepaalde hersengebieden in deze netwerken met elkaar in verbinding staan en interacteren, hoe deze hersengebieden voedingsgerelateerde informatie verwerken, en hoe deze gebieden bijdragen aan verzadiging en betrokken zijn bij de regulatie van voedingsgerelateerd gedrag.

In hoofdstukken 3 tot en met 5 heb ik geprobeerd macroscopische met microscopische kennis te combineren. Dit verschaft inzicht in de cellulaire mechanismen die ten grondslag liggen aan neurale netwerkactiviteit en -connectiviteit en aan gedrag. Daartoe heb ik in hoofdstuk 3 een techniek ontwikkeld waarmee specifieke projecties in het brein geactiveerd kunnen worden op cellulair niveau en waarmee tegelijkertijd het effect van deze activatie op activiteit en connectiviteit in het hele brein gemeten kan worden. Deze techniek, die we DREADD-phMRI genoemd hebben, combineert twee bestaande technieken, namelijk chemogenetica waarmee neuronen geactiveerd of geïnhibeerd kunnen worden, en functionele MRI. In de studie beschreven in

hoofdstuk 3 hebben we twee projecties geactiveerd die onderdeel uitmaken van het mesocorticolimbische systeem, dat betrokken is bij belangrijke aspecten van de regulatie van voedingsgerelateerd gedrag. Na cellulaire activatie van de twee projecties door middel van chemogenetica, detecteerden we activiteit door middel van functionele MRI in deze projecties, maar ook detecteerden we responsen in gebieden waarvan we weten dat ze verbonden zijn met deze projecties. Dit toonde aan dat DREADD-phMRI in staat is om netwerkactiviteit in het gehele brein te meten na cellulaire activatie van specifieke neurale projecties. Dit geeft de cellulaire basis weer van de indirecte maat van neurale activiteit zoals die met functionele MRI gedetecteerd wordt en vormt daarmee een eerste brug van het macroscopische niveau van een functionele beeldvormende techniek als MRI naar een meer microscopisch niveau van cellulaire activatie van hersenprojecties. Deze kennis over de cellulaire basis van de functionele MRI response is ook toepasbaar op humane functionele MRI data. De patronen in de responsen die we detecteerden na activatie van het mesocorticolimbische systeem gaven naast bevestiging van de huidige kennis ook nieuwe inzichten in activiteit van het mesocorticolimbische systeem.

Hierop volgend hebben we ons onderzoek meer richting het microscopische niveau opgeschoven, terwijl we de cellulaire technieken die we in hoofdstuk 4 gebruikten wel bleven combineren met macroscopische uitkomstmaten, zoals gedrag. Met een multidisciplinaire benadering hebben we de rol van het mesocorticolimbische systeem en van de neurotransmitter dopamine in 'eetlust' voor zout bestudeerd. 'Eetlust' voor zout verwijst naar het proces waardoor zout, dat van nature aversief is voor ratten, aantrekkelijk en belonend wordt wanneer een dier zout-gedepriveerd wordt, dus wanneer het in een staat van ernstig zouttekort wordt gebracht. Hoe neurale circuits deze verandering in waardering van zout bewerkstelligen was vooralsnog onduidelijk. Door verschillende macroscopische en microscopische technieken, zoals 'fiber photometry', chemogenetica, gedragsfarmacologie, en immunohistochemie in te zetten in dieren die zout-gedepriveerd waren, konden we de rol van dopamine en het mesocorticolimbische systeem in 'eetlust' voor zout bestuderen. Hiermee konden we tevens kennis over de werkingsmechanismen van bepaalde neuronen in specifieke hersengebieden linken aan gedragsgerelateerde uitkomstmaten, daarmee een verbinding vormend tussen microscopische en macroscopische inzichten. We vonden onder andere dat de nucleus accumbens, een hersengebied dat onderdeel uitmaakt van het mesocorticolimbische systeem, de motivationele aspecten van 'eetlust' voor zout medieert, maar niet de hedonische aspecten ervan, en dat dit niet afhankelijk is van dopaminerge neurotransmissie in de nucleus accumbens. Deze resultaten geven meer inzicht in hoe het brein

voedingsgerelateerd gedrag reguleert.

Aan het einde van de macroscopische naar microscopische schaal hebben we onderzocht wat de afferente neuronen, dus de informatie-aanvoerende neuronen, zijn van een specifieke set van neuronen die een centrale rol spelen in de regulatie van energie balans. Door te ontrafelen wat de, vooralsnog onbekende, afferente neuronen van een specifieke neuronenpopulatie zijn, hebben we meer microscopisch inzicht gekregen in de cellulaire organisatie van dit voedingsgerelateerde neurale netwerk.

Ten slotte hebben we met de in de Appendix beschreven experimenten getracht om microscopische bevindingen naar een macroscopisch niveau te tillen. Hiertoe hebben we het brein van muizen, waarin we bepaalde neuronen die betrokken zijn bij de regulatie van voedingsgerelateerd gedrag aangekleurd hadden, transparant gemaakt. Daardoor zijn de individuele neuronen en hun uitlopers in een geheel, intact, 3D brein te zien, en later ook te analyseren. Dit heeft ons begrip van de organisatie van voedingsgerelateerde neurale netwerken verbeterd.

Samenvattend, dit proefschrift kan gezien worden als een poging om bruggen te slaan tussen verschillende begripsniveaus in hersenwetenschappelijk onderzoek. Ik heb getracht om de vertaalslag van proefdieronderzoek naar humaan onderzoek te maken, door de waarde van hersenwetenschappelijk onderzoek naar voedingsgerelateerd gedrag in proefdieren voor humaan onderzoek aan te tonen. Daarnaast heb ik getracht om neurofysiologische kennis over onderliggende moleculaire en cellulaire werkingsmechanismen in verbinding te brengen met de organisatie en het functioneren van neurale netwerken die betrokken zijn bij de regulatie van voedingsgerelateerd gedrag.

Dankwoord

Eindelijk is het zover, het dankwoord! Dat betekent dat de rest van mijn proefschrift af is! En dat was nooit gelukt zonder de hulp van velen. Voor die directe en indirecte hulp wil ik iedereen ontzettend bedanken. Er zijn echter een paar mensen die ik specifiek wil noemen.

Roger, ruim zes en een half jaar geleden klopte ik bij je aan of ik misschien mijn eerste stage in jouw lab mocht lopen. Wat was ik blij dat je dat goed vond en dat je me vervolgens ook nog eens wilde begeleiden bij het schrijven van mijn eigen PhD proposal. Ondanks dat ik dat plan niet kon uitvoeren, bood jij me een promotieplek aan. Daar ben ik nog steeds erg blij mee en je ook dankbaar voor. Ik heb veel van je geleerd de afgelopen jaren en je enthousiasme voor zo'n beetje alles rond voeding en energie balans werken aanstekelijk. Ik vond het fijn dat we bij jou de vrijheid hebben gekregen om onderzoek te doen naar datgene wat we zelf interessant vinden, en dat je ons op die eigen wegen altijd wist te voorzien van de nodige tips en tricks en ook van je kritische vragen en gedachtespinsels. Ik vind het vooral bewonderenswaardig dat jij je hard blijft maken voor 'de menselijke maat' binnen het UMC en dat je erin slaagt om te zorgen voor zo'n leuke, gezellige onderzoeksgroep. Bedankt voor de leuke en leerzame jaren!

Rick, iets later klopte ik ook bij jou aan, voor een tweede stage. Bedankt voor het vertrouwen dat je in mij had om die stage te gaan doen, ook al was het dan een onderzoek naar een onderwerp dat tamelijk ver van jouw bed (of bench) af stond, in de MR troffen onze interesses elkaar. Dat ik daarna mijn promotie ook deels op jouw groep mocht doen, heeft me heel veel geleerd en daar ben ik je dankbaar voor. Ik wil je ook bedanken voor je zeer uitgebreide en leerzame feedback op mijn stukken, daar heb ik zeker beter door leren schrijven. Verder was het fijn om resultaten aan jou te laten zien, omdat jij er toch altijd nog wel weer wat moois in zag. Door af en toe mee te kijken door die roze bril, zag het er vaak een stuk rooskleuriger uit. Bedank voor de kans om na mijn PhD ook mijn eerste postdoc in jouw groep te mogen doen. Ondanks dat die periode ook alweer achter ons ligt, heb ik er veel van geleerd.

Han, bedankt dat je me wegwijs hebt gemaakt in de wondere wereld van de wetenschap. Bedankt voor je nimmer aflatende enthousiasme, dat erg inspirerend werkte, en je goede en gezellige begeleiding tijdens mijn eerste stage. Je bent er zelfs in geslaagd om een beetje van je enthousiasme voor 'wetenschappelijk' bakken op mij over te dragen, wie had dat ooit gedacht! Je zeer nauwkeurige keukenweegschaal wordt veelvuldig gebruikt. ;-)

Newbies, I found it rather confronting when our group name changed from Newbies to Oldies-but-Goldies. Therefore, I still thank the Newbies, because honestly, we'll always be newbies to life! ;-) Thanks for the chats, the coffees, the moments to complain, to relax, to share each other's struggles, and to celebrate each other's victories!

Jeroen, bedankt voor de leukste tijd uit heel mijn PhD. Van alle experimenten denk ik nog met het meeste plezier terug aan ons zout-werk. Ik vond het ontzettend leuk om samen met jou een heus team te vormen en met je te kunnen sparren over de volgende stappen in ons master experiment of in het leven in het algemeen. Ik heb ontzettend veel van je geleerd, denk bijvoorbeeld aan fatsoenlijke statistiek of fatsoenlijke plaatjes maken, maar vooral hoe je je op de juiste momenten maximaal inspant, om dan op andere momenten lekker te kunnen relaxen. Heerlijk ook om te zien hoe je om wist te gaan met druk en andere 'factoren', ook daar heb ik heel wat van afgekeken. ;-)

Shanice, dank voor je gezelligheid en hulp bij zowel het zout-werk als het rabies-werk. Dank dat ik je zelfs een jaar na het afronden van je stage nog steeds lastig mocht vallen met vragen over hoe je alles ook alweer afgerond had terwijl ik met verlof was. Zonder jouw hulp was het nooit zo mooi geworden als het nu is. Heel veel succes met je PhD en geniet vooral van je kleine spruit, dat blijft het allermooiste en het allerbelangrijkste, geloof me!

Mieneke, allereerst dank voor al je praktische hulp tijdens mijn PhD. Het opereren, perfuseren, samen magen ontleden en ballonnen fröbelen. Ik heb altijd erg genoten van onze lunches, de gezelligheid om met jou samen te werken en onze gedeelde interesses in bijvoorbeeld geloof en groentetuinen. Je moet me nog maar eens een paar lesjes geven, want ik was dit jaar vergeten op te schrijven wat in welk bakje zat... De tuin was dus een grote verrassing! Ik ben ontzettend blij dat jij mijn paranimf wilt zijn!

Julia, we always got along well, but especially in the final stage we had the chance to work together more often. I loved our coffee-laptop-dates and it really helped me to stay motivated and get it all finished. Although I never knew if I had to speak English, Dutch or Afrikaans (although the latter would have been problematic) and neither did the bar tender, I enjoyed all the conversations about work, relationships, houses, jobs, family and whatsoever. Thanks for being my paranimf!

Wim, Gerard, Michel en Milou, dank voor jullie eindeloze stroom aan hulp, in welke vorm dan ook! Voor alle hulp bij de analyses of een wederom vastgelopen 9.4, en voor alle input op mijn output. Maar bovenal heel veel dank dat ik met jullie altijd zo leuk kon praten over van alles en nog wat, zoals het leven, geloof, wetenschap, werk, vriendschappen en vitamines! Ik mis die ontspannende momenten nu al.

Annette, Geralda en Caroline, dank voor jullie hulp in welke zin dan ook, voor alle spoedjes, voor de hulp bij het opzetten van alle technisch nogal uitdagende scans, voor het fixen van vastgekleefde coils en doorgebrande spoelen, en voor het bijspringen in tijden van 'nood'!

Inge, Roland en Keith, dank voor al jullie praktische hulp, maar veel meer nog voor alle gezelligheid en leuke gesprekken. Ik heb ervan genoten!

Verder alle andere collega's van zowel het BCRM als van de in vivo NMR groep, van kamergenoten tot studenten, van alle dierverzorgers tot analisten, van mede Nudge-itters tot schoenen-adviseurs, van collega's tot bijzonder leuk kraambezoek, van staf tot schoonmakers, ik wil iedereen heel erg bedanken voor de leuke, gezellige en inspirerende tijd. Zonder jullie aanwezigheid, motiverende woorden, gezelligheid, en directe of iets minder directe hulp was het misschien wel nooit gelukt, maar was het in ieder geval veel minder leuk geweest.

Herman Finkers, ondanks dat u zich met een aan zekerheid grenzende waarschijnlijkheid niet bewust bent geweest van het feit dat u mij tot steun bent geweest tijdens dit promotietraject, wil ik u toch bedanken voor het feit dat u dat wel degelijk bent geweest. Bedankt dat u laat zien dat religie, kunst en humor zich eigenlijk allemaal met hetzelfde bezig houden. Graag zou ik daar 'wetenschap' nog aan toe willen voegen. Uw geweldige humor, goede grappen en interessante gedachtegangen hebben mij de afgelopen jaren steeds weer doen ontspannen wanneer de werkdruk me even naar het hoofd steeg. Ik wil u bedanken dat u, in mijn ogen, laat zien dat wetenschap en geloof een perfect duo zijn. Omdat een poëet nou eenmaal het best bedankt kan worden door iets uit zijn oeuvre te citeren, wil ik dat graag doen aan het einde van dit dankwoord.

De moeders van de wonderbaby's, wat blijft het bijzonder om zoiets geweldigs en moois als het krijgen van een kind samen meegemaakt te hebben. Ik vond het superfijn om tussen al het promotiewerk door heerlijk ongegeneerd met jullie te kunnen praten over alle leuke en minder leuke (en zelfs genante) dingen die

bij onze zwangerschappen, bevallingen en daarna bij de wonderbaby's kwamen kijken. Ik denk met veel plezier terug aan de nachtelijke WhatsApp-gesprekken als we weer eens allemaal zaten te voeden. Dank voor alle afleiding van mijn PhD-werk en toch ook voor de interesse daarin.

Vriendinnen, De meisjes en Puur, dank voor de gezelligheid, de afleiding, de motiverende woorden en steunbetuigingen, de wandelingen, de etentjes, en de spontane en minder spontane dates. Ondanks dat we, zoals waarschijnlijk elke vriendschap, onze pieken en ook dalen hebben gekend, ben ik jullie dankbaar voor alle mooie momenten die we samen hebben meegemaakt. Dank ook dat jullie mijn, soms eindeloze, klaagzangen over het werk en mijn momenten van victorie hebben willen aanhoren en er altijd nog leuk op wisten te reageerden ook!

Alle familie die altijd zo betrokken is geweest, ooms en tantes, neven en nichten, dank jullie wel voor jullie betrokkenheid en voor alle ontspannende momenten!

Opa en oma, jullie zijn een belangrijke motivatie geweest voor mij om dit proefschrift af te ronden. Altijd waren jullie geïnteresseerd in hoe het er nu mee stond. Ik vond het zo leuk dat ik jullie mocht rondleiden op het lab en in de stallen, en hoe jullie daarna toch wel echt van de ratten besnuffeld waren. Dank dat we bij jullie mochten logeren, heel vroeger en ook wat minder vroeger om weer even bij te tanken. Dank voor de goede gesprekken, zelfs die ene keer op 1 januari tot bijna drie uur 's nachts. Toen ik jullie ooit vroeg of jullie wel eens aan jullie keus voor elkaar getwijfeld hadden, was opa's volmondige 'nee, nog nooit!' een hele mooie reden om door te blijven zoeken tot ik Robert vond. Dus niet alleen dank voor de gezelligheid en de interesse in mijn werk, maar bovenal dank voor jullie wijze adviezen!

Mijn zussen, broer, schoonzussen en zwagers. Irene, Karin en Bas, en Alex, wat zijn we toch een heerlijk ongestructureerd zooitje. Totaal verschillend en toch ook zoveel dat ons bindt. Ik heb heel veel zin om weer meer tijd met jullie door te brengen en kan niet wachten op alle leuke dingen die we nog gaan beleven! Irene, dank voor je rust, hoe je me leest en hoe je me altijd weer herinnert aan waar het ook alweer echt om gaat in het leven. Karin, dank voor je vrolijkheid, je eerlijkheid, hoe je dingen oppakt en aanpakt, en je alles-verbindende familieliefde. Wat moesten we zonder jou..? Eerlijk, ik zou het niet weten. Bas, goeie keus heb je gemaakt, wees zuinig op d'r! Alex, dank voor je hulp bij onze talloze verhuizingen en vele klusjes in ons huis, maar meer nog, dank voor je

doorzettingsvermogen en gezelligheid. Wouter en Maartje, Naneth en Tim, wat fijn dat ik jullie er als bonus-broers en -zussen bij heb gekregen! Dank voor jullie interesse en voor alle leuke tijd die we tot nu toe samen gehad hebben. Ik zie uit naar alles wat nog komen gaat!

Ad en Cobi, thanks for raising the man of my dreams. Hij en, mede daardoor, ook jullie waren onmisbaar in dit hele project. Dank voor jullie interesse in mijn werk, de betrokkenheid en voor alles dat jullie voor ons gedaan hebben en nog steeds doen. Jullie zijn werkelijk geweldige schoonouders! En Cobi, het zij je vergeven dat je steeds vroeg hoe het er nu met mijn studie voor stond. ;-)

Pap en mam, jullie stonden aan mijn begin. Dank jullie wel dat jullie me hebben opgevoed zoals jullie dat gedaan hebben, voor de stimulans om vooral te gaan doen wat ik leuk vond. Jullie hebben me geleerd dat als je echt je hart volgt, je uiteindelijk vanzelf goed wordt in wat je doet en op je plek terecht komt. Dank dat jullie al vroeg de wetenschapper in mij herkend hebben, maar me ook altijd de mogelijkheden hebben geboden om andere opties te kiezen. Bedankt ook dat jullie me waar nodig bescherming geboden hebben, maar ook dank jullie wel dat jullie altijd vertrouwen in mij hebben gehad en zelfs in de afronding van dit tamelijk intense PhD traject. Ik ben dolblij dat het achter me ligt en zie de toekomst met vertrouwen tegemoet, ook weer zoiets dat ik aan jullie te danken heb. Ik hou van jullie!

Robert en Noah, wat ben ik een ontzettend gezegend mens dat ik jullie in mijn leven heb! Ik ben dolgelukkig met jullie twee en oh zo dankbaar voor het gezin dat wij vormen! Lieve Noah, ik hoop dat je me niet teveel hebt hoeven missen tijdens de afronding van dit boekje. Ik ben blij dat we de tijd nu dubbel en dwars kunnen inhalen. Je bent een echt wonder! Lieve Roob, wat kan ik nog zeggen dat jij niet allang weet? Ik heb er lang over nagedacht hoe ik je hier kan bedanken, maar woorden schieten tekort. Op de pieken en ook in de soms diepe dalen was jij daar om me te helpen, te steunen en me lief te hebben. Je wist me er altijd aan te herinneren dat pieken en dalen van werk uiteindelijk allemaal relatief zijn. Het echte Leven met jou, Noah en Hem, dat is waar het allemaal om draait. Dank voor wie je bent en dat je mijn man bent. Ik kan me geen betere wensen. Ik hou zielsveel van je. Zoals Herman Finkers dat zo mooi zegt, ik heb je liever dan geluk!

Daarboven in de hemel - Herman Finkers

Weet u, ook ik ben niet compleet knettergek, ik heb HBS gehad.
Dus ik ben een man van wetenschap, van feiten en zo meer.
Als iets niet is bewezen, geloof ik het niet zo zeer.
Als men glashard aan kan tonen dat ik me vergis,
pas dan zal ik geloven dat er geen hemel is.

Ik zat in een tv-program, een soort van kruisverhoor.
Men vroeg mij daar: 'Zeg Herman, één ding heb ik niet goed door:
Je hebt toch HBS gehad? Dat is geen kattepis.
Hoe kun je dan geloven dat er een hemel is?'

Ik zat in een tv-program en 't ging nog verder mis.
Er werd me haarfijn uitgelegd hoe ik me vergis:
'De hemel is iets achterhaalds, er wacht ons boven niets.
De hemel, wees nou eerlijk, is een verzonnen iets.'

Verzonnen, dacht ik, jaja...
'De veertigste van Mozart en de liedjes van Jacques Brel
zijn ook ooit verzonnen', zei ik, 'toch bestaan ze wel.'
Iets kan zijn verzonnen en daardoor juist bestaan.
Dat soms iets niet verzonnen is, neemt men zomaar aan.
Mijn lied is ook verzonnen en hoor hoe het bestaat.
Ik zing het graag omdat daarmee de hemel opengaat.

Dus daarboven in de hemel zien wij elkander weer,
daar drinken wij een glaasje met Onze Lieve Heer.
Ook hij die nooit geloofde, heft daar met ons het glas
en kan dan maar niet geloven dat hij ooit op aarde was.

Dus daarboven in de hemel zien wij elkander weer,
daar maakt Andries Knevel ruzie met de Heer:
'Zoals 't er hier aan toe gaat', zegt hij, 'strookt niet met de leer.'
'Dat klopt,' zegt God, 'en daarom heerst er hier zo'n fijne sfeer.'

Daarboven in de hemel zien wij elkander weer,
daar drinken wij een glaasje met Onze Lieve Heer.
Ook hij die nooit geloofde, heft daar met ons het glas
en kan maar niet geloven dat hij ooit op aarde was.

Daarboven in de hemel...

List of Publications

J.W. de Jong, **T.J.M. Roelofs**, F.M. Mol, A.E. Hillen, K.E. Meijboom, M.C.M. Luijendijk, H.A. van der Eerden, K.M. Garner, L.J.M.J. Vanderschuren, R.A.H. Adan. *Reducing ventral tegmental dopamine D2 receptor expression selectively boosts incentive motivation.* Neuropsychopharmacology 40: 2085–2095 (2015)

L. Boekhoudt, **T.J.M. Roelofs**, J.W. de Jong, A.E. de Leeuw, M.C.M. Luijendijk, I.G. Wolterink-Donselaar, G. van der Plasse, R.A.H. Adan. *Does activation of midbrain dopamine neurons promote or reduce feeding?* International Journal of Obesity 41: 1131-1140 (2017)

T.J.M. Roelofs, J.P.H. Verharen, G.A.F. van Tilborg, L. Boekhoudt, A. van der Toorn, J.W. de Jong, M.C.M. Luijendijk, W.M. Otte, R.A.H. Adan*, R.M. Dijkhuizen*. *A novel approach to map induced activation of neuronal networks using chemogenetics and functional neuroimaging in rats: A proof-of-concept study on the mesocorticolimbic system.* NeuroImage 156: 109-118 (2017) *Shared last authorship

J.P.H. Verharen, J.W. de Jong, **T.J.M. Roelofs**, C.F.M. Huffels, R. van Zessen, M.C.M. Luijendijk, R. Hamelink, I. Willuhn, H.E.M. den Ouden, G. van der Plasse, R.A.H. Adan, L.J.M.J. Vanderschuren. *A neuronal mechanism underlying decision-making deficits during hyperdopaminergic states.* Nature Communications 9:731 (2018)

J.P.H. Verharen*, **T.J.M. Roelofs***, S. Menting-Henry, M.C.M. Luijendijk, L.J.M.J. Vanderschuren, R.A.H. Adan. *Limbic control over the homeostatic need for sodium.* Scientific Reports 9:1050 (2019) *Shared first authorship

T.J.M. Roelofs, M. Straathof, A. van der Toorn, W.M. Otte, R.A.H. Adan, R.M. Dijkhuizen. *Diet as connecting factor: functional brain connectivity in relation to feeding-related stimuli assessed with resting-state functional MRI in rats.* Under review at Journal of Neuroscience Research.

M. Straathof, M.R.T. Sinke, **T.J.M. Roelofs**, E.L.A. Blezer, R.A. Sarabdjitsingh, A. van der Toorn, O. Schmitt, W.M. Otte, R.M. Dijkhuizen. *Distinct structure-function relationships across brain regions and connectivity scales in the rat brain*. In preparation.

T.J.M. Roelofs, M.C.M. Luijendijk, A. van der Toorn, G. Camps, P.A.M. Smeets, R.M. Dijkhuizen, R.A.H. Adan. *Good taste or gut feeling: what fulfils? Oro-sensory stimulation and gastric distention generate distinct brain activation patterns in rats.* In preparation.

T.J.M. Roelofs, S. Menting-Henry, L.M. Gol, A.M. Speel, K.M. Garner, M.C.M. Luijendijk, V.H. Wielenga, K.K. Conzelmann, R.A.H. Adan. *Modified rabies virus tracing technology goes viral! Optimization of whole-brain input mapping to leptin receptor-expressing neurons in the lateral hypothalamus by assessing the effect of different TVA titers on tracing efficiency and specificity.* In preparation.

Curriculum Vitae

Tessa Roelofs was born on 15 January 1990 in Zutphen, the Netherlands. In 2008, she graduated from high school, Baudartius College, in Zutphen, and started her Bachelor's in Biomedical Sciences at Utrecht University which she obtained *cum laude*. From 2012 to 2014 she was enrolled in the Research Master Neuroscience and Cognition (*cum laude*) at Utrecht University. During her Master's Tessa further pursued her interest in the regulation of feeding behaviour. Her first scientific internship was in the lab of Prof. Dr. Roger Adan in Utrecht, where she studied the role of dopamine D2 receptors in the ventral tegmental area. Her second research project was in the group of Prof. Dr. Rick Dijkhuizen, where she optimized a functional Magnetic Resonance Imaging protocol in rats with which she investigated the effects of ghrelin administration on brain activity. During her Master's she was selected for the NWO Graduate Program 2012-2013, which allowed her to write her own PhD proposal. Although not financially supported by this program, participating in the NWO Graduate Program resulted in the opportunity for her to start her PhD with Prof. Dr. Roger Adan and Prof. Dr. Rick Dijkhuizen in 2014. During the 4 years following, she investigated the neural circuits involved in the regulation of feeding behaviour, the results of which are presented in this thesis. In 2018-2019 she was employed as a postdoctoral fellow at the lab of Prof. Dr. Rick Dijkhuizen, where she studied the interaction between Alzheimer's Disease and stroke.


FSC
www.fsc.org
MIX
Paper from
responsible sources